Similitude augmentation in sub-scale flight test model design
An MDAO based similarity maximization approach

Raju Kulkarni, A.

DOI
10.4233/uuid:6f0eaa80-e52e-4a03-b92b-cae847f12906

Publication date
2022

Document Version
Final published version

Citation (APA)
Raju Kulkarni, A. (2022). *Similitude augmentation in sub-scale flight test model design: An MDAO based similarity maximization approach*. [Dissertation (TU Delft), Delft University of Technology]. https://doi.org/10.4233/uuid:6f0eaa80-e52e-4a03-b92b-cae847f12906

Important note
To cite this publication, please use the final published version (if applicable).
Please check the document version above.

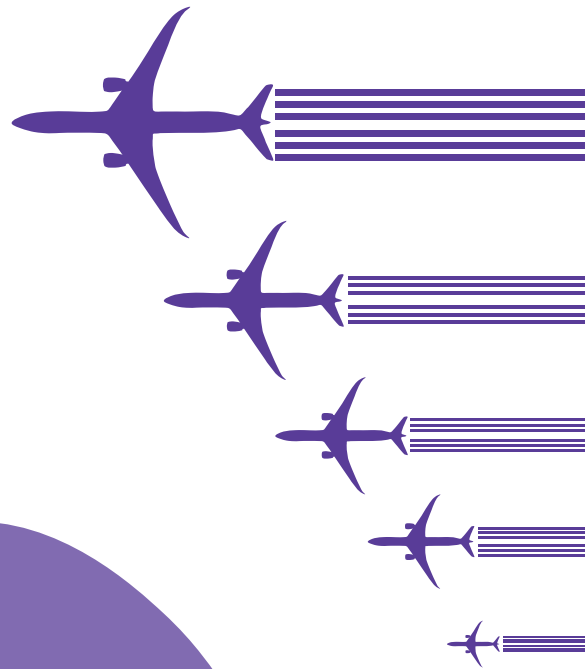# Similitude Augmentation in Sub-scale Flight Test Model Design

An MDAO based Similarity Maximization Approach

Akshay Raju Kulkarni

SIMILITUDE AUGMENTATION IN SUB-SCALE FLIGHT TEST MODEL DESIGN

AN MDAO BASED SIMILARITY MAXIMIZATION APPROACH

SIMILITUDE AUGMENTATION IN SUB-SCALE FLIGHT TEST MODEL DESIGN

AN MDAO BASED SIMILARITY MAXIMIZATION APPROACH

Dissertation

for the purpose of obtaining the degree of doctor
at Delft University of Technology
by the authority of the Rector Magnificus prof. dr. ir. T.H.J.J. van der Hagen,
chair of the Board of the Doctorates,
to be defended publicly on
Thursday 17 November 2022 at 12:30 o'clock

by

Akshay RAJU KULKARNI

Master of Science in Aerospace Engineering,
Delft University of Technology, The Netherlands
born in Bharuch, India.

This dissertation has been approved by the promotors.

Composition of the doctoral committee:

Rector Magnificus,	chairperson
Prof. dr. ir. L.L.M. Veldhuis	Delft University of Technology, *promotor*
Dr. ir. G. La Rocca	Delft University of Technology, *promotor*

Independent members:

Prof. dr. D. A. von Terzi	Delft University of Technology
Prof. dr. P. Krus	Linköping University, Sweden
Prof. dr. J. Morlier	ISAE-SUPAERO, France
Prof. dr. ir. M. Voskuijl	Nederlandse Defensie Academie
Dr. H. W. Jentink	Koninklijk Nederlands Lucht- en Ruimtevaartcentrum
Prof. dr. A. Gangoli Rao	Delft University of Technology, *reserve member*

Keywords:	Sub-Scale Flight Testing, Degree of Similitude, Flight Dynamics, SFT model design
Printed by:	Proefschriftmaken
Cover Page:	Designed by Spoorti Ramesh Sadarjoshi and Akshay Raju Kulkarni

An electronic version of this dissertation is available at
`http://repository.tudelft.nl/`.

पुराणमित्येव न साधु सर्वं न चापि काव्यं नवमित्यवद्यम् ।
सन्तः परीक्ष्यान्यतरद्भजन्ते मूढः परप्रत्ययनेयबुद्धिः ॥

Every idea(scripture) is not good simply because it is old or scriptures say so;
nor should the idea be condemned simply because it is new.
The wise resort to the old or new ideas after (proper) examination;
the ordinary are led by the opinions of others.

-*Kālidāsa*
(Excerpt from the book Malvika-Agnimitra)

SUMMARY

By 2050, the aviation industry is expected to grow by 250-300% of its current air traf-
fic. If left unchecked, the corresponding increase in atmospheric and noise pollution
will have a catastrophic impact on the environment. Thus, improvements in aircraft
design are urgently needed for a sustainable growth of the aviation industry. The per-
formance and behaviour of existing tube-and-wing aircraft have been refined and im-
proved so much in the past decades that further improvements are barely possible. Con-
sequently, by 2050, breakthrough solutions in the form of unconventional design con-
figurations, novel propulsion systems and operation models are required to meet the
ambitious goals stated in Europe's vision for Aviation.

However, the design of unconventional aircraft is particularly challenging as it of-
ten involves integrated multi-functional components for which legacy data is unavail-
able. Thus, appropriate means to assess their performance and behaviour are needed to
lower their industrial development risk. Sub-scale Flight Testing (SFT), an experimental
approach involving the free-flight testing of sub-scale models with an on-board power-
plant, shows promise in the evaluation of the in-flight motion of a given aircraft configu-
ration and its response to control inputs. In the past, SFT has been used in a wide-range
of flight tests to study the effect of novel technologies on the aircraft flight behavior, to
assess systems integration feasibility and as a proof-of concept for unconventional de-
signs.

The actual benefit and validity of SFT mainly depends on the design of the SFT model
used for the test. A well designed SFT model can show a similar behaviour to the full-
scale aircraft such that any observation on the scaled device can be directly used to pre-
dict the full-scale performance. However, ensuring similarity between SFT model and
full-scale aircraft is challenging due to the differences in their size and flight conditions.
In addition to guaranteeing similitude, SFT model must comply with multidisciplinary
design requirements such as safe completion of the mission, adhering to restrictions im-
posed by local authorities and selecting suitable flight-control and measurement equip-
ment.

Three main methodologies to design a SFT model, namely, classical similitude the-
ory (1950), similitude theory based on governing equations (1964) and computational
scaling (1989) can be found in the literature. The classical similitude theory, based on
dimensional analysis, is the most widely used methodology for SFT model design. How-
ever, this theory adopts a simplistic scaling approach that leads to significant compro-
mises in the similitude between the SFT model and full-scale aircraft. Furthermore, it
does not offer the possibility to include the aforementioned multidisciplinary require-
ments. The similitude theory based on governing equations requires rigorous mathe-
matical analysis and can only be applied to a limited number of cases.

The computational scaling approach is the state of the art methodology to design
SFT models. This approach uses computational methods iteratively, generally in an Mul-

tidisciplinary Analysis and Optimization (MDAO) framework, to maximize the similarity between the SFT model and full-scale aircraft while accounting for all the necessary requirements. Although, the computational scaling methodology proposed in the literature shows promise in designing SFT models for diverse test objectives, it has not attained sufficient methodological and technological maturity necessary to improve the quality of SFT.

Engineers have to expend significant time and resources to formalize and execute their computational scaling problem. Furthermore, the benefits and limitations of computational scaling approach over other SFT model design methodologies have not been quantified in the literature yet. Thus, to address these three main gaps in the literature, namely, (i) the lack of formalized MDAO based computational scaling methodology, (ii) high computational complexity and cost and (iii) the assessment of computational scaling with respect to geometric scaling, the following research question is formulated:

To what extent can the value and applicability of SFT be improved by using the MDAO based computational scaling approach in the SFT model design process?

Thus, the objective of this dissertation was to identify and develop an MDAO based computational scaling approach that is applicable to a wide-range of SFT objectives and supports engineers in quickly formalizing their SFT model design problem.

To achieve this objective, the **MDAO based similarity maximization methodology** is developed in this research work to extend the computational scaling approach. A novel figure of merit that quantifies the extent of similitude between the SFT model and the full-scale aircraft called the **Degree of Similitude (DoS)** is proposed in this work (where, DoS = 1 implies complete similitude and DoS < 1 implies differences in model and full-scale aircraft behaviour) which can be used as an objective function to maximize the similitude of the SFT model and the full-scale aircraft. This is a generalized figure of merit applicable to a wide range of SFT design problems.

After complete MDAO, if DoS = 1 cannot be achieved, a methodology to assess the applicability of the optimal similitude SFT model (with DoS < 1) for a given SFT objective has been formulated in this dissertation using the figures of merit **Behavioural Indicator Matrix (BIM)** and **Allowable Scaling Error (ASE)**. These synthetic measures aid designers in determining whether meaningful results can be gathered from SFT for a given model design. The development of such a methodology also allows the comparison of the similarity of scaled model produced using simple geometric scaling approach with computationally-scaled design, thereby addressing the aforementioned challenge (i.e., is a computationally-scaled model better than a geometrically-scaled one?).

In order to implement and demonstrate this methodological approach, two main technological developments were made as follows:

- **Scaled Model Design and Engineering Engine (SMDEE)** is a computational framework, that automates the modelling and multi-disciplinary analyses tasks in MDAO based computational scaling approach proposed above. At the core SMDEE lies a Knowledge Based Engineering tool called the Multi-Model Generator that supports designers in quickly and automatically generating the SFT model geometry, aspect models and weight & balance data. SMDEE is a configuration agnostic

framework and can be used to design SFT models to assess the behaviour of any unconventional aircraft.

- **Parallel Execution Environment** speeds up the SMDEE execution by distributing complex and time-consuming computational analyses over different computers that are free and available on the local network. The benchmark studies performed in this dissertation show that the parallel execution environment speeds up the execution time of one complete MDAO with 500 design iterations from 12 weeks to 1 week. Thus, the parallel execution environment is a key enabler of computational scaling by making it viable in the limited time available for SFT model design.

These methodological and technological developments are used to formulate and execute seven different case studies of incremental complexity for both conventional and unconventional aircraft design (ranging from 4 disciplines & 25 design variables to 8 disciplines & 46 design variables). For every study, the computationally-scaled SFT model consistently showed better similitude (i.e., DoS) to full-scale aircraft as compared to geometrically-scaled model. Furthermore, the computationally-scaled model matched better with full-scale aircraft Behavioural Indicator Matrix as compared to geometrically-scaled models. This shows that the DoS is a suitable figure of merit to quantify the extent of similitude and can be used in future computational scaling problems.

Based on the initial studies with the computational scaling approach, it is clear that one SFT model may not be sufficient to predict the complete flight behavior of a full-scale aircraft but a catalog of tailored sub-scale models is necessary. Recommendations are provided to extend the proposed MDAO based computational scaling approach to develop such a catalog of SFT models.

SAMENVATTING

Tegen 2050 zal de luchtvaartindustrie naar verwachting gegroeid zijn met 250-300% ten opzichte van het huidige luchtverkeer. Indien hier niets aan wordt gedaan, zal de overeenkomstige toename in luchtvervuiling en geluidsoverlast een catastrofale impact hebben op het milieu. Voor een duurzame groei van de luchtvaartindustrie zijn er daarom dringend verbeteringen in het vliegtuigontwerp nodig. De prestaties en eigenschappen van bestaande conventionele "tube-and-wing" vliegtuigen zijn in de afgelopen decennia zo verfijnd en verbeterd dat verdere verbeteringen nauwelijks nog mogelijk zijn. Als gevolg hiervan zijn er tegen 2050 baanbrekende oplossingen in de vorm van onconventionele ontwerpconfiguraties, een nieuw voortstuwingssysteem en een nieuw luchtvaartope- ratie model nodig om de ambitieuze doelen te bereiken die zijn vastgelegd in de Europese visie op de luchtvaart.

Het ontwerp van onconventionele vliegtuigen is echter bijzonder uitdagend, omdat het vaak om geïntegreerde multifunctionele componenten gaat waarvoor geen bestaande data beschikbaar is. Er zijn daarom methoden nodig die de prestaties en eigenschappen bepalen van onconventionele vliegtuigen en daarmee hun industriële ontwikkelingsrisico's verminderen. Testvluchten met schaalmodellen, ook wel "Sub-scale Flight Testing" (SFT) genoemd, is een experimentele benadering waarbij dergelijke "SFT-modellen" met een voortstuwingssysteem aan boord worden getest. SFT is veelbelovend in de evaluatie van de beweging van een gegeven vliegtuigconfiguratie tijdens de vlucht en diens reactie op besturingssignalen. In het verleden is SFT gebruikt voor een breed scala aan testvluchten om het effect van nieuwe technologieën op de vliegeigenschappen van vliegtuigen te bestuderen, de haalbaarheid van systeemintegratie te beoordelen en als concept-validatie model voor onconventionele ontwerpen.

Het daadwerkelijke voordeel en de validiteit van SFT hangt voornamelijk af van het ontwerp van het SFT-model dat voor de test wordt gebruikt. Een goed ontworpen SFT-model kan soortgelijke eigenschappen hebben als het vliegtuig op ware grootte, zodat elke observatie op het SFT-model direct kan worden gebruikt om de prestaties op de volledige schaal te voorspellen. Het is echter moeilijk om de gelijkenis tussen het SFT-model en het volledige vliegtuig te garanderen, gezien de verschillen in grootte en vliegcondities. Naast het garanderen van de gelijkenis moet het SFT-model ook voldoen aan multidisciplinaire ontwerpvereisten zoals het veilig voltooien van de missie, het naleven van de regels opgelegd door de lokale autoriteiten en het selecteren van de juiste vluchtbesturings- en meetapparatuur.

In de literatuur zijn drie hoofdmethodologieën te vinden om een SFT-model te ontwerpen, namelijk de klassieke gelijkheidstheorie (1950), de gelijkheidstheorie gebaseerd op fundamentele vergelijkingen (1964) en het rekenkundige schalen (1989). De klassieke gelijkheidstheorie, gebaseerd op dimensionale analyse, is de meest gebruikte methode voor het ontwerpen van SFT-modellen. Deze theorie hanteert echter een simplis- tische schalingsmethode die leidt tot aanzienlijke afwijkingen in de gelijkenisgraad tussen

het SFT-model en het vliegtuig op ware grootte. Bovendien biedt het niet de moge- lijkheid om bovengenoemde multidisciplinaire eisen mee te nemen. De gelijkheidstheorie gebaseerd op fundamentele vergelijkingen vereist een rigoureuze wiskundige analyse en kan slechts op een beperkt aantal gevallen worden toegepast.

Rekenkundige schaling is de meest recente aanpak voor het ontwerpen van SFT-modellen. Deze methode gebruikt iteratieve rekenkundige methoden, meestal in een Multidisciplinair Analyse en Optimalisatie (MDAO) kader, om de gelijkenis tussen het SFT-model en het volledige vliegtuig te maximaliseren, waarbij er rekening wordt gehouden met alle noodzakelijke vereisten. Hoewel de in de literatuur voorgestelde rekenkundige schalingsmethode veelbelovend lijkt bij het ontwerpen van SFT-modellen voor verschillende testdoelen, heeft het nog niet het vereiste methodologische en technologische niveau bereikt dat nodig is om de kwaliteit van SFT te verbeteren.

Ingenieurs moeten veel tijd en middelen steken in het formaliseren en uitvoeren van hun rekenkundig schalingsprobleem. Bovendien zijn de voordelen en nadelen van de rekenkundige schalingsmethode ten opzichte van andere SFT-ontwerp methoden nog niet gekwantificeerd in de literatuur. Om deze drie belangrijkste gaten in de literatuur aan te pakken, namelijk (i) het ontbreken van een geformaliseerde op MDAO gebaseerde rekenkundige schalingsmethode, (ii) de hoge eisen aan rekenkracht en infrastructuur en de bijhorende kosten en (iii) de beoordeling van rekenkundige schaling ten opzichte van geometrische schaling, is de volgende onderzoeksvraag geformuleerd:

In hoeverre kan de waarde en de toepasbaarheid van SFT worden verbeterd door het gebruik van een op MDAO gebaseerde rekenkundige schalingsmethode in het ontwerpproces van SFT-modellen?

Derhalve was het doel van dit proefschrift het identificeren en ontwikkelen van een op MDAO gebaseerde rekenkundige schalingsmethode die van toepassing is op een breed scala aan SFT-doelstellingen en die ingenieurs ondersteunt bij het snel formaliseren van hun SFT-model ontwerpprobleem. Om dit doel te bereiken is in dit onderzoek de op MDAO gebaseerde methodologie voor maximale gelijkenisgraad ontwikkeld om de rekenkundige schalingsmethode uit te breiden. Een nieuw prestatiegetal dat de mate van overeenkomst tussen het SFT-model en het vliegtuig op ware grootte kwantificeert, wordt voorgesteld in dit werk. Dit prestatiegetal, dat **"Degree of Similitude" (DoS)** wordt genoemd (waarbij DoS = 1 een volledige gelijkenis aangeeft en DoS < 1 wijst op verschillen in het gedrag van het model en het vliegtuig op ware grootte), kan worden gebruikt als een doelfunctie om de gelijkenis van het SFT-model en het vliegtuig op ware grootte te maximaliseren. Dit is een algemeen prestatiegetal dat toepasbaar is op een groot aantal SFT-ontwerpproblemen. Na volledige MDAO, indien DoS = 1 niet kan worden bereikt, is een methode geformuleerd in dit proefschrift om de toepasbaarheid van het SFT-model met optimale overeenkomst (met DoS < 1) te bepalen voor een gegeven SFT-doelstelling met behulp van de parameters **"Behavioural Indicator Matrix" (BIM)** en **"Allowable Scaling Error" (ASE)**. Deze prestatiegetallen helpen ontwerpers te bepalen of SFT betekenisvolle resultaten kan opleveren voor een bepaald modelontwerp. De ontwikkeling van een dergelijke methode laat ook toe de gelijkenis van eenvoudig geometrisch geschaald model te vergelijken met een model dat gemaakt is door een rekenkundig geschaald ontwerp, waarbij de bovengenoemde vraag wordt aangepakt (d.w.z.,

is een rekenkundig geschaald model beter dan een geometrisch geschaald model?). Om deze methodologische aanpak te implementeren en te demonstreren, zijn de volgende twee technologische ontwikkelingen gerealiseerd:

1. De **"Scaled Model Design and Engineering Engine" (SMDEE)** is een rekenkundig kader dat de modellering en multidisciplinaire analysetaken automatiseert in de op MDAO gebaseerde rekenkundige schalingsmethode die hierboven is voorgesteld. De kern van SMDEE is een "Knowledge Based Engineering" programma, de "Multi-Model Generator" genaamd, dat ontwerpers ondersteunt bij het snel en automatisch genereren van de SFT-model geometrie, abstracties en gewichts- en balansgegevens. De SMDEE is onafhankelijk van de configuratie en kan gebruikt worden om SFT-modellen te ontwerpen om zo de vliegeigenschappen vast te stellen van een willekeurig onconventioneel vliegtuig.

2. De **"Parallel Execution Environment"** versnelt de uitvoering van de SMDEE door de complexe en tijdrovende rekenkundige analyses te verdelen over verschillende computers die vrij en beschikbaar zijn op het lokale netwerk. De referentiestudies in dit proefschrift tonen aan dat de Parallel Execution Environment de uitvoering van één complete MDAO met 500 ontwerp iteraties inkort van 12 weken tot 1 week.

Deze methodologische en technologische ontwikkelingen worden gebruikt om zeven verschillende casussen van toenemende complexiteit te formuleren en uit te voeren voor zowel conventionele en onconventionele vliegtuigontwerpen (variërend van 4 disciplines 25 ontwerpvariabelen tot 8 disciplines 46 ontwerpvariabelen). Voor elke casus leidde het rekenkundig geschaalde SFT-model consistent tot een betere gelijkenis (d.w.z. DoS) met het vliegtuig op ware grootte, in vergelijking met het geometrisch geschaalde model. Bovendien kwam het rekenkundig geschaalde model beter overeen met de Behavioural Indicator Matrix van het vliegtuig op ware grootte dan de geometrisch geschaalde modellen. Hieruit blijkt dat de DoS een geschikt prestatiegetal is om de mate van gelijkenis te berekenen en dat dit kan worden gebruikt bij toekomstige rekenkundige schaalproblemen.

Op basis van de eerste studies met de rekenkundige schalingsmethode is het duidelijk dat één SFT-model wellicht niet voldoende is om alle vliegeigenschappen van een vliegtuig op ware grootte te voorspellen, maar dat een reeks van op maat gemaakte SFT-modellen noodzakelijk is. Er worden aanbevelingen gedaan om de voorgestelde op MDAO gebaseerde rekenkundige schalingsmethode uit te breiden zodat een catalogus van SFT-modellen kan worden ontwikkeld.

CONTENTS

LIST OF ABBREVIATIONS

AAM	-	Advanced Air Mobility
ASE	-	Allowable Scaling Error
ATAG	-	Air Transport Action Group
BI	-	Behavioural Indicator
BIM	-	Behavioural Indicator Matrix
CG	-	Center of Gravity
CM	-	Capability Module
COTS	-	Commercial Off the Shelf
CST	-	Class Shape Transformation
DEE	-	Design Engineering Engine
DNW	-	German-Dutch Wind-tunnel
DoS	-	Degree of Similitude
HLP	-	High Level Primitives
HQ	-	Handling Quality
KBE	-	Knowledge Based Engineering
MDAO	-	Multidisciplinary Analysis and Optimization
MMG	-	Multi-Model Generator
OML	-	Outer Mold Line
PHALANX	-	Performance, HAndling qualities and Loads ANalysis toolboX
S & C	-	Stability and Control
SFT	-	Sub-scale Flight Testing
SI	-	Sensitivity Index
SMDEE	-	Scaled Model Design and Engineering Engine
SMI	-	Scaled Model Initiator
TRL	-	Technology Readiness Level
VGM	-	Variable Geometry Model
WT	-	Wind-Tunnel Testing
W & B	-	Weight and Balance
UML	-	Unified Modelling Language
xDSM	-	eXtended Design Structure Matrix

1

INTRODUCTION

In this chapter, we take a bird's eye view of the aviation industry, its importance to the growth of human civilization and the risks posed by rapid growth of aerospace sector to the environment. To tackle the global environmental concerns, aviation industry must incorporate novel technologies and unconventional aircraft designs in commercial operations which poses two main challenges. First, the prediction of in-flight behaviour of unconventional configurations without experimental or legacy data is challenging . Second, radical changes to design are often prone to distrust from the stake holders such as airlines and certification authorities which must be addressed before introducing a design into commercial operation. Preliminary studies indicate that Sub-scale Flight Testing (SFT), a testing method that is rapidly gaining scientific interest, could be effective in tackling both these problems. Nevertheless, the reliability of SFT is largely affected by the methodologies used for designing the SFT models, which requires further investigation and advancement. To this end, we formulate a set of research questions aimed at extending SFT design methods beyond the state of the art and propose a research framework to answer them.

1

1.1. AVIATION IN 2020: A BIRD'S-EYE VIEW

Air transport is a major contributor to global economic prosperity. Aviation provides the only rapid worldwide transportation network, which makes it essential for global business and tourism. Air transport facilitates world trade. It helps countries contribute to the global economy by increasing access to international markets and allowing the globalisation of production. The increased accessibility plays a vital role in facilitating economic growth, particularly in developing countries. Aviation's global economic impact (direct, indirect, induced and tourism catalytic) was estimated at \$3.5 trillion, equivalent to 4.1% of world gross domestic product (GDP) [1].

The number of passengers using air-travel has increased by 300% since the beginning of 21st century [2]. Not only have the number of passengers increased, the distance they travel has also grown. The number of passenger-kilometers [1] has doubled from 4 trillion km in 2010 to nearly 8 trillion km in 2020 [3, 4]. The growth in airline passengers has also seen a corresponding increase in the number of flights [5–8]. As per ATAG report, 2019 saw 46.8 million commercial flights worldwide [1]. With the number of flights, the safety of passengers flying has also increased. As per ICAO's security report [9], the number of accidents has reduced from 94 in 2010 to 53 in 2019. The corresponding fatalities per billion passengers has gone down from 300 in 2010 to 50 in 2019.
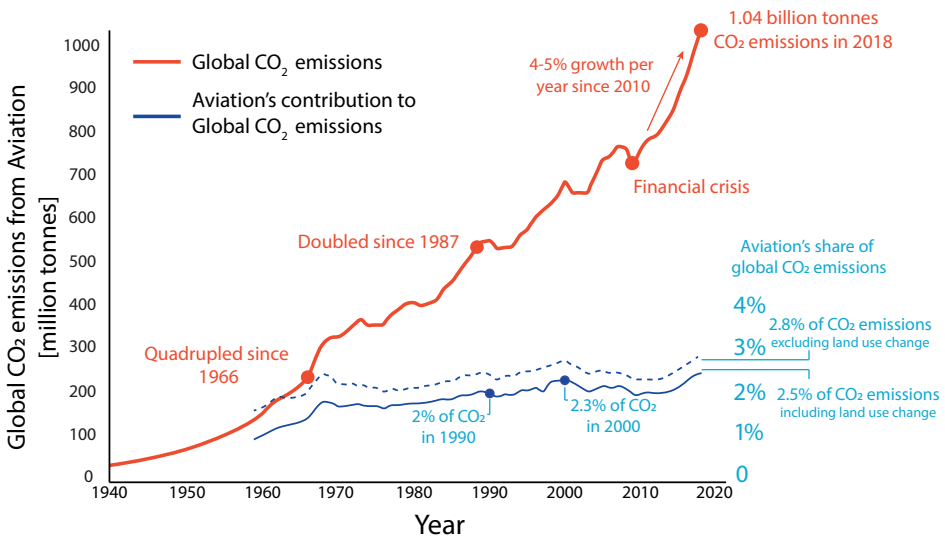
Figure 1.1: Graph of variation aircraft CO2 emissions from aviation industry over the years with an overview of its proportions compared to worldwide CO_2 emissions
Source: Lee et al. [10] © Hannah Ritchie under CC BY-SA 3.0

This massive air-transport machinery is kept in safe operation by 87 million workers and 33000 aircraft flying world-wide [1]. Such a massive infrastructure leaves a significant imprint on the environment. In 2019, over 350 billion litres of aviation fuel was

---

[1]passenger kilometers = number of passengers x the number of kilometers travelled per passenger

consumed. Combustion of such large quantities of fuel releases atmospheric pollutants such as CO_2, NO_x and SO_x in the atmosphere [1]. As per calculations by Lee et al. [10], 1.04 billion tonnes of CO_2 was produced by aviation industry worldwide. To put things in perspective, this is 2.5% of the global human induced CO_2 emissions (Figure 1.1) and 12% of CO_2 emissions from all transport sources.

As of 2020, the economic and social benefits of aviation are clear, with the growth of the aviation sector being important for all countries, developed and developing. However, these benefits also come with an environmental cost. For aviation to grow sustainably, it is vital that the industry balances the growth in air travel with the associated adverse climate and environmental effects. The global aviation sector is aware of this responsibility and has started taking concrete actions in the direction of sustainable aviation [4, 11].
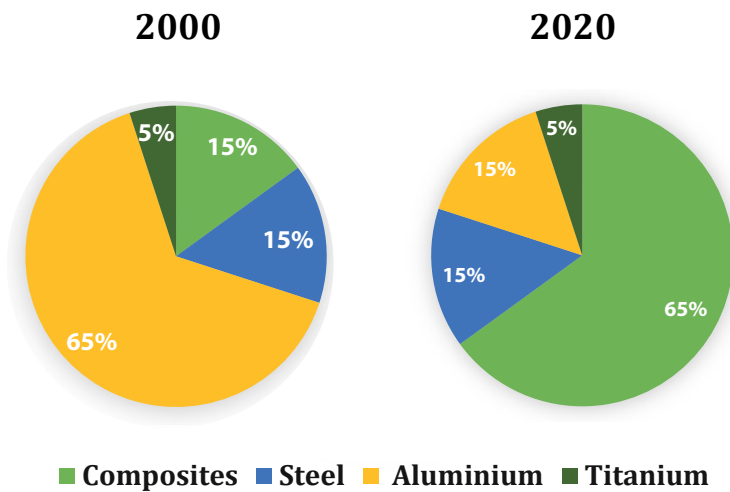
Figure 1.2: Evolution of material composition of aircraft in the last decade showing how airline manufacturers have moved from aluminium dominated designs to composite material dominated designs
Source: Air Travel – Greener by Design[12]

To this end, aircraft industry is improving the performance of its sub-systems such as the engines, the heating, ventilation and air-conditioning systems etc. For example, ceramic matrix composites allow the engines to operate at a higher temperature, resulting in better fuel efficiency [12]. Furthermore, manufacturers are increasingly using lightweight materials such as carbon fibre composites to build aircraft components, particularly the wings, which improves fuel efficiency through decreasing weight and enabling advanced aerodynamics. The Boeing 787 and 777X, Airbus A220 and A350XWB aircraft use these cutting-edge materials and technologies to deliver exceptional gains in environmental performance. Figure 1.2 shows how the material composition of aircraft has evolved in the last decade.

In addition to improving the design of the aircraft, airline operators are increasingly

1

reducing their carbon footprint by using sustainable aviation fuels. In 2019, 40 million litres of sustainable aviation fuel was used by commercial flights [13]. This was blended with traditional fuel in over 65,455 flights from five international airports (Los Angeles, San Francisco, Bergen, Oslo and Stockholm) [13]. The current sustainable fuels used by the aviation industry accounts for about 1% of the fuel used in aviation globally.

The combined effect of design improvements and the use of sustainable fuels is the reduction of global fuel consumption. As per a report by International Council on Clean Transportation, in the last decade, the aviation sector has an average yearly reduction of 1.5% in fuel consumption per tonne-km (see Figure 1.3).
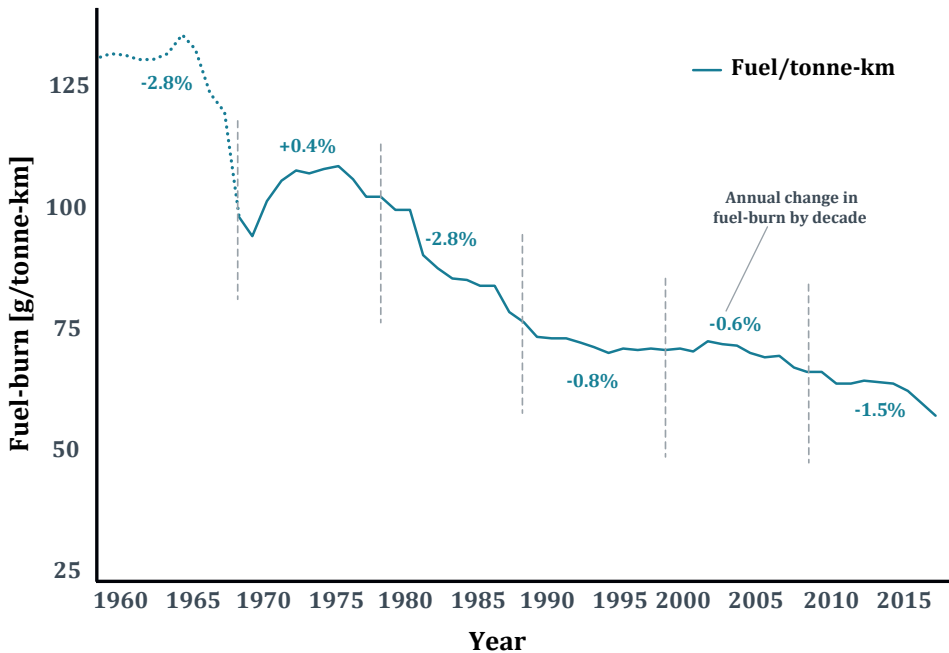
Figure 1.3: Improvements of up to 50% in fuel-burn efficiency in the last fifty years (1970-2020) © International Council on Clean Transportation under CC BY-SA 3.0

Furthermore, aviation industry is reducing its carbon footprint by using carbon offset when reducing one's own emissions becomes unfeasible. It is a way to compensate for CO_2 being produced in one sector, by helping to fund a project which reduces CO2 emissions in another sector. These offsets can be generated by a range of different programs around the world, in renewable energy, forestry protection or reforestation. These developments have led to a reduction in carbon footprint and fuel consumption per tonne-km of flight. All these measures have helped reduce the carbon footprint of the aviation industry.

In the last two decades, the aircraft noise emissions have reduced too. From 2000 to 2019, noise exposures due to aviation sector reduced by 50% while enplanements rose 37% in United States of America [14]. In Europe, the average noise around airports is

still close to 2005 levels despite growth in traffic[11, 15]. This has been made possible by the implementation of new operating restrictions (*Balanced Approach Regulation (EU) 598/2014*) which limit or reduce the operational capacity of an airport if the noise regulations are not complied with. It also includes the banning of operations by so-called 'marginally compliant' aircraft [2].
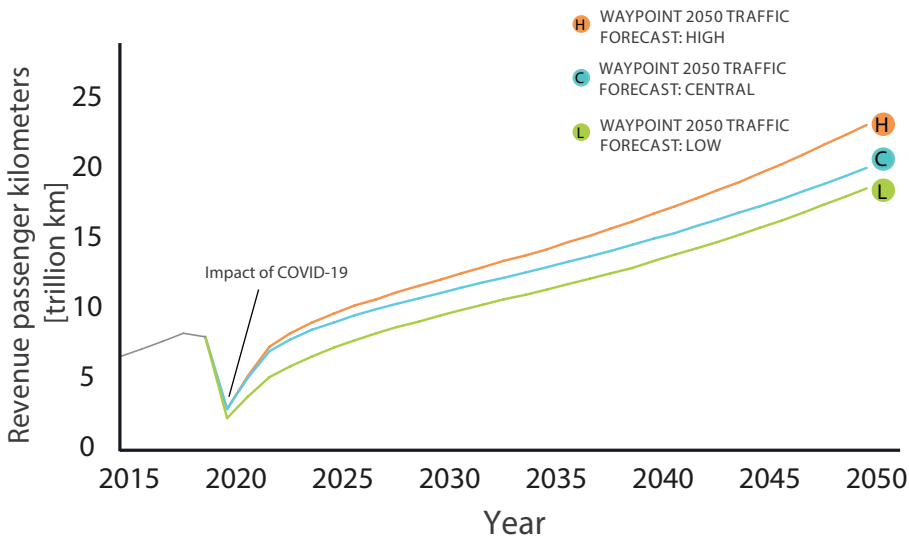
Figure 1.4: Projected growth in he Aviation industry for three different traffic growth rates including the dip experienced due to COVID-19 pandemic [4]
© Air Transport Action Group under CC BY-SA 3.0

The efforts of the aviation sector in the reduction of aircraft fuel consumption and the consequent alleviation of the impact of carbon footprint and noise emission are commendable. Nevertheless, these improvements are not commensurate with the expected growth in traffic. Air Transport Action Group's (ATAG) Waypoint 2050 [4] performed a study to estimate air traffic until 2050 taking into account the impact of COVID-19 (Figure 1.4). This graph shows that the (forecasted) growth of aviation industry is 250-300%. However, the associated reduction in any category of emissions is projected at less than 50% [4].

Thus, the current efforts in reducing the environmental impact is insufficient to support sustainable air-transportation of the future. This can be attributed to two main reasons. First, the aviation industry is heavily dependent on conventional tube-and-wing aircraft of varying specifications (Figure 1.5) whose performance and behaviour have been refined and improved so much in the past decades that further improvements are barely possible. The improvements observed and forecasted are largely due to developments at sub-system level and ground-operating procedures. Second, the expectations from aviation industry are changing. This means that the operations, the flight times and

---

[2]the compliance requirements are defined using the noise certification limits specified in ICAO Annex 16, Volume I, Chapter 3

1

the comfort of the passengers must be improved which comes at a cost, namely, increase in the per-capita carbon footprint of an airline. In the following section, we look at how aerospace industry should look like in 2050 and what steps must be taken to sustainably improve the aviation industry to meet the expectations of various stake holders.
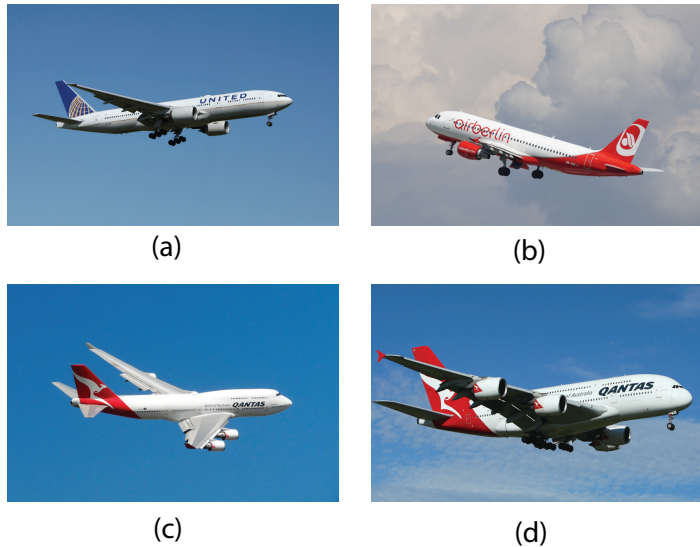
Figure 1.5: Examples of conventional tube-and-wing aircraft used commercially (a) Boeing 777-222(ER) - maximum take off weight of 299 tonne & range of 15.840 km (b) Airbus A320-214 - maximum take off weight of 93.5 tonne & range of 6.940 km (c) Boeing 747-438ER - maximum take off weight of 397 tonne & range of 13.490 km (d) Airbus A380-842 - maximum take off weight of 575 tonne & range of 15.700 km
Credits: ©Pixabay from Pexels, ©Renet Pascual from Pexels and ©Raf Jabri from Pexels under CC0 1.0

1.2. AVIATION IN 2050: LOOKING BEYOND THE HORIZON

In 2050, the passenger experience will be integrated, seamless, energy-efficient, diffused inter-modal system taking travellers and their baggage from door to door, safely, affordably and quickly [4]. Technology and procedures in use in the year 2050 will allow a 75% reduction in CO2 emissions per passenger kilometre and a 90% reduction in nitrogen oxide (NO_x) emissions. Furthermore, the perceived noise emission of flying aircraft will be reduced by 65% as compared to the capabilities of an aircraft in 2000.

Several potential pathways to reach these goals by 2050 have been identified by Waypoint 2050 [4]. Each scenario considers varying degree of improvements in four main areas, namely, improved aircraft technology (i.e., use of unconventional aircraft designs as shown in Figure 1.6), improvements in operations in aviation industry, effective deployment of sustainable aviation fuels (i.e., reduction in crude-oil dependence) and offsetting/investing in out-of-sector carbon reduction measures.
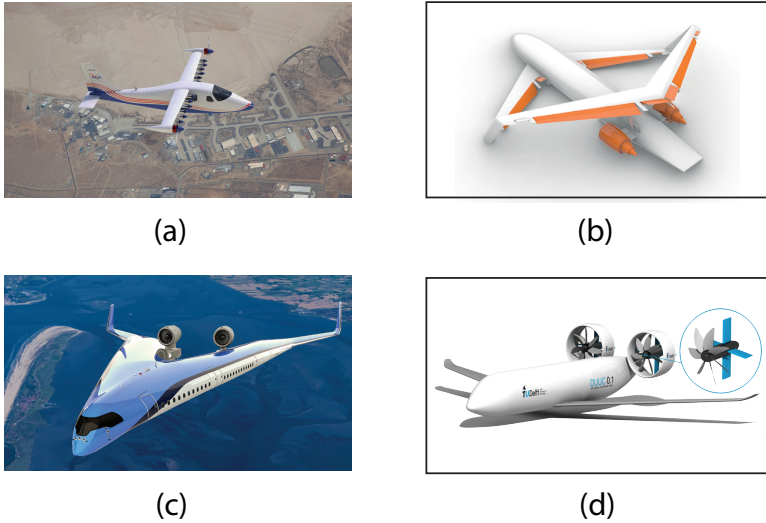
Figure 1.6: Artist's concept image showing (a)NASA's first all-electric X-plane, the X-57 Maxwell, (b) Box-wing aircraft, (c) V-shaped blended-wing body, the Flying-V, (d) Delft University Unconventional Concept (DUUC). These example configurations include technology and design modifications that could help in meeting the aviation industry's goals of 2050
Credits: (a) NASA Langley/Advanced Concepts Lab, AMA, Inc., (b) TU Delft, (c) TU Delft / Edwin Wallet, (d) TU Delft / Nando van Arnhem

Of the reductions expected in 2050, effective deployment of sustainable aviation fuel is expected to contribute 50-75% of the reductions. The improvements in operations in expected to be under 10%. And the improvements in aircraft technology is expected to contribute between 15-45% of the reduction in CO_2 emissions. The short-comings of the target will be covered with offsetting. Figure 1.7 shows the scenario where the industry pushes for improvements in all the areas with the least dependence on carbon offsetting.

The deployment of sustainable aviation fuel and operational improvements are logistical challenges. However, in aircraft technology, in addition to overcoming logistical challenges, significant scientific breakthroughs are necessary to demonstrate tangible improvements. This in turn requires improved understanding and investigation of processes and phenomena occurring in flight.

A broad range of technologies can contribute to aircraft fuel efficiency improvement and emissions reduction. These developments can be attributed to improvements in aerodynamics, use of lightweight materials and structures, equipment and systems, adoption of radical aircraft configurations, effective use of energy management and electrification and advancement in combustor technologies.

ATAG in their report 'Waypoint 2050' [4], show a number of technology improvement scenarios which can help reduce CO_2 by 2050. In order to have a significant impact on CO_2 emission reduction, unconventional aircraft designs powered by sustainable aviation fuel or electric propulsion must enter into service by 2050 (see T_4 in Figure 1.8) [4].
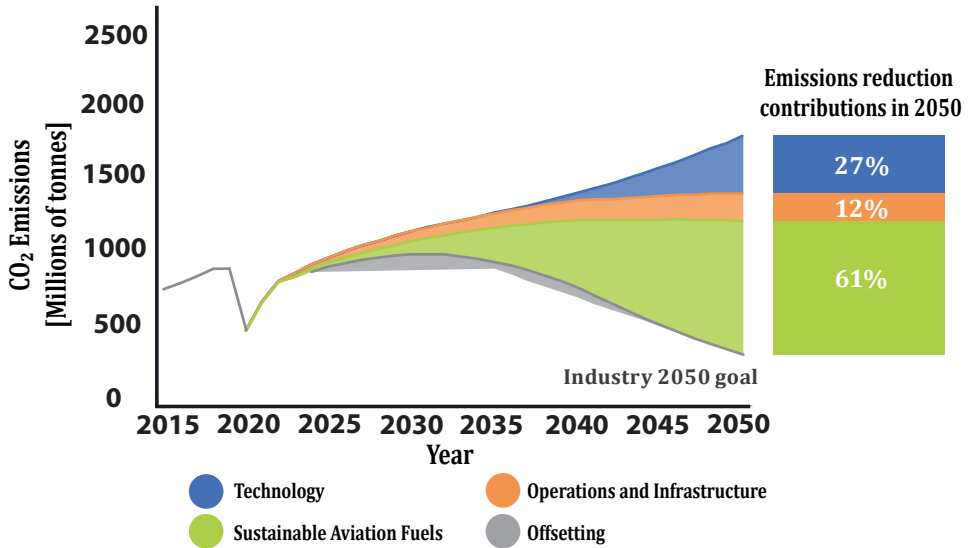
Figure 1.7: Projected CO_2 reduction from different sources of improvements as outlined by ATAG [4]

© ATAG as published in WAYPOINT 2050

Researchers and designers in the aviation industry understand this challenge and are working towards the development of both unconventional designs and radical technologies such as those addressed in Figure 1.6 [16–22]. However, the path from conceptual design to the entry into service involves a number of barriers, where, engineers have to accurately assess the in-flight behaviour and performance of their designs without the support of legacy (experimental) data. In the following sections, the challenges of introducing unconventional designs into service and potential solutions are discussed.

1.3. ENHANCING CONFIDENCE ON CONCEPTUAL DESIGN

The seriousness of the efforts in the improvement of aircraft technology can be observed from the fact that over 250 aircraft concepts are under development/investigation today [4]. Of these, over 30 are intended for commercial scale operations. Currently, most of these developments are based on "paper" designs with Technology Readiness Level (TRL) under 5.

Past experiences show that many (conventional) "paper" designs, when manufactured at full-scale and flight-tested, demonstrated deficiencies in their flight behavior such as stability and control (S&C) characteristics and handling qualities that resulted in expensive rework, which in turn adversely affected the overall performance of the aircraft [23, 24]. Examples of such deficiencies include, stall break due to raked wing tips in Boeing 767-400, wing drop/roll-off due to propeller-induced effects in Lockheed Martin C-130J, missed predictions concerning aft loading on the main wing and effectiveness of the horizontal tail in flight with the Boeing 777, etc. [24]. Worryingly, most of these
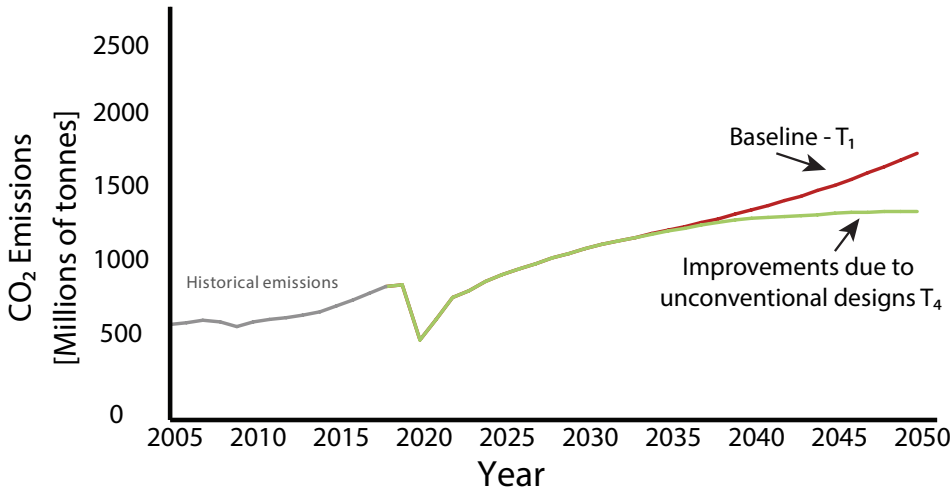
Figure 1.8: Projected reduction in CO_2 with increased efforts in improving aircraft technology [4] © ATAG as published in WAYPOINT 2050

configurations that needed re-design were derivatives of pre-existing aircraft, let alone the risk-laden unconventional designs (i.e., not the tube-and-wing aircraft with 2 or 4 turboprop/turbofan engines) that are the need of the future.

Concretely, the aviation industry must develop new certification procedures to ensure the undisputed safety level required for commercial aviation. For example, with blended-wing body where the distinction between the fuselage, wing and tails are blurred, the rules that were applicable to the conventional tube-and-wing aircraft no longer hold good. In addition to formulating concrete rules for certification, aviation industry will also have to develop appropriate processes to introduce the unconventional designs to various stake holders such as the passengers, investors and the airlines to attract investments and to create trust.

Sustained effort and investment of time and resources is essential to support aviation industry to transition to unconventional configurations. The first step in this endeavour is to develop the ability to accurately analyze the aircraft flight-behavior in the early stages of design process to kick-start the certification process and to address fundamental issues on flight mechanical behaviour of a given aircraft design to prevent costly rework before production of the aircraft. Furthermore, the results of such analysis can be used to demonstrate the value of the proposed designs to various stake holders.

Many virtual (computer-based) and (sub-scale) physical tests are normally used during the design process to assess the model behaviour. Nonetheless, the only way to fully ascertain the behaviour of an aircraft is through full-scale flight testing [25]. However, the cost of manufacturing a prototype (*the physical system for which the predictions are to be made* i.e., a full-scale aircraft) is estimated to be in the order of 300-800% of the market price of an aircraft currently in operation [26, 27], which makes full-scale flight testing in the initial stages of aircraft design process economically unviable.

1

An alternative to using prototype in flight testing in early design stages is to use sub-scale models in flight testing. A well designed sub-scale model can show a similar behaviour to the full-scale prototype such that any observation on the scaled device can be directly used to predict the performance of the prototype. When sub-scale models are used as part of free-flight testing (i.e., experiments carried out in open atmosphere with all the measurement apparatus inside the model devoid of any external constraints such as tethers) and the models complete the test mission with an on-board power-plant without a man on-board, the testing method is known as powered free-flight testing [28–30]. In most literature as well as in this dissertation, powered-model free-flight testing is called Sub-scale Flight Testing (SFT).

These smaller models can be quickly manufactured at a fraction of the cost of the prototype and the associated risk of performing experiments with such models is much lower than the full-scale aircraft. Although, the cost of a SFT model depends on the size of the model and the equipment used for the test, elaborate SFTs can be performed at 0.1% of the cost of a full-scale aircraft[3].

SFT can be used for demonstration, phenomenological testing and simulation of the full-scale aircraft behaviour. SFT provides a research environment for the study of phenomena involving large range of motions (e.g., pitch, roll, yaw, etc.) that can add to the current numerical analysis and wind-tunnel testing capabilities. The inherent potential of SFT to predict the in-flight behaviour of aircraft designs of the future makes SFT an attractive testing method to the designers. Furthermore, these free-flying models are powerful demonstration tools that can be used effectively to enhance the confidence of various stakeholders. Thus, the effective use of SFT will allow designers to analyze their designs quickly, accurately and affordably, which will in turn accelerate the introduction of unconventional aircraft designs that have lower (adverse) impact on the environment. This forms the key motivation for this dissertation.

1.4. Sub-scale Flight Testing: Growth & Challenges

1.4.1. Current Trends in SFT

The literature reviewed for this dissertation indicates that SFT has been used in a wide-range of flight tests to study aircraft flight behaviour (i.e., static & dynamic stability, control characteristics and handling qualities), effect of novel technologies on flight behavior, effect of power-plant on landing and take-off distance, systems integration feasibility and as a proof-of concept for unconventional designs. Thus, SFT is primarily used to assess the flight motion of a given aircraft configuration and its response to control inputs. The flight motion includes both the motion of the center of gravity and the motion of different components such as flexible wings and their effect on overall flight behaviour.

The first reported SFT dates back to 1970 but more than 90% of the reviewed SFTs have been performed after 2005 (Figure 1.9). The tests performed before 2005 involved the construction of large models whose size ranged between 30% and 50% of the full-scale aircraft. Such large models (typically span size larger than 4 m) were needed to accommodate the large components and measuring devices necessary for testing. Early

---

[3]This number is computed based on the cost of commercially available measurement equipment, flight control equipment and propulsion system

tests (only 2 were found in the English-language literature before 2000) were expensive and limited to a consortium of well-funded research organizations and large commercial entities such as National Aeronautics and Space Administration (NASA), Boeing, Lockheed Martin etc.

The sharp increase in SFT after 2001 can be attributed to five main factors, namely, (i) miniaturization and improved performance of electronics, (ii) increased affordability of electronics, (iii) availability and affordability of Commercial Off The Shelf components (COTS) such as landing gear, ducted fans, small jet engines, pressure probes, (iv) surge in Advanced Air Mobility (AAM) and (v) increased use of rapid prototyping techniques. The impact of these developments on SFT will be discussed in detail in Chapter 3.
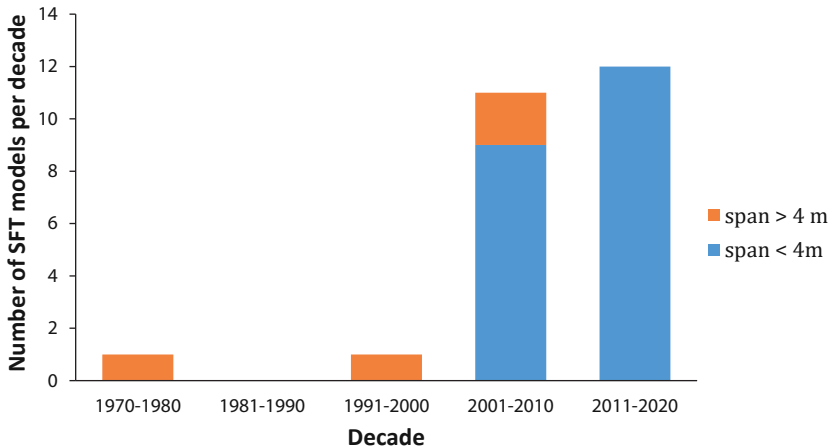
Figure 1.9: Growth in the number of SFT models reported in the literature since 1970 and the reduction in the size of the SFT model after 2005

The miniaturization of electronics and COTS components in the recent years has opened up avenues for sub-scale model designs whose size can now vary over a range from 50 cm span (with micro-measurement devices) to over 4 m (with powerful yet small jet or electric engines) [31–34]. This opens new regions of sub-scale model design space which can be exploited to diversify SFT applications. Moreover, the reduction in the cost of equipment used in SFT has allowed the larger scientific and engineering community to perform SFT. As a consequence of these developments combined with the need to assess the in-flight behaviour of unconventional aircraft designs, interest in SFT has grown in the recent years. An exhaustive list of all the SFTs performed to date and available in the literature is provided in Chapter 3.

1.4.2. CHALLENGES IN SFT

SFT enhances the accessibility of dynamic testing (e.g.,short-period motion, dutch roll, etc.) to larger engineering community and shows potential in improving the quality of flight dynamics testing by eliminating model constraints (see Chapter 2). However, use of SFT introduces a number of challenges. The key challenge lies in guaranteeing the

1

similarity between SFT model and full-scale aircraft, which is difficult to achieve due to the differences in size (of the model and the prototype) and flight conditions.

Furthermore, additional considerations such as guaranteeing model safety throughout the mission, adhering to the design restrictions imposed by the local authorities, selecting suitable measurement and flight control equipment and development of an optimal SFT mission must be made during SFT model design. All these design requirements coupled with similitude requirements make SFT model design a multi-disciplinary problem.

Thus, the reliability of SFT results is largely affected by the methodology used to design the SFT model. A number of design approaches have been proposed in the literature such as the classical similitude theory, similitude theory based on governing equations and the computational similitude theory to design similar SFT models (see Chapter 4).

Majority of the SFT model designs available in the literature are based on the classical similitude theory as it does not require a rigorous analysis. However, the classical similitude theory often leads to an over constrained problem leading to significant compromises in the similitude between model and prototype (details in Chapter 4). Furthermore, the multidisciplinary design requirements of the SFT model discussed in the preceding paragraph cannot be accounted in classical similitude theory. Thus, the SFT models obtained from classical similitude theory are often not truly similar to the prototype and are unsuitable for the simulation of prototype behaviour.

The computational Similitude Theory is the state of the art approach which uses computational methods iteratively (often within Multidisciplinary Analysis and Optimization (MDAO) framework) to design a similar SFT model (explained in Chapter 4). However, computational scaling has only been used for a limited number of aerodynamics and aeroelastic problems. The reasons for its lack of widespread adoption are summarized below:

1. A formal methodology to implement computational scaling approach is missing in the literature. Thus, engineers have to develop a suitable methodology for their problem before actually using computational scaling.

2. Engineers either use computational scaling or geometric scaling but never both together which prevents the comparison of their similitude with full-scale aircraft. As a result, the benefits of using the analysis intensive computational scaling approach over other methods remains unquantified.

3. To support MDAO based computational scaling approach, the SFT model design process must be automated to enable the design in the limited time available. However, such an automation is rarely undertaken as the process is laborious, time-consuming and error-prone and therefore not feasible in the limited time available for the SFT model design.

4. In order to improve the accuracy of computational scaling, medium/high computational methods are necessary. However, the associated computational infrastructure necessary to execute such a resource intensive MDAO process is generally not available to SFT engineers which limits the use of computational scaling.

1

Thus, to improve the quality of SFT (i.e., similitude with full-scale aircraft), the adoption of computational scaling design approach must be streamlined by lowering its methodological and technological barriers. To this end we formulate a set of research questions aimed at extending SFT design methods beyond state of the art in the following section.

1.5. DISSERTATION OBJECTIVE

Based on the literature review performed in this research work, the key challenge in SFT model design process (and SFT) lies in designing similar SFT models. Although, the computational scaling methodology proposed in the literature shows promise, it has not attained sufficient methodological and technological maturity necessary to improve the quality of SFT. To bridge this gap in the scientific body of knowledge, the following research question is formulated:

To what extent can the value and applicability of SFT be improved by using the MDAO based computational scaling approach in the SFT model design process?

This research question can be answered by achieving the following objectives:

- To identify and develop an MDAO based computational scaling approach that is applicable to a wide-range of SFT objectives and supports engineers in quickly formalizing their SFT model design problem.

- Development of enabling technologies for computational scaling, which:

  - supports the quick and automated parametric design of the SFT model

  - assists in rapid pre/post-processing activities for the computational analysis of SFT model

  - aids engineers in performing complex and time-consuming computational analysis in the limited time available for the SFT model design

- Compare the similitude of geometrically scaled model and computationally scaled model (designed using the methodology formulated in this dissertation) to the full-scale aircraft behaviour for different SFT objectives to quantify the value of using computational scaling or lack of it thereof.

1.6. RESEARCH OUTLINE

To address the research question formulated in the preceding section and to meet the objectives, this dissertation is divided into four main parts, as shown in Figure 1.10.

Part I - Review and Reflection establishes the current state of the art in Sub-scale Flight Testing, which includes:

1. The different analysis methods that are used in a typical design process and their relative merits and demerits and the summary of the potential benefits that SFT can bring to aircraft design process to complement the analysis methods currently in use (**Chapter 2**).

1

Part I:
Review and Reflection

Part II:
Identification and development
of methodology

Part III:
Results & Case-studies

Part IV:
Conclusions
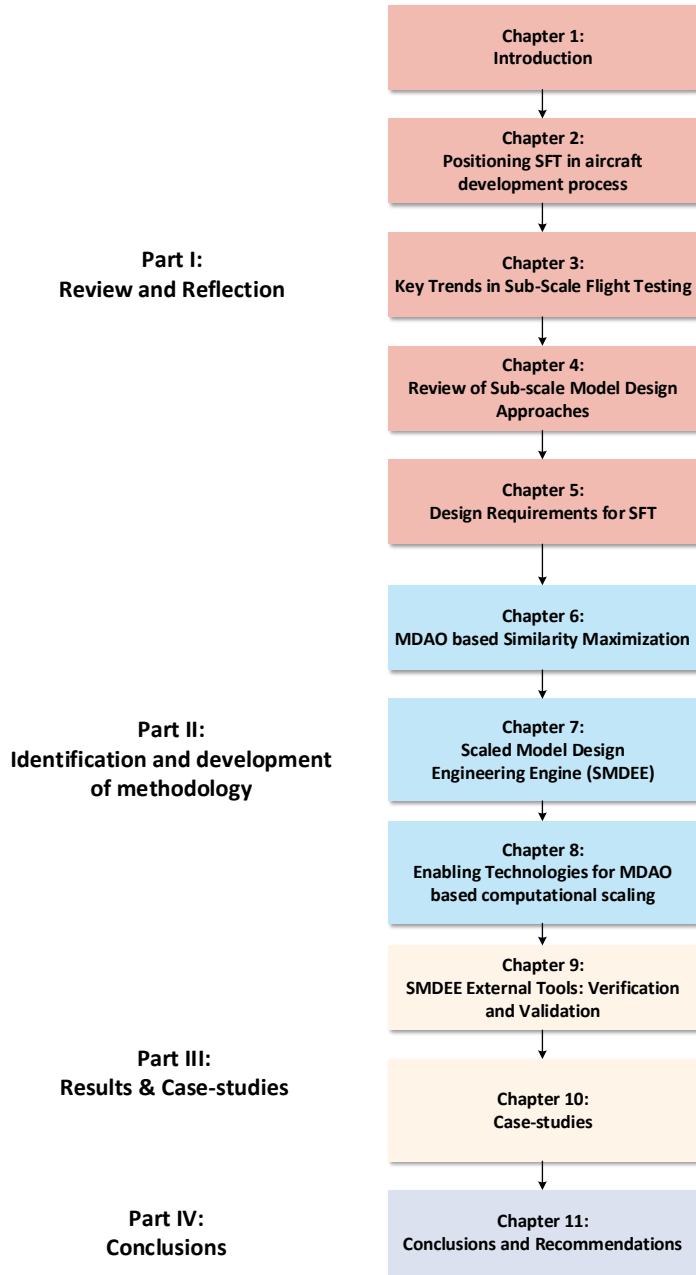
Figure 1.10: Dissertation Outline

2. The overview of past SFTs, the applications of past SFTs and the developments in

allied fields which supports the widespread use of SFT. Based on the review of past SFTs, the key tasks in SFT are identified and their associated challenges (**Chapter 3**).

3. A review of different methods used in the design of sub-scale models and the strengths and weaknesses of each of the methods (**Chapter 4**).

4. An overview and classification of the all the multi-disciplinary design requirements that are applicable to SFT and their incorporation in the SFT model design process (**Chapter 5**).

Part II - Identification and Development of Methodology explains the development of MDAO based computational scaling approach and enabling technologies, which includes:

1. A detailed treatment of MDAO based similarity maximization approach to support the SFT model design and the critical methodological barriers in the use of such methods and their mitigation strategies (**Chapter 6**).

2. The description of the implementation of the proposed methodology using advanced design methods such as Multi-disciplinary Design Analysis and Optimization (MDAO) and Knowledge Based Engineering (KBE) which has led to the development of the Scaled Model Design and Engineering Engine (SMDEE) (**Chapter 7**).

3. The explanation of enabling technologies developed in this dissertation that allow the use of the SMDEE in the short time available for the SFT model design (**Chapter 8**). These technologies include the extension of the existing KBE tool called the Multi-Model Generator and the development of parallel execution environment to speed up the disciplinary analysis needed by the SMDEE.

Part III - Results and Case-studies discusses the key results of this dissertation, which includes:

1. The verification and validation of the disciplinary analyses tools used in SMDEE by comparing the results of computational simulation with experimental tests to identify the sources of uncertainties and errors in the results (**Chapter 9**).

2. Seven case-studies of incremental complexity are performed with the aim of demonstrating the effectiveness of the proposed methodology and the use of SMDEE. Relevant discussion is provided to show how SMDEE can enable and improve the SFT model design process as compared to the classical similitude theory (**Chapter 10**).

Finally, in **Part IV - Conclusions**, relevant conclusions from the different phases of the research are compiled and discussed (**Chapter 11**). Apart from the main observations drawn from the research, recommendations for future work are also provided. In addition to meeting the objectives of the dissertation, the author believes that these chapters together will support the oncoming research in augmenting similitude in the SFT model design process.

I

REVIEW AND REFLECTION

2

POSITIONING SFT IN THE AIRCRAFT DEVELOPMENT PROCESS

In this chapter we discuss the capabilities and applications of different testing methods employed in the design of an aircraft. Many of these testing methods (such as wind-tunnel testing, material testing) have been used for a long time to evaluate the in-flight behaviour and performance of a design. Discussing the relative merits and challenges of various testing methods in conjunction with SFT allows us to understand the potential of SFT and pin-point the key stages in aircraft design process where SFT could be beneficial. In addition, we classify different testing methods based on the test objective and position them within a typical aircraft design life-cycle.

2.1. Testing Techniques in Aircraft Design

In most literature, as described in Chapter 1, the value and benefits of performing SFT vis-a-vis other testing methods have not been discussed. Computational simulation, experimental simulations using sub-scale models (including ground-based testing methods such as wind-tunnel testing, impact testing, etc.) and full-scale flight testing are the three main testing methods. However, full-scale flight testing is impractical in the conceptual and preliminary design stages of an unconventional aircraft. Therefore, we limit the discussion to computational and experimental simulations in this chapter.

2.1.1. Computational Simulation

Computational simulation uses software to analyse the behaviour of a prototype. Software such as Computational Fluid Dynamics (CFD), Finite Element Methods (FEM), Multi-body Dynamics (MBD) etc. help predict the flight behavior of an aircraft [36–38]. Such methods typically discretize a complex geometry into a sub-set of simpler geometrical entities (such as quadrilateral and triangular faces) and apply governing equations to each discrete entity to predict the aircraft behaviour. The discrepancies introduced by discretization, the assumptions and approximations in the governing equations used in the simulation and the numerical noise, all together, lead to errors in the predicted results [39, 40].

Very fine discretization with higher order governing equations may alleviate these inaccuracies, but significantly increases the computational cost, rendering the use of such simulations untenable in the conceptual and preliminary design stages, when many different aircraft configurations and variants need to be investigated. For example, in Direct Numerical Simulation (DNS), one of the most accurate CFD simulation technique, the computational effort scales with the third power of Reynolds number, which typically ranges from 5 to 30 million, depending on aircraft size and operating conditions. On the other hand, most numerical methods based on lower order and semi-empirical equations are predominantly developed and validated for conventional designs. Thus, their applicability to unconventional aircraft designs is unclear.

Aircraft design is a typical multidisciplinary problem. However, many computational methods are generally used for mono-disciplinary analysis. For example, CFD is used to study aerodynamics and FEM is used for structural analysis. Thus, designers are faced with the task of combining multiple disciplinary results to estimate the design behaviour such as the study of flight dynamics or aeroelasticity. In the process, the errors, assumptions and uncertainties in each of these disciplinary analyses may propagate downstream in design process and lead to erroneous conclusions about a prototype's behaviour. For example, in the estimation of aircraft flight dynamic behaviour, different types of disciplinary data (aerodynamic, weight and balance, propulsion etc.) must be provided to a flight-dynamics toolbox (Figure 2.1). However, the inaccuracies in these disciplinary analyses can result in cases where stable designs are deemed unstable and vice-versa. To prevent this, engineers need to acquire clear understanding of the capabilities and limitations of their computational simulations, which is done by validating computational results with experimental simulations.
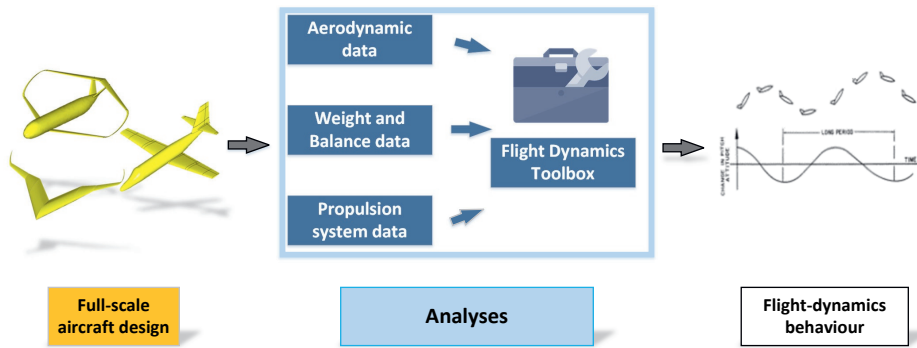
Figure 2.1: Methodology to estimate flight dynamics behaviour using computational simulation or ground based testing (discussed in Section 2.1.2) by studying the aircraft behaviour per discipline and then combining the disciplinary analysis using a flight-dynamics tool box.

2.1.2. EXPERIMENTAL SIMULATION

As discussed in Chapter 1, sub-scale aircraft models can be employed to study the behaviour of the full-scale aircraft [29, 41–44]. These smaller models can be manufactured quickly and at a fraction of the cost of the prototype (typically less than 0.01% of the market price of an aircraft depending on the test [27, 45–49]). Moreover, the risk of performing experiments with such models is much lower than the full-scale aircraft. Sub-scale models can either be used in ground-based facilities or for free-flight tests (see Figure 2.2). Irrespective of the type of tests, the results of experimental simulations performed using sub-scale models must be ***scaled-up***. Scaling-up the model test results involves correcting all the discrepancies that occur in the simulation of prototype behaviour due to the differences in the size, shape and mass of prototype and model. These discrepancies are known as ***scale-effects***. A detailed treatment of scale effects and different methods to address them is provided Chapter 4.

GROUND BASED TESTING

Ground-based tests are performed in large facilities (such as wind-tunnels, material testing laboratories and (aero-) engine test rigs [51–54]) that simulate the prototype operating environment artificially to extract high-quality data to predict prototype behavior at specified flight conditions. These facilities enable better control on the test conditions than free-flight tests, thereby reducing the uncertainties in the measurements. These tests are mainly used to obtain a general understanding of the implications of new-technologies and innovations in design, where, numerical or analytical methods are unreliable due to the limited knowledge of the underlying phenomenon (see examples in Table 2.1) [55, 56]. The models used in these tests are generally intended as proof of concept and do not mimic a specific full-scale design or vehicle (neither geometry nor in-flight behaviour). In certain cases, ground based testing is used to simulate the behaviour of specific vehicle/design [48, 57, 58]. However, these testing methods have limited applicability as explained in the following sections.

2
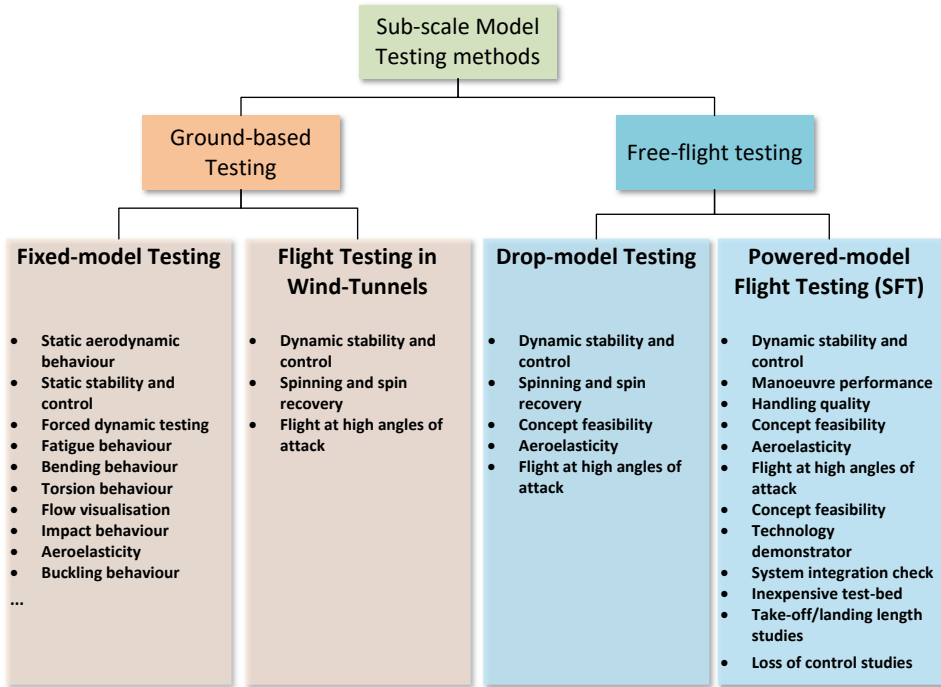
Figure 2.2: Classification of testing methods that are based on sub-scale models and their common applications found in the literature [41, 47, 50]

Fixed-model testing

Ground-based Testing is classified into two sub-groups, namely, fixed-model testing and flight testing inside wind-tunnels (Section 2.1.2). In fixed-model testing, sub-scale models are attached to the test equipment with rigid supports that limit the motion of the model. Typical facilities allow one or two degrees of freedom but the sophisticated testing facilities such as those operated by NASA and DNW (German Dutch Wind Tunnels) allow up to six degrees of freedom. Some applications of fixed-model tests are listed in Figure 2.2. Fixed model tests are used to evaluate both static and dynamic behaviour of a model. Examples of fixed model static tests used in aircraft design cycle are tabulated in Table 2.1.

The fixed model testing methods have evolved so much in the last century that they are able to generate high-quality data [41, 42, 48, 72] that can be directly used to evaluate the prototype static behaviour. In addition to these static tests, fixed model tests are also used to perform dynamic tests. These tests are known as forced dynamic tests as the models are forced to perform a dynamic manoeuvre using an actuator [48, 58, 72]. Typically, all dynamic tests that require aerodynamic forces are performed in the wind-tunnels. These forced dynamic tests can be divided into two sub-groups as follows:

1. **Flight dynamics**: involves the study of combined effect of aerodynamic forces and inertia forces acting on the model (see Figure 2.3). Forced-dynamic tests are used

2

Table 2.1: Overview of static testing methods used in ground-based testing

Test type	Description	References
Aerodynamics	typically performed using a wind-tunnel. The goal of such tests is to acquire high-quality data that provides information on the force and moments acting on the model in different flight conditions (angles of attack, side-slip angles, flight mach number, movable deflections). In addition, such tests are also used to study the flow around the model.	[41, 49, 57–59]
Structural	provide insights into the structural (bending, torsion, fatigue and buckling) strengths of different components of a model for the first few modes as the scaled model is stiffer than the full-scale aircraft. Structural engineers gain insights from these tests to predict full-scale structural behavior.	[52, 60–62]
Propulsion	The propulsion tests are classified into two categories: • Isolated tests: to study the performance of engines at different flight conditions which is usually performed in specific engine test chambers. • Engine integration tests: inclusion of a propulsion unit often modifies the airflow around the airframe and therefore the associated forces and moments acting on the model which is generally performed in wind-tunnel.	[51, 56, 63–65]
Aeroelasticity	study the coupled effect of aerodynamic forces and elastic forces. These aeroelastic phenomena are shown using Collar's triangle of forces in Figure 2.3.	[66–68]
Aeroacoustics	to identify noise sources in an aircraft and quantify their magnitude. Such tests are typically performed in wind-tunnels using a microphone array. For nuisance effects, both in-flow microphones and and far-field scans are evaluated.	[69–71]

2
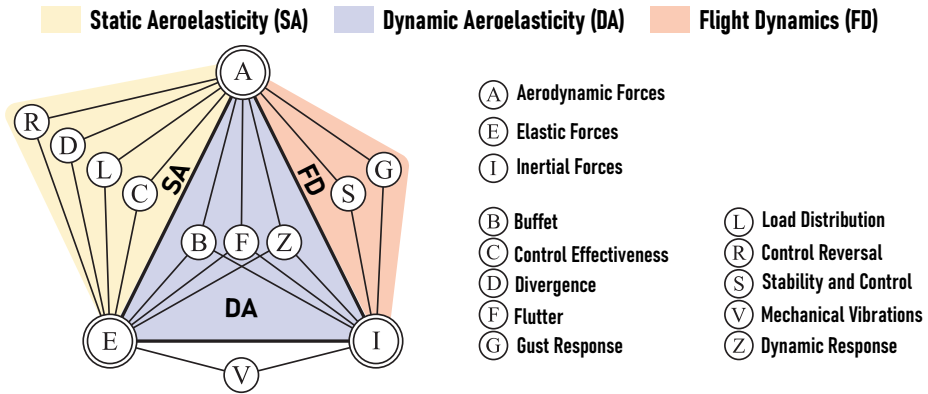
Figure 2.3: Collar's Triangle of Forces showing aeroelastic and flight dynamics phenomena occurring as a consequence of interaction between aerodynamic, elastic and inertial forces [67]. Tests are performed to study each of these phenomena to ascertain the in-flight behaviour of a design.

to estimate aerodynamic derivatives such as the variation of force and moments due to pitch, roll and yaw rates of the aircraft. The aerodynamic derivatives are then used with propulsion and weight & balance database of the aircraft in a flight dynamics model to determine prototype flight dynamics behaviour as shown in Figure 2.1.
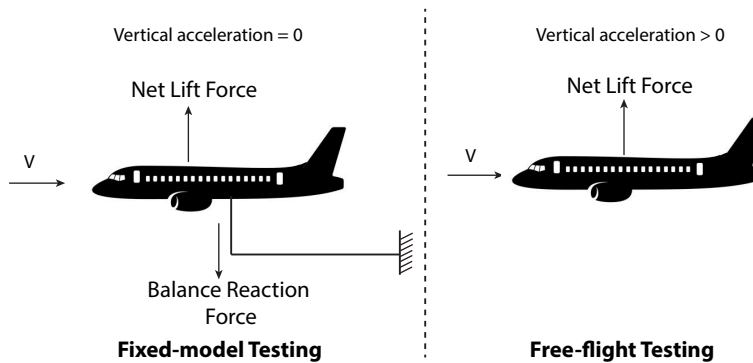
Figure 2.4: Example comparing a fixed-model testing (degrees of freedom < 5) and free-flight testing. Here, the balance reaction force counteracts the net lift force of the model which results in zero vertical acceleration, which is not included in the dynamic response. Whereas, in free-flight testing (discussed in Section 2.1.2), the effect of non-zero vertical acceleration is accounted.

This method would work well if the aerodynamic derivatives predicted using the wind-tunnel testing could be directly used in flight dynamics toolbox. In practice,

this is not possible due to two reasons. First, the motion of the models is forced (in one or more degrees of freedom as allowed by the testing facility). As a result, the natural dynamics response of the model is not studied (see example in Figure 2.4). Second, the models are attached to the wind-tunnel using stings that affect the flow around the model and thus the aerodynamic forces and moments (see Figure 2.5) [48, 73]. If connected at the center of gravity (CG) they affect the aircraft aerodynamics and thus the flight dynamics.

Conventional rotary test balance (attachment behind center of gravity) (a)   **6 DoF Model positioning mechanism (attachment at center of gravity) (b)**   **6 DoF Model positioning mechanism (attachment behind center of gravity) (c)**
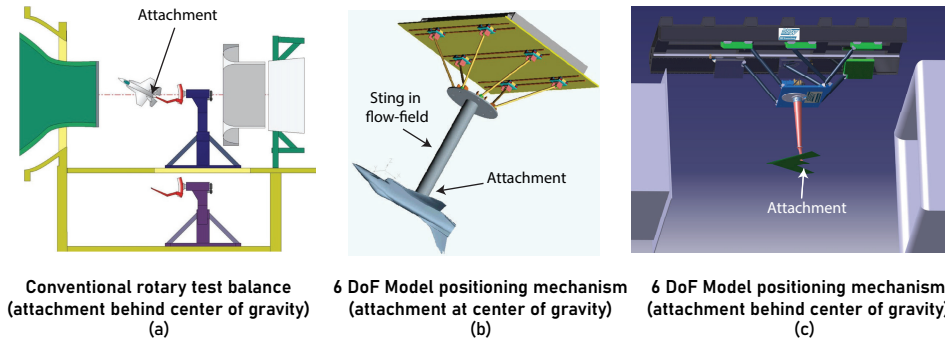
Figure 2.5: Different test rigs available at the state of the art DNW Tunnels to perform forced dynamic motions, where, the stings are either far behind the CG (Figure (a) and (c)) or the sting perturbs the flow-field (Figure (b)) affecting the prototype behaviour estimation [48, 58].

In a study performed by NASA with the X-48B model, Vicroy [74] found that the effect of the shape of the attachment sting on the pitching moment of the aircraft is significant. Three different types of stings were used in the wind-tunnel to determine the pitching moment coefficient as shown in Figure 2.6 and compared with the (averaged) data obtained from 50 different flight tests at similar conditions. The y-axis of the figure is redacted for confidentiality reasons. However, the scale of the graph shows that support stings affect both the magnitude and the trend of pitching moment.

Therefore, the stings are often connected behind the CG to ensure that the perturbance of the stings on the flow dynamics is limited. However, this comes with negative consequences. For example, when pure pitching moment is desired, connecting the sting behind the CG will also induce plunging motion as a result, such tests cannot be directly used to predict full-scale aircraft behaviour [48].

The effect of attachment location on the aerodynamic derivatives is best illustrated with an in-house study where a RANS simulation of the pitching moment of a swept wing was performed. The pitching moment was studied about five different attachment points as shown in Figure 2.7. The motion of the root section of the wing at different time instances for these attachment points is depicted in Figure 2.8.

Consequently, the movement of the attachment point changes the static and dynamic derivatives used in estimating the flight-dynamics behaviour. The longitu-
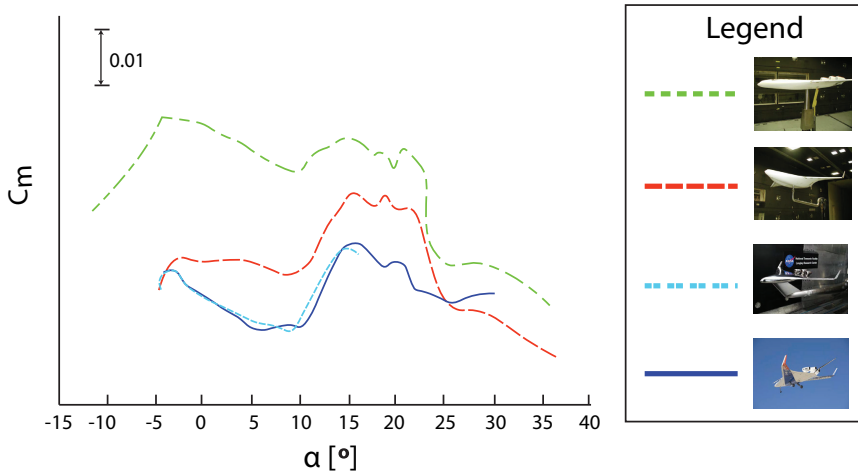
Figure 2.6: The variation of moment coefficient with respect to angle of attack tested at Reynolds number of 6 million when three differently shaped stings are used and compared with a free-flight test model [74]
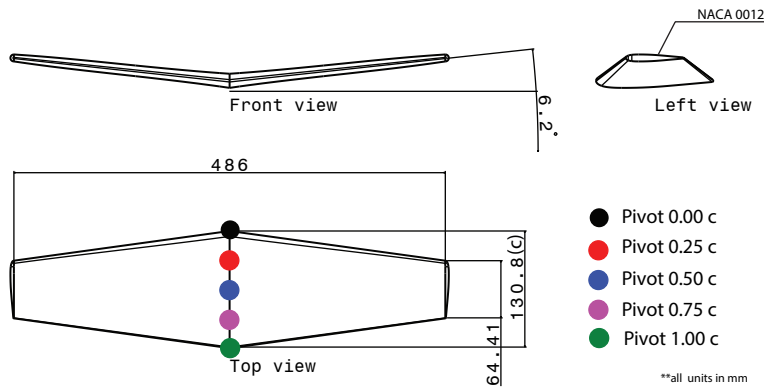
Figure 2.7: Geometry of the model used in RANS simulation to evaluate the effect of five different attachment location on aerodynamic derivatives

dinal derivatives for different locations of attachment point are as shown in Figure 2.9. The graph shows that the static derivatives C_{M_α} (moment derivative with respect to angle of attack) changes by 10% when the attachment point is moved from leading-edge to the trailing edge of the wing and C_{Z_α} (z-force derivative with respect to angle of attack) by 0.5%. However, the dynamic derivatives $C_{Mq} + C_{M_{\dot{\alpha}}}$ (moment derivative with respect to rotation rate and rate of change of angle of attack) change by nearly 35% and $C_{Zq} + C_{Z_{\dot{\alpha}}}$ (z-force derivative with respect to rotation rate and rate of change of angle of attack) change by 110%. Thus, the impact

2
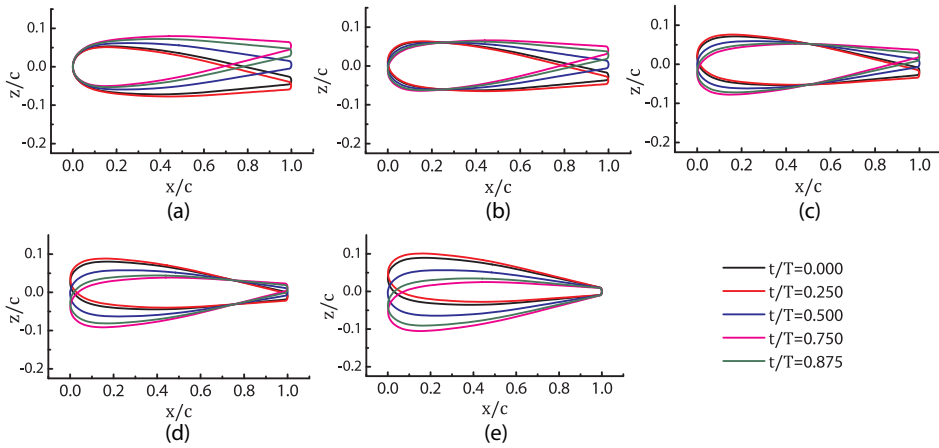
Figure 2.8: Motion of root section of the wing at different time instances where the attachment point is at (a)leading-edge of the section, (b) quarter-chord of the section, (c) half-chord of the section, (d) three-quarter chord of the root section and (e) trailing-edge of the section
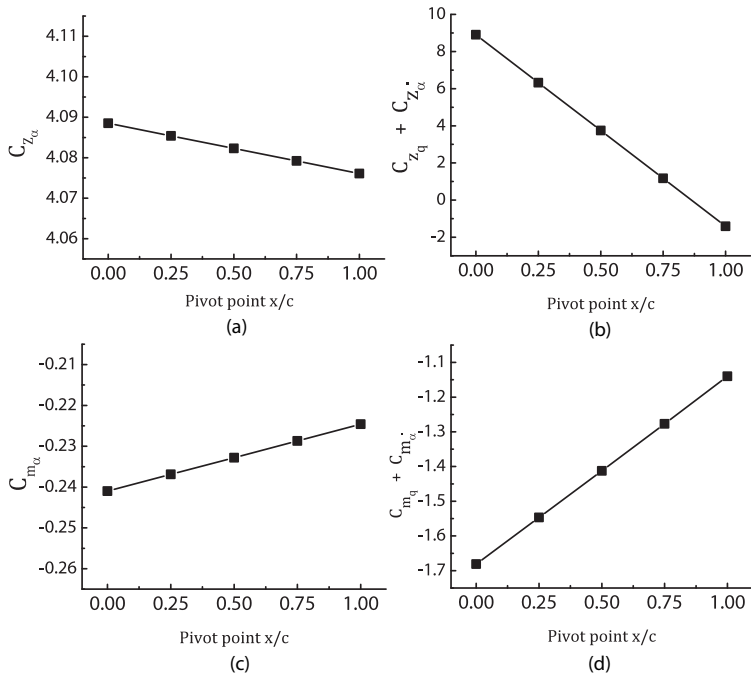
Figure 2.9: Variation of longitudinal aerodynamic derivatives at different attachment locations shown in Figure 2.7

of attachment location on dynamic derivatives is much more significant than the static derivatives. It is important to note that these results only depict the situation of a single-wing simulation. The changes in the moment derivatives due to shift in attachment point of a full aircraft is expected to be higher due to larger moment arm.

Although the 6 degrees of freedom wind tunnels [48, 58] are capable of complex simultaneous multi-axes motions and single axis constant amplitude and frequency sinusoidal motions, they can only solve the first challenge of degrees of freedom. The challenge associated with sting attachment induced effect persists.

2. **Aeroelasticity** : involves the study of combined effect of aerodynamic, inertial and elastic forces on the model as shown in Figure 2.3 (e.g., buffet, flutter and dynamic response). These critical aeroelastic conditions can be found by observing either the free oscillation of the structure following an initial disturbance or by the response of the structure to an external periodic excitation. In the former method, the airspeed is increased until a maintained oscillation of a specific amplitude occurs. In the latter method, one or several exciters (eccentric rotating masses, air-pulse exciter, etc.) are used to excite the oscillation. At each airspeed, the amplitude response is recorded for varying exciter frequencies. The critical condition is found when the amplification becomes very large [66]. Forced dynamic testing is often used to determine the optimum location of engines or external fuel tanks. It has also become clear [66] that rigid body degrees of freedom (i.e., translation and rotation of the airplane as a whole) have an influence on the flutter of swept wings and tails. However, it is impractical to allow all the degrees of freedom corresponding to free flight conditions in a wind-tunnel. Thus, engineers simplify the problem by separating the constituent motion of the airplane in the symmetric and asymmetric types and examining them separately.

Flight Testing in Wind-tunnels
In order to overcome the challenges in forced dynamic testing, engineers have moved towards indoor (wind-tunnel) flying sub-scale models. Tests that allow free-flight of sub-scale models inside the wind-tunnels are known as indoor-model flight tests. Here, the models perform free motions in the available space (i.e., the models have all six degrees of freedom). Spin tests, vertical drop tests, and hover tests performed in wind-tunnel are examples of indoor-model flight testing [75–77]. Most of these tests are not truly free-flight tests because they use strings to prevent damage to the model and the facility. However, it has been found that such string supports tend to alter the dynamic behaviour of the model too [41, 73].

The specifications and the capabilities of the test-facility determine the size of the model, the test-conditions, and the manoeuvres that can be performed. As per estimates by Owens et al. [72], for free-flight tests in wind-tunnel, the largest model dimension should be $1/5^{th}$ of the wind-tunnel length to ensure sufficient maneuvering space. Consequently, the models end up being so small (typically less than 1 m) that they are prone to significant *scale-effects* (details in Chapter 3).

Thus, the constraints imposed by the test-facility either prevent large models from performing the full-range of motions necessary to study the prototype behavior or de-

mand the use of smaller models, thereby leading to scale effects. Notable exceptions are the very large wind-tunnels operated by NASA and DNW, which can house sufficiently large models to prevent scale effects [48, 58, 72].

These state of the art ground-based testing facilities offer better control over the test conditions than smaller wind-tunnels and free-flight testing methods, which reduces uncertainties in the measurements. Additionally, ground-based measurement equipment potentially have higher sensitivity, which ensures better resolution of model output (i.e., they are more accurate). However, even these state of the art methods have technical limitations as described in the preceding paragraphs. Besides, the increased control on the test conditions and improved accuracy of measurement comes at a cost. In addition to the cost of the model, per-day cost of these facilities can run into thousands of euros, where, a test-campaign generally ranges from 2-3 weeks. Moreover, the waiting time to access such scarce test facilities can stretch to months. To overcome these limitations, free-flight testing has been used an alternative.

FREE-FLIGHT TESTING

In free-flight testing, experiments are carried out in open atmosphere with all the measurement apparatus inside the model. Free flight testing always provides 6 degrees of freedom, which allows the study of the coupled effect of all forces acting on the model. This feature is the reason why free-flight testing is especially used to study the *dynamics* of aircraft model. Furthermore, unlike ground based testing or computational simulation, there is no need to combine the results of individual disciplinary analyses, as the relationship between the tightly coupled disciplines is directly manifested in its flight behaviour. For example, unlike the process shown in Figure 2.1, the flight dynamics behaviour of the sub-scale model can be directly evaluated during a free-flight test, as shown in Figure 2.10. The flight dynamics response is a coupled reaction to aerodynamic, inertia and elastic forces acting on the model. In addition, these results can be further analyzed using an appropriate system identification process to arrive at disciplinary data that can be used to validate other experimental or computational methods [78, 79].
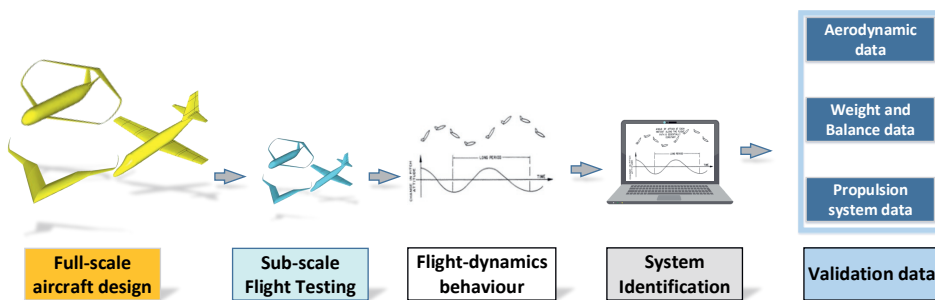
Figure 2.10: Methodology to estimate flight dynamics behaviour using sub-scale flight testing, where, the coupled effects of aerodynamic and inertial forces are directly manifested in the model flight dynamics behaviour. Further insights on model's performance per discipline can be gleaned by performing system identification studies.

DROP-MODEL TESTING

Free-flight tests are classified into drop-model tests and powered-model flight tests as shown in Figure 2.2. In drop tests, the model is launched into the atmosphere with external aids such as launchers (ground-based or rocket) or dropped from another aircraft or helicopter [80–82].

Until 2000, drop-model testing was the preferred free-flight testing method because miniature equipment (such as flight control system, compact propulsion system, radio-controlled actuators, etc. suitable for sub-scale model) was not available in the market and most well-funded research organizations like NASA (which were predominantly involved in past free-flight tests) had easy access to drop/launch vehicle. At the same time, the need of expensive drop/launch equipment is the main reason this testing approach is scarcely employed. Moreover, this testing method ignores the effect of airframe/propulsion integration which can be a relevant contributor to the model behaviour. To overcome these challenges, powered models are used, as discussed in the following section.

SUB-SCALE FLIGHT TESTING (SFT)

Tests with models that perform the mission with an on-board power-plant are called SFT [28–30]. Since SFT does not require a launch equipment, it can be a cost effective testing approach to study aircraft dynamics. However, fitting all the measurement equipment, energy source for the power-plant such as fuel or batteries and the flight control equipment in the limited space of the model is a challenge in the execution of SFT. As discussed in Chapter 1, in the last decade, the improvements and miniaturization of electronics and COTS components, complemented by advancements in rapid prototyping techniques, have opened up avenues to exploit SFT. For example, with the availability of miniature battery powered engines, it is possible to have model installations with a wide-range of thrust over weight ratio, as the weight of the scaled model is much lower than the full-scale aircraft. Thus, these latest developments offer engineers the flexibility to perform varied SFTs while still maintaining the necessary similarity requirements (discussed in Chapter 4).

Nevertheless, SFT is afflicted by the problem of scale effects like all sub-scale model experimental testing methods. In addition, engineers wishing to perform SFT must consider three other factors:

1. The model flies in open atmosphere, which introduces uneven turbulence, gusts, etc. that affects the model behaviour.

2. The model needs to be certified by competent authorities before it can be flown for testing. Certification of models for SFT has not reached the universality that has been achieved for full-scale aircraft and every country has its own set of rules and local certification authorities to oversee SFT activities. In general, these authorities assess the potential damage in case of a crash and check whether the model can safely complete the required mission. Thus, based on their risk perception, local authorities can impose restrictions on the model size and test conditions. For example, in the Netherlands, where the rules are derived from European regulations for drones [83], SFTs require a certificate before flight, which are categorized into

open (mass < 25 kg), *specified* (mass > 25 kg and span < 3 m) or *certified* category (25 kg < mass < 150 kg and span > 3 m). More details can be found in the Dutch Government website [84].

3. SFT models are completely unsupported. Therefore they must be able to take off and land (with appropriate consideration for the required landing gear) and enable the test pilot to fly the test mission in an accurate and repeatable manner (by accounting the required model flying qualities) .

These critical considerations determine the very feasibility of SFT and eventually the accuracy with which full-scale aircraft behaviour and performance can be predicted. Thus, these factors must be taken in careful consideration while designing the sub-scale model to ensure that the actual value of SFT is harnessed.

These issues combined with the limitations imposed by COTS components make SFT challenging. For example, the restrictions imposed by the authorities, combined with the (limited) range of operations of radio-controlled devices that are typically used in SFT, make the simulation of the complete mission including transonic cruise impossible. Nevertheless, SFT can be used to study certain parts of the mission, where all the disciplines are coupled and the results of multiple SFTs can be used in conjunction with other testing methods to predict full-scale flight behaviour (Chapter 6)..

2.2. TESTING METHODS AND THE AIRCRAFT DESIGN PROCESS

In the early stages of aircraft life-cycle, several tests must be performed from the conception till first flight to analyze aircraft performance and in-flight behaviour. These tests consist of physical experiments or computer-based simulation, as described in the preceding sections. Each of these tests can be be broadly grouped into one of three categories based on the test objective [41, 85, 86], namely:

1. **Phenomenological tests:** preliminary tests intended to improve fundamental understanding of the underlying phenomena or evaluate the impact of new technology and innovations on the prototype behaviour. Such tests are a part of fundamental research and generally not intended for the evaluation of a specific prototype design.

2. **Demonstrator tests:** to provide a proof-of-concept of new designs and novel technologies and to show that different aspects of the model can be integrated together in flight. These tests are intended to enhance the confidence of various stakeholders such as investors, airlines and the general public.

3. **Simulation tests:** to simulate the full-scale flight behaviour and draw relevant correlation to the prototype flight behaviour. These tests are intended to evaluate the performance of specific vehicle design.

This classification of tests is mapped over the key steps in the development of an aircraft as shown in Figure 2.11. Fundamental research, innovative ideas and advancements in technologies (both in aerospace industry and the allied fields) trigger the de-

2
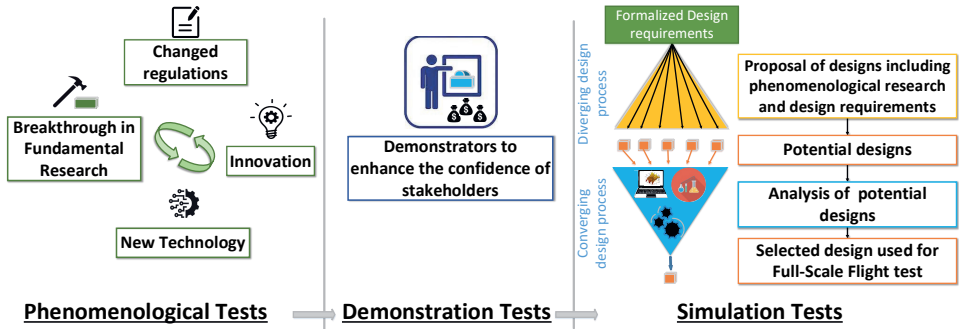
Figure 2.11: An overview of different types of test methods and their role in different phases of development of an aircraft from conception till the first full-scale flight

velopment of a new aircraft that incorporate these progresses. Typically, such break-throughs are an outcome of phenomenological tests. These tests are performed to get a preliminary understanding of the physics and to estimate the potential gains from incorporating such developments.

For example, distributed electric propulsion shows promise in improving aircraft performance [22]. However, the aerodynamic interaction between the wing and the propellers is not well understood [56, 64, 65]. To improve their understanding, engineers perform a preliminary test with a (simple) wing and a propeller. The models used for such tests are not designed based on a specific vehicle but are minimum viable products to study a specific behavior.

Ground-based tests are the most used methods for phenomenological tests [56, 64–66, 68]. Although computational simulation is used for phenomenological testing, they are generally accompanied by ground-based validation tests to quantify the impact of the underlying assumptions and approximations in the computational simulation [64, 87]. Until last decade, free-flight testing was not used for phenomenological tests, as the method was considered too expensive for preliminary studies and the accuracy of measurements from such tests was insufficient to make pertinent conclusions [41]. This has changed in the recent years and engineers are employing this method much more frequently in phenomenological tests [28, 88–90]. Examples are shown in Chapter 3.

Since phenomenological tests are based on mono-disciplinary analysis and the models used in such tests are minimum viable products, engineers are confronted with two main questions:

1. Are the results of such tests sufficient to evoke the confidence of stakeholders such as airlines, investors and the general public?

2. Do these (mono-disciplinary) benefits actually translate into meaningful gains when all the sub-systems are integrated in an aircraft where multi-disciplinary effects are in action?

In the design of conventional aircraft, these question can be answered by experienced aircraft manufacturers as they are able to estimate the impact of phenomeno-

logical benefits (determined using ground-based testing and computational simulation) on the overall aircraft performance and behavior based on legacy information. Furthermore, the stakeholders are not skeptical about such improvements as the topology of the aircraft does not change significantly.

However, in the case of unconventional designs, where legacy information is missing, demonstrator tests are used by engineers (see Figure 2.11) to enhance the confidence of the stakeholders by demonstrating the effect of the proposed improvements on the relevant disciplines. This type of test can be performed using a sub-scale model in free-flight as they offer a natural environment to perform multi-disciplinary analysis as explained in Section 2.1. In the last decade, computational methods have been used to demonstrate multi-disciplinary aircraft system integration and are generally called Digital System Models or Digital Twins [91]. And, to the best of author's knowledge, ground-based testing methods have not been used for demonstrator testing.

Once engineers are satisfied with the results of phenomenological and demonstrator tests, they formalize the set of requirements based on which the aircraft is designed. Numerous designs, that incorporate the design requirements and the novel technology that has been studied using phenomenological tests (see Figure 2.11), are proposed at the start of the design. However, not all designs can be brought into production. Thus, multiple rounds of trade-off studies are performed, where, every round reduces the contending designs until a handful of designs remain, which are evolved, matured and optimized until one design comes out.

Table 2.2: Comparison of different testing methods described in Section 2.1 based on their applicability to different test objective

Test-type	Ground-based Testing	Computer Simulation	Sub-scale Flight testing
Phenomenological Tests	✓	?	✓
Demonstrator Tests	✗	✓	✓
Simulation Tests	✓	?	✓

✓ is Applicable, ✗ is Not applicable and ? is Applicable after validation with other tests

These trade-off studies are based on simulation tests. In the past, ground-based tests, computer simulations and sub-scale flight tests have been used for simulation tests and their specific applications have been listed in Figure 2.2. The initial trade-off rounds are generally based on lower order computer simulations [92, 93]. However, as the design pool becomes smaller, higher order computational methods, ground-based tests and SFTs are employed [28, 41, 48, 58, 73, 89, 90, 94, 95]. Here, the ground-based tests are generally used to perform mono-disciplinary analysis and the computer simulations and SFT are used for multi-disciplinary analysis. These higher order analysis can reveal shortcomings of designs unseen in the early phases of design and prevent expensive last-minute rework.

Based on the discussion provided in this section, the applicability of different testing methods per test objective is summarized in Table 2.2. Notably, sub-scale flight testing is

the only testing method employed for all three types of tests. The ground-based tests are not used for demonstrator tests and the computer simulations are generally not trusted without a validation using sub-scale model test. The possibility of using SFT in different phases of aircraft development makes it a useful tool in the aircraft design process. However, owing to the reasons described in Section 2.1.2, the widespread use of SFT has not been possible. In the following section we summarize the pros and cons of SFT, based on which, a detailed review of developments in SFT will be performed and a proposal for future progress in SFT will be made.

2.3. SUMMARY: SFT IN AIRCRAFT DESIGN PROCESS

On the basis of what has been discussed so far, the strong points of SFT, in contrast to other testing methods can be summarized as follows:

1. SFT enhances the accessibility of dynamic testing environment (for aeroelasticity and flight dynamics) to the larger engineering community, as it does not require investment is expensive infrastructure, such as wind tunnels.

2. SFT demonstrates the potential to improve the quality of dynamic testing, as no supporting (and perturbing) devices such as stings and strings are necessary to constrain the model in SFT.

3. SFT provides a natural setup for simulating aircraft behaviour that is influenced by multiple disciplines.

4. SFT is a method that can be used for phenomenological tests, demonstrator tests and simulation tests. It is useful in all phases of aircraft development, which is not always possible with other testing methods.

In order to harness these benefits, ***challenges*** posed by SFT must be overcome. The key challenges of SFT can be summarized as follows:

1. SFT is prone to scale-effects, which must be accounted for in the design of the sub-scale models.

2. Compared to other testing methods, SFT poses additional constraints in the design phase as engineers must ensure the model can safely complete the required mission, as the model remains unsupported for the entire duration of the test.

3. If local authorities impose any constraints on the size and test conditions of SFT, they must be accounted in the design phase.

4. Despite miniaturization of COTS components and electronics, fitting them within the limited space of a SFT model while accounting for mass and inertia (discussed further in Chapter 5-7) is a formidable task for the designers.

5. SFT model's range of operations is largely limited to sub-sonic conditions [1].

---

[1]This is based on the current limitations imposed by COTS equipment and certification authorities. In the future, with sufficient improvements in technology and relaxation in certification requirements, miniature models might be able fly long distances at transonic and possibly supersonic speeds.

6. SFT is performed in open atmosphere which introduces errors and uncertainties in measurements due to gusts, inhomogeneous turbulence, etc.

These challenges can be broadly classified into three categories, namely, the challenges that affect the multi-disciplinary design of the sub-scale model (1-5); the challenges posed by the limitations in the available technologies or equipment (5); and those that are are inherent to the testing method (6).

Whilst the practical challenges in performing SFT and the limitations imposed by the equipment and electronics used in SFT are largely discussed in the literature, the developments and challenges associated with the design of sub-scale model are not [45, 47, 96]. Thus, for the remainder of this dissertation, we mainly discuss the challenges associated with the multi-disciplinary design of the sub-scale model with relevant references to other practical challenges where necessary. This original contribution is one of the main objectives of this paper. In the following sections, we discuss the past applications of SFT, the design strategies used in those tests, the state of the art design methods that are available today and how they can be exploited to improve the applicability and value of SFT.

2

3

KEY TRENDS IN SUB-SCALE FLIGHT TESTING

Sub-scale Flight Testing has been in use since the last 50 years. Numerous SFT models have been designed and manufactured in this period. The design of these SFT models and their eventual effectiveness in predicting full-scale aircraft behaviour is largely dependent on the advancements in measurement equipment, flight-control systems, manufacturing techniques and the test-objective over the last 50 years. In this chapter, we identify the key milestones in SFT model design and describe the enabling developments in allied fields (such as electronics and manufacturing). Furthermore, various SFTs that have been addressed in the literature are discussed with a focus on their application and objectives. Based on this literature study, we determine the key tasks that must be performed to successfully complete SFT and the challenges they pose in the design of SFT model, which must be overcome to further the state-of the art in SFT model design.

3.1. Milestones in SFT

The key milestones in the history of SFT are shown in Table 3.1 . The first reference in the literature of the use of SFT in aircraft design process to simulate full-scale behavior was done in 1979 as part of the the HiMAT (Highly Maneuverable Aircraft Technology) program by NASA [97–100]. This aircraft was a departure from small balsa wood models, where 44% scaled composite model of a fighter aircraft weighing 450 kg was used to test aircraft behavior. The HiMAT model was designed to reproduce the manoeuvre and pull-up behaviour at high loading conditions (12g at sub-sonic and 10g at supersonic speeds).

3

Table 3.1: Timeline of key milestones in the realization of SFT based on the information available in the literature

Milestone	Year / Inception Date	References
Tests with balsa models that have geometrical shape similar to the prototype (results not recorded in the literature)	**pre-1979**	-
First SFT model reported in the literature (model having 10 m span and 450kg mass)	**1979**	[97–100]
Introduction of rapid prototyping and composite materials in the manufacture of sub-scale models	**1998**	[50, 101, 102]
First miniature SFT model built and tested (span smaller than 4 m)	**2006**	[72]
First computationally scaled model designed and tested	**2010**	[103]

Such (large) SFT models, which were built before 2005, were affected by long manufacturing times and high costs. In 1990s, industrial techniques known as rapid prototyping were developed to manufacture models quickly at low cost. The materials used in rapid-prototyping in the 1990s were typically plastics. As a result, the properties and structural behaviour of the scaled model were markedly different from that of the prototype. Cho et al. [101] were among the first to develop similarity rules (discussed in Chapter 4) in manufacturing. These techniques were quickly adopted in the construction of wind-tunnel models. Chuk and Thomson [102] compared different manufacturing techniques used in wind-tunnel model design. However, the models developed using these methods were limited to testing under low loads as the materials used in rapid-prototyping were low strength plastics. Casaburo et al. provides an insight into rapid prototyping techniques used for construction of models. In the last decade, composite layup and 3D printing of metals [104] have become popular in model construction,

which allows high loads on model during tests. In the case of SFT, composite layups and metal 3D printing have been predominantly used since 2005.
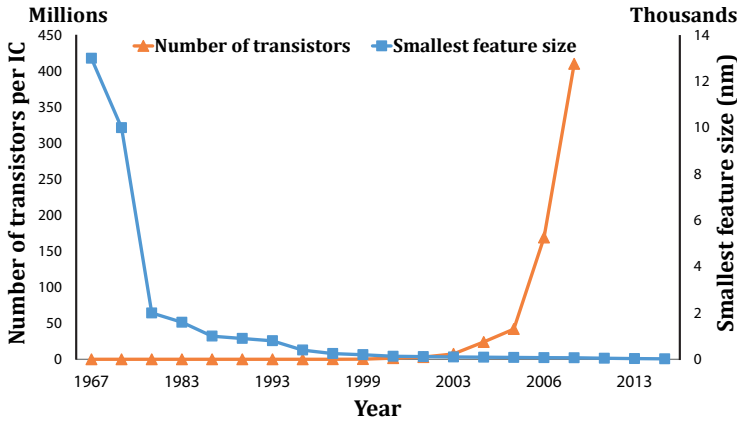
Figure 3.1: Miniaturization of electronics due to exponential increase of number of transistors per integrated circuit (IC) and the reduction in the size of transistors

The next breakthrough came in the form of miniature models, i.e., models less than 30% size of the prototype, that were made possible by the miniaturization of on-board equipment [30, 72, 105]. These include miniature turbo-jet engines, landing gear, inertial measurement units, pneumatic systems, servomotors, etc. Before 2000, these components had to be manufactured specially for SFT, which increased the cost and waiting times for tests.
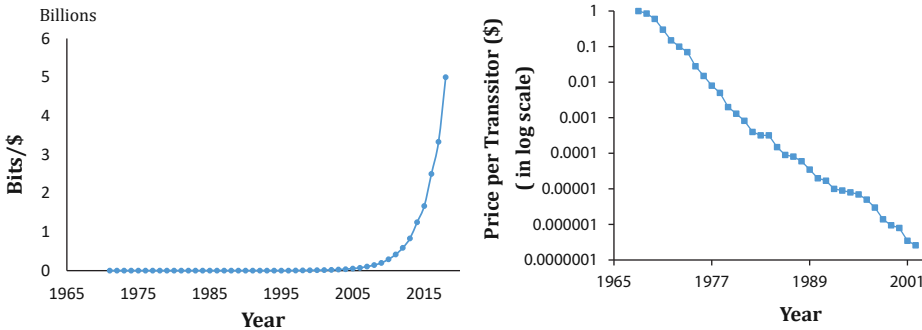
Figure 3.2: Improvements in cost-effectiveness of electronics

Today, a large variety of such equipment is available commercially off-the-shelf [31–34]. Since these components are manufactured in bulk, their costs have come down significantly. Furthermore, designers have a large catalogue at their disposal to choose the right equipment for the test at hand. Finally, a lot of effort also goes into optimizing the shape, size and weight of such equipment. This improves the performance of the

equipment and consequently enables tests in wider range of flight conditions such as speed, altitude, angles of attack etc.

At the core of these components lie a set of integrated circuits (ICs) that are essential to enable communication between the pilot and the SM in flight, power the sensors needed to measure various flight parameters and store the measured data for further analysis. The size of these ICs and their mass greatly affect the design of SM. Broadly, the size of an IC is determined by two factors, namely, the maximum number of transistors that can be fit inside an IC and the size of each transistor (known as minimum feature size). The review by Kurzweil [106] shows that there is an exponential drop in the size and cost of ICs and the storage capabilities of ICs have grown exponentially (Figure 3.1 and 3.2).

All these developments translated into improvements in the electronic products used in SFT. For example, micro Secure Digital memory cards (SD cards), when introduced in 2005, had memory of up to 125 megabytes(mb) [107, 108]. This low storage capacity was one of the bottlenecks in the use of SFT. For example, a typical SFT of 30 minutes measuring at 100 Hz with aeroprobe (approximately 20mb), inertial measurement unit (IMU) (approximately 30mb) and 10 unsteady pressure sensors measuring at 50 kHz (approximately 300-500mb) surpasses the capabilities of SD card from 2005. Thus, all the measurements cannot be made simultaneously in one SFT. Today, SD cards have storage capacity of 1 terabyte, while their size has almost remained the same. Thus, many more parameters can be measured and stored in a single flight without storage capacity limitations.

Not only has the miniaturization improved the capabilities of different devices but it has also enabled tests which were not possible using sub-scale models. For example, Bunge et al. [109] installed 16 differential pressure sensors on the wings of 1/4 scale PA-18 Super Cub, which proved to be sufficiently accurate. Such in-flight surface pressure measurement capabilities on SFT models were non-existent before 2005. Furthermore, miniature autopilot systems like Pixhawk, which have come into existence after 2008, have opened up the possibility of autonomous flight and on-board computer-vision [110]. Such systems are enabling widespread use of SFT by reducing the pilot effort and improving the safety of the SFT models.

Another major reason for the surge in SFT models after 2005 is the increasing prevalence of Unmanned Aerial Systems (now called Advanced Air Mobility (AAM)), which are smaller (compared to general aviation aircraft) and cheaper than conventional aircraft [111, 112]. These are intended to improve the urban mobility of the future. The AAM aircraft design process generally includes the flight test of both sub-scale models and full-scale aircraft, whose size is often comparable to SFT models of conventional passenger/military aircraft. Thus, the growing interest in AAM aircraft has also added to the increase in number of SFTs and resulted in the improvement of SFT components and design practices.

In the last decade (2010-2020), utilizing these advancements, many tests have been conducted using varied design approaches, manufacturing methods, and test objectives. Table 3.2, 3.3 and 3.4 list different sub-scale aircraft models that have been recorded in the literature and specifically used for SFT. While these tables present a brief description of individual tests, the detailed treatment of manufacturing methods, control-laws, and

specifications of on-board equipment are not included. In the remainder of this section, we analyze the overall trends in SFT concerning the objective of the test and the applications of SFT. Based on this analysis, we formulate the key tasks that must be performed to successfully complete SFT.

3.2. Test-Objective based Classification of SFT

As discussed in Chapter 2, SFT can be classified into three categories, namely, demonstrator, phenomenological and simulation tests. Of all the SFT reviewed in the literature addressed here, 52% of the models were used for demonstration, 20% to study specific phenomena, and 28% to simulate the full-scale flight behavior. This is shown in Figure 3.3. In the following paragraphs, we categorize different classes of SFT applications based on the type of test they require.
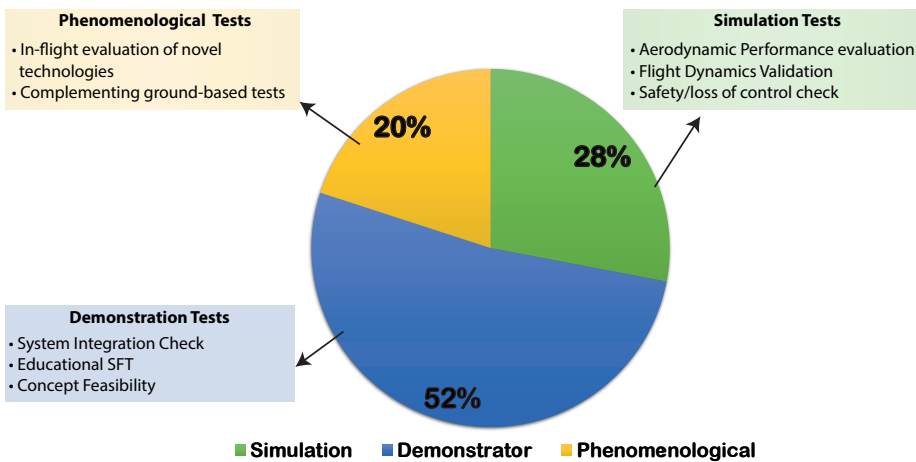
Figure 3.3: Distribution of SFT based on test objective and the classification of applications per test objective.

3.2.1. Applications Requiring Demonstration Tests

Applications that use demonstration SFT models are categorized into the following classes:
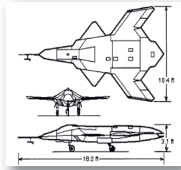
1. **System integration**: to study whether different sub-systems can work together while ensuring a safe and efficient flight for a given design. Examples of such system integration tests are the Faser project [72], DUUC project [113, 114] and the Eclipse Project [44, 105]. Such tests are also used to improve SFT techniques by assessing the performance of different COTS components in flight. For example, SFT to develop data acquisition, transmission and storing techniques also belong to this category.

2. **Educational SFT**: employed to teach students the principles of flight, aircraft design, and manufacturing techniques.

3. **Concept feasibility**: models that are not designed with any particular prototype design as a reference. They merely act as an engineer's impression of prototype design.

Examples of SFT intended for demonstration are shown in Table 3.2. The design effort in these tests is not as high as the simulation tests and the phenomenological tests because the model is not required to behave exactly as the prototype (even if its design exists at the time of demonstration tests). Accommodating all the on-board equipment within the model and ensuring that the model can complete the mission safely are the only requirements. Therefore, in most cases, engineers do not use a specific design approach when designing demonstrator SFT model (as shown with NA in Table 3.2) but only strive to design a model which can complete the mission safely.

Table 3.2
Past sub-scale flight tests used for demonstration testing

Model Image	Model name and goal	Organizations	Design approach	Refs.
	X-36b (1997) Demonstrate tail-less stealth design using a model which was approximately 565 kg and a span of 5.3 m	NASA	Geometric Scaling (28%)	[115, 116]
	FASER (2006) System integration test to study flight data acquisition system and techniques on a conventional aircraft	NASA	NA	[72]
	RAVEN (2008) Teaching aid to educate students on the principles of SFT design, manufacture and testing	Linköping University	Geometric scaling (13.8%) & Froude number scaling	[30]
			Continued on next page	
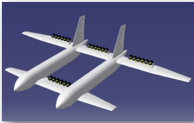
Table 3.2 – continued from previous page

Model Image	Model name and goal	Organizations	Design approach	Refs.
	ECLIPSE (2009) Flying demonstrator for circulation control devices and fluidic thrust vectoring to replace the conventional ailerons	BAE Systems, Imperial College London, Universities of Cranfield, Leicester, Liverpool, Manchester, Nottingham, Southampton, Warwick, Wales and York	NA	[43, 44, 105, 117, 118]
	ECO-Sport (2010) Teaching aid to educate students on the principles of SFT design, manufacture and testing¯	Linköping University	NA	[119]
	GL-10 (2010) Demonstrate the transitions from hover to wing borne flight and from wing borne flight back to hover in a reliable and repeatable way	NASA	NA	[120]
	Flexi-Bird (2010) Sub-scale model to study environmental and safety issues	Warsaw University of Technology, University of Stuttgart, ONERA, Airbus, NLR, FOI Stockholm	NA	[121, 122]
	DUUC (2016) Concept feasibility study demonstrating propulsive empennage	TU Delft	Geometric Scaling (5.5%)	[20, 114]
	Avistar Elite (2019) System integration test to validate flight data acquisition system in flight	Technical University of Munich	NA	[123]

Continued on next page

Table 3.2 – continued from previous page

Model Image	Model name and goal	Organizations	Design approach	Refs.
	ALBATROSS (2019) Concept feasibility study of semi aero-elastic wing-tips for improved efficiency	Airbus	NA	[124]
	MAVERICK (2020) Concept feasibility study of blended wing body that promises environmental performance benefits	Airbus	NA	[125]
	DEP STOL (2020) Concept feasibility study to explore aero-propulsive coupling effect in distributed electric propulsion aircraft⁻	Northwestern Polytechnical University	NA	[126]
	Flying-V (2020) Concept feasibility study of a Flying-V aircraft	TU Delft	Geometric Scaling (4.65%)	[127, 128]

3.2.2. APPLICATIONS USING PHENOMENOLOGICAL TESTS

Phenomenological SFT models are employed in two main types of applications:

1. **In-flight evaluation of novel designs and technologies**: preliminary test to understand the potential impact of unconventional design, novel control-system or technology on the overall flight performance and behaviour. For example, to validate flight control laws or to study the noise of emission of an unconventional aircraft during approach.

2. **Complementing ground testing**: tests that cannot be performed using ground based tests such as the evaluation of the effect of a propulsion unit design on take-off length. [29, 129]

Here, design is more involved than demonstration tests, as the specific phenomenon being tested must be replicated in addition to satisfying the requirements of a demonstrator test. There are a number of design methods that are typically used to design sub-scale models (discussed further in Chapter 4). For phenomenological tests, engineers often apply the simplest scaling method, known as geometric scaling. The results of such tests are only applicable to the prototype if there are no scale effects, which is difficult to avoid in practice. Nevertheless, geometrically scaled models are considered to be sufficient to get a preliminary qualitative understanding of the prototype behavior [41, 42]. Table 3.3 lists examples of SFT used in phenomenological testing.

3

Table 3.3
Past sub-scale flight tests used for phenomenological testing

Model Image	Model Description	Organizations	Design approach	Refs.
	Super-Ximango (2008) Test to characterize aerodynamic performance and stability	University of Arizona, Advanced Ceramics Research	Geometric Scaling (20%)	[130]
	DEMON (2009) Extension of ECLIPSE model to get a better understanding of underlying aerodynamic phenomena	BAE Systems, Imperial College London, Universities of Cranfield, Leicester, Liverpool, Manchester, Nottingham, Southampton, Warwick, Wales and York	Computationally scaled model of ECLIPSE model	[43, 44, 105, 117, 118]
	PTERA (2014) Test to characterize aerodynamic performance and stability	NASA	Geometric Scaling (11%)	[29]
	GA-USTAR (2017) Test to understand stall/upset aerodynamic behaviour of a Cessna 182 model	University of Illinois at Urbana–Champaign	Geometric Scaling (20%)	[131]

Table 3.3 – continued from previous page

Model Image	Model name and goal	Organizations	Design approach	Refs.
	Super-STOL (2019) Test-bed to determine the effect of propeller, wing, and flap design on maximum achievable lift coefficient	Massachusetts Institute of Technology	Geometric Scaling (30%)	[129]
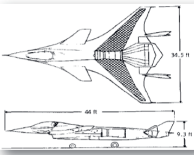
3.2.3. Applications employing Simulation Tests

Simulation tests are used to study the performance or in-flight behaviour of specific full-scale aircraft design after sufficient design maturity has been attained (Figure 2.11). Although the applications of simulation tests appear similar to that of phenomenological tests, the difference is that the results of the former are only applicable to a specific vehicle configuration and the latter is intended for generalized understanding of the underlying phenomenon. Simulation SFT have been used in the following applications:

1. **Aerodynamic performance evaluation**: drag estimation, high angle of attack behavior, and high side-slip angle characteristics

2. **Flight dynamics evaluation**: estimation of stability and control derivatives, manoeuvre performance, and handling qualities

3. **Safety and loss of control situation**: simulate extreme flight envelope scenario to determine the safety of a design
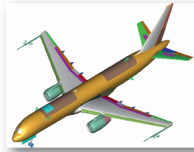
Table 3.4
Past sub-scale flight tests used for simulation testing

Model Image	Model name and goal	Organizations	Design approach	Refs.
	HiMAT (1979) Simulate the manoeuvre performance of the prototype with a model that handles 12g at sub-sonic and 10 g at supersonic speed	NASA	Computationally Scaled (44%)	[97–100]
			Continued on next page	

Table 3.4 – continued from previous page

Model Image	Model name and goal	Organizations	Design approach	Refs.
	NEXST-1 (2005) Simulate the supersonic aircraft drag prediction. The results of the test were correlated with CFD which showed a good match	Japan Aerospace Exploration Agency, Sankoh Software DEPT. Co. LTD	Geometric Scaling	[90]
	AirSTAR (2006) Simulate prototype flight dynamics and loss-of control situations	NASA	Geometric Scaling (5.5%) & Froude number scaling	[89, 132]
	X-48B (2007) Simulate flight performance, stability characteristics, high angle of attack behavior, and high side-slip angle behavior of blended-wing body	NASA, Boeing	Geometric scaling (8.5%)	[88, 133, 134]
	Generic Future Fighter (2010) Test to study vortex induced at the canard of a fighter-aircraft and its effects on the aircraft	Linköping University	Computationally Scaled (13%)	[135, 136]
	Cirrus SR22T scaled (2018) Test for dynamics model validation by matching inertia	University of Illinois at Urbana-Champaign	Geometric Scaling (21%) & Mass Scaled	[79, 137]

Table 3.4 – continued from previous page

Model Image	Model name and goal	Organizations	Design approach	Refs.
	e-Genius Mod (2019) Test with modified airfoils to match full-scale glider behaviour	University of Stuttgart	Computationally Scaled (33.3%)	[28]

It is interesting that computationally scaled models (discussed further in Chapter 4) have been mainly used in simulation SFT cases, which makes scaling for simulation very challenging. Despite numerous simulation SFT tests, only a handful of simulation SFT results have been validated. In some cases such as X-48B, e-Genius Mod and NEXST [28, 90, 134], the authors claim similitude between the model and the prototype but very little quantitative information is provided. Examples of past simulation SFTs are shown in Table 3.4.

3.3. Key tasks in SFT

Based on the review of the literature, we have identified and classified the key tasks that must be performed to accomplish SFT. These tasks can be grouped into four main sub-categories (Figure 3.4), as follows:

1. The design of the SFT model

2. Manufacture of the model and installation of COTS components

3. Planning and execution of flight test

4. Interpretation and scale-up of SFT results to predict the prototype behaviour.

While many works in the literature deal with one or two of the these categories, all of them are rarely treated together. Nevertheless, it is important to note that these tasks are inter-linked. A bad design makes the model unsuitable for flight or poorly similar to the prototype whereas bad realization (i.e., manufacturing or flight test) of SFT will adversely affect the quality of the results, thus, rendering the test useless. Thus, every SFT design must holistically deal with these aspects to improve the applicability and use of SFT. This is discussed further in Chapters 4 - 7. Each sub-category of tasks is briefly described in the following sections.

3.3.1. SFT Model Design
Certification Compliance: Unlike other testing methods, no direct constraints are imposed on the size of the model in SFT as long as the model can take-off, perform the required mission and land safely. To alleviate the risk of damage in the event of crash,
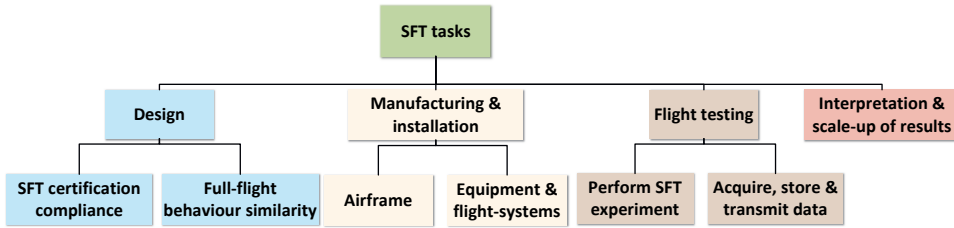
Figure 3.4: Overview of key tasks in SFT

3

most governmental authorities impose certification requirements, which typically include the maximum weight of the model and the dimensions of the flight box of the model (i.e., the farthest distance in the airspace to which the model can be flown from the point of lift-off). These requirements must be taken into consideration during the design of the model. For example, if the flight-box is small, the model needs to make sharp turns, which can lead to high forces on the model and must be accounted in the structural design of the model.

Furthermore, the mission profile of SFT (i.e., a detailed description of an aircraft's flight path and its in-flight activities) needs to be such that the model can perform the manoeuvres of interest within the available airspace. For example, in the study of flight dynamics behaviour, the SFT model must be able to return back to its equilibrium after being perturbed from steady level flight within the flight-box to successfully complete the test. Inability to finish the required motion or manoeuvre within the flight box, renders the SFT unusable to for that study.

Similarity to the prototype: The key aim of a sub-scale model simulation test is to predict prototype behaviour, which is possible only if the behaviour of the sub-scale model is similar to prototype. In the context of similarity, numerous questions must be answered. For example, when is a model said to be similar to a prototype? What methods can be used to make sure that a model behaviour is similar to the prototype? Furthermore, even in case of similarity between a model and the prototype, how can the results of SFT be used to predict full-scale behaviour.

These questions have been asked for over a century in numerous fields. Chapter 4 provides a detailed overview of the evolution of similitude criteria and how they can be used in the design of sub-scale model to ensure with the prototype. Despite numerous similitude criteria, the applicability of the these criteria is often limited owing to vast differences in the test conditions of the model and the prototype.

3.3.2. MANUFACTURE OF AIRFRAME AND INSTALLATION OF COTS COMPONENTS

Once designed, the SFT must be manufactured, which involves two main tasks, namely, manufacture of the airframe and installation of equipment necessary for SFT (Figure 3.4). The airframe typically includes the skins, ribs, spars, frames, bulkhead etc. Often, for sub-scale models under 0.5 m span, the monocoque structure is sufficient (i.e., skins carry all the structural loads) [138]. However, for larger models, other structural

components might be necessary depending on the mission. The equipment includes the engines, landing gear, batteries, actuators, flight controller etc. and the components needed to measure the flight behaviour such as pitot tubes, inertial measurement units, accelerometers etc. Depending on the requirements and scale of the model, these components are either purchased commercially off the shelf or manufactured in-house to meet specific requirements.

3.3.3. FLIGHT TEST AND DATA ACQUISITION

At the end of manufacturing phase, the SFT must be performed which includes training the pilot, multiple ground tests and performing the required mission. Furthermore, appropriate mechanism should be set in place to capture, store and transmit data collected by various equipment in flight. Reader is referred to the work of Sobron et al. [47], Jordan et al. [89], Kuehme et al. [29] and Hueschen [139] for more details on the selection and integration of equipment and its use for testing.

3.3.4. INTERPRETATION OF THE SFT RESULTS

After the required measurements are recorded, they must be used to predict the prototype behaviour (in simulation and phenomenological tests). This process is known as ***scale-up*** of results. As a general rule, scale-up is only possible if the model experiences shape of the streamlines, forces and moments that are similar to the prototype (i.e., their ratios are equal) as discussed in Chapter 4.

Often, complete similarity of the flow-field (i.e., velocity, density and acceleration at different points in flow over space and time), forces and moments is not possible due to differences in shape, size and test-conditions of the model. In such cases, engineers utilize partially similar models (i.e., only certain forces, moments and streamlines are similar) to study a specific aspect of full-scale aircraft behaviour. Furthermore, the methodology of scaling up the SFT results in case of partially similar models also depends on the design approach. A detailed treatment of different SFT model design strategies, different types of partial similarity (also known as scaling laws), the conditions for similarity per SFT model design approach and the corresponding methodology for the scale-up of results is discussed in Chapter 4.

4

A REVIEW OF SUB-SCALE MODEL DESIGN APPROACHES

The fundamental purpose of a sub-scale model is to predict (a specific aspect of) the behaviour and performance of prototype, which is only possible if model behaviour is similar to prototype. As discussed in Chapter 3, the design of the sub-scale model drives the extent of similarity between model and prototype. Thus, similarity requirements must be an integral part of sub-scale model design process to ensure similitude. Numerous similitude theories have been developed in the last century that can be used in the sub-scale model design process to establish similarity between model and prototype. In this chapter, we trace the developments in similitude theories (1761 - present), which range from simple dimensional analysis to the state of the art computational scaling approach. Furthermore, we identify the critical bottlenecks in the current sub-scale model design approaches that will be addressed in the remainder of this dissertation to improve sub-scale model design process and SFT.

A sub-scale model should be designed such that its in-flight behaviour is similar to the prototype, at least for those features that must be studied. In order to determine similarity (or the lack thereof), numerous theories, also known as similitude theories, are available. Attempts to develop such theories started well before the inception of flight, when engineers looked at approaches to avoid *"costly mistakes"* in the design of hydraulic structures, channels and harbors, hydraulic machines and ships [86]. The design approaches for similitude are not limited to SFT. Indeed, most of the concepts discussed in this section originated from the design of sub-scale models other than SFT, although they are applicable to SFT too.

Some of the pioneers who developed theories for model testing were famous scientists such as Froude, Stokes and Reynolds (Section 4.1) [140–142]. While their scaling laws are used till date, they were not an integral part of the model design process until the Buckingham π-theorem [143] and fractional analysis [144] were conceived to formalize the idea of similitude (Section 4.2). These two developments were expanded to formulate the classical similitude theory (Section 4.4). Kline [145] proposed the use of governing equations and approximation theory to establish similitude (Section 4.5). However, this similitude theory had its challenges (Section 4.5.3), which were later overcome by the computational similitude theory developed in the 1990s (Section 4.6). A timeline of evolution of these theories is shown in Table 4.1.

Table 4.1: Evolution of sub-scale model design approaches

Design approach	Year of inception	References
Dimensional Analysis	1761	[140–142, 146]
Model Laws	1915[1]	[85, 86, 143–145, 147–149]
Scaling Laws	1951[2]	[25, 41, 42, 85, 86, 145, 150, 151]
Classical Similitude Theory	1950	[25, 41, 42, 85, 86, 150, 152]
Similitude using governing equations and approximation theory	1965	[85, 145, 147]
Computational Similitude Theory	1990	[103, 147, 153–155]

4.1. DIMENSIONAL ANALYSIS

Dimensional Analysis is a general method by which we deduce information about a phenomenon based on the premise that a phenomenon can be described by a dimensionally

---

[1]Numerous model laws were formulated much before 1915. However, their utility in establishing similitude and generalization only happened after the introduction of Buckingham's π-Theorem.

[2]The idea of scaling laws seemed to be present earlier than this. However, the first formal application and articulation of this idea appears in the work of Langhaar [86].

correct equation constructed using physical parameters that influence the phenomenon [85, 86, 145]. This method can be used to simplify the high-dimensional problems by reducing the number of system parameters, thereby reducing the number of variables to be considered in a test. In addition, dimensional analysis is useful in establishing dimensionless numbers [85, 86, 145] that are convenient figures of merit used to compare the characteristics of a prototype and its model, irrespective of their size. In aerospace applications, dimensional analysis has been used to establish various dimensionless numbers to compare aircraft of varying sizes. Coefficient of lift (C_L), coefficient of drag (C_D), moment coefficient (C_M), coefficient of pressure (C_P), coefficient of thrust (C_T), Reynolds number (Re), Froude number (Fr), Strouhal number (Str) are some commonly used dimensionless numbers.

4.2. MODEL LAWS

Dimensional homogeneity is a sufficient condition to establish a dimensionless number. However, not all dimensionless numbers are meaningful. A dimensionless number can only be used if it influences the phenomenon being tested. For example, nondimensional boundary layer thickness expressed as a ratio of boundary layer thickness to length of a runway is not useful, as the size of the model has no impact on this dimensionless number. However, when the dimensionless number is expressed as the ratio of boundary layer thickness to the mean aerodynamic chord of the model, the dimensionless number can be effectively used to compare model and prototype behaviour.

Mathematically, model laws can be expressed using the following relationship:

$$N_{model_i} = N_{prototype_i} \tag{4.1}$$

where, $i = 1,...,m$, N is a relevant dimensionless number and m is the number of relevant dimensionless terms that are necessary to evaluate the similarity between the model and the prototype [85, 86, 143–145, 147]. Examples of dimensionless numbers used in model laws are Reynolds number, Euler number, Mach number, Froude number, Strouhal number etc. Model laws have been well documented for numerous engineering problems. Eventually, these laws can be easily used without performing laborious dimensional analysis. Some examples of dimensionless numbers commonly used to establish model laws are shown in Table 4.2. There are two methods to determine the dimensionless numbers that must be used in model laws, namely:

1. Fractional Analysis: Rayleigh [144] proposed that the key forces (occasionally energy terms) that affect the phenomenon must be selected by *intuitive* reasoning. The ratios of these forces are then used to predict the model laws using dimensional analysis

2. π-theorem [143, 145]: If m different parameters affect a phenomenon being studied, where the parameters are defined as $q_1, q_2, q_3....q_m$ and can be represented as follows:

$$f(q_1, q_2, q_3..., q_m) = 0 \tag{4.2}$$

then, Equation 4.2 can be re-written as:

$$F(\pi_1, \pi_2, \pi_3, ..., \pi_n) = 0 \tag{4.3}$$

where, $n = m - k$, k is equal to the number of parameters in Equation 4.2 that do not combine into non-dimensional form and $\pi_1, \pi_2, \pi_3, ..., \pi_n$ are non-dimensional parameters. Depending on the phenomenon being studied, the transformation from Equation 4.2 to Equation 4.3 can be mathematically complex. For more details on this transformation in π-theorem, the reader is referred to the work of Langhaar, Kline and Buckingham [86, 143, 145]. These π-terms, when resolved properly, can be used as the dimensionless numbers in the model laws. Thus, the term N in Equation 4.1 can be substituted by these π-terms.

Table 4.2: Dimensionless numbers commonly used to establish model laws in different simulation problems

Problem being studied	Dimensionless numbers
Incompressible flow	⁻Reynolds number, pressure coefficient, Froude number, Weber number
Compressible flows	Reynolds number, Mach number, Prandtl number, specific heat ratio
Flow-excited vibration	Strouhal number
Internal compressible flows	Reynolds number, Mach number, pressure coefficient
Boundary layer thickness	Reynolds number, Womersley number

Challenges in establishing model laws: Experimenters need to know *"a priori"* all the physical variables $(q_1, ..., q_m)$ that influence the test in order to establish the model laws that must be used. In case the model laws are obtained using π-theorem one could end up with π-terms that are completely meaningless if one or more physical variables are not considered. Often, these π-terms are useful when they are defined in hindsight, after understanding the underlying phenomena. For example, if a model is used to predict the drag of a prototype, it is important to include the boundary layer thickness as a physical variable in the application of π-theorem. Without boundary layer thickness, Reynolds number will not be a π-term, which results in a flow dissimilarity between the model and the prototype. In the case of fractional analysis, model-laws are established purely based on intuition of experimenters, which could lead to erroneous conclusions as demonstrated by Kline [145].

Furthermore, once these model laws are defined, engineers aim to make sure that all the model laws are satisfied [85, 86, 145, 147–149]. However, matching all model laws

may not be possible owing to differences in the model, shape, size and test conditions. For example, a football and a section of a wing can have the same Reynolds number. However, the development of boundary layer is not same for the two because of the dissimilarity in their geometrical shapes which results in differences in the airflow around them and the forces acting on them. Thus, the differences in geometrical shapes and the consequent affect of the flow around the body and forces must be accounted for, which is done using scaling laws.

4.3. SCALING LAWS

Scaling laws are necessary to define the relationship between a prototype and its model. Such laws are useful in describing their relative geometrical shapes, the flow around their bodies and ratios of forces acting on the model and prototype, such that they are not vastly different in their behaviour as explained in the preceding section. Langhaar [86] mathematically described the scaling laws between a prototype and a model using the following relations:

$$x^{'} = K_x x, \qquad y^{'} = K_y y, \qquad z^{'} = K_z z, \qquad t^{'} = K_t t, \qquad m^{'} = K_m m \qquad (4.4)$$

where (x, y, z) and $(x^{'}, y^{'}, z^{'})$ are the Cartesian reference frames of the prototype and the model respectively in which each point on the prototype and the model adhere to the relationship in Equation 4.4. t and $t^{'}$ are the time-periods of the motion of prototype and the model. m and $m^{'}$ are the masses of prototype and model. K_x, K_y, K_z, K_t and K_m are constants and known as *scale factors*. The exact value of K_x, K_y, K_z, K_t and K_m are chosen based on the objective of SFT and the test conditions.

These scaling laws are general conditions that must be satisfied when the values of model laws of the prototype and the model are the same. It is not necessary to use all scaling laws simultaneously. Only those scaling laws pertaining to the phenomenon being studied must be used. Six main groups of scaling laws can be identified as follows [25, 85, 86, 145, 147–150]:

1. **Geometric scaling law:** If the prototype and the model have the same shapes, the model is said to be geometrically scaled. Mathematically, $K_x = K_y = K_z$ condition must be satisfied to obtain a geometrically scaled model.

2. **Mass and Inertia scaling law:** When the ratio of masses of all homologous parts of the prototype and the model are kept equal, the two systems are mass scaled. Achieving this type of scaling is challenging due to two reasons. First, mass distribution directly affects inertia which must be accounted for when rotational motion is involved. Second, mass is a function of material density and volume, which in-turn is a function of geometry. Thus, the masses of prototype and model are directly affected by their geometry and the choice of material.

3. **Time scaling law:** For cyclic phenomenon, time scaling is equal to the ratio of time-period of motion of the model and the prototype. For non-cyclic processes, the model is time scaled if both the prototype and the model move such that the

ratio of the time needed to complete any given fraction of the total path to the total time of the motion are equal for the two systems. In other words, K_t is constant throughout the experiment.

4. **Kinematic scaling law:** If the prototype and the model have the same shape of streamlines, they are said to be kinematically similar. Mathematically, kinematic similarity is achieved when every fluid particle around the prototype and the model satisfies the following equations:

$$u' = \frac{K_x}{K_t}u, \qquad\qquad v' = \frac{K_y}{K_t}v, \qquad\qquad w' = \frac{K_z}{K_t}w \qquad (4.5)$$

$$a'_x = \frac{K_x}{K_t^2}a_x, \qquad\qquad a'_y = \frac{K_y}{K_t^2}a_y, \qquad\qquad a'_z = \frac{K_z}{K_t^2}a_z \qquad (4.6)$$

where, u', v', w' and u, v, w are the velocities and a'_x, a'_y, a'_z and a_x, a_y, a_z are the accelerations of the fluid particles around the model and the prototype in x, y, z directions respectively.

5. **Dynamic scaling law:** If the homologous parts of a prototype and its model experience forces whose ratio is constant, the two systems are dynamically scaled. Mathematically, based on Equation 4.4, dynamic similarity can be expressed as follows:

$$F'_x = \frac{K_m K_x}{K_t^2}F_x, \qquad\qquad F'_y = \frac{K_m K_y}{K_t^2}F_y, \qquad\qquad F'_z = \frac{K_m K_z}{K_t^2}F_z \qquad (4.7)$$

where, F'_x, F'_y, F'_z and F_x, F_y, F_z are the net forces experienced by the fluid particles moving around the model and the prototype in x, y, z directions respectively. By combining Equations 4.6 and 4.7, we can conclude that dynamic similarity exists, if the systems are kinematically similar and the mass distributions are similar (i.e., mass scaled).

6. **Structural scaling law:** The scaled model closely reproduces the structural response of the full-scale vehicle [1]. Here, the structural deformation of the model must be similar to the prototype, which is only possible if the stiffness of the model (ratio of the force applied and model deflection) is the same as the prototype at all locations in the model. [151, 153, 156–159] The original structural scaling laws proposed by Goodier and Thomson [151] did not include aeroelastic effects, which are critical in aircraft problems. Wissmann [158] proposed scaling laws for aeroelastic problems in the 1960s. Although structural scaling has been used in ground testing of aircraft, it has not yet been used for aeroelastic testing in flight.

Scaling laws implementation challenge: The implementation of different scaling laws is difficult, especially kinematic and dynamic scaling, owing to challenges in estimating the parameters in Equations 4.5 - 4.7 . This has led scientists to excessively rely on on

geometric scaling, which allows them to easily fix the scaling factors before the start of the experiment. Before 1960, most authors recommended the use of geometric scaling, claiming that similar shapes implied similar flow properties. In fact, this is not true because the stream lines around the model do not scale geometrically with the size of the model. This is because the flow field does not scale as per euclidean geometry but a type of non-euclidean geometry known as differential geometry [147]. Consequently, Equations 4.5, 4.6 and 4.7 cannot be satisfied.
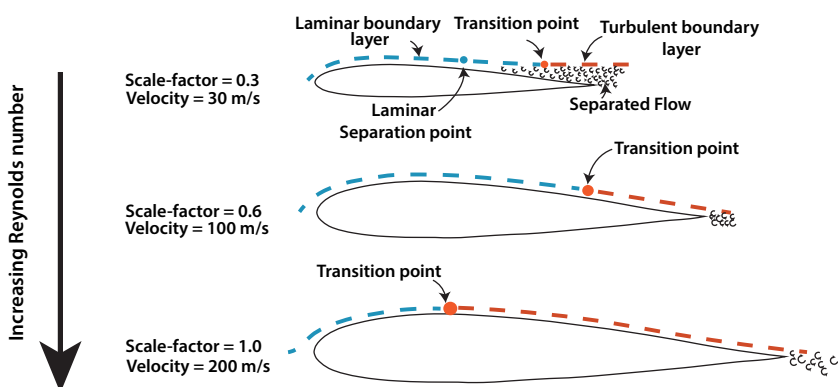
Figure 4.1: Geometrically scaled models do not guarantee geometrically scaled shapes of the boundary layer. This is because the model scales as per Euclidean geometry whereas the flow-field does not [147]. Here, the 30% scaled model has completely different flow characteristics as compared to the prototype due to separation. In case of 60% scaled model, the streamlines have similar shapes but different transition point, which must be corrected to predict prototype behaviour.

For example, for a model with lower Reynolds number (i.e., smaller model with lower testing velocity) as compared to the prototype, the boundary layer changes the flow field so much that it is not representative of the flow field around the prototype. For models with lower Reynolds number, the flow has lower momentum and separates when the flow slows down and pressure increases. This is shown in Figure 4.1, where, two models are scaled geometrically (30% & 60%). The results of SFT using a 30% scaled model in this case will not be representative of the prototype behaviour due to separation. The 60% scaled model has similar shape of streamlines as the prototype but the transition location is different, which much must be accounted and corrected using appropriate numerical or analytical methods to predict prototype behaviour. Thus, geometric scaling is usually neither necessary nor a sufficient condition to establish similitude [147].

Furthermore, surface finish (i.e., surface roughness, debris, insect remains, etc.) also affects the transition location [160–162]. Typically, the effect of surface roughness, which is an artefact of manufacturing and maintenance is not included in geometric scaling. In fact, ensuring the geometric scaling of the roughness can be challenging and would significantly escalate the manufacturing cost of the model. Thus, (complete) geometric

scaling is usually neither necessary nor sufficient condition to ensure similitude [147].

Additionally, the flow fields (artefact of geometrical shape) also have a significant impact on static and dynamic stability, required control power, propulsion, etc. These secondary effects must be carefully assessed during SFT model design. For example, flow separation might make the control surfaces ineffective leading to the complete loss of model.

4.4. CLASSICAL SIMILITUDE THEORY

The classical similitude theory is one of the most widely used method in sub-scale modelling problems. [25, 41, 42, 85, 86, 148–150, 152] The concept of classical similitude theory is captured best by the definition provided by Langhaar [86], which is as follows: *A function f' is similar to function f, provided the ratio for f' / f is a constant, when the functions are evaluated for homologous points and homologous times. The constant ratio, f' / f = K_f, is called the scale factor.*

f and f' are abstract scalar function defining a state of the prototype and the model. In this definition, the homologous point refers to the same relative position on the reference frames in which the two systems are described and the homologous time refers to the same fraction of time period in which the two systems describe the paths of their trajectories. Notably, homologous times are only used to study time variable states.

This definition of Langhaar [86], though accurate, is rather abstract. The challenge of reducing the complex design aspects of models and prototypes into an *"abstract scalar function"* makes the use of this definition difficult. Years of research in the field of sub-scale flight testing have been invested in finding the right scalar function (i.e., similitude criteria). [25, 85, 86, 148–150, 152]

In essence, classical similitude theory is the process of reducing complex design parameters associated with prototypes and their models into tangible scalar functions, such that they can be measured and effectively used to compare the behavior of model and prototype. In this paper, we attempt to summarize and unify the different versions of classical similitude theory using one set of nomenclature and definitions and then maintain it consistently to allow readers to easily understand the state of the art.

The model laws and scaling laws are primitive attempts at arriving at the scalar function described by Langhaar [86]. However, individually these laws cannot be used effectively to design a sub-scale model owing to the limitations listed in the preceding sections. Classical similitude theory combines model laws and scaling laws to establish similitude. The model laws and scaling laws that must be satisfied for a phenomenon being studied are determined by studying a large number of past experiments. These model laws and scaling laws that must be satisfied to study prototype behaviour are known as *similitude criteria*. The similitude criteria needed for common applications are well documented by Wolowicz et al. [42] and forms the basis for a majority of sub-scale model tests.

Once the similitude criteria that affect the phenomenon being tested are selected, they lead to a set of equations whose solution determines the size, shape, mass and inertia of the model and the test conditions. The general methodology of implementing classical similitude theory is shown with the Unified Modeling Language (UML) activity

diagram in Figure 4.2. The classical similitude theory can be used for a myriad of problems, one such problem is shown with Example A.1 in Appendix A to help the reader get an understanding of classical similitude theory.
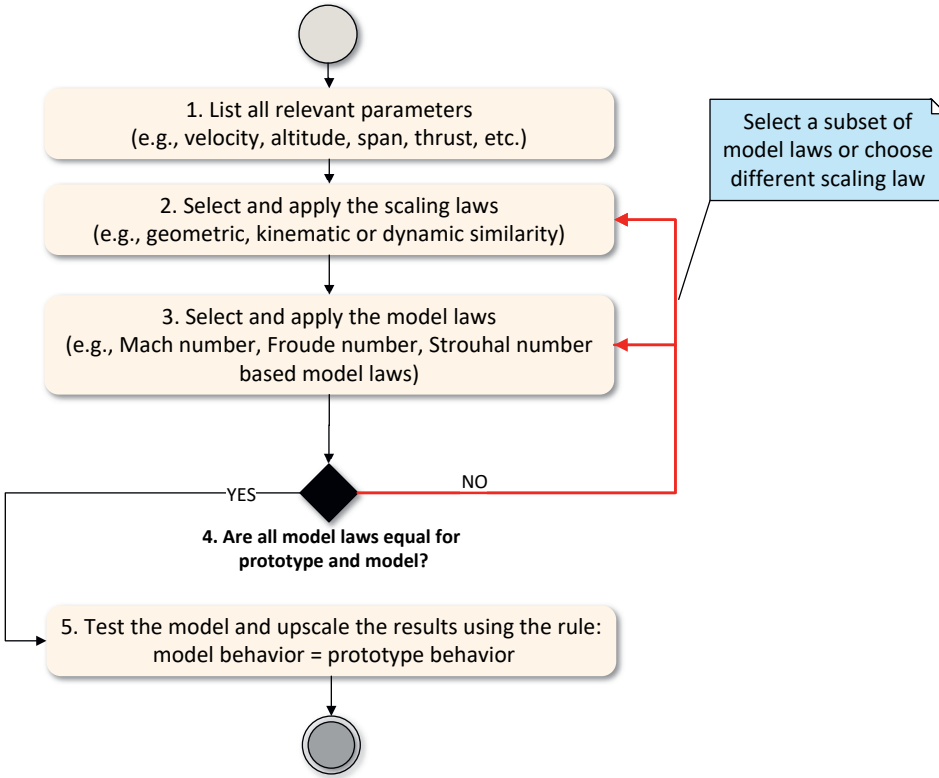
Figure 4.2: UML activity diagram capturing the tasks in classical similitude theory

Limitations of classical similitude theory: While the key benefit of using classical similitude theory is that the labor involved in determining the similitude criteria is very small and the associated mathematics required to solve them is not rigorous [145], it has a practical limitation that constantly challenges the scientists known as the *scale effects*. All relevant model and scaling laws (called similitude criteria) must be solved together to arrive at a sub-scale model whose size, shape, and the test conditions are such that its behaviour is similar to the prototype. However, solving such similitude criteria leads to an over constrained problems. In particular, model laws cannot be satisfied simultaneously due to certification requirements, limitations of the testing equipment, cost limitation, etc. as shown in Appendix A.

These over-constrained problems are often solved by selecting some of the model law(s) based on experience and ignoring others (see Appendix A). The discrepancy in

the results owing to the ignored model laws are termed as scale effects. These scale effects are corrected either using legacy information from previous tests (if available) or by resorting to the experience of the engineer. This might be possible for conventional designs where flight data of similar full-scale aircraft are available. Whereas, for unconventional designs, due to lack of data, results prone to scale effects cannot be scaled up.

4.5. SIMILITUDE WITH GOVERNING EQUATIONS AND APPROXIMATION THEORY

4.5.1. SIMILITUDE THEORY BASED ON GOVERNING EQUATIONS

Kline [145] proposed the use of analytical methods (governing equations) to overcome the limitations of classical similitude theory. He argued that a similitude criterion that is applied to every infinitesimal element of a model will apply to the whole body, as long as both the model and the prototype belong to the same class of problems. He defined *a class of problems* as a group of problems that obey the same governing equations and boundary conditions. Kline defined similitude between any two systems as follows [145]:

"If two systems obey same governing equations and boundary conditions and if values of all coefficients in these equations and boundary conditions are made the same, then the two systems must exhibit similar behavior provided a unique solution to this set of equations and boundary conditions exist."

As a consequence, even without solving the governing equations, sufficient information to establish a similitude between the model and the prototype can be obtained by comparing the coefficients of the normalized governing equations. An obvious problem in comparing the coefficients in the governing equations is the variation of values due to the differences in the size of the model and the prototype. Kline further proposed a two-step approach to normalize governing equations and the associated boundary conditions to allow the comparison of coefficients as follows [145]:

1. make all the variables in the governing equations dimensionless

2. make all the equations dimensionless

He called this approach normalization of governing equations. A normalized equation contains two sets of terms. The first set is composed of dimensionless independent variables that affect the phenomenon under study (i.e., variables in the original dimensional governing equations). The second set is made up of dimensionless physical parameters which are system properties or physical constants. For example, the Navier-Stokes equation, ignoring the time dependent terms and the z-components terms, is reduced to dimensionless form as follows:

x-momentum equation:

$$\overline{u}\frac{\partial \overline{u}}{\partial \overline{x}} + \overline{v}\frac{\partial \overline{u}}{\partial \overline{y}} = -\frac{\Delta p_L}{\rho U^2}\left(\frac{L}{\delta}\right)^2 \frac{\partial \overline{p}}{\partial \overline{x}} + \frac{\nu}{UL}\left(\frac{\partial^2 \overline{u}}{\partial \overline{x}^2} + \left(\frac{L}{\delta}\right)^2 \frac{\partial^2 \overline{u}}{\partial \overline{y}^2}\right) \tag{4.8}$$

y-momentum equation:

$$\overline{u}\frac{\partial\overline{v}}{\partial\overline{x}} + \overline{v}\frac{\partial\overline{v}}{\partial\overline{y}} = -\frac{\Delta p_L}{\rho U^2}\left(\frac{L}{\delta}\right)^2\frac{\partial\overline{p}}{\partial\overline{y}} + \frac{\nu}{UL}\left(\frac{\partial^2\overline{v}}{\partial\overline{x}^2} + \left(\frac{L}{\delta}\right)^2\frac{\partial^2\overline{v}}{\partial\overline{y}^2}\right)$$

(4.9)

here, the dimensionless independent variables are

$$\overline{x} = \frac{x}{L}, \qquad \overline{y} = \frac{y}{\delta}, \qquad \overline{u} = \frac{u}{U}, \qquad \overline{v} = \frac{v}{V}, \qquad \overline{p} = \frac{p}{\Delta p_L}$$

(4.10)

and the dimensionless physical parameters are

$$\pi_1 = \frac{UL}{\nu}, \qquad \pi_2 = \left(\frac{L}{\delta}\right)^2, \qquad \pi_3 = \frac{\Delta p_L}{\rho U^2}$$

(4.11)

where, L is the length of the object, δ is the boundary layer thickness, U and V are the x- and y-component of the velocity far upstream, Δp_L is the largest pressure difference between two points on the body, x is the x-coordinate, y is the y-coordinate, u is the x-component of the velocity, v is the y-component of the velocity, ν is the kinematic viscosity, ρ is the density, and p is the pressure. It can be noted that π_1 is the Reynolds number and π_3 is the coefficient of pressure.

Thus, if the model and the prototype belong to the same class of problems and have a unique solution in the domain of the tests, the similitude criteria are the coefficients of the normalized governing equations and the associated boundary conditions. These similitude criteria must then be satisfied by performing appropriate *transformations*, thus altering the shape and size of the model and varying the test conditions suitably so that model and prototype have the same coefficients. This is shown using the activity diagram in Figure 4.3. In addition, the application of this iterative process is shown using Example B.1 in Appendix B.

A key consequence of the application of this theory is that the model and prototype, in general, do not retain the same shape i.e., the model is not geometrically scaled. Consequently, these changes may result in model designs that do not belong to the same class of problems as the prototype. In other words, the model and the prototype may not follow the same governing equations. For example, if inviscid theory governing equations are used to model the flow properties, it might be applicable to the full-scale aircraft which has a thin boundary layer. However, for a distorted sub-scale model, the same governing equations might not be applicable anymore. Thus, similitude cannot always be established. In some cases, the reverse is also true, i.e., the model and the prototype belong to the same class of problems only after transformation. Kline [145] demonstrated specific cases where the model and the prototype belong to the same class of problems after the transformation. For example, he showed how distorting the models helps in capturing compressibility effects (see Appendix B) [145].

However, despite the best efforts in transforming the model, similitude criteria cannot be satisfied [163]. Consequently, like the classical similitude theory, the issue of scale
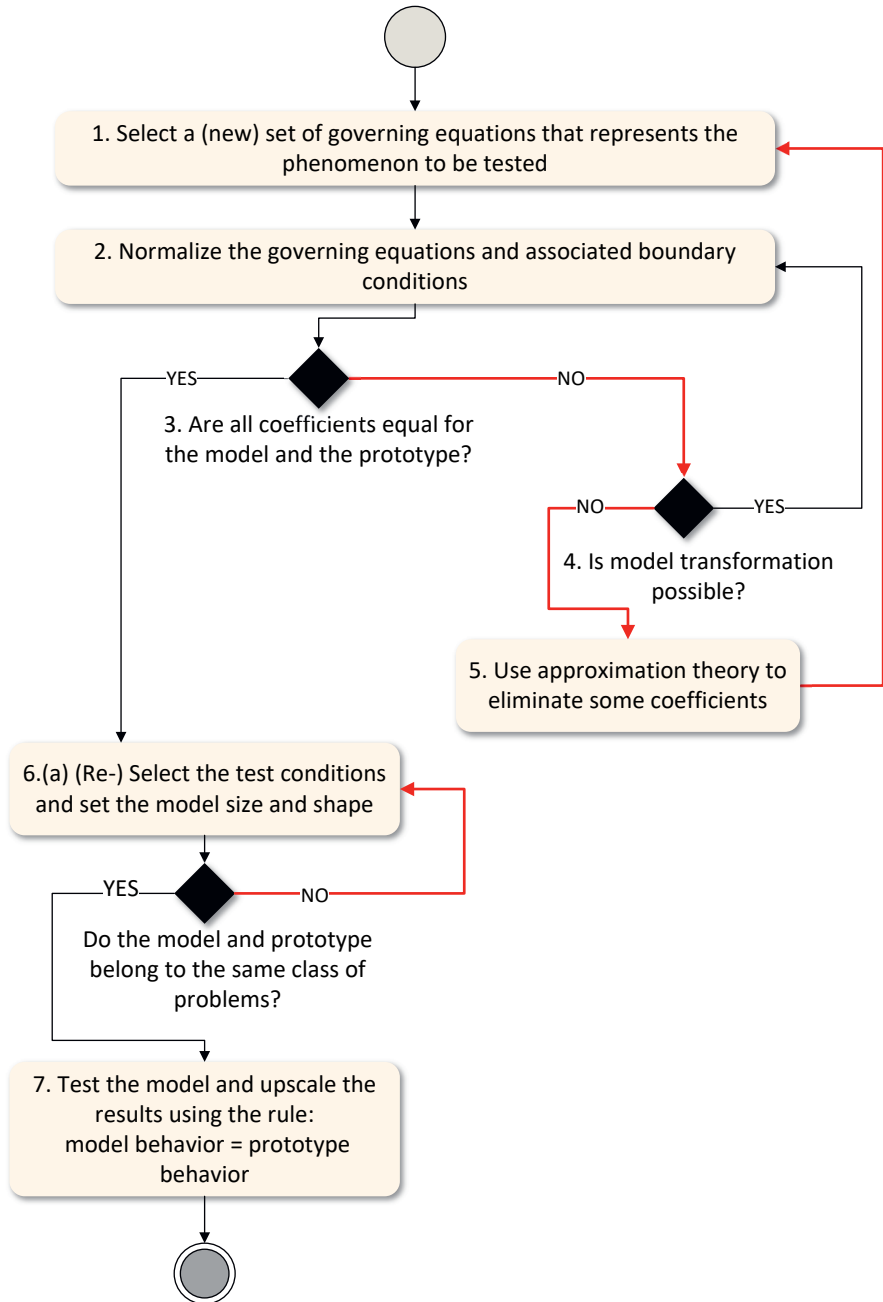
Figure 4.3: UML activity diagram of similitude theory using governing equations and approximation theory

effects persists as all coefficients cannot be matched simultaneously. Nevertheless, when sub-scale models are designed using similitude criteria based on governing equations, better results than classical similitude theory can be obtained, as the former takes the entire flow field into account in the design, unlike the latter, which uses generalized laws. Furthermore, the method employing governing equations provides insights into which similitude criterion might be ignored as explained in the following section.

4.5.2. Governing Equations and Approximation Theory to establish Similitude

The coefficients of governing equations in Kline's [145] method are analogous to model laws and scaling laws in classical similitude theory [85]. Just as all model laws and scaling laws cannot be matched, all the coefficients in the governing equations cannot be matched. To overcome this problem, Kline introduced approximation theory [145] that allows the experimenters to ignore those model laws that are not completely necessary for the simulation of the phenomenon. Application of approximation theory is shown as part of Example B.1 in Appendix B.

Kline [145] proposed a careful consideration of the normalized governing equations. If any coefficient in the normalized governing equation is insignificant as compared to the scale of the equations (i.e., $<< 1$), the coefficient is ignored as it has little or no effect on the similitude. This method of simplifying the similitude criteria is known as approximation theory [145]. Thus, after setting appropriate test conditions and selecting the model shape and size, if all the coefficients cannot be matched, certain terms that do not contribute to the phenomenon being tested are neglected after careful mathematical analysis. If no coefficient can be eliminated by applying the approximation theory, test conditions and/or model shape and size must be altered (i.e., transformed, see activity diagram in Figure 4.3).

One could argue that neglecting terms in governing equations is comparable to ignoring model laws in classical similitude theory. Nonetheless, there is a significant difference. In classical similitude theory, we ignore model laws by intuitive feeling. However, Kline's approximation theory neglects coefficients only after analyzing its significance in the governing equations. For example, in the normalized Navier-Stokes equation (see Equation 4.8 and 4.9), for very high Reynolds number problem, one might be tempted to ignore the terms multiplied by the inverse of Reynolds number in the absence of governing equations. This approximation is not correct because L/δ term may have a high numerical value. Consequently, the product of L/δ and $1/Re$ shown in Equation 4.8 and 4.9 may not be insignificant. Since insights about the combined influence of various π terms derived using the π-theorem is not available in classical similitude theory, ignoring π terms becomes challenging.

4.5.3. Limitations of Similitude Theory with Governing Equations and Approximation Theory

Including governing equations and approximation theory in establishing similitude criteria offers several improvements over classical similitude theory such as improving the rationale in selecting dimensionless numbers, reducing dependence on legacy information and experience of the experimenters, and developing appropriate justification

for discarding dimensionless numbers from similitude criteria. Nevertheless, establishing similitude criteria using governing equations and approximation theory poses other challenges, namely:

1. The governing equations are not always available. Even if the governing equations are obtained, ensuring that model and prototype belong to the same class of problems is difficult.

2. The governing equations combined with boundary conditions often do not have a unique solution (indicated using red arrows in Figure 4.3). Thus, similarity criteria cannot be established with the selected governing equations and a different set of governing equations must be selected or developed.

3. The differences in the size of the model and the full-scale aircraft make it challenging to match all the similitude criteria by transforming the coefficients of governing equations (by altering the model geometry and test conditions). Even in cases where it is possible, it is a laborious and time-consuming task.

4. Normalizing governing equations is a rigorous mathematical effort. Furthermore, establishing normalized governing equations and the associated approximation theory for multiple disciplines is often impossible.

5. Combined use of governing equations and approximation theory cannot guarantee similitude as all the coefficients for both model and prototype must be equal. Only in some specific cases, similitude is possible. In other words, following all the steps shown in the Figure 4.3 does not guarantee a similar sub-scale model.

6. This method provides a Boolean output, i.e., whether similitude is achieved or not. It does not express the extent of similitude when all the similitude criteria are not satisfied. For example, it would be useful for experimenters to know that their model has attained 80% of similarity for the phenomenon being tested, which can be used in the scale-up process by assigning uncertainty values to scaled-up values of performance parameters. Unfortunately, this figure of merit cannot be extracted from any of the methods describe thus far.

4.6. COMPUTATIONAL SIMILITUDE THEORY

The method proposed by Kline [145] focused on establishing normalized governing equations and then utilizing them without actually solving these equations. An alternative approach is to solve these governing equations to determine the similitude criteria. Baker et al. [85] were the first to demonstrate the use of the solution of governing equations to establish a similitude relationship. While the examples shown by Baker et al. [85] could be solved analytically, unfortunately, most similitude problems are complicated and not easily solvable.

With improvements in computing power and the development of powerful solvers, many governing equations have become numerically solvable, albeit approximately by discretization such as Computational Fluid Dynamics (CFD) and Finite Element Methods. This opens up the possibility of comparing the behavior of the model and the prototype to ensure they match before starting with complex and expensive manufacturing

and testing activities. Although these computational methods have their limitations as detailed in Section 2.1, they can be used for preliminary design of sub-scale models. After execution of SFT, the results can be used to study the uncertainty of the methods and validity of underlying assumptions in the computational simulations. Bushnell [164], in his review, opines that "*numerical simulations can increasingly include the influences of the various scaling issues. Computational methodologies are becoming the approach of choice for (flight behaviour) prediction, with the wind tunnel increasingly relegated to a supporting computational tool validation role*". Thus, these computational methods can be used as a bridge to link the in-flight behaviour of the sub-scale model and the full-scale aircraft as explained in the following paragraphs.

The approach of solving governing equations to arrive at an approximate solution using computational analysis is a significant departure from the method proposed by Kline, where, similitude is established without actually solving the governing equations. In this section, we group all the sub-scale model tests that use computational analysis to establish scaling laws into a broad category known as *computational scaling laws*. The models developed using computational scaling laws are called computationally scaled models. For problems with single disciplines, many authors refer to computational scaling with the name of the discipline. For example, aerodynamic scaling, structural scaling, thermal scaling, etc. [50].

Despite the capabilities of computational tools, comparing the behavior of the prototype and its model is challenging. Similar to Kline's approach, results of computational analysis of the prototype and its model cannot be directly compared owing to differences in scale. Thus, the results of the computational analysis must be non-dimensionalized to enable the comparison. Furthermore, depending on the problem, the result of the computational analysis might be a very large data-set. For example, in the case of aerodynamic analysis, the result includes forces and moments on the body at different location, velocity scans around the model, the pressure distribution, boundary layer information etc. Comparing such large data-sets is challenging in itself, let alone arriving at a figure of merit that establishes an extent of similitude between the model and the prototype that can be used by the designer to alter model shape and size to enhance the similitude.

Thus, establishing a function, which is composed of non-dimensional parameters affecting the phenomenon being tested, to quantify the *extent of similitude* between prototype and scaled model is a key step in computational scaling approach. This aspect of computational scaling was already recognized by engineers at NASA in the 1970s when they tried to design a 44% sub-scale fighter aircraft which mimicked the aerodynamic behavior of its full-scale counterpart [97–99]. However, the methods developed were only suitable for the specific models developed in HiMAT. After this, most of the SFTs were largely designed using classical similitude theory as shown in Chapter 3 and no developments have been seen with respect to computational scaling until 2005.

In allied sub-scale model testing fields such as wind-tunnel testing, new methods to estimate the extent of similitude have been developed in the last two decades. Pettersson and Rizzi developed functions based on coefficient of lift, drag, and moments to design wind-tunnel test models whose behavior was similar to the prototype [165]. Similar functions have been used to design models for sub-scale flight testing by Bergmann

et al. in glider design [28]. Functions to study aeroelastic similitude have been formulated by multiple authors such as French, Mas Colomer et al., Pereira et al. and Ricciardi et al. [103, 153, 155, 157]. Ricciardi et al. established a fundamental criterion to compare the extent of similitude, called Model Assurance Criterion (MAC), between the structural mode shapes of model and prototype.

Most of these functions are aimed at specific application of aerodynamics or aero-structural analysis using a specific testing methods such as wind-tunnel testing. However, such functions can be formulated for SFT too. As formulating a function of extent of similitude for different applications (e.g., flight dynamics simulation, wind-tunnel testing, etc.) is a time-consuming effort, designers would benefit from a generalized function such as the **Degree of Similitude (DoS)**, which is formulated in this research. DoS is a synthetic measure to establish the extent of similarity and discussed in detail in Chapter 6.

Depending on the phenomena being tested and the flight behaviour to be studied, different formulations of extent of similitude functions can be used to design numerous models, where, each model predicts specific aircraft characteristics. Once a figure of merit is formulated to estimate the extent of similitude, designers can iterate over the design of their models by varying test conditions, size and shape of the model till they arrive at a design which is similar to the prototype for the phenomenon being tested. This is illustrated using the activity diagram in Figure 4.4. Different techniques have been used for design iterations of sub-scale models, as discussed in Section 4.6.1.

The key difference between the preceding similitude theories and the computational similitude theory is that, in the latter case, the iterative design cycle does not result in a generally applicable scaling. For example, the model laws in classical similitude theory shown in Table 4.2 is applied to any model for a given type of problem. In computational scaling, for a specific combination of prototype design and the test objective, a unique scaling law is established to arrive at a model whose response can be scaled up to predict a specific feature (or set thereof) of the prototype behaviour, i.e. the feature defining the test objective. Some examples of test objectives include, simulation of short-period motion, simulation of dutch-roll, study of spin characteristics, study of flutter behaviour or combinations thereof. In general, these computational scaling laws are based on iterative procedures to transform model design and/or test conditions to ensure similitude, as explained in the following section (see red line in Figure 4.4).

4.6.1. Iterative methods for Computational Scaling
Numerical optimization is an obvious choice to enable efficient modification of the sub-scale model design and test conditions to achieve the highest similarity with the prototype. French [103] was one of the first to use optimization in the application of structural similitude. He demonstrated the use of optimization to match the stiffness distribution over the wing. Here, the figure of merit for the extent of similitude was the difference between the normalized deflection along the span of the wing of the model and the prototype. French [103] showed with physical testing that such an optimization-based scaling technique was indeed effective in achieving similarity. While French [103] specifically used this method for the design of wind-tunnel models, similar techniques can be used to design models for SFT.
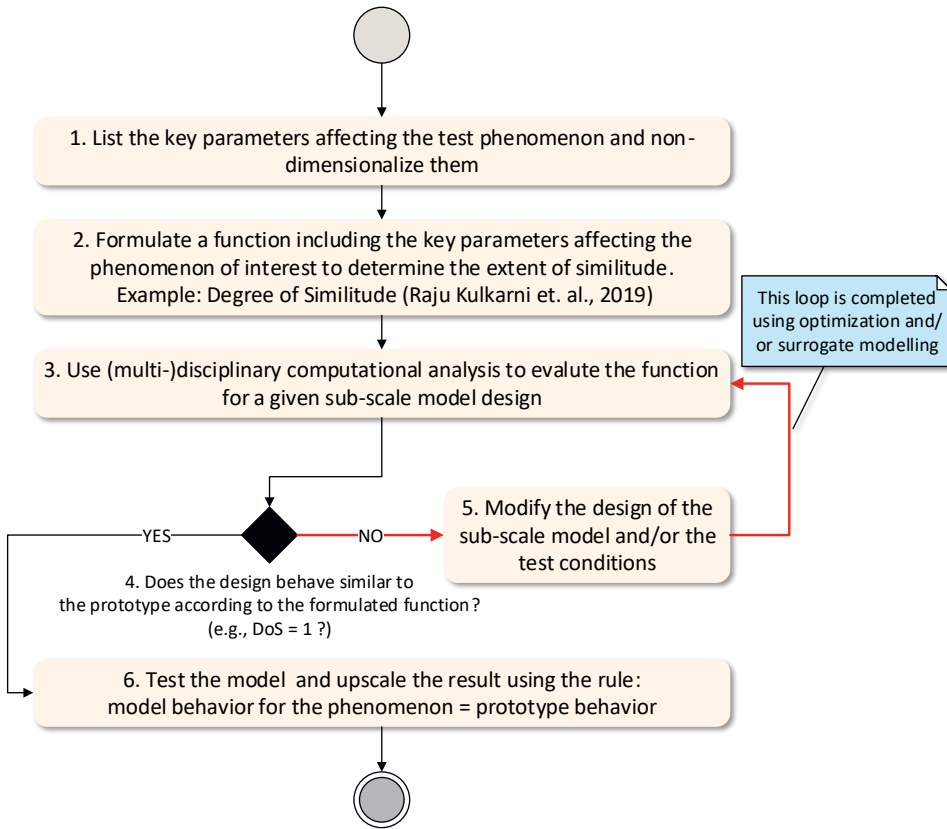
Figure 4.4: UML activity diagram of methodology for computational scaling

Most engineering problems are multi-disciplinary. As a consequence, the use of the methods described in Sections 4.4 and 4.5 can be challenging, as multiple governing equations and a broader set of similitude criteria must be satisfied to design a model similar to prototype. Optimization based scaling laws are much more versatile as they rely on Multi Disciplinary Analysis and Optimization (MDAO) strategies to account for the coupled effects of the various disciplines. In such MDAO problems, the objective function is the figure of merit quantifying the extent of similitude (such as DoS), the design variables are the parameters defining the geometry of the model and the test conditions, and the constraints are a combination of manufacturing and mission requirements, including those set by certification authorities (see Chapter 6).

For example, Pereira et al. [155] used MDO in aeroelasticity problems by ensuring homologous pressure distribution over the model and the prototype while matching the reduced natural frequencies. The design variables were the rib thicknesses under manufacturing constraints. Many other complicated similitude problems in the field of aeroelasticity are solved using optimization [153, 157, 166] as described in the review by Mas

Colomer et al. [153].

The applicability of computational scaling is not limited to aeroelasticity. For example, this method shows great potential in the study of aircraft flight dynamics behavior, where the model must demonstrate multiple-disciplinary similarity with the prototype (i.e., similar aerodynamic behavior, structural behavior and mass distribution). Other studies which include aeroacoustics, aero-propulsive interactions, aero-thermal design, unmanned aerial vehicle design, etc. can also benefit from this method. The computational scaling method is largely unexplored, but demonstrates very high potential. A full exploitation will depend on the ability to address the challenges discussed in Section 4.6.2.

4.6.2. CHALLENGES IN COMPUTATIONAL SCALING

Computational scaling laws are the state of the art in sub-scale model design method for all physical testing methods including SFT. Nevertheless, the state of practice lags behind. There are numerous reasons for this which are detailed as follows:

1. The formulation of the objective function to establish scaling laws is challenging because the design space may be large when all the relevant parameters that affect the phenomenon are selected. Furthermore, most of the formulations of extent of similitude in use today are aimed at specific applications such as aerodynamics and aeroelasticity. Thus, engineers have to expend significant time and resources to formulate a representative figure of merit for other applications.

2. Developing (accurate) computational disciplinary analysis tools, which can be used in an optimization, is a knowledge and labour intensive task.

3. Most computational analyses require repetitive pre/post-processing activities (e.g., generation of computational grids for CFD and FE analysis, post-processing of flow analysis, etc.), which are laborious, time-consuming and error-prone. Because, an iterator is used to modify the design, these pre/post-processing activities must be automated which requires non-trivial investment of time and resources.

4. Even if the disciplinary analysis tools are available and automated, combining them together in a multi-disciplinary analysis framework, selecting the right MDO architecture and optimization algorithm can be challenging tasks, which requires specific knowledge of MDO and numerical optimization techniques.. In other words, barriers associated with MDO must be lowered for experts in the field of SFT to make full use of its potential.

5. The benefits of optimization based scaling laws can be negatively affected by the use of high-order, high-fidelity and time-consuming analyses in the optimization process. To keep the computational time compatible with the usability of SFT in the design process, surrogate-model techniques can be very effective. These surrogate models are analytical approximations of the actual high-fidelity analysis and are orders of magnitude faster to evaluate, thus making the optimization effort time manageable.

4.7. Catalog of Sub-scale Models to Mitigate Scale-effects

In spite of using the appropriate sub-scale design approach and incorporating all the requirements, a critical problem in sub-scale flight testing lies in overcoming scale effects. While scale-effects cannot be eliminated in all the problems, they can be mitigated by not *overloading* the similitude problem. With overloading, we intend the situation where one sub-scale model is expected to replicate many more non-dimensional parameters than physically possible for the combination of model size and test conditions. For the example shown in Appendix A, no suitable model can be found that simultaneously replicates the Reynolds number and Froude number of the prototype; such a similitude problem is said to be overloaded. Consequently, one sub-scale model cannot completely simulate the prototype behavior for the phenomenon being tested.

Szücs proposed the theory of partial modeling to overcome the overloading problem in sub-scale model testing [147]. Partial modeling involves the sub-division of a complex system into sub-systems called partial models and studying each of the partial models separately to understand a specific aspect of prototype behaviour. Szücs then proposed the combination of results of partial model tests to predict the behavior of the complex system. When this concept was first proposed in 1980, the implementation was rather abstract without a concrete methodology.

With the introduction of computational scaling, we can use Szücs' postulate to simulate prototype behavior by designing, manufacturing, and testing a ***catalog of sub-scale models*** i.e., multiple sub-scale models, each one designed to offer the best similarity as required to a specific test condition or phenomenon. The results of these tests are then integrated to determine the overall prototype behavior. However, integrating the results of sub-system can be quite challenging to implement. Thus, for the progress of SFT research, an appropriate methodology to create the catalog of sub-scale models must be identified and formalized.

One approach is to use equations of motions to list all the parameters relevant to characterize prototype behavior and then classify them into sub-groups. Thereafter, per sub-group, a scalar function like the must be formulated (e.g. Degree of Similitude (DoS) discussed in Chapter 6). For each DoS, an optimal model (i.e., DoS = 1) must be designed using computational scaling and tested. The results of these tests can be combined together to predict prototype behavior.

For example, the aerodynamic derivatives ($C_{m_q}, C_{z_q}, C_{z_\alpha}$ and C_{m_α}), non- dimensionalized mass and inertia can be used in the formulation of DoS for one model to study short-period motion and aerodynamic derivatives (C_z, C_{x_u} and C_{z_u}) can be used in the formulation of DoS for another model to study phugoid motion. Where, C_{m_α} and C_{m_q} are the derivatives of moment with respect to angle of attack and rotation rate respectively, C_{z_α}, C_{z_u} and C_{z_q} are the derivatives of force in z-direction with respect to angle of attack, velocity and rotation rate respectively and C_{x_u} is the derivatives of force in x-direction with respect to velocity. The behaviour of the two models can be studied together to predict the longitudinal behaviour of the prototype.

The number of designs in a catalog directly impacts the overall cost, effort and time needed to simulate prototype behavior. Hence, a cost-benefit analysis of utilizing a cat-

alog of sub-scale models must be performed before embarking on the process. If the size of this catalog is too large, SFT is not viable as its unique selling proposition of being an affordable simulation method is lost. The catalog size can be decreased by reducing the number of governing parameter sub-groups and thereby the number of designs. Besides, each sub-scale model should be manufactured modularly. As a result, if two or more models have similar components, they can be reused. For example, if the tail design changes, while the rest of the components are unaltered, modular design can be used to just replace the tail. Thus, a catalog of modularly designed sub-scale models using computationally scaling has the potential to mitigate scale-effects.

4.8. Design methods employed in SFT

Despite the increased use of SFT to study unconventional aircraft designs, it is interesting to note that many SFTs have no equivalent full-scale counterpart, i.e., there is no full-scale aircraft design (about 36% of the 25 SFTs reviewed). As a result, they do not use any of the similitude methods discussed in the preceding sections. About 48% of the 25 SFT models reviewed in this paper were geometrically scaled (shown in Figure 4.5). The primary reason for this is the ease of applying geometrical scaling as compared to other scaling laws. Nonetheless, the response of geometrically scaled models is often prone to scale effects, which leads to significant uncertainty in results. Thus, the results of tests are mostly relevant to demonstration tests. Finally, 16% of the models that were studied were computationally scaled. This type of scaling ensures that the specific disciplinary behavior of the model is similar to that of the prototype. It is interesting to note that engineers working on HiMAT [98, 99] utilized principles of computational scaling as early as 1976. However, the complexity of performing computational analysis in those days prevented the widespread use of this method. With tremendous improvements in computational power, researchers have been using computational scaling more frequently in the recent years.
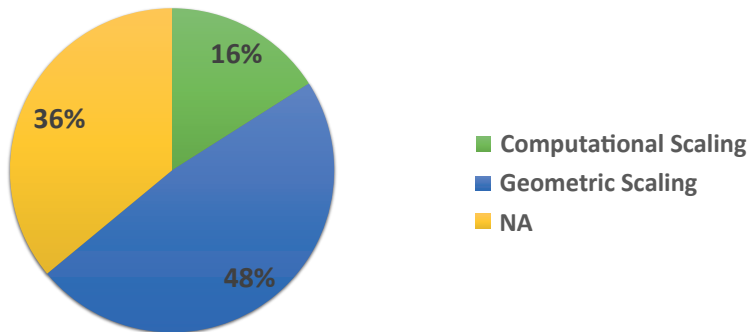
Figure 4.5: Distribution of 25 SFTs (reviewed in this paper) based on design approach. Here, 'NA' implies scaling criteria are not used at all as there is no full-scale aircraft design and the SFT is solely intended for demonstration tests.

Review of design approaches shows that engineers performing SFT recognize the im-
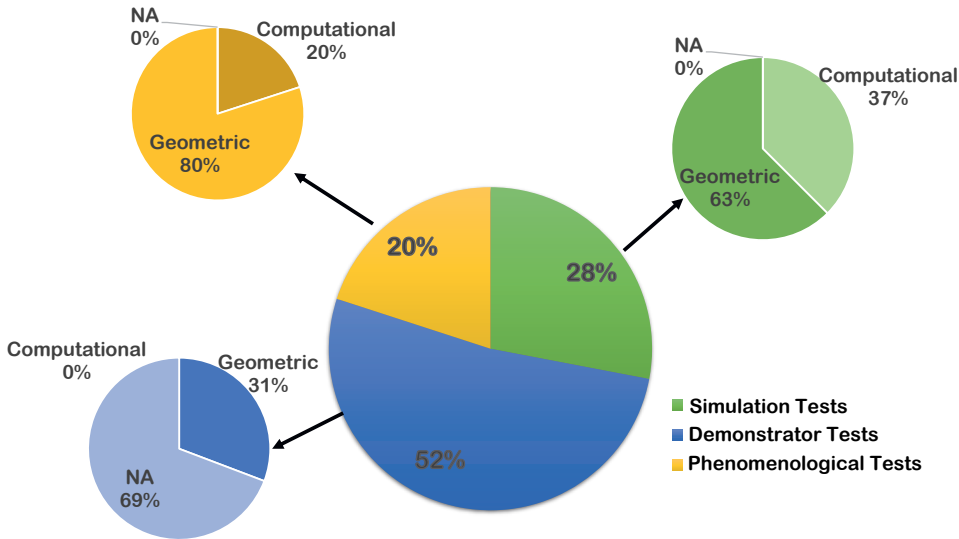
Figure 4.6: Distribution of SFT based on design approach per test objective

portance of sub-scale model design approach for a given test objective. The distribution of SFT based on design approach per test objective is shown in Figure 4.6. It is observed that engineers avoid complicated and resource-intensive computational scaling when designing models for demonstration tests. In most cases (69%), no scaling criteria are used at all. Conversely, in simulation and phenomenological tests, either geometrical scaling or computational scaling is used to design the sub-scale model, which is essential in scaling up the results of SFT. Nevertheless, in both simulation and phenomenological tests, the majority of the models are designed using geometric scaling despite their susceptibility to scale effects.

For aeroelastic tests performed in wind-tunnels, the benefits of computationally scaled models over geometrically scaled models have been demonstrated [103]. Similar studies have been performed for SFT models by Bergmann et al. [28], where they demonstrated the improved similarity in lift, drag and moment with the prototype of the computationally scaled model as compared to geometrically scaled model.

However, research work demonstrating improvements in similarity with computational scaling in SFT models are limited to static characteristics and have not yet demonstrated improvements in dynamic behaviour (e.g., flight dynamics). This is primarily because SFT was considered too complicated in the past (before 2005) for most research entities as discussed in Chapter 1 and has not received the same attention and funding as other testing methods to perform comparative studies of different scaling approaches. Furthermore, the impact of the inaccuracies in computational methods and the longer time needed to perform the optimization on the overall SFT process has not been studied. Nevertheless, based on the evidence provided by ground based tests, computational simulations and static SFTs [28, 50, 103, 159, 167, 168], computational scaling shows

promise in improving SFT, which must be investigated further by scientific community.

4.9. Discussion: Extending Computational Scaling

The miniaturization of electronics and COTS components has greatly boosted the use and applicability of SFT. Yet, SFT seems to be mostly used for demonstration purposes (where the scaled model does not even have a full scale counterpart). It seems, scaling effects are the most urgent challenge to overcome to make SFT a (new) powerful assessment method for aircraft designs, particularly for the unconventional designs under investigation to address sustainable aviation goals.

Design automation and numerical multidisciplinary optimization appear to be the new enablers to push SFT forward. Nonetheless, computational similitude theory, which encompasses these advanced design methods, has not been effectively utilized (only 16% of designs reviewed in this paper use computational scaling). This is due to the barriers associated with the use of computational scaling as discussed in Section 4.6.2, which include:

1. ill-defined and/or missing disciplinary requirements for SFT model design (Chapter 5)

2. unclear methodology for formulating an objective function to estimate the extent of similitude (Chapter 6)

3. integration of disciplinary analyses to arrive at a converged design (Chapter 6)

4. time-consuming and laborious repetitive pre/post-processing activities for every computational simulation (Chapter 8)

In the remainder of this dissertation, the aim is to enhance the accessibility of computational scaling by developing a methodology that can be effectively used to lower the barriers in computational scaling. A pre-requisite to improving the computational scaling design process is to understand the different requirements that must be satisfied by the designers to safely perform SFT. The typical requirements of SFT model design are discussed in Chapter 5. Based on these requirements, a methodology to improve computational scaling is discussed in Chapter 6 and 7.

5

DESIGN REQUIREMENTS FOR SFT

To benefit from SFT and realize its value, numerous SFT model design requirements must be satisfied. A comprehensive list of these requirements is not found in the literature. In addition, these requirements (where formalized) are mono-disciplinary and therefore unsuitable for multidisciplinary SFT model design process. In this chapter, the key SFT model design requirements are identified, classified and discussed in detail. Furthermore, disciplinary analyses (and their requirements) which were hitherto not considered but have a significant impact on SFT model behaviour are addressed. Finally, the collected requirements and design considerations are collated into a N^2 diagram to support (multidisciplinary) SFT model design.

5.1. SFT model Design Requirements per Discipline

The goal of a sub-scale model is different from that of a full-scale aircraft. Consequently, the requirements associated with the two are dissimilar. For example, in full-scale aircraft design, the number of passengers, airport gate size, the range of the aircraft, cruise mach, climb and cruise ceilings, approach speed, one-engine-inoperative flight path and take-off requirements are considered based on industrial use-cases. In the case of sub-scale flight testing, the key goal is to replicate (a part of) the full-scale aircraft behaviour.

At the beginning of the sub-scale model design process, the phenomenon that should be studied and the details of the test range are known. Based on these details, the key requirements for the model and its mission should be formalized. In this section, we study the requirements posed by the six most important disciplines that have been used in past SFTs. This information is obtained from experts' interview and the literature. As discussed in Chapter 2, SFT is best used for dynamic tests (i.e., flight dynamics and aeroelasticity). Thus, only those requirements that are relevant to dynamic tests are discussed here.

5.1.1. COTS Equipment

COTS equipment can be categorized into sensor components, power components, data & transmission components and support equipment. The use of COTS equipment in SFT is recommended to prevent the increase in cost and complexity associated with components manufactured in-house. Thus, engineers must select appropriate equipment based on the SFT model mission and safety requirements. Some common requirements associated with the COTS components are listed in Table 5.1. Typically the requirements associated with COTS components influence the aerodynamics, weight and balance, propulsion and flight mechanics. This is discussed further in Section 5.3.

5.1.2. Structures

The structural discipline involves the design of the airframe (i.e., skin panels, frames, floors for the fuselage and ribs, spars, stringers and floor for the wing and movables). Figure 5.1 shows different airframe components used in SFT. Typically, the floors in sub-scale models are necessary to place appropriate COTS components. With the exception of the floors and the skin panels, the other structural elements are optional (i.e., they are only used if the monocoque structure cannot withstand the loads imposed during different flight phases). The structural elements become much more important when the flight box is small as the model needs to make a fast and steep turn, which can result in forces as high as 8g on the structural components.

The key structural requirements concern the stress, strains, displacements and the mass of the various components used in SFT model. These are detailed in Table 5.2. The structural requirements are mainly meant to ensure structural integrity of SFT model in flight. The main coupled effect of the structural requirements is on the weight & balance because the weight of the component typically increases with maximum allowable stress on the body for a given material. For non-rigid models, the aerodynamic behaviour might change (with respect to original SFT model design) when the model experiences large deflections. The structural requirements do not have direct impact on flight dy-

Table 5.1: Overview of requirements imposed on COTS equipment and the disciplines affected by the selection of COTS equipment

Requirement Name	Description	Disciplines affected
Redundant Flight control system	Loss of a movable, transmitter, receiver, servos or regulators should not lead to complete loss of the model	Aerodynamics & Flight Mechanics
Sustained power source	Should power all the on-board equipment throughout the mission	Flight Mechanics
Power source redundancy	Sufficient redundant power to get the model back to ground in case of power failure	NA
Propulsion & Similitude	Produce the required thrust (Section 5.1.5)	Propulsion, Aerodynamics & Flight Mechanics
Equipment weight	COTS equipment weight should not exceed the target weight (Section 5.1.3)	Weight & Balance
Inertial Measurement Unit (IMU) accuracy	Should measure 3D linear and angular accelerations, velocities, position and GPS location as per accuracy requirements determined by the objective of SFT.	Aerodynamics & Flight Mechanics
Autopilot system	If used, should consistently match the programmed airspeed, roll, pitch, yaw and altitude	Aerodynamics & Flight Mechanics
Airspeed and heading	Should satisfy the accuracy requirements determined by the objective of SFT.	Aerodynamics & Flight Mechanics

5

(a) Fuselage structure

(b) Wing structure
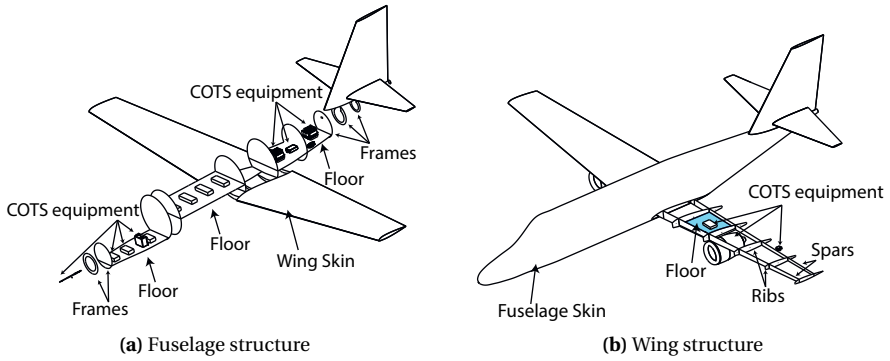
Figure 5.1: Structural components typically used in SFT

namics (not including control reversal, flutter, divergence, see Figure 2.3). However, the influence of structural requirements on the weight & balance and aerodynamics disciplines indirectly affects the flight dynamics behaviour. For example, the change in the structural design changes the maximum take-off weight and center of gravity location which in turn affects the moment arm and the moment coefficients in flight dynamics analysis.

Table 5.2: Overview of requirements imposed on structural components and the disciplines affected by structural design

Requirement Name	Description	Disciplines affected
Skin strain	For composite laminates maximum 2D principle strain should not exceed the limits set by disciplinary experts (typically 3000/6000 micro-strain)	Weight & Balance
Maximum structural displacement	Should not alter the aerodynamics of the model or hinder the functioning of the COTS equipment	Aerodynamics
Modal behaviour	For aeroelastic studies, the model must replicate the first few mode shapes	Weight & Balance, Flight Mechanics
Structural mass	Should meet the target structural weight requirements (Section 5.1.3)	Weight & Balance, Flight Mechanics

5.1.3. WEIGHT AND BALANCE

The weight and balance discipline includes the evaluation of model mass, inertia, and center of gravity location (see Table 5.3). These attributes of the model are determined based on the design of structural components and the selection of COTS components.

The weight & balance characteristics are critical in SFT model design as they influence the selection of the propulsion system, the trim flight condition and the range and duration of the mission.

Table 5.3: Overview of requirements imposed on weight and balance discipline and the disciplines influenced by the weight & balance characteristics of SFT model

Requirement Name	Description	Disciplines affected
Maximum model weight	Model mass should: • be less than the mass limit set by authorities • allow the model to fly the mission for required duration	Flight Mechanics
Inertia Scaling	The mass distribution of the model should be similar to prototype (see inertia scaling Chapter 4)	Flight Mechanics
Mass Scaling	The mass of the model should be similar to prototype (see mass scaling Chapter 4)	Flight Mechanics
CG location	CG location should ensure: • the model is statically stable (except unstable aircraft simulation) • the moment coefficients are similar to the prototype (w.r.t center of gravity for flight mechanics analysis and 0.25 mean aerodynamic chord for aerodynamics)	Aerodynamics and Flight Mechanics

The weight & balance requirements mostly affect the flight mechanics behaviour of the model. The model mass and CG location influences the static stability of the model and the model inertia determines the dynamic stability of the model. In addition to model safety, the weight and balance requirements drive multiple similitude requirements. To match the flight dynamics behaviour the mass and inertia of the model must be scaled proportionately. This can either be done using classical similitude theory or using non-dimensional mass and inertia as described in Chapter 6.

The location of CG also affects the aerodynamic moments and their dimensionless coefficients. This knowledge is effectively used by engineers to move the CG location by moving COTS components or adding ballast masses, which helps in matching the moments acting on the model and the prototype. From the studies performed in this dissertation, one can conclude that the weight & balance requirements are the most important characteristics to ensure similitude of flight dynamics behaviour. The impact

of weight & balance requirements on the overall similarity between the model and the prototype are quantified in Chapter 10 for specific use cases.

5.1.4. AERODYNAMICS

There are two main aerodynamics requirements on SFT model, namely, similarity of flow-field between the model and the prototype and preventing in-flight stall to guarantee model safety (see Table 5.4). The aerodynamic flow (kinematic) similarity requirement is the most studied similitude condition. Consequently, most of the available literature (>90% of similitude papers in this dissertation) on similitude theory is written with a prism a of flow similarity.

Table 5.4: Overview of requirements imposed on aerodynamic behaviour

Requirement Name	Description	Disciplines affected
Matching aerodynamic stability and control derivatives	Should be the same to ensure similarity of streamlines, forces and moments between the model and the prototype relevant to the test objective (refer to the work of Nelson [169] for complete list of derivatives)	Flight Mechanics
Stall behaviour	Should not stall in any phase of the mission (exception: stall characteristics study)	Flight Mechanics

In classical similitude theory, the requirement is to achieve kinematic similarity for aerodynamics. However, with computational scaling, this can be done by matching (dimensionless) stability and control derivatives of the model and the prototype. The detailed rationale of matching the derivatives is provided in Chapter 6. Replicating stall behavior of prototype is another important requirement, as the stall behavior investigation is a classic motivation for SFT. Furthermore, the stall behaviour is is also an issue in flight mechanics studies using heavier SFT models when the model needs to be trimmed at angles of attack close to the stall angle.

Aerodynamic requirements mainly affect the flight dynamics behaviour of the model. Thus, in any similitude design for flight dynamics, aerodynamics plays a critical role. These requirements also have an effect on the structures and the weight & balance modules. The aerodynamic forces acting on the model determines the strain and displacements of the structural components, which in turn affects the weight of the structural components and the model.

5.1.5. PROPULSION

For SFT models, the propulsion system (such as propellers or miniature jet engine) is critical as it enables free-flight testing. The propulsion requirements are shown in Table 5.5.

The propulsion requirements mainly affect the flight mechanics and the aerodynamics behaviour. The location of the propulsion system affects the thrust location, which consequently affects the model flight dynamics behaviour. The aero-propulsive interac-

Table 5.5: Overview of requirements imposed on propulsion system and the disciplines affected by the selection of propulsion system

Requirement Name	Description	Disciplines affected
Matching coefficients	Thrust and torque coefficient should be equal to prototype	Flight Mechanics
Aero-propulsive interaction	Should not significantly alter the flow around the model as compared to prototype	Aerodynamics
Reliability	Should not malfunction (such as loose blades etc.)	Aerodynamics
Model fit	Should fit well with the airframe	Weight & balance
Efficiency	Should consume power commensurate to on-board power source (e.g. battery or fuel tanks)	Flight Mechanics

tion often influences the flow around the model and alters the aerodynamic behaviour of the model. Thus, engineers must ensure that the aero-propulsive effects do not make the model aerodynamics dissimilar to prototype aerodynamics. Finally, the weight, size and attachment location of the propulsion system also impact the weight & balance discipline as discussed in Section 5.1.1.

5.1.6. FLIGHT MECHANICS

Unlike other sub-scale model testing methods, in SFT, flight mechanics plays a pivotal role irrespective of the objective of the test. Since the model needs to take-off, fly the mission (within the available space/flight box for testing) and land safely, stability and control characteristics of the model must be carefully studied to ensure that the model can complete the required mission (see Table 5.6). Often, the certification authorities also set requirements on the flight mechanics of the model (e.g., model should be statically stable).

Moreover, if flight dynamics behaviour of a full-scale aircraft is assessed using SFT, additional similarity requirements (listed in Table 5.6) such as the similarity of eigenvalues must be satisfied to ensure that the model's dynamic response is similar to prototype (examples in Chapter 6 and 10). The trim flight conditions obtained after flight mechanics analyses determines the baseline model flight condition about which aerodynamic forces and moments are measured. These forces and moments in-turn influence the aerodynamic similarity. Thus, the model must be designed such that the stability and control derivatives experienced at trim conditions should be similar to prototype derivatives.

Typically, the requirements associated with flight mechanics are assessed at the end of a design iteration as this discipline requires inputs from other disciplines such as aerodynamics, weight & balance, propulsion systems etc. This is discussed further in Section 5.3.

Table 5.6: Overview of requirements imposed on flight mechanics behaviour and the disciplines influencing flight mechanics behaviour

Requirement Name	Description	Influencing Disciplines
Matching Eigevalues	The dynamic behaviour of model and prototype should be similar	NA
Trim conditions	Should allow the aerodynamic derivatives of the model and the prototype to be similar	Aerodynamics
Static Stability	Should be statically stable (exception: study of unstable aircraft)	Weight & balance
Dynamic stability	Should be dynamically stable (exception: study of unstable aircraft)	
Control power	Should have sufficient control power to manoeuvre the aircraft in case of a malfunction	Weight & balance
Test within flight box	Model should be safely manoeuvred in the limited flight box while replicating the required phenomena necessary to study prototype behaviour	Structures
Handling and Flying qualities	Should be such that the pilot should not be overwhelmed by tasks throughout the mission	NA

5

5.2. DISCIPLINES NOT CONSIDERED IN PAST SFT MODEL DESIGN

The requirements discussed so far are based on the experiences gained from past SFTs. These designs were generally obtained using classical similitude theory or governing equations. Furthermore, the designs were based on mono/bi-disciplinary analyses (if at all). However, with the introduction of computational similitude theory, many aspects of SFT model design, which were previously impossible, can be considered at early design stages. This eliminates last minute rework and tedious corrections during post processing. In the following sections, additional design considerations that can be accounted in future computational scaling process to improve SFT model design are discussed.

5.2.1. MANUFACTURING CONSTRAINTS

With the advancements in manufacturing and material technology, one can manufacture sub-scale models in various ways using different materials. The selection of the manufacturing technique depends on the time available for manufacturing, the structural requirements of the mission, the budget, required precision and the materials that can be used in manufacturing.

The manufacturing technique and the material used in the process directly affect the SFT model design features such as surface finish, trailing edge radius, gap between movable and the fixed part of the wing, etc. These features affect the aerodynamics and the weight and balance of the model, thereby, affecting the flight behavior. Nevertheless, the implication of manufacturing technique and material are generally not included during the design phase for two reasons. First, rules of thumb to predict the implication of manufacturing techniques on model design are not available. Second, such rules of thumb cannot be generalized due to substantial variation in requirements from one design to another (especially with novel aircraft configurations). This can only be overcome by using computational analyses to evaluate the impact of designers decision on the overall model design, which is enabled by computational scaling approach.

5.2.2. ATMOSPHERIC CONDITIONS

Addressing the uncertainties in scaled model response is a critical challenge that must be address by experimenters. Undoubtedly, ground-based testing methods can use much more sophisticated and precise measurement instruments as compared to SFT because there are no limitations on the weight, size, and shape of these equipment in ground-based testing. Moreover, the uncertainties posed by atmospheric turbulence in SFT can be lowered in controlled environment of ground-based testing. Nevertheless, ground-based testing methods are ill-equipped to study several aspects of flight-behavior as discussed in Section 2.3. Engineers are reducing model uncertainties by improving the precision of the on-board measurement equipment [45, 123], developing mathematical models to correct the effects of atmospheric turbulence [170] and repeating the tests multiple times [74]. These developments should be included in the SFT model design process to improve its quality.

5.2.3. HANDLING QUALITIES

SFT requires a pilot to fly the sub-scale model. The pilot can either be a human or a trained computer that performs the test. In most SFTs, there is little or no time available to build an auto-pilot system. In such cases, it is essential to design sub-scale models whose handling and flying qualities are such that the pilot effort remains acceptable during the entire SFT mission. However, the handling qualities and the pilot effort are quite different for remote-controlled models as compared to a prototype owing to the differences in their size, mass and inertia, in addition to the fact that pilot is not on-board the aircraft.

Williams [171] proposed standards for specifying Unmanned Aerial Vehicles (UAV) handling qualities. Although UAVs have different objectives and requirements as compared to SFT models, the similarities in their size and piloting technique (unmanned flight) opens the possibility of reusing UAV standards for SFT. Thus, the proposed UAV handling qualities can be adapted to the needs of SFT and used in computational scaling to ensure that pilot does not get overwhelmed. Dantsker et al. provides an example for such flight testing automation [172].

5.3. COMBINING ALL THE DISCIPLINARY REQUIREMENTS

The literature survey performed to enumerate SFT model design requirements reveals that individual disciplinary experts worked in silos of design with little or no interaction with other disciplines. This results in inconsistent designs even after months of SFT model design synthesis and analysis. The adjustments made to overcome these inconsistencies often results in loss or reduction of similitude. Thus, the use of Multidisciplinary Design Analysis and Optimization (MDAO) to design consistent and compliant SFT model becomes imperative.

Based on (multi-disciplinary) requirements identified in this chapter, appropriate Multidisciplinary Analysis and Optimization SFT design framework must be developed to support the design of compliant SFT model. This involves the selection of apt disciplinary analysis tools and mapping the requirements on objective function, design variable and constraints (details in Chapter 6). A N^2 diagram, an intermediate step in the mapping process, represents functional or physical interfaces between system elements to systematically identify, define, design, and analyze them. It applies to both hardware and/or software interfaces [173]. Various disciplinary requirements imposed on SFT models are discussed and the disciplinary couplings are formalized using an N^2 diagram as shown in Figure 5.2.

This N^2 diagram (Figure 5.2) summarizes the engineering competences necessary to perform SFT model design and their key outputs necessary to determine the compliance of SFT model requirements. It is interesting to note that the key disciplines used in SFT model design are similar to the disciplines of prototype design. Thus, the N^2 diagram of the model and the prototype disciplinary analyses (and their inputs and outputs) can look quite similar.

However, the objectives, requirements and constraints of prototype design are different from SFT model. For example, the objective of SFT is to mimic prototype behaviour whereas the prototype has specific commercial/military objectives (range, payload, speed, etc.). Thus, in order to tackle SFT model design problem, the follow up of
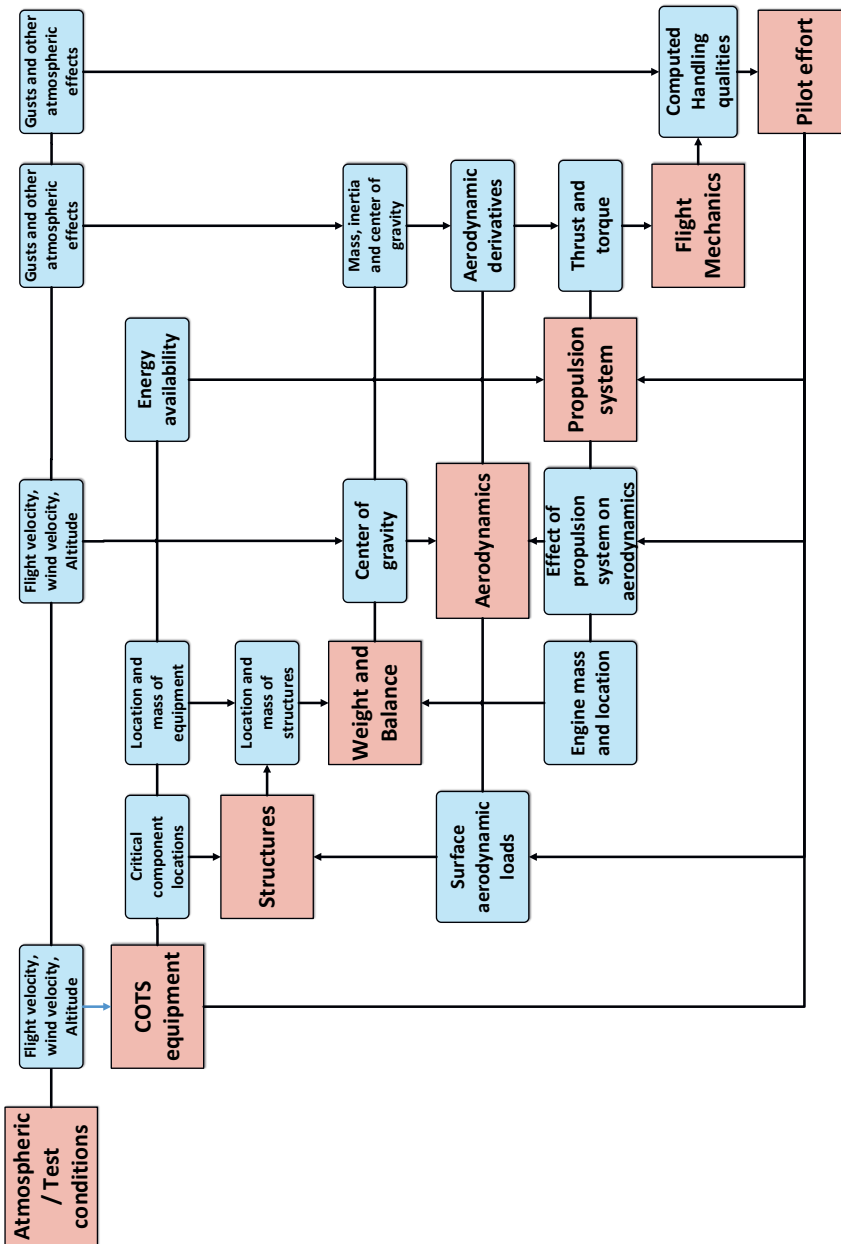
Figure 5.2: N^2 diagram of disciplinary analyses necessary for SFT model design and their key outputs required to assess SFT design requirements compliance discussed in Section 5.1

this N^2 diagram would be the formulation of fundamental optimization problem, where, the design variables, objective and constraints are formalized based on the requirements as discussed in Chapter 6.

5.4. SUMMARY: SFT REQUIREMENTS

In this chapter, we identified, enumerated and classified the requirements associated with SFT model design per discipline. This effort has filled the gap of ill-defined/missing requirements discussed in Chapter 4. The requirements enumerated in this chapter can be further extended depending on the test objectives and the limitations imposed by certification authorities.

Although, the N^2 chart shown in this chapter provides an overview of the system level challenges and a starting point for MDAO, it does not provide engineers with sufficient support in formulating the objective functions, determining the design variables and constraints and development of automated tools and methods necessary to perform MDAO. In Chapter 6, a methodology to incorporate MDAO in SFT model design process is discussed in detail.

5

II

METHODOLOGY

6

MDAO BASED SIMILARITY MAXIMIZATION OF SFT MODELS

The requirements discussed in Chapter 5 indicate the need for the adoption of Multidisciplinary Design Analysis and Optimization (MDAO) approach to address SFT model design problem. Thus, the next step is to formulate such an MDAO problem. In this chapter we propose a generalized approach for computational scaling problems by formalizing a novel figure of merit to estimate the extent of similitude between the model and the prototype called the Degree of Similitude (DoS). Furthermore, constraints, disciplinary analyses and their key inputs and outputs necessary for SFT model design are derived from the requirement analysis performed in Chapter 5. Finally, an example SFT model design problem formalization with MDAO architecture is illustrated to clarify the proposed method.

6.1. PROBLEM STATEMENT

The SFT sub-scale model design requirements pinpoint the multi-disciplinary nature of the design problem and suggest the adoption of a formal MDAO approach to design SFT models. In general, an MDAO problem can be stated as,

minimize

$$f(z, x, y(x, z)) \tag{6.1}$$

with respect to

$$z, x \tag{6.2}$$

such that

$$g(z, x, y(x, z)) \geq 0 \tag{6.3}$$
$$h(z, x, y(x, z)) = 0 \tag{6.4}$$

where f is the objective function, g and h are inequality and equality constraints respectively, z is the vector of global design variables (applicable to multiple disciplines), x is the vector of local design variables (applicable to single discipline) and y is the vector of state variables for all disciplines, which are determined by the multidisciplinary analysis system. This is often indicated in literature as MDA . For a given discipline i, the state y_i , is obtained by the respective set of governing equations. We can write the governing equations for the N disciplines as,

$$\mathcal{R}_i(z, x_i, y_i(z, x, y_j)) = 0 \tag{6.5}$$

where,

$$i = 1, ..., N.$$

Thus, in order to use MDAO in the design of SFT models, different aspects of the MDAO problem such as the objective function, the constraints, the design variables and the state variables must be formulated. In the case of the SFT model design MDAO problem, f, the objective function, is a synthetic measure of the extent of similitude between the model and the prototype, x is a vector of local design variables that are typically composed of sub-scale model characteristics (such as scaling factor, geometrical shape, etc.), z is a vector of global design variables that are derived from test-conditions (altitude, velocity, etc.), y is a vector of state variables obtained by the respective set of governing equations, g and h are vectors of constraints based on the requirements identified in Chapter 5.

Thus, the aim of applying MDAO to the SFT model design is to simultaneously find the shape/size of the SFT model and the flight test conditions. Interestingly, when applying MDAO to the prototype design, flight conditions (range, speed, mass etc.) are mostly

fixed parameters. However, in case of SFT, the selection of test condition is left to the discretion of engineers which adds an extra layer of complexity in the SFT model design.

As discussed in Chapter 4, to date, identification of relevant design and state variables and formulation of an appropriate objective function remains an open challenge in computational scaling approach. In the following sections, each of these challenges are discussed and a novel methodology to formulate the objective function and identify design and state variables which is generally applicable to all the SFT model design problems is proposed.

6.2. OBJECTIVE FUNCTION: DEGREE OF SIMILITUDE

The objective of any design exercise for sub-scale model is to ensure similarity of the model and the full-scale aircraft behaviour. Thus, the requirements listed in Chapter 5 that guarantee the similarity between the model and the prototype constitute the objective function. However, the qualitative requirements described in the preceding chapter are not suitable for assessing the compliance of (multiple) requirements. In any case, satisfying all the similitude requirements is often not possible due to the differences in the test conditions of the model and the prototype. To overcome this challenge, we propose a novel and generic figure of merit called the **Degree of Similitude (DoS)** which can be used as an objective function in any sub-scale model design process irrespective of the configuration of the model or the phenomenon being studied.

6.2.1. OBJECTIVE FUNCTION REQUIREMENTS

To support MDAO based similitude maximization, one figure of merit expressing the extent of similitude should be developed which can be used to compare two or more sub-scale model designs to select the most similar model. The requirements on such a figure of merit (objective function) can be summarized as follows:

1. The requirements shown in Chapter 5 are extensive and not all of them must be satisfied for a given test. Thus, appropriate methods must be formalized to support the identification of relevant similitude requirements for a given SFT objective (Section 6.2.2)

2. The qualitative similitude requirements provided in Chapter 5 should be translated into quantitative values that can be used to formulate an objective function (Section 6.2.2)

3. When all the identified similitude requirements cannot be satisfied, appropriate means of ranking these requirements in the order of their influence on the behaviour being studied must be developed to allow engineers to leave those requirements that do not significantly affect the similitude (Section 6.2.4)

In the following sections, these requirements are utilized to formulate a suitable objective function, which can be adapted for use in a variety of (MDAO based) SFT model design problems.

6.2.2. SIMILITUDE REQUIREMENTS: IDENTIFICATION AND QUANTIFICA-
TION

The list of similitude requirements provided in Chapter 5 are exhaustive and generally applicable to diverse SFTs. However, engineers must select a subset of these requirements that are relevant to their test. For example, the quantification of the modal behaviour of a sub-scale model is not important in the case where short-period motion of a rigid aircraft must be studied.

The governing equations provide an insight into the dependent and independent parameters that affect the phenomenon being tested. Based on these parameters, the similitude requirements specific to the problem being studied can be identified. For example, the equation of motions can be used to determine that lift and drag forces are relevant parameters affecting Phugoid motion of an aircraft and must be incorporated in the objective function used for determining the extent of Phugoid motion similitude between the model and the prototype.

Once the constituent parameters relevant to a test are identified, they can be quantified by means of non-dimensional coefficients. As discussed in Chapter 4, non - dimensional coefficients are the only means of comparing the performance of a sub-scale model and the full-scale aircraft. Thus, all the similitude requirements must be expressed as functions of non-dimensional numbers. The aerodynamic requirements can be expressed as non-dimensional aerodynamic derivatives. The inertia coefficients can be reduced to normalized radius of gyration and the mass can be made non-dimensional using critical dimensions and the density of fluid flow as shown in Equations 6.6 and 6.7.

$$K_y = \frac{1}{c} \cdot \sqrt{\frac{I_{yy}}{m}} \tag{6.6}$$

$$\mu_c = \frac{m}{\rho S c} \tag{6.7}$$

where, I_{yy} is inertia about the y-axis, m is the mass of the aircraft, S is wing area, ρ is density and c is mean aerodynamic chord of the wing.

Based on the selected non-dimensional terms affecting the phenomenon being studied, the quantified similitude requirements can be mathematically represented as follows:

all similitude requirements are satisfied when

$$\epsilon_i = 0 \tag{6.8}$$

for,

$$i = 1, 2, ... n$$

where, ϵ_i is known as scaling error and given by the formula

$$\epsilon_i = |C_{i_p} - C_{i_m}| \tag{6.9}$$

Here, n is the number of dimensionless coefficients relevant to the problem at hand, C_{i_m} is the ith relevant dimensionless coefficient of the model and C_{i_p} is the ith relevant dimensionless coefficient of the prototype.

The difference in the non-dimensional coefficients of the model and the prototype is called the scaling error as it is caused by the difference in the size and the testing condition of model and the prototype. If all the similitude requirements are satisfied, (all) the relevant non-dimensional coefficients of the model and the prototype would be equal. Therefore, the coefficients of the governing equation becomes equal and the behaviour of the model and the prototype are similar.
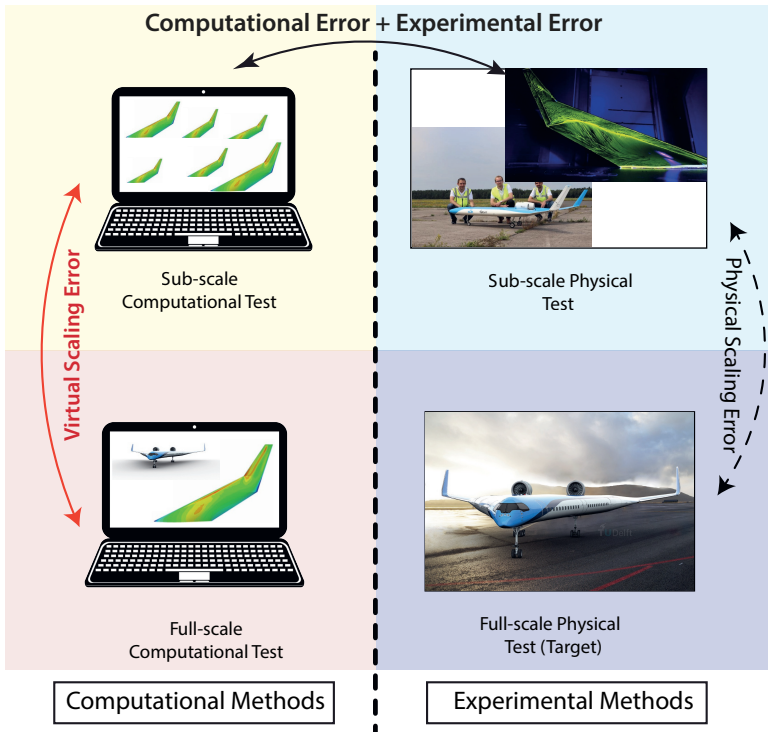
Figure 6.1: Schematic representation of scaling errors

Equation 6.10 [169], for example, is the lift equation obtained from the equations of motion of an airplane. If C_L (lift-coefficient) is an important parameter affecting a given phenomenon, C_L for the prototype and the model must be the same. Which also implies, aerodynamic coefficients, C_{L_u} (change in lift due to change in velocity), C_{L_α} (change in lift due to change in angle of attack),C_{L_q} (change in lift due to change in pitch-rate), $C_{L_{\dot\alpha}}$ (change in lift due to rate of change of angle of attack), $C_{L_{\delta_e}}$ (change in lift due to change in elevator deflection) and $C_{L_{\dot\delta_e}}$ (change in lift due to rate of change of elevator deflection) should be the same for model and prototype.

$$C_L = C_{L_u} \frac{\Delta u}{V} + C_{L_\alpha} \Delta \alpha + C_{L_q} \frac{qc}{2V} + C_{L_{\dot{\alpha}}} \frac{\dot{\alpha}c}{2V} + C_{L_{\delta_e}} \delta_e + C_{L_{\dot{\delta}_e}} \frac{\dot{\delta}_e c}{2V} \qquad (6.10)$$

In order to assess whether the similitude requirements are satisfied, the values of the relevant non-dimensional coefficients for both the prototype and the model must be calculated. This can be done either using experimental methods or by computational methods. The scaling error obtained from experimental methods is often called ***Physical Scaling Error*** and the scaling error obtained by means of computational methods is called ***Virtual Scaling Error***. Figure 6.1 provides an overview of different scaling errors.

The objective of all the testing methods is to determine the full-scale physical test response. Nevertheless, as discussed in Chapter 2, full-scale aircraft tests are infeasible in the early design stages which prevents the quantification of physical scaling error of new or unconventional aircraft designs. Thus, only virtual scaling error can be used to determine the similitude requirements.

However, computational tests are not accurate and are often prone to errors due assumptions and uncertainties in the computational models and experimental tests have their errors as discussed in Chapter 2. Thus, the idea is to predict the prototype behaviour by flying a SFT model whose scaling error is minimized using computational simulations within an MDAO framework (i.e., minimum virtual scaling error) and then evaluating and accounting for the computational error and experimental error by comparing the results of physical SFT with the results of virtual SFT obtained from MDAO based computational analysis (see Figure 6.1). This can be mathematically expressed as follows:

$$Q_p = Q_m \pm \epsilon_v \pm \epsilon_c \pm \epsilon_e \qquad (6.11)$$

where, Q is the quantity of interest, subscripts p and m indicate prototype and model respectively, ϵ_v is the virtual scaling error, ϵ_c is the computational error and ϵ_e is the experimental error.

In view of the available time and resources, the scope of this dissertation is limited measuring and minimizing the virtual scaling error, whilst the task of building and flying the SFT model designed in this work and quantifying the computational error is left to follow-up research work.

6.2.3. DEGREE OF SIMILITUDE

In Section 6.2.2, the mathematical formulation to quantify the similitude requirements was discussed. Nevertheless, like the classical similitude theory and Kline's Governing Equation theory (see Chapter 4), the quantification of similitude requirements only yields a list that enumerates the extent to which each of the similitude requirements have been satisfied. However, when multiple sub-scale models need to be compared, a vector of similitude requirements per design is not a convenient metric to evaluate and select an appropriate design. Thus, these similitude requirements must be combined to arrive at one figure of merit that can be used to compare the extent of similitude.

Such a generalised synthetic measure that meets all the requirements discussed in Section 6.2.1 has not been formulated so far. Although application specific formulation

have been provided by some authors in the past, as discussed in Chapter 4, they are not generally applicable to sub-scale model design process. To this end, a figure of merit called the Degree of Similitude that satisfies all the requirements listed in Section 6.2.1 and provides engineers with an opportunity to compare the extent of similitude of different models using a unique synthetic measure is proposed in this research work.

The **Degree of Similitude (DoS) is defined as the function of weighted sum of normalized virtual scaling error.** Mathematically the DoS can be expressed as:

$$DoS_{test} = 1 - \sum_{i=1}^{n} w_i * \frac{|C_{i_p} - C_{i_m}|}{|C_{i_p}|} \tag{6.12}$$

where, n is the number of dimensionless coefficients, C_{i_m} is the ith relevant dimensionless coefficient of the model obtained using a computational analysis, C_{i_p} is the ith relevant dimensionless coefficient of the prototype obtained using computational analysis and w_i is the degree of influence of the ith coefficient on the phenomenon being tested when subject to the condition:

$$\sum_{i=1}^{n} w_i = 1$$

The subscript *test* indicates that the DoS formulation is specific for a given SFT and can be modified as necessary for different test objectives. This is particularly useful in supporting the design of catalog SFT models to test the full-scale aircraft behaviour (discussed in Chapter 4). Examples of different DoS formulations and their implications on similitude will be discussed further in Chapter 10. In case the value of $C_{i_p} = 0$, the DoS becomes infinite. In such cases, the C_{i_p} value can be made non-zero by adding an infinitesimal value.

(a) DoS behaviour when Equation 6.12 is used   **(b)** DoS behaviour when Equation 6.13 is used
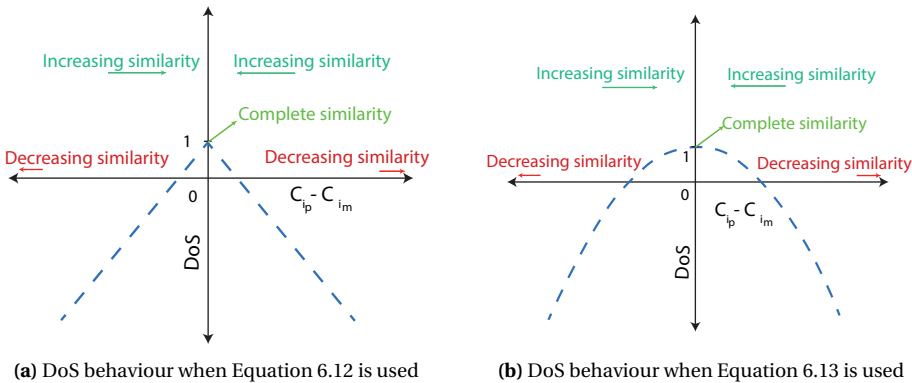
Figure 6.2: General trend-line for the variation of DoS with changing Virtual Scaling Error computed using a single non-dimensional coefficient

As per this definition, when the DoS is 1, all the relevant coefficients of the model and the prototype are equal and consequently their behaviour for the phenomenon under consideration is similar. This is shown graphically in Figure 6.2a for one non-dimensional coefficient. As the virtual scaling error increases, the degree of similitude decreases and consequently the similarity of the behaviour of the model and the prototype decreases. Conversely, when the virtual scaling error decreases, the value of the DoS increases and hence the similarity between the model and the prototype. As the definition of the DoS includes the absolute value function, the objective function might be infeasible for certain optimization algorithms owing to discontinuity at the DoS value of 1. In such cases, an equivalent formulation of the DoS can be used as shown in Equation 6.13. The behaviour of such a DoS function with respect to changing virtual scaling error composed of one non-dimensional coefficient is shown in Figure 6.2b. Nevertheless, for the remainder of this dissertation, the formulation of the DoS as shown in Equation 6.12 will be used.

$$DoS_{test} = 1 - \sum_{i=1}^{n} w_i * \left(\frac{C_{i_p} - C_{i_m}}{C_{i_p}} \right)^2 \tag{6.13}$$

As the number of non-dimensional coefficients used in the computation of virtual scaling error increases, the trends remain the same but achieving a DoS of 1 becomes challenging. In most practical applications, the DoS of 1 cannot be achieved. Nevertheless, designs which have a DoS close to 1 can be used, provided, the relative importance of the different non-dimensional coefficients affecting the phenomenon being tested are accounted (i.e., degree of influence) and the overarching system performance parameters for the phenomenon being tested are not significantly different for the model and the prototype. Both these concepts are discussed in the following sections.

6.2.4. DEGREE OF INFLUENCE

If we were to use the definition of the DoS provided in the preceding section without including **Degree of Influence**, Equation 6.12 would be re-written as:

$$DoS_{test} = 1 - \sum_{i=1}^{n} \frac{|C_{i_p} - C_{i_m}|}{n|C_{i_p}|} \tag{6.14}$$

Such a formulation would only include the different non-dimensional coefficients used in the associated governing equations including the relative importance of these coefficients on the phenomenon being tested. Therefore, the relative importance of different coefficients on the phenomenon would not be exposed to the optimizer which uses this DoS as its objective function.

For example, a set of similitude requirements to study short-period motion can be formulated using the coefficients:

- C_{z_α}: change of lift coefficient with changing angle of attack

- C_{z_q}: change of lift coefficient with changing pitch rate

- C_{m_α}: change in moment coefficient with changing angle of attack

- C_{m_q}: change in moment coefficient with changing pitch rate

- μ_c: non-dimensional mass as defined in Equation 6.7

- $K_Y{}^2$: the non-dimensional radius of gyration

The model behaviour in short period motion is best characterized by damping and frequency which is much more sensitive to changes in mass and inertia properties as compared to the aerodynamic coefficients as will be discussed further in Chapter 10.

While the sensitivity of damping and frequency for varying dimensionless coefficients is inherently captured in the governing equations, it is not included in Equation 6.14. As a consequence, the optimizer might change the design of the sub-scale model in such a way that the virtual scaling error of aerodynamic coefficients is much lower than the virtual scaling error of the mass and inertia coefficients. This might be useful in obtaining a DoS that is closest to 1 but the short-period motion damping and frequency of the model and the prototype will be significantly different.

To overcome the problem, where, the optimizer tries to change the design to match those coefficients which are less relevant to the phenomenon being tested when the DoS of 1 cannot be achieved, degree of influence is incorporated in Equation 6.14. ***The degree of influence provides a rank-list of different similitude requirements to the DoS based on their relative importance in the phenomenon being tested.*** This helps the optimizer to satisfy the similitude requirements in the order of their importance and maintaining the implicit information of the governing equations intact while ensuring similitude.

The ranking of different similitude requirements can be done in two ways. The experience of the engineers based on lessons learnt from preceding tests can be used to rank the different coefficients and their relative weights. Alternatively, systematic sensitivity analysis can be performed using the governing equations to determine the relative weights of the coefficients based on their rank. Hamby [174], in his review of sensitivity analysis techniques provides numerous ways to rank the coefficients.

In the remainder of this dissertation we will use the Sensitivity Index proposed by Hoffman and Miller [175]. They advocate the use of each parameter's entire range of possible values in order to assess the parameter sensitivities. The "sensitivity index" (SI) is calculated using,

$$SI = \frac{D_{max} - D_{min}}{D_{max}} \qquad (6.15)$$

where D_{min} and D_{max} represent the minimum and maximum output values obtained from computational or experimental simulation, respectively, resulting from varying the input over its entire range. This figure-of-merit provides a good indication of parameter and model variability. The specific implementation of this sensitivity analysis method to the SFT model design is discussed further in Chapter 10 (see Equations 10.13 and 10.14).

In addition to infusing the rank-list of coefficients in the objective function, Degree of Influence also helps engineers leave out those coefficients that do not significantly influence the phenomenon being tested. This reduces the similitude requirements that must be satisfied thereby making the optimization problem simpler. As a consequence,

the probability of finding a sub-scale model whose DoS is 1 becomes higher. Nevertheless, for a sufficiently complex problem, there might be no design that has the DoS of 1. In the following section we discuss this scenario further.

6.2.5. MODEL SELECTION WHEN DOS < 1

Despite the best efforts, DoS of 1 cannot be achieved most of the time owing to differences in size and testing conditions of the model and the prototype. However, after complete optimization, even if the model has a DoS less than 1, SFT model designs need not be outrightly rejected. Under some circumstances, designs with DoS < 1 behave *"almost"* like the prototype. In this section, we define the conditions under which such models (DoS < 1) can be used in SFT to predict the prototype behaviour.

In case DoS<1, in addition to the DoS, the ***Behaviour Indicator Matrix (BIM)*** is proposed in this dissertation to determine the similarity between the model and the prototype behaviour. BIM is a matrix of non-dimensional terms called the ***Behaviour Indicators (BI)*** that can be used to describe the model or prototype behaviour for the phenomenon being tested. Eigenvalues are examples of behaviour indicators in the study of dynamic stability. Typically, each BI is a function of the coefficients and variables used in computational scaling and are determined using governing equations. A general mathematical representation for BIM is given as follows:

$$\mathbf{BIM_m} = \begin{bmatrix} BI_{m_1} & BI_{m_2} & BI_{m_3} & BI_{m_4} & ... & BI_{m_n} \end{bmatrix} \tag{6.16}$$

$$\mathbf{BIM_p} = \begin{bmatrix} BI_{p_1} & BI_{p_2} & BI_{p_3} & BI_{p_4} & ... & BI_{p_n} \end{bmatrix} \tag{6.17}$$

where, subscripts m and p stand for the model and the prototype respectively, n is the number of behaviour indicators necessary to understand the aircraft behaviour for the given phenomenon and the terms BI can be expressed as follows:

$$BI_{m_i} = f(C_{m_1}, C_{m_2}, C_{m_3}...C_{m_k}) \tag{6.18}$$

$$BI_{p_i} = f(C_{p_1}, C_{p_2}, C_{p_3}...C_{p_k}) \tag{6.19}$$

where, i = 1, 2, 3, 4,....n, C refers to the dimensionless coefficients in the similitude requirements that influence the behaviour indicator for models and the prototype (represented by subscripts m and p respectively) and k is the number of coefficients that affect a behavioural indicator.

Once the BIM is constructed, the virtual scaling error can be calculated as shown in Equation 6.20 with Δ**BIM**. If the maximum BI is less than **Allowed Scaling Error (ASE)**, the model can be used to study the full scale behaviour for the phenomenon being tested. The ASE is a function of the prototype BIM as shown in Equation 6.22.

$$\Delta\mathbf{BIM} = \mathbf{BIM_p} - \mathbf{BIM_m} \tag{6.20}$$

subject to the condition

$$ASE \geq max(|\Delta\mathbf{BIM}|) \tag{6.21}$$

where,

$$ASE = g \cdot BIM_{selected}/100 \tag{6.22}$$

$BIM_{selected}$ is the element in $\mathbf{BIM_p}$ that contributes to $max(\Delta\mathbf{BIM})$

here, g in Equation 6.22, is a percentage of maximum value in prototype BIM. This percentage is based either on the sensitivity of the BIs to the coefficients of the similitude requirements used in Equation 6.16 and 6.17 or on the experience of the disciplinary expert. This is best illustrated using the example of the pure-pitching motion of an aircraft. The behaviour of an aircraft in such a motion is defined using the damping ratio (ζ) and the natural frequency (ω), where,

$$\zeta = f(C_{m_q}, C_{m_\alpha}, C_{m_{\dot{\alpha}}}) \tag{6.23}$$

$$\omega = f(C_{m_\alpha}) \tag{6.24}$$

and,

$$\mathbf{BIM_p} = [\zeta_p, \omega_p] \tag{6.25}$$

$$\mathbf{BIM_m} = [\zeta_m, \omega_m] \tag{6.26}$$

Here, ζ and ω are the BIs for pure-pitching motion, C_{m_α} is change in moment coefficient with changing angle of attack, C_{m_q} is change in moment coefficient with changing pitch rate and subscripts m and p stand for the model and the prototype respectively. In order to determine the ASE for this test, the value of g in Equation 6.22 must be determined. In order to do this, a sensitivity analysis of the BI to different coefficients must be studied.

Nelson [169] studied the sensitivity of change in normalized angle of attack with time for different damping factors pure pitching aircraft motion as shown Figure 6.3. Such a study can be used to study the validity of a SFT model design for a given test objective. For example, if the model and the prototype damping and frequency are as follows,

$$\zeta_p = 1.3 \times 10^{-3} \tag{6.27}$$

$$\omega_p = 7.09 \times 10^{-3}$$

$$\zeta_m = 0.65 \times 10^{-3}$$

$$\omega_m = 8.01 \times 10^{-3}$$

thus,

$$\Delta\mathbf{BIM} = [0.65 \times 10^{-3}, -0.92 \times 10^{-3}] \tag{6.28}$$

because, $BI_{selected} = \omega_p$ and $g = 20\%$ (see Figure 6.3 for details)

$$ASE = 0.2 \times \omega_p = 1.418 \times 10^{-3}$$

since,

$$ASE > max(|\Delta\mathbf{BIM}|)$$

in this case, the SFT model design can be used to study the longitudinal behaviour of the full-scale aircraft.
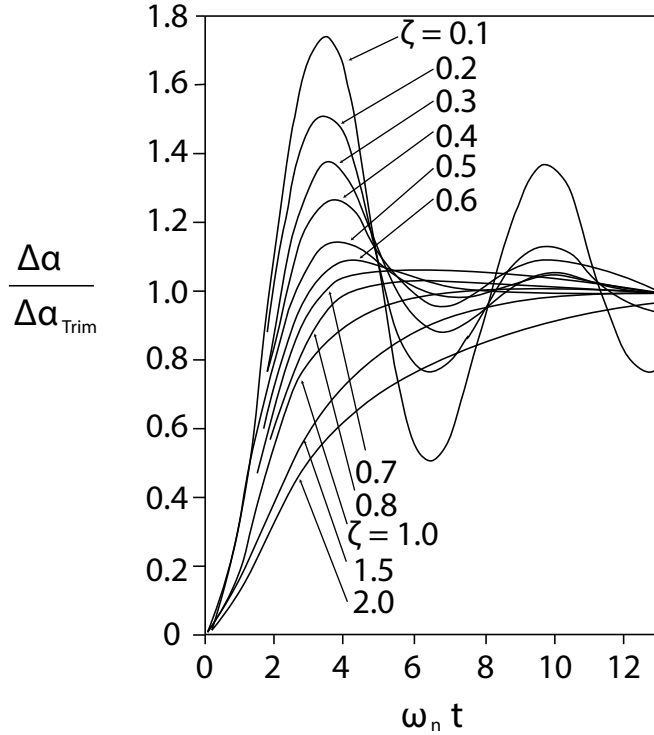
Figure 6.3: Variation of normalized angle of attack with time at different damping values [169]. For up to 20% variation in damping factor, the aircraft behaviour does not change significantly. Thus, if the prototype has $\zeta = 0.1$ and the model has $\zeta = 0.3$, both the model and the prototype exhibit underdamped behaviour (i.e., similar behaviour). Conversely, if the model has a $\zeta = 0.8$, then it becomes critically damped exhibiting different longitudinal behaviour.

Thus, models can be used to study the prototype behaviour despite having DoS < 1, provided, the following conditions are satisfied:

1. The coefficients used to determine the BI are not in a (significantly) different flight conditions. For example, if the C_{Z_α} of the model is calculated at stall angle whereas the prototype C_{Z_α} is evaluated in linear range (low angles of attack), the underlying phenomenon for the model and the prototype would be significantly different (i.e., different boundary layer, sudden loss of control at stall, etc.). Thus, extrapolation of results becomes challenging.

2. The BI and all the relevant coefficients have a continuous behaviour as shown in Figure 6.3. With discontinuous and fluctuating behaviour, similarity of the model and the prototype behaviour cannot be guaranteed

At the end of computational scaling, the model BIs might not be able to satisfy the bounds of ASE (i.e., Equation 6.21). In such cases, engineers can study a sub-set of the problem. For example, instead of studying the complete short period motion, engineers can use SFT to validate the accuracy of their computational tools in predicting C_{M_q} and C_{Z_q}, which are challenging to determine using other experimental methods. This validation step can be used to determine the uncertainty of the full-scale aircraft behaviour predicted by computational tools. In such studies, the effect of novel technologies on a given phenomenon cannot be studied. For example, the effect of distributed propulsion on short period motion cannot be studied when the SFT model is designed using a DoS formulation composed of a sub-set of non-dimensional coefficients affecting the phenomenon.

6.3. DISCIPLINARY ANALYSES AND THEIR DESIGN AND STATE VARIABLES

For the SFT model design problem, a number of disciplines are necessary as outlined in Chapter 5. In the following paragraphs, different disciplinary analyses tools necessary for the SFT model design, their input parameters and the associated state variables (outputs of disciplinary analysis) are discussed briefly.

6.3.1. PREREQUISITES: MODELLING AND MESHING DISCIPLINES

To support the SFT model design, we aim to implement an MDAO system of type "Geometry-model in the loop" (details in Chapter 7). Such MDAO systems have a parametric CAD model as one of the disciplines. This approach is necessary when other disciplines need refined geometry information such as meshes.

The geometric modelling discipline should generate the CAD model of the aircraft outer mold line based on user inputs. The user inputs for geometric modelling can be divided into wing, fuselage and connecting element inputs as shown in Figure 6.4. In other words, this discipline must convert the design parameters which are integers and floats (based on conceptual design) to a CAD model which can be used by other disciplines for synthesis and analysis of the SFT model. An important aspect of this discipline is the inclusion of scaling factor as an input parameter. This parameters allows users to provide full-scale aircraft dimensions as input and then apply a scaling factor to the entire component. For example, the user can provide a wing design with a span of 30 m and apply a scaling factor of 0.1 with reduces the entire wing size isometrically to generate a smaller wing of span 3 m.

In addition to generating the geometry, this discipline should also discretize the geometry to generate meshes for various disciplinary analysis. Ideally, the generation of geometry and the mesh should be automated to enable MDAO for computational scaling. The detailed explanation of how these inputs are used to generate (automatically) the CAD model and the associated input format for each of these elements is provided in Chapter 7 and Appendix C.
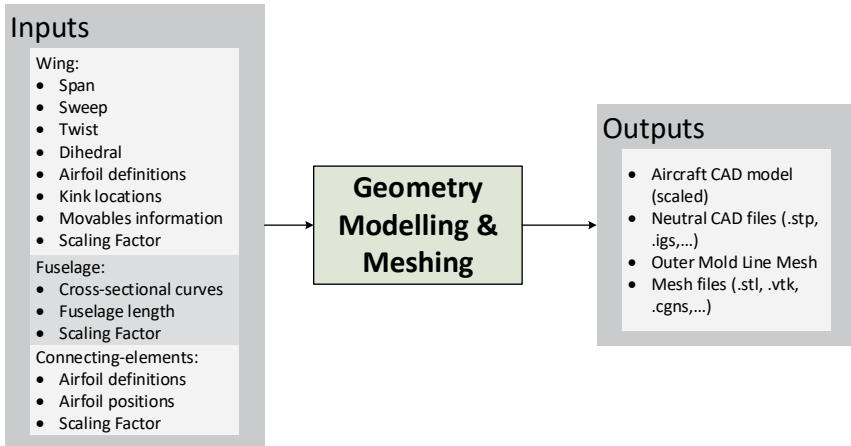
Figure 6.4: Inputs and outputs necessary to generate the SFT model geometry and mesh

The airframe modelling discipline uses the outer mold line of the aircraft to generate the airframe components such as ribs, spars, frames, bulk-heads etc. The locations and the material properties of these components are user inputs (see Figure 6.5 and the shape of these bulkheads are a combination of user input and the outer mold line of the aircraft. This discipline should also be able to generate meshes suitable for structural analysis. This is important to assess the structural integrity of the model in flight.
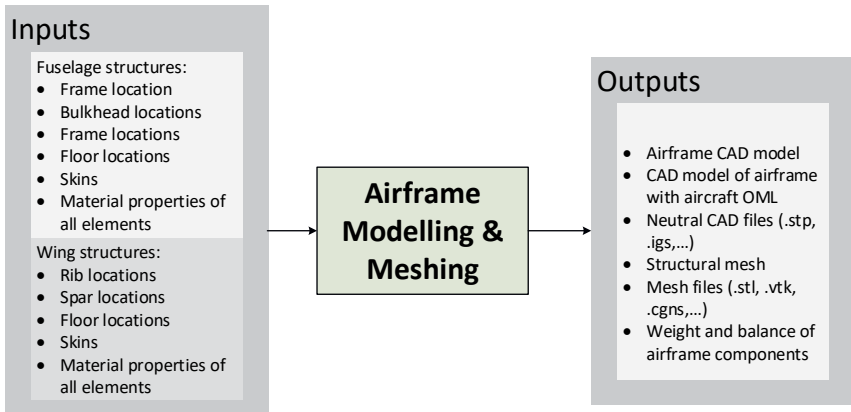
Figure 6.5: Inputs and outputs necessary to generate the SFT airframe geometry and mesh

Like geometry generation, the modelling and meshing of airframe components and their positioning in the CAD model must be automatic for use in MDAO applications. In addition, to positioning the airframe components, based on the geometry and material properties of the components, the disciplinary analysis should also generate the mass and center of gravity location of individual components for weight and balance estima-

tion.

6.3.2. COTS EQUIPMENT

Generally, a large database of different COTS equipment is available to the user. Depending on the test objectives and the SFT model design, the user must select relevant components that must be used by COTS discipline from a predefined database (see Figure 6.6). This database can be updated by the user if necessary.
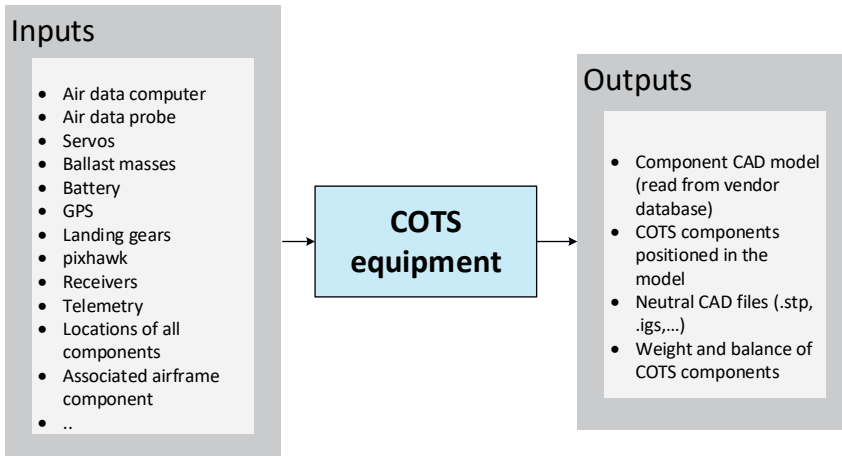
Figure 6.6: Inputs and outputs necessary to generate and position COTS equipment

Based on user inputs, either the bounding box of the component or the geometry file (.stp/.igs if provided by the vendor) must be read from the database by this disciplinary analysis tool. The bounding boxes or geometry of the COTS equipment must be used to ensure that there is sufficient clearance space available to install and remove COTS components. Furthermore, this discipline should position the COTS components at the appropriate location chosen by the user and determine suitable attachment location on the airframe to prevent the detachment of equipment in case of gusts/sudden manoeuvres.

6.3.3. PROPULSION SYSTEM ANALYSIS

Propulsion system ensures that sufficient power is available throughout the mission to perform the tests. Typically, most modern SFT rely on battery powered fans to propel the model. However, some larger models (>100 kg) use small turbojet engines. Often, propulsion system is acquired commercially off the shelf. In such cases, the geometry model, thrust and torque that can be produced by the engine is provided by the vendor. If the model is produced in-house, appropriate analyses must be performed to determine engine performance.

Based on the user selection of the engine (from the available database), their location and the number of batteries, the components are positioned on the model and weight and balance of all the COTS equipment is determined (see Figure 6.7). Furthermore,
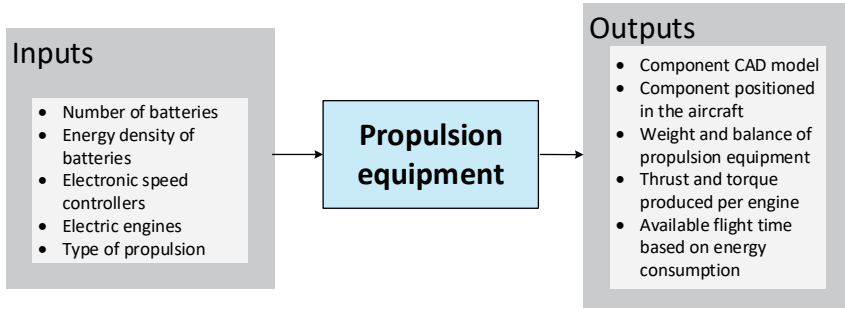
Figure 6.7: Inputs and outputs for propulsion system synthesis

the attachment to airframe is also determined in this discipline. Finally, the flight time available for the mission is calculated based on the energy consumption of the selected engine and the available on-board battery.

6.3.4. AERODYNAMICS ANALYSIS

Aerodynamics analysis is a key discipline when SFT is used to study Flight Dynamic and Aeroelastic similarity of the model and the prototype. This discipline requires a mesh suitable for aerodynamic solver, the test conditions and boundary conditions (depending on the type of analysis) as an input (Figure 6.8).
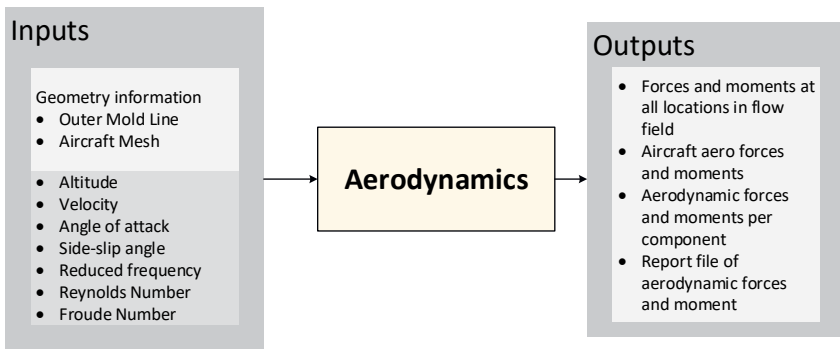
Figure 6.8: Inputs and outputs for aerodynamic analyses

Based on the inputs, an aerodynamic solver (such as panel method, RANS, Euler, etc.) is executed to determine the forces and moments acting on different components, overall aircraft and points of interest in the flow field. These results are used by other disciplines such as flight mechanics to determine the stability and control of the aircraft and the objective function to determine the DoS.

6.3.5. STRUCTURAL ANALYSIS

The structural analysis discipline is used to study the structural strength and stiffness to ensure the safety of the model in flight. In the case of aeroelastic analyses, structural analysis is also necessary to determine the flexibility of the model and the similarity of model shape deformation with prototype shape deformation [153, 157]. Often, for flight dynamic assessments, where rigid the SFT model is sufficient, the structural analysis is not performed at every iteration. A check is performed at the end of the optimization to ensure that the selected design does not deflect significantly.
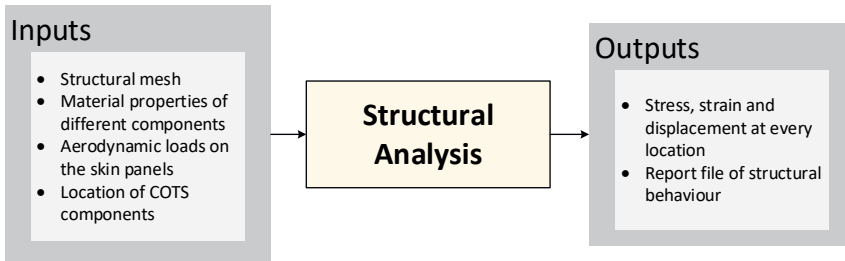
Figure 6.9: Inputs and outputs necessary to perform structural analyses

To perform these analyses, the structures discipline requires a mesh of aircraft and airframe components suitable for structural analyses, the aerodynamic loads, the location of COTS components and the material properties of aircraft components as input. Based on this, a structural solver (such as NASTRAN, ABAQUS, etc.) is employed to determine the stress, strains and displacements at all the locations desired by the user (Figure 6.9).

6.3.6. WEIGHT & BALANCE ANALYSIS

This discipline is necessary to determine the mass, inertia and the center of gravity location of individual components (COTS and airframe), aircraft sub-systems (wings, fuselage, engines) and the overall aircraft. This discipline is critical for flight mechanics analysis as all the forces and moments are calculated about center of gravity. Furthermore, the inertial forces and moments acting on the aircraft are determined by this discipline.
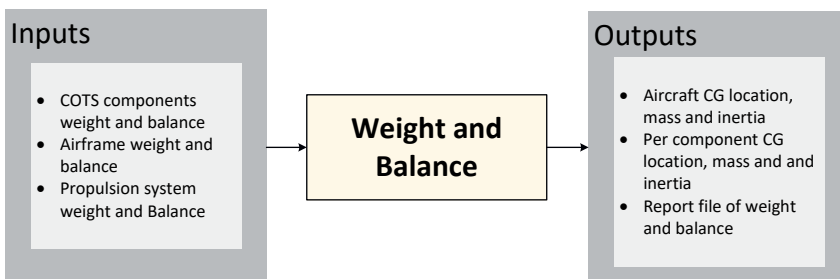
Figure 6.10: Inputs and outputs necessary to perform Weight & Balance analyses

This discipline requires information of COTS components, airframe and the propulsion system as input (see Figure 6.10). These inputs are not user input but are obtained from the outputs of other disciplines such as COTS equipment and airframe design.

6.3.7. FLIGHT MECHANICS ANALYSIS

Flight mechanics analysis discipline is important to assess the feasibility of a SFT mission irrespective of the phenomenon to be simulated. This discipline is necessary to determine the static stability of the model, dynamic stability, the trim condition and the available control power at trim condition.

To evaluate these characteristics of the model, the discipline needs information about the aerodynamic forces and moments acting on the aircraft at different flight conditions (angles of attack, side-slip angles and mach number), the weight and balance data of the aircraft (center of gravity location, mass and inertia), the test conditions, the location of the engine and the thrust and torque provided by the engine as shown in Figure 6.11.
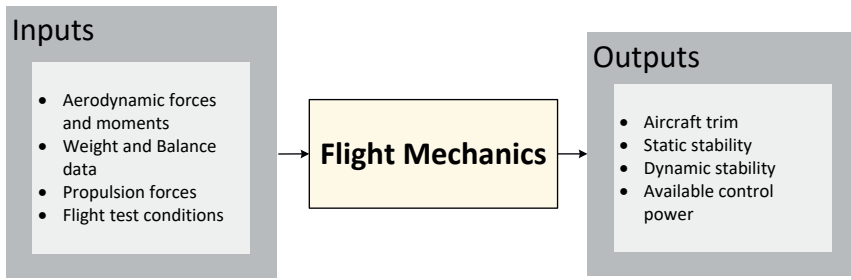
Figure 6.11: Inputs and outputs for flight mechanics analyses

6.4. CONSTRAINTS

The role of the constraints is to determine whether the given design can complete the mission safely while gathering all the relevant measurements to assess the performance and behaviour of the SFT model. These constraints are only related to the characteristics of sub-scale model and are not influenced by the full-scale aircraft behaviour. Some examples of constraints are:

1. the model should be statically stable

2. the model should be dynamically stable

3. the maximum stresses (σ) and strains (ϵ) experienced by the aircraft components during the mission within permissible limits set by disciplinary experts

$$\sigma_{max} < \sigma_{allowable} \tag{6.29}$$

$$\epsilon_{max} < \epsilon_{allowable} \tag{6.30}$$

4. the maximum weight of the aircraft

$$w_{max} < w_{allowable} \tag{6.31}$$

5. the minimum sensitivity of pressure probes used to measure surface pressure distribution

6. the model should be trimmable in flight

7. the model should be flyable by the ground based pilot within the flight box (important for facilities which impose visual line of sight)

These constraints are imposed using mathematical expressions in the optimization framework. The exact limits on the constraints are set based on test condition and the capabilities of the facility. A classic example of the SFT model constraint is the maximum weight of the model should be under 25 kg.

6.5. EXAMPLE PROBLEM FORMULATION USING DOS

A simple example problem is discussed in this section. Here, (MDAO based) computational scaling problem must be formulated to maximize the short-period motion similitude at a given altitude and test velocity. The model must maintain geometric similarity with the prototype. Furthermore, all COTS components must fit inside the model without intersection with other COTS/airframe components and the model must be statically stable. Mathematically, this problem can be formulated as follows:

maximize

$$DoS = f(C_{z_\alpha}, C_{z_q}, C_{m_\alpha}, C_{m_q}, \mu_c, K_Y) \quad \text{(See Equation 6.12)} \tag{6.32}$$

with respect to

$$\lambda \tag{6.33}$$

subject to:

$$h > 0 \tag{6.34}$$

$$\phi_{i,j} > 0 \tag{6.35}$$

where, h is the static margin, λ is the isometric scaling factor and ϕ is the clearance between i^{th} COTS components and j^{th} airframe/COTS components. All other coefficients remain the same as discussed in Section 6.2.4.

Since the model needs to be geometrically similar to the prototype, only isometric scaling factor (see Chapter 4) can be be varied. Thus, the scaling factor becomes the only design variable. The DoS is the objective function. The static margin and the component clearance are the constraint.

A UML activity diagram to maximize the similitude (DoS) between the model and the prototype is shown in Figure 6.12. The activities enumerated in Figure 6.12, can be accomplished by combining different disciplinary analyses discussed in Section 6.3. In principle, all the disciplinary inputs which are not state variables (of another discipline)
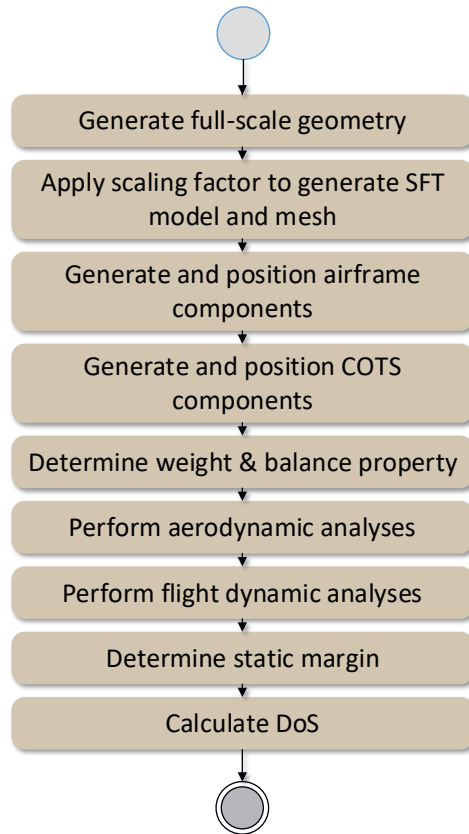
Figure 6.12: UML activity diagram of the key steps that must be performed to solve the MDAO problem shown in Equations 6.32 - 6.35

can be used as a design variable for the SFT model design MDAO problem. Since (model) scaling factor is the only design variable in this example, all other disciplinary inputs for these disciplines must be set by the user (often referred to as model settings/parameters) or they must be an output of another discipline (i.e., coupling variables).

Once the required disciplinary analyses, design variables and coupling variables are determined, an important consideration in implementing MDAO is to organize the disciplinary models, approximation models (if any), and optimization software [176]. For the example represented in Equations 6.32-6.35, the key tasks shown in Figure 6.12 are converted into a formal MDAO architecture represented by eXtended Design Structure Matrix (xDSM) [176] as shown in Figure 6.13.

In addition to demonstrating the formalization of MDAO problem and architecture, this example demonstrates the complexity of the SFT model design. Even with one design variable and two constraints, nine disciplinary analyses must be performed to determine the DoS of one model. In order to perform a full-blown optimization with geometry and mesh generation and medium/high fidelity aerodynamics/structural analyses,

the SFT model design time can become significantly larger than the time available to perform SFT itself.

Thus, performing these iterative disciplinary analyses manually becomes infeasible. This calls for the use of design automation techniques to perform the disciplinary analyses quickly and automatically to support the SFT model design. In Chapter 7 and 9 the methodology developed in this research work to automate these disciplinary analyses is discussed in Detail.

6.6. Discussion: Novelty in the Proposed Method

The extension of MDAO based computational scaling approach to maximize the similitude between the model and the prototype is the novelty of this work. In particular, the generally applicable figure of merit, Degree of Similitude (DoS), formulated in this dissertation to capture the extent of similitude between the model and the prototype helps in streamlining the SFT model design problem formulation. In addition, the proposed MDAO based computational scaling approach aids engineers in designing a catalog of SFT models (see Chapter 4) necessary to test different behavioural aspects of the prototype.

Guaranteeing complete similitude between the model and the prototype is impossible for most SFT design problems. In case of incomplete similarity, a formal methodology to assess the validity of the SFT model design for a given test objective was missing in the literature. Engineers often used empirical methods to account for the errors and approximations. Such methods were case-specific and not formalized or generic to allow an objective assessment of the SFT model. In this dissertation, synthetic measures such as Behavioural Indicator Matrix and Allowable Scaling Error have been proposed to allow the objective analysis of the validity of a SFT model for a given test objective.

The extended and formalised MDAO based computational scaling approach proposed in this dissertation coupled with a method to assess the validity of SFT models for a given test in case of incomplete similitude, lowers the barriers associated with computational scaling and provides a systematic methodology to adopt computational scaling in the design process. This gives engineers more time to focus on the development of disciplinary analysis tools and their integration that would otherwise be severely limited due to the time lost in formulating a suitable problem.

To enable this MDAO based computational scaling approach, a number of technical challenges concerning the automation of the SFT model design and multidisciplinary analysis needs to be addressed to reduce the design lead time by eliminating repetitive, laborious and time-consuming activities. How these challenges are address is discussed in the following chapters.

6
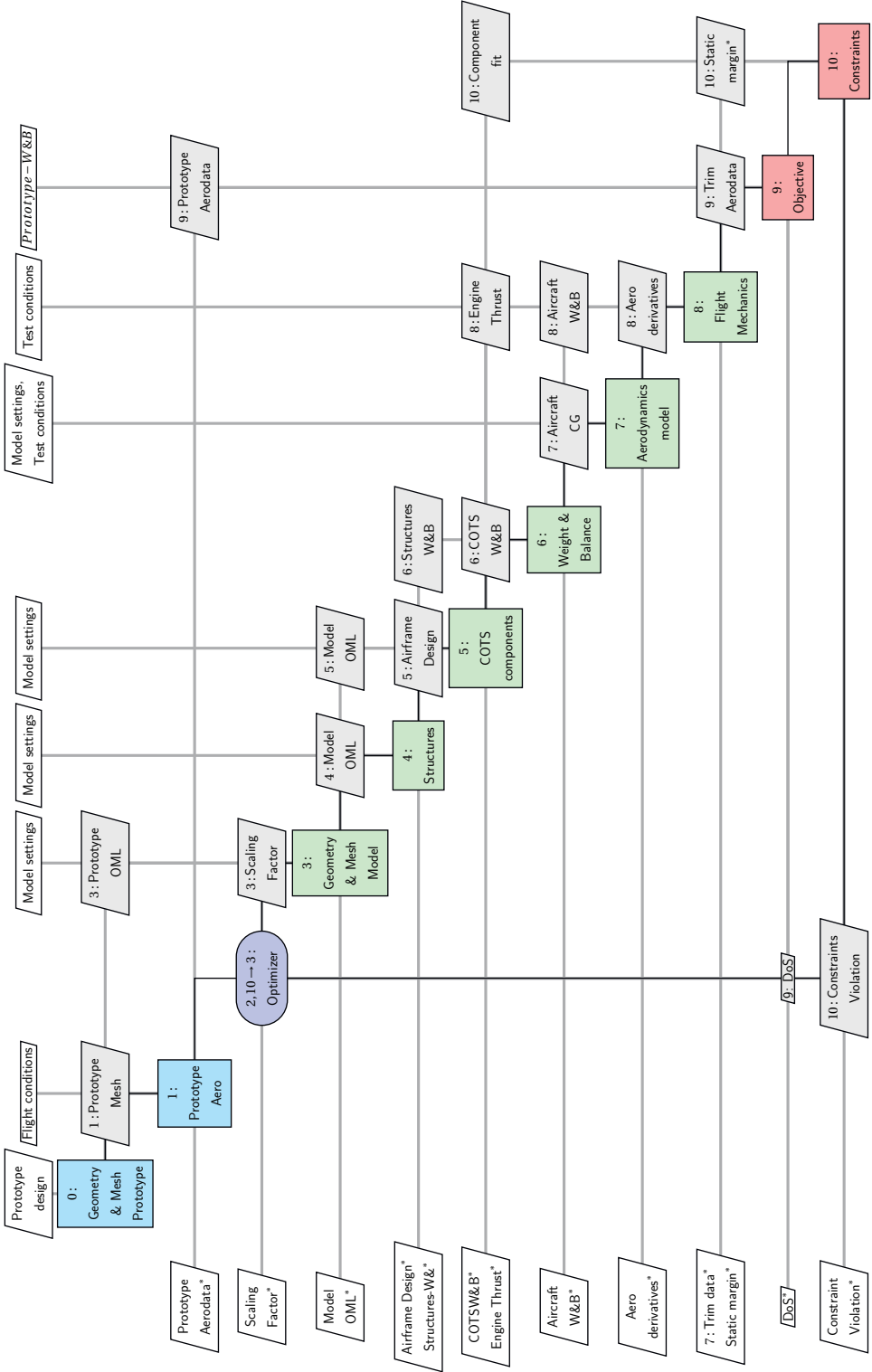
Figure 6.13: xDSM to solve the MDAO problem shown in Equations 6.32 - 6.35

7

SCALED MODEL DESIGN AND ENGINEERING ENGINE (SMDEE)

In this chapter, we discuss a scalable framework to enable the SFT model design using MDAO. Based on the discussion in the preceding chapter, we conclude that geometry in the loop MDAO framework is necessary to tackle the SFT model design problem. Design Engineering Engine (DEE), a geometry in the loop MDAO framework, has shown promise in addressing full-scale aircraft design problems in the past. An adaptation of DEE, called Scaled Model Design and Engineering Engine (SMDEE), has been developed in this work to specifically support the SFT model design. The SMDEE framework described in this chapter is a key enabler of the MDAO based similarity maximization technique discussed in Chapter 6.

Parts of this chapter have been published in AIAA SciTech conference (2019) and AIAA Aviation conference (2019) [177, 178]

In order to accomplish the synthesis and analysis tasks discussed in Chapter 6, the ability to generate and manipulate geometry representations of SFT model becomes indispensable. These geometry representations may be updated during each optimization loop (if required) and suitably modified for various analysis tools. Consequently, the geometry generator becomes the key element of the whole approach.

Numerous examples can be found in the literature on full-scale aircraft design where a MDAO framework has been implemented with the geometry in the loop [179–182]. A schematic of such an MDAO framework with geometry in the loop his shown in Figure 7.1.
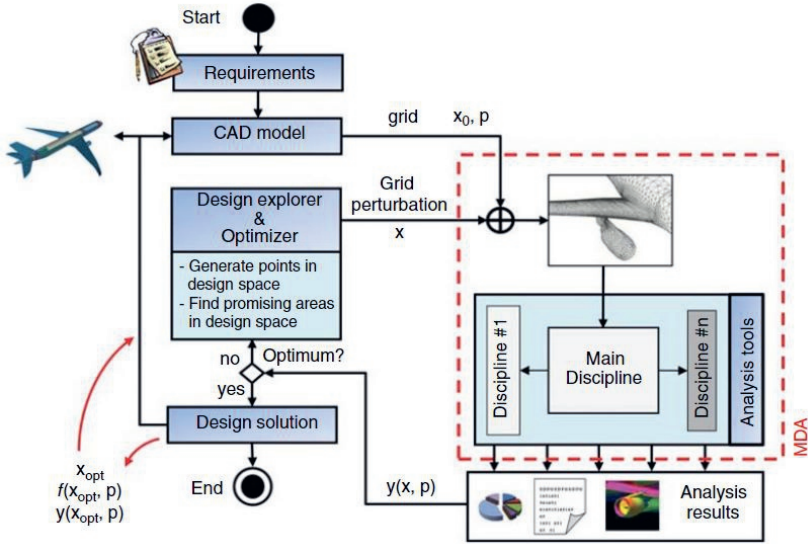
Figure 7.1: The MDAO design system with integrated geometry generation capability [183]

The development of a geometry in the loop MDAO framework to support the SFT model design poses numerous challenges at system architecture level, which include analysis capability, geometry manipulation and optimization. These challenges are generic and applicable to many complex MDAO problems. La Rocca [184] identified these challenges and translated them into a collection of needs to enable the MDAO design approach, which are also applicable to the SFT model design problem. Some of the key needs include the ability to support automation, integrate in-house and commercial tools at multiple levels of fidelity, parametrically model complex geometries and enable pre/post-processing activities.

For the last two decades, a conceptual design framework used to tackle geometry in the loop MDAO problems, called the Design and Engineering Engine (DEE), is under development at Delft University of Technology to support and accelerate conventional / unconventional full-scale aircraft design [184]. The DEE paradigm shown is a generic template of a design system to support engineers in formalizing and implementing complex MDAO problems. The paradigm and functional components of the DEE will be

briefly reviewed in Section 7.1. The DEE framework serves as the basis for the development of a MDAO framework for the design of SFT models called the Scaled Model Design and Engineering Engine (SMDEE). Numerous features of the DEE are (re)used in the SMDEE and certain features are extended where necessary. The development and implementation of the SMDEE features are discussed in Section 7.3.

7.1. DESIGN AND ENGINEERING ENGINE (DEE)

The DEE is a multidisciplinary collection of design and analysis tools to automatically interface and exchange data and information. The DEE supports and accelerates the MDAO of complex products, through the automation of the non-creative and repetitive design activities [184]. In this thesis, the focus will be on an aircraft DEE (both sub-scale and full-scale). The paradigm of the Design and Engineering Engine is illustrated Figure 7.2. This is a simplified representation of the system with only the main communication lines.
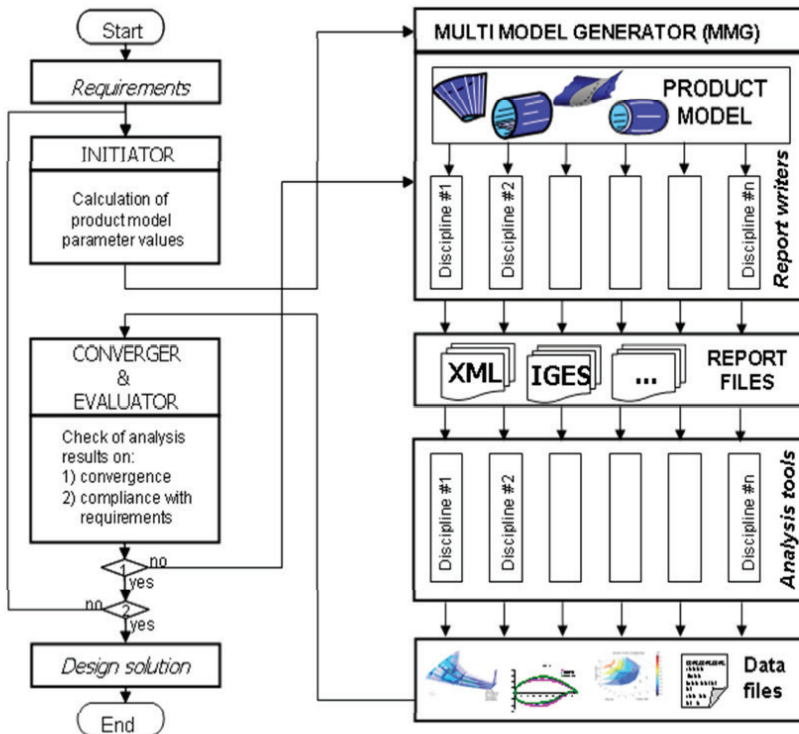
Figure 7.2: The Design Engineering Engine Paradigm [185]

The DEE is an integrated design system built up of loosely coupled modules, which can vary in number and type according to the design case at hand. The DEE paradigm can be customized based on the user needs. For example, the SMDEE for the SFT model design is a specialization of the DEE Framework (Section 7.3). Depending on the design

case, different analysis modules can be included or left out of a specific DEE implementation. The architecture of the DEE is composed of six main components. Each component is briefly discussed in the following sections. For the detailed discussion on the DEE, reader is referred to the work of La Rocca [184].

7.1.1. MULTI-MODEL GENERATOR (MMG)
The MMG is a software tool based on Knowledge Based Engineering system [185] conceptualized by La Rocca [184] with the twofold intent of:

1. providing designers with a parametric modeling environment to generate models of conventional and novel aircraft configurations

2. automate the generation of input data and specific disciplinary models for various disciplinary analysis tools.

The MMG is able to automatically and quickly generate geometry models of varied aircraft configurations based on an initial set of input values. The generated models are further manipulated by the MMG to obtain aspect models (e.g. surface and volume meshes) that are used as input for disciplinary analyses. The MMG will be discussed in detail in Section 7.2.

7.1.2. INITIATOR
Initiator is a collection of tools and methods that provides an initial set of input values to the MMG to automatically instantiate aircraft CAD model. Prototype Initiator for the conceptual design of a complete full-scale aircraft (conventional and unconventional) has been developed at TU Delft [186]. This includes tools and methods for the conceptual design of the wings, fuselage, engines, internal structures and determination of the weight and balance and aerodynamic loads based on customer requirements, regulations and handbook design methods [186]. Initiator combines these tools and methods to arrive at a feasible initial solution to be fed to the MMG before the start of a full-blown MDAO/convergence process.

7.1.3. DISCIPLINARY ANALYSES TOOLS
Engineers need to perform multi-fidelity analyses using both commercial and in-house tools (such as panel methods, RANS, FEM etc.) to enhance confidence on their designs. The DEE is an ideal framework to plug varied disciplinary analysis tool depending on the project needs. Furthermore, the MMG can automatically generate the input aspect models (abstraction of aircraft CAD model such as meshes) needed for disciplinary analysis to speed up the design process and enable MDAO. The advantage of using the DEE is that the different disciplinary analysis tools can exchange data among themselves or via the MMG as needed. For example, a structural analysis module can use the loads computed by an aerodynamic analysis module to determine the deflections in the model.

7.1.4. CONVERGER AND EVALUATOR
Converger and Evaluator gathers the disciplinary analyses results and post-processes them to determine the feasibility of the design (i.e., convergence of various analyses)

and assess its performance based on the objectives set by the designer. This feasibility and performance assessment capability is typically provided by an optimizer. After assessing the design, optimizer typically proposes a new set of design variables (based on optimization or design of experiments algorithm) which become input parameters to the MMG. Consequently, the MMG modifies the aircraft model and produces updated analyses data. In case the optimizer is unable to satisfy the initial requirements, the loop is terminated and the initiator will have to synthesize a different aircraft to restart the loop.

7.1.5. COMMUNICATION FRAMEWORK
A key challenge in the design of complex products such as an aircraft is the management of data and information flow between different design synthesis and analysis tools (represented using a set of connectors in Figure 7.2). The DEE proposes the use of agent-based architecture to speed up the design process. An agent-based communication framework (developed by Berends and Van Tooren[187]) mimics the organizational structure of a design team, where various human actors work and interact in a flexible service oriented approach rather than in a rigidly predefined procedural scheme [184]. This agent based system enables fast set-up and reconfiguration of a MDAO workflow for different design problems. Typically, web-services (installed on different servers/computers) are used to link different tools (discussed further in Chapter 9).

7.2. MULTI-MODEL GENERATOR (MMG)
At the heart of the DEE lies the Multi-model Generator (MMG). The MMG provides a modeling system where a number of predefined parametric modules (components) are available, which the designer can adjust and combine to assemble large number of aircraft configurations and configuration variants [184]. The MMG serves two main purposes, namely, automatic generation of CAD models using parametric definition of (full-scale) aircraft geometry and the creation of aspect models that become input for specific disciplinary analyses. The ability to automatically generate and analyze aspect models helps in significantly speeding up the design process, which in turn helps engineers in advancing from *back of the envelope calculations* to medium and high fidelity analysis. Consequently, the maturity and performance of the design improves over time.

The MMG has been developed using a Knowledge Based Engineering system. A KBE system is based on Object Oriented Programming (OOP) paradigm that includes run-time caching, dependency tracking and lazy-evaluations. The first and second generation KBE systems (such as ICAD[1] and Genworks GDL[2]) only included a geometry kernel to aid in the designers with model analyses. Modern KBE systems such as ParaPy[3] include meshing libraries and application programming interfaces to commercial tools in addition to geometry kernel to further speed up the design automation process.

The KBE system is a key enabler of the MMG because it allows engineers to capture the aircraft concepts and categories and not just specific instances. This has been made

---

[1] no longer in service
[2] https://www.genworks.com/
[3] https://www.parapy.nl/

possible by means of OOP classes called High Level Primitives (Section 7.2.1) and Capability Modules (Section 7.2.2), which can be exploited to define specific aircraft designs. The MMG was originally implemented using ICAD KBE system. Thereafter, it has been re-implemented in both Genworks GDL and ParaPy with significant advancements from the original capabilities and structure. In the remainder of this dissertation, the different constituents of the MMG will be explained using the (latest) ParaPy implementation. Nevertheless, the fundamental concepts of the MMG remain unaltered from the first version.

7.2.1. High-Level primitives

The Multi-Model Generator (MMG) supports both unconventional and conventional aircraft design. A review of aircraft designs currently being investigated shows that aircraft configurations can be generated by composing a handful of components (aircraft abstraction features) such as wings, fuselage, engines, tails etc. in varying parametric permutations and combinations. In other words, most aircraft configurations that are considered as the future of aviation are a specialization of these aircraft abstraction features.

La Rocca [184] defined a number of functional blocks to capture elements of similarity among (significantly) different aircraft configurations and use them as the parametric modules for modeling. These modules are named High Level Primitives (HLPs). The name HLP is chosen in contrast with the low level primitives used in conventional CAD systems. Their implementation forms the basis of the Multi Model Generator. A High Level Primitive (HLP) is a KBE artifact that contains both declarative and procedural knowledge, where the latter consists mostly of the specific operations to generate the geometry of the given HLP instance. The encapsulated knowledge is different and specific for each HLP and cannot be shared/reused by other primitives [184].

Nevertheless, the same HLP can be used to model different functional elements of the aircraft. For example, wing primitive, can be used to model different wing parts of an aircraft such as winglets, canard wings, vertical horizontal tails and the movable components such as rudders, ailerons, etc. [184]. The object oriented paradigm suits the case as the HLPs can be modeled as classes that can be instantiated as objects for different set of attribute values.

In its current version, two main categories of aircraft HLPs have been identified in the MMG, namely:

1. **Outer Mold Line (OML) primitives**: primitives to define the outer shape and size of the aircraft (e.g., lifting-surfaces (wings), fuselage, engine etc.)

2. **Internal Components primitives**: primitives to define the shapes and sizes of components internal to the aircraft (e.g., wing structural elements, fuselage structural elements, fuel tanks etc.)

La Rocca [184] demonstrated that it is possible to assemble a large number of aircraft configurations having radically different OML topologies by defining just four High Level Primitives, such as Wing, Fuselage, Engine and Connection-element (to join the other wings into a continuous and watertight surface) (Figure 7.3). A detailed explanation of HLPs in the current implementation of MMG is provided in Appendix C.
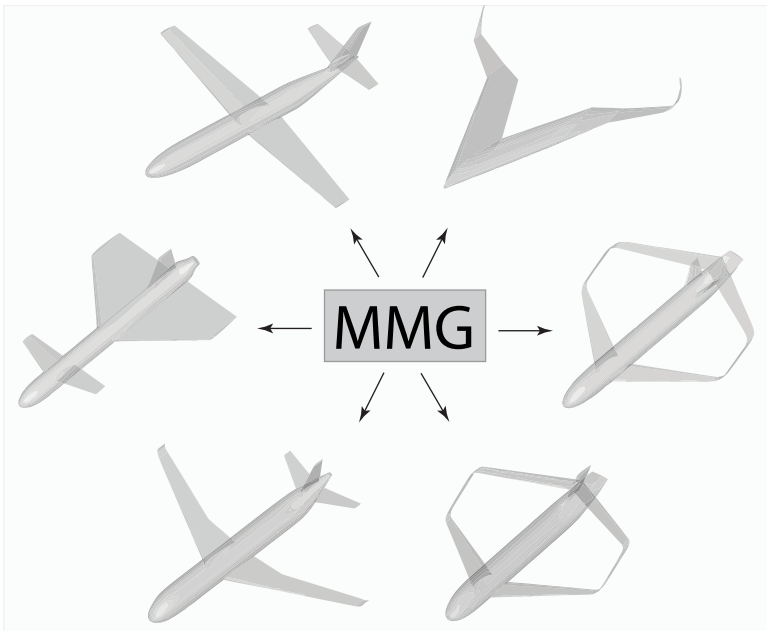
Figure 7.3: Generation of different aircraft configurations and their variants in the MMG

7.2.2. CAPABILITY MODULES

Capability modules have been implemented in the MMG to address the challenge of developing consistent and synchronized aspect models to support and speed-up the work of disciplinary experts. A Capability Module (CM) is a KBE artifact that contains procedural knowledge. CMs are generalized methods that support disciplinary analyses. A CM is generally linked to a HLP and enhances the functionality of HLP. For example, a CM does not autonomously generate geometrical entities (wings, fuselage, engines, etc.) on its own but modifies the geometry generated by HLP to support mesh generation for aerodynamic solver.

CMs capture the abilities and knowledge of the engineer in the form of rules. In particular, they generate different abstractions of the master geometry model for a range of disciplines discussed in Chapter 5 and 6. The generation of these geometrical abstractions, also known as aspect models, is laborious and time-consuming (especially for high-fidelity tools) but essential in the pre/post-processing of disciplinary analyses. Fortunately, a large part of these pre/post-processing activities are systematic and repetitive. Thus, the way designers process the general purpose CAD model of an aircraft into an aspect model (i.e., input model suitable for Fluent[4], FlightStream[5] or some other analysis tool), is independent of the aircraft configuration.

By means of interviews, direct observation and other dedicated knowledge acquisition techniques [188, 189], specialists' working practice can be elicited, which can in-

---

[4]https://www.ansys.com/products/fluids/ansys-fluent
[5]https://www.darcorp.com/flightstream-aerodynamics-software/

turn be used to transform a general purpose CAD model into a set of aspect models. Example CMs typically used in aircraft design are shown in Figure 7.4.
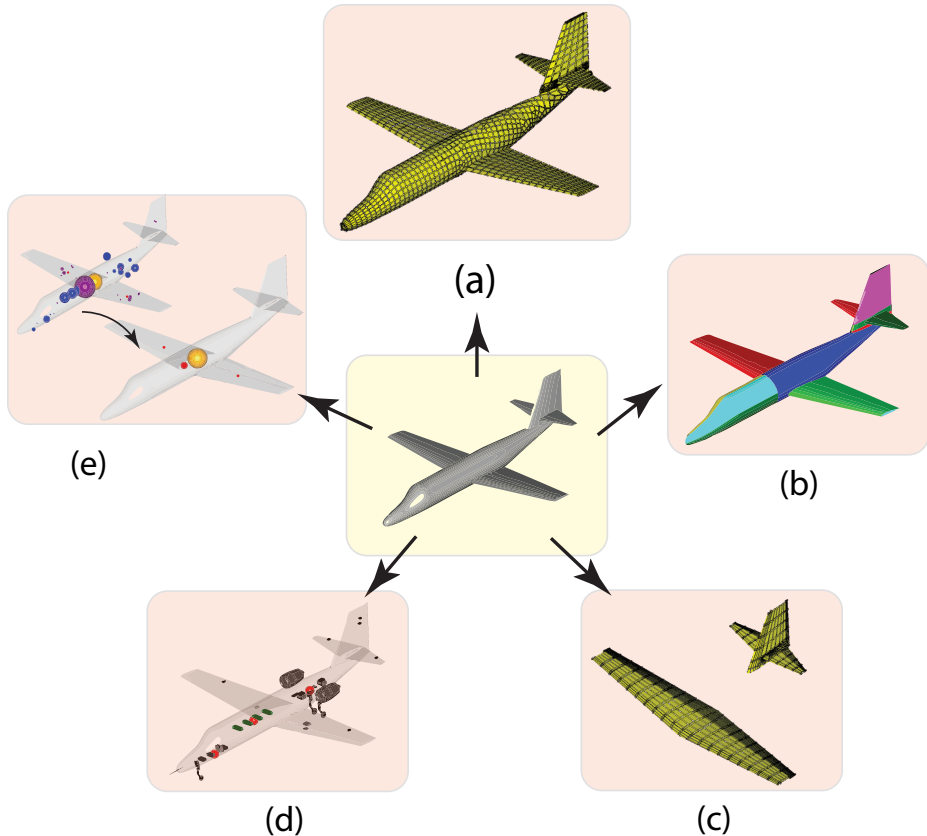
Figure 7.4: Some examples of the pre-processing activities that can be performed by different CMs on a given aircraft HLP, as follows: (a) The outer surface of the aircraft is translated into mesh suitable for aerodynamics analysis (b) outer skin panels of the aircraft are segmented sets of meshable surfaces to generate aerodynamics/structural meshes (c) relevant surfaces are extracted from aircraft HLP to generate meshes for wing structural analysis (d) module positioning the COTS equipment at appropriate location in the model (e) system of distributed points is generated to determine the center of gravity of the aircraft based on the positioning and masses of different aircraft components

The aspect model generated by the MMG capability model can either be a direct input to (in-house built/external) analysis tool or could be an input to another pre-processing tool which provides input to analysis solver. For example, the aircraft surface segmentation by the MMG (shown in Figure 7.4 (b)) can be fed into PATRAN[6] which

---

[6]https://www.mscsoftware.com/product/patran

generates the mesh file to be input into NASTRAN[7] for FEM analysis whereas positioning of COTS equipment and determination of weight & balance properties (Figure 7.4 (d) & (e)) are directly used to assess aircraft performance and/or behaviour. In the preceding versions of the MMG (built in ICAD and GDL), there was no link to a meshing module. Thus, external pre-processing tools were necessary to perform mesh based disciplinary analyses. In the current implementation of the MMG (using ParaPy), Salome meshing module[8] is available within the KBE software. This has led to the development of configuration agnostic meshing modules (i.e., the meshing CM remains the same independent of the aircraft configuration being studied). This not only improves the applicability of the MMG for a wide variety of aircraft configurations, but also improves the user control on mesh generation and reduces the post-processing burden on the MMG application developers. These configuration-agnostic features of the MMG are discussed in Chapter 8.

7.2.3. USER/OPTIMIZER ROLE IN MMG

The HLPs and CMs cannot substitute the designers in their decision making. Despite their generative capabilities, these software modules cannot judge the quality and the validity of the data received as input by the designers (or optimizers) that set the input values in the MMG application. HLPs and CMs are means to create a flexible, robust and automated modeling environment capable of delivering valid output for the given input in a fraction of time needed to perform the same task manually.

In cases where optimizer is used as shown in Figure 7.2, the optimizer proposes designs on the basis of the evaluation of objectives and requirement using adequate search algorithms. Ultimately, the responsibility of deciding the configuration to be modeled and judging the design quality lies with the designer/optimizer (with adequate support from analyses tools). Thus, HLPs and CMs do not directly steer the design but help the designers (and/or optimizers) in decision making by enabling quick and automated design space exploration.

7.3. SCALED MODEL DESIGN AND ENGINEERING ENGINE

Scaled Model Design and Engineering Engine (SMDEE) is an adaptation of the DEE specifically aimed at supporting the SFT model design problem discussed in Chapter 6. A schematic of the SMDEE as used in this research work is shown in the Figure 7.5. Indeed, a large part of the framework closely matches with the DEE as the SMDEE is a specific instance of the DEE. The key elements of the SMDEE are described in the following paragraphs.

Prerequisites: The SMDEE is developed to support the SFT model design for simulation tests. Since the simulation tests are aimed at mimicking specific aircraft configuration, a (converged) full-scale aircraft design must be provided as an input to the SMDEE. This can be in the form of paper design without any CAD representation. Such a design can also be obtained by running the full-scale aircraft initiator as shown in Figure

---

[7]https://www.mscsoftware.com/product/msc-nastran
[8]https://www.salome-platform.org/user-section/about/mesh
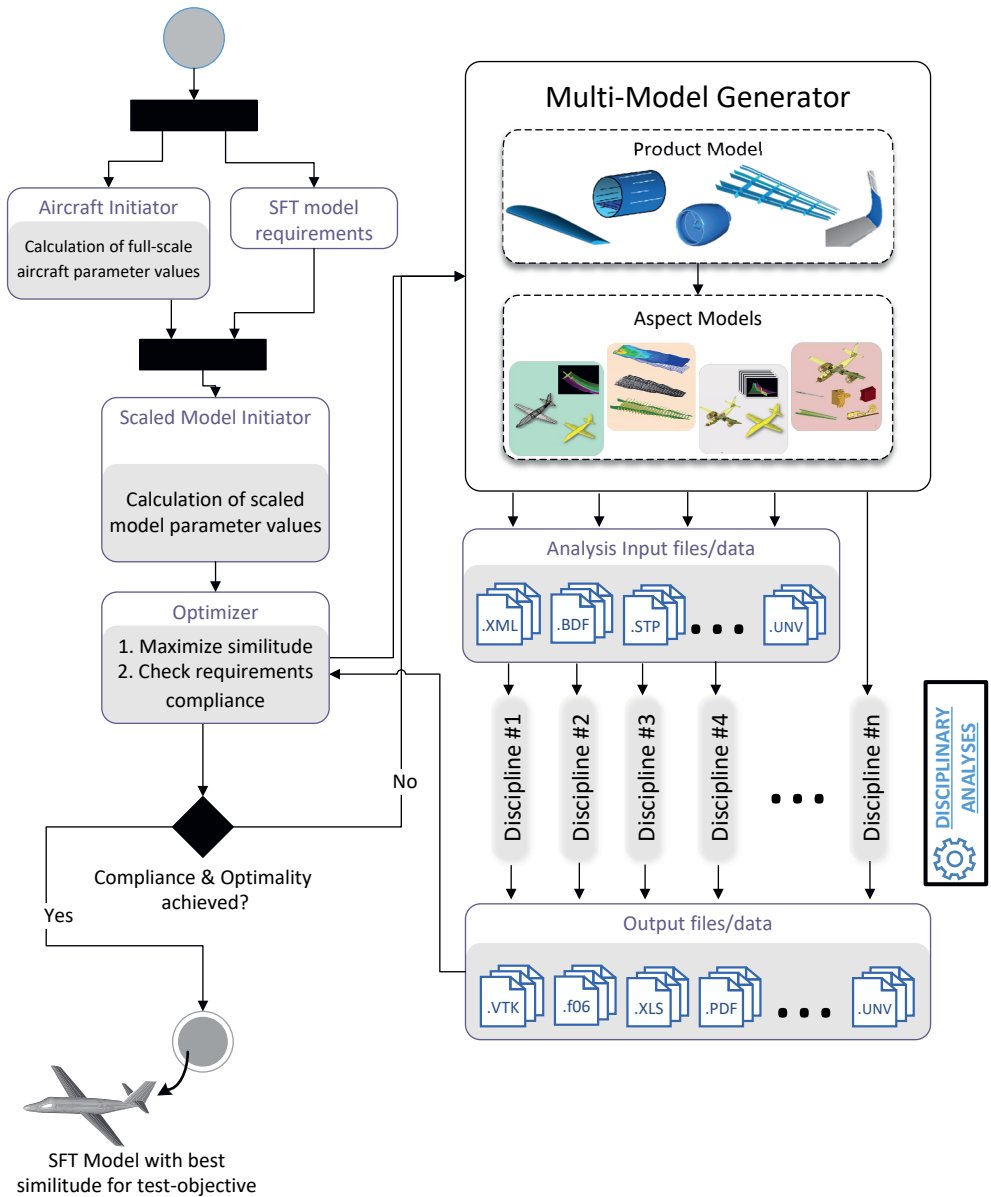
Figure 7.5: Scaled Model Design and Engineering Engine: an instantiation of the DEE paradigm

7.5. In addition, different stakeholders (disciplinary experts, test engineers, designers etc.) must agree on the requirements that the final the SFT model must satisfy. This is typically a sub-set of the requirements listed in Chapter 5.

Scaled Model Initiator: The Scaled Model Initiator (SMI) is a collection of tools and methods intended to provide an initial design of a scaled model. This initial design is the input to the optimizer that performs the task of computational scaling. The SMI is discussed further in Section 7.4

Optimization and Compliance: The aim of the the optimization is to maximize the similitude between the model and the prototype. The optimizer should ensure that the scaled model satisfies the requirements discussed in Chapter 6. Typically, commercial optimization algorithms that support constrained optimization work well for most computational scaling problem as shown in Chapter 10. However, dedicated algorithms might be necessary for complex problems where many phenomena must be studied using a single SFT.

Multi-model Generator: The tasks of the MMG remains the same as discussed in Section 7.2. However, the capabilities of the MMG have been extended to include the ability to model a (sub-)scale aircraft, position COTS equipment and generate aspect models for disciplinary analyses specifically aimed to support the SFT model design (see Section 7.5 for details).

Disciplinary Analyses: The aspect models generated by the MMG are used to determine the extent of similarity and requirement compliance of a given scaled model. These disciplinary analyses can be performed either using commercial software or in-house tools. The number and type of disciplinary analyses largely depends on the requirements and the phenomena being replicated using the scaled model. Some of the analyses used in this research are described in Chapter 9.

Execution and communication Infrastructure: Designers depend on medium/high fidelity analyses to predict the performance of their designs. Such analyses require significant computational resources, which largely affect the execution time. The execution time can be high enough to make the optimization unfeasible in the time allocated for SFT. Thus, appropriate infrastructure must be constructed to support computational scaling. Furthermore, the transfer of data and information between different components of the SMDEE and the external tools is a critical challenge. The execution and communication infrastructure will be discussed in Chapter 8.

7.4. SCALED MODEL INITIATOR (SMI)

Once the conceptual design of full-scale aircraft is (almost) complete and the requirements and objectives of SFT are clear, the SFT model design process starts. In this phase, an initial parametric definition of the SFT model (based on full-scale aircraft design generated by the aircraft initiator[9]) is necessary to invoke the MMG. Furthermore, the test conditions for SFT (i.e., the test velocity and altitude), must be known to start DoS calculation. Finally, an initial design of the SFT model structural components, selection of

---

[9]Aircraft initiator is intended for full-scale aircraft design. The SMI is a separate tool developed in this research to support the SFT model design.

COTS components and their positioning is required to determine the compliance of a model with the requirements. To this end, the SMI has been developed in this research work to aid the designers with the initial set-up of the SFT model definition and test condition, which is done as follows:

- **Test conditions & Model OML size**: The test conditions and initial sizing of the OML are typically performed using the Classical Similitude Theory as discussed in Chapter 4. Depending on the phenomenon being studied, the user can select Geometric Scaling, Froude number Scaling, Reynolds number scaling or a combination thereof. A python script is used in the SMI to calculate the scaling factor and the test conditions using classical similitude theory.

- **Selection and positioning of COTS components**: The COTS components that are used in the SFT model are dependent on the objective of the test and the size of the model. Thus, selection of COTS equipment and the number of floors where these components must be accommodated must be decided by the user. The SMI supports the user by providing an extendable database from which components can be chosen. Furthermore, the location of the floors (i.e., whether they should be housed in fuselage or wings and where) should be provided by the user. These positioning inputs are relative to the length of the fuselage or span of the wing (see Appendix C for details).

  Selection of the propulsion components is slightly more challenging as the engine (and the number of batteries on-board) needs to be adapted with the changing size and weight of the model. Furthermore, estimating the weight of the SFT model without complete CAD is challenging as there are no empirical rules for weight estimation (unlike full-scale aircraft). Engineers can use an approximate SFT model mass and simplified rules proposed by Raymer [190] to select an initial engine from the database. Typically, for aircraft under 3m span, engines are available from 50 N up to 200 N [34] which are sufficient to fly models up to 60 kg (and heavier if the model is aerodynamically efficient).

  Other than the database, SMI does not provide any synthesis support for the selection of COTS equipment as lower order tools and methods are not available. Furthermore, such tools are not easy to develop due to the variability in test conditions, objectives and model shape. Nevertheless, an initial selection of COTS equipment is sufficient to trigger the design process in the SMDEE. The higher order analyses tools in the SMDEE further checks whether the selected components can sustain the mission and the optimizer modifies the design suitably to make the model compliant to requirements selected by the stakeholders at the start of the design process.

- **Structural component positioning**: The SFT model structure could be one of two types, namely, monocoque or space-frame structure. Monocoque structure is a construction in which the outer skins bear the stresses. Thus, only the external skin panels bear all the loads in monocoque structures. In case of monocoque structure, depending on the material of the skin, the initial skin thickness must be

provided by the user and the MMG uses the OML to generate the skin panels (i.e., the airframe structure).

In the SFT model design, the space-frame components are ribs, spars, frames, floors, etc. (see Figure 5.1). Preliminary studies indicate that monocoque structures (with sufficient skin thickness) are well-suited for rigid aircraft studies (discussed further in Chapter 9). However, in cases where flexible models must be designed, space-frame structure is chosen.

In case of space-frame structure, the user must choose the number and position of ribs, spars and frames. For this, the location of floor panels and the rules proposed by Raymer [190] are used for initial sizing as shown in Table 7.1.

Table 7.1: Overview of structural design rules proposed by Raymer [190]

	Lower bound	Upper bound	Nominal Value	Units
Front Spar	0.2	0.3	0.2	fraction of (local) chord length from leading edge [-]
Rear Spar	0.6	0.75	0.75	fraction of (local) chord length from leading edge [-]
Rib spacing	0.2	0.8	0.3	m
Bulkhead Locations	[-]	[-]	N.A	Locations where wing /tails/pylons attach to fuselage
Frame spacing	0.2	0.8	0.3	m

The floor location and size is a user input as discussed in the preceding paragraph. Based on the floor location, SMI automatically adds frames (if housed in fuselage) or ribs (if housed in wings) around the floor to support it (see Figure 5.1). The nominal values shown in Table 7.1 are provided to the MMG as initial values to generate the CAD model of the airframe. In case the user decides to have multi-spar system or add ribs at specific locations (in addition to the ribs generated based on pitch requirements shown in Table 7.1), additional components can be added using an input file.

Role of the user: SMI is semi-automated and is only intended to support engineers in making design decisions for the initial design. These decisions are further fine-tuned by the optimizer depending on the design variables selected for the problem (see Examples in Chapter 10).The user decisions are essential and irreplaceable in the current state of practice where consolidated design rules are not available yet for the initial design of a SFT model. In the future, after sufficient empirical data is available, a completely automated SMI might be possible.

7.5. MULTI-MODEL GENERATOR TO SUPPORT SFT MODEL DE-SIGN

The MMG is also used in the SFT model design because the aircraft abstraction features / functional elements (wing, fuselage, engines, etc.) remain the same for full-scale and sub-scale aircraft. However, their size and shape could vary. Although the MMG allows engineers to vary the size and shape of the model in its parametric definition of functional elements, it does not include the ability to geometrically/aerodynamically scale the model. Furthermore, certain structural and COTS equipment are only needed in a sub-scale aircraft such as pressure-probes, inertial measurement units, etc. Suitable primitives must be developed to support the SFT model design. To this end, the current full-scale aircraft MMG is extended to accommodate the SFT model design. These enhancements, which are the key enablers of the MDAO based computational scaling, are discussed in Chapter 8.

7.6. DISCUSSION: SCOPE AND APPLICABILITY OF SMDEE

In this chapter, we illustrated the features of the SMDEE to support the design of sub-scale models which is an instantiation of conceptual design framework, the DEE. As the use of SFT becomes widespread, the requirements associated with the SFT model design and the corresponding disciplinary analyses will also change. The modularity of the SMDEE will easily allow engineers to plug newer disciplinary analysis tools to the framework and quickly generate synchronized aspect models. Additionally, the automation benefits obtained from the MMG eliminates the delays caused by manual labour, human errors and fatigue induced by repetitive tasks, thereby making the SMDEE a key enabler of computational scaling approach discussed in Chapter 4.

Nevertheless, the use of the SMDEE does not offer any guarantees on the assessment provided by external disciplinary tools (i.e., compliance with similarity, safety and measurement requirements). The results produced by the SMDEE is as good as the tools used in disciplinary analyses. Furthermore, the SMDEE has no control on the time needed for analyses themselves, as it only reduces the time associated with the pre/post-processing.

In the following chapters, we discuss the enabling technologies developed in this dissertation to support MDAO based computational scaling. Furthermore, we also discuss the accuracy and cost of disciplinary analyses used in this dissertation.

8

ENABLING TECHNOLOGIES FOR MDAO BASED COMPUTATIONAL SCALING

Extension to the Multi-Model Generator (MMG) to support the parametric design and analysis of a SFT model and the development of the parallel execution environment to reduce the execution time of external disciplinary analyses tools are the two main technical developments to support MDAO based computational scaling. These developments are discussed in detail in this chapter.

Since its inception, different aircraft configurations could be modelled using the MMG by combining different HLPs, although, certain adjustments were needed at the code level to model unconventional configurations. This necessitated expert programming knowledge and code-architecture understanding from the designer. In the case of the SFT Model design, where the designers are not necessarily programmers, adjusting the code within the rather short design lead-time is untenable.

Thus, the capabilities of the MMG have been extended to make it configuration agnostic, which allows designers to set the position and orientation of different HLPs and the MMG will automatically generate the geometry and aspect models without requiring modification to the code. The benefits and implementation of this configuration agnostic framework are discussed in Section 8.1.3. In addition to enhancing the HLP of the MMG, a number of capability modules have also been enhanced to support the SFT Model design. These are discussed in Section 8.2

Despite design automation with the SMDEE, the framework (i.e., the SMDEE together with external analysis tools) can take weeks to obtain an optimized SFT model. To this end, infrastructural improvements have been made to the SMDEE execution environment to enable parallel execution of disciplinary tools, which are essential enablers of the SMDEE as they reduce the optimization time from weeks to days, thereby enabling MDAO based similarity maximization. The development of a parallel execution environment and its impact on MDAO based similitude maximization is discussed in Section 8.3.

8.1. Enhancement of High-Level Primitives in MMG

The High-Level Primitives used in the MMG for the SFT Model design are the same as those used for full-scale aircraft design as discussed in Section 7.2 and Appendix C. In addition to the HLPs for full scale aircraft, two main enhancements have been made to the MMG to support the SFT model design process as follows:

1. Scaling of OML and airframe components which is applicable to all HLPs involved with the geometric modelling of the SFT Model

2. Modelling and positioning of COTS components

Each of these will be discussed briefly in the following paragraphs.

8.1.1. Scaling of OML and Airframe Components

Scaling can be performed in numerous ways as discussed in Chapter 4. However, in order to perform computational scaling, the CAD model of such scaled models must be generated quickly and automatically. Such scaling is not only limited to geometrical scaling but also includes scaling in a specific direction, scaling of one functional component, scaling of a specific feature such as airfoil as shown in Figure 8.1. All the HLPs explained have been enhanced to allow scaling of the models based on user input.

8.1.2. COTS Component Modelling

Modelling of COTS components was not included in the original version of the MMG as they are not used in full-scale aircraft design. Developing a HLP to model a wide
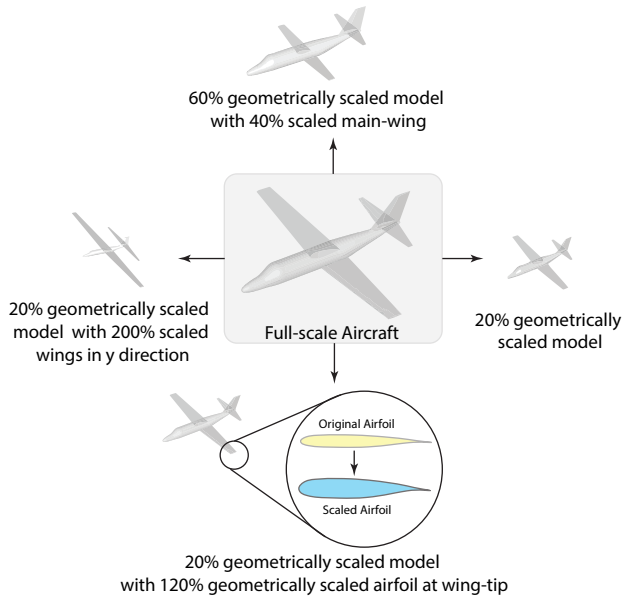
Figure 8.1: Different scaling capabilities available in the MMG to support the SFT Model design
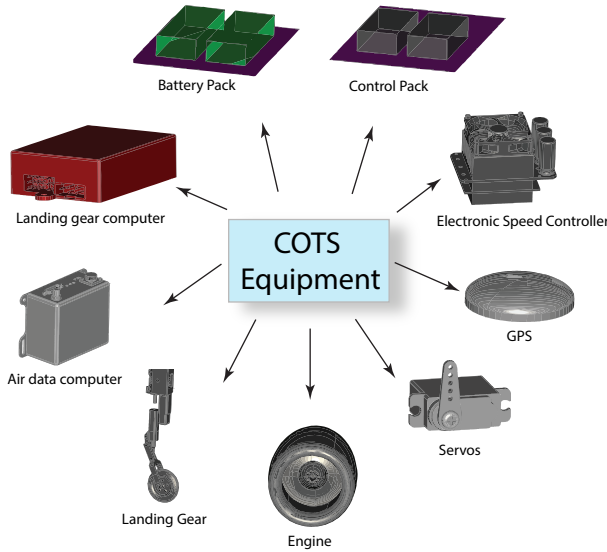
Figure 8.2: Geometry of different COTS equipment imported by the MMG to support the SFT Model design

variety of COTS components available in the market is impractical. However, geometry information of these COTS components is necessary to ensure that they do not interfere

with other components of the SFT model.

Typically, most vendors provide a neutral CAD file (.stp/.igs) with the product specification. This information is stored in a database of the COTS components available in the MMG and read by the MMG to generate the geometry of the model. If such geometry files are not available, dimensions of the component can be stored in the COTS equipment database to generate a bounding box which are used to check the clearance with other airframe/structural components. Example of COTS equipment models imported by the MMG from COTS equipment database are shown in Figure 8.2. Figure 8.3 shows examples of COTS components positioned by the MMG in two aircraft models.

(a)   (b)
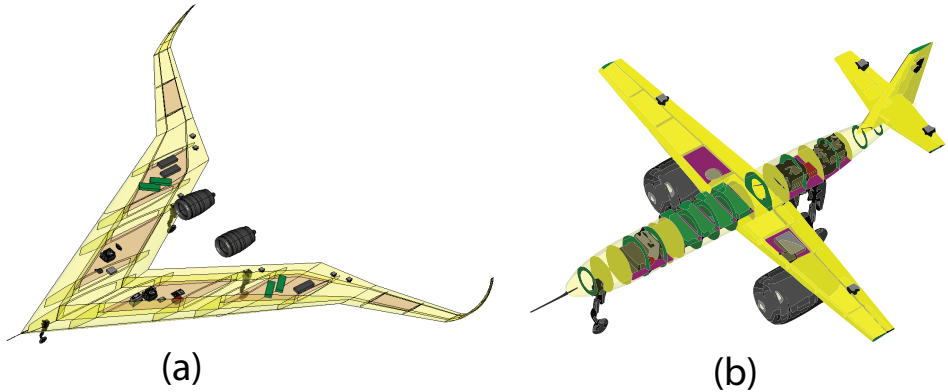
Figure 8.3: A snapshot of COTS equipment positioned at appropriate floors by the MMG on a scaled model of (a) Flying-V and (b) Cessna Citation II aircraft

8.1.3. CONFIGURATION AGNOSTIC MODEL DESIGN USING MMG

The role of the SMDEE is to support the designer by providing the SFT model of varied aircraft configurations. Naturally, the MMG must be able to support the design of a large variety of configurations. As discussed in Section 7.2, this is possible using OML HLPs. Nevertheless, in the past versions of the MMG, adjustments had to be made at the code level to generate different topologies of aircraft configuration. For example if the designers had to move from a blended-wing body configuration to conventional tube and wing aircraft, they would have to manually add or remove Fuselage HLP (class). This required a detailed understanding of the code and consumed considerable time before the actual synthesis and analyses tasks could be performed. To overcome these challenges, in the current version of the MMG, a configuration agnostic model design algorithm has been formulated.

As illustrated in fig 7.10, the MMG reads the wing user input file (see Appendix C) which contains the geometry information (such as the leading edge points, trailing edge points, airfoils, twist, dihedral etc.) of all wing components (in the MMG, lifting surfaces are called wing components). Subsequently, if a fuselage has been defined by the user, the geometry information (such as the cross-section location and radius, the fuselage length, fuselage tail-cone dimensions etc.) of the fuselage is read, a CAD model is gen-
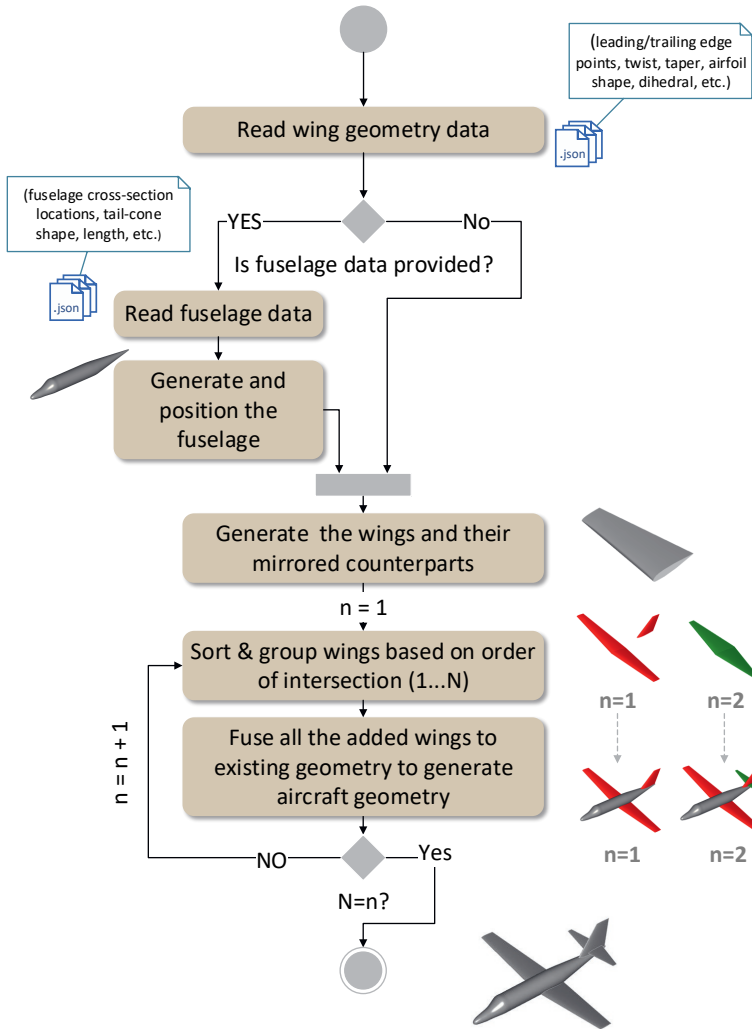
Figure 8.4: UML activity diagram of the process implemented in the MMG to generate configuration agnostic aircraft geometry

erated and positioned with appropriate orientation. In case a fuselage is not defined, wing only aircraft is generated. Furthermore, wing geometries and their mirrored counterparts (if requested by the user) are generated.

In order to generate meshes for aerodynamic and structural analysis, the meshing kernel needs one shell/surface/solid. Thus, different wing and fuselage components must be fused to generate one aircraft shell object. To this end, the MMG groups wings based on the wing intersection with other components. For example, if a conventional aircraft is used, the MMG first identifies all the wings that intersect with the fuselage (primary element) and groups such wings together (called primary wing group). In the next

iteration, any wing that intersects with the the primary wing group is grouped together (called secondary wing group). This process is iterated until all the wing components are grouped (see Figure 8.4). In case of a design without fuselage, the MMG selects the wing that intersects with most number of wings as the primary element and then uses it to determine the primary wing group. Typically, the wing at the root section of a flying wing concept is chosen as the primary wing.

The grouping is necessary to fuse (i.e., Boolean shell operation to unite different wing surfaces) the components together. If all the wings and fuselage are fused at once, there is a risk that geometry kernel starts fusion using secondary wing group component (such as the horizontal tail shown in Figure 8.4) and the fuselage/primary wing that do not intersect. Thus, the order of fusion needs to be set by checking which components intersect. After generating each group, they are fused together to generate the aircraft as shown in Figure 8.4.

The underlying MMG code is not written for a specific configuration but to assess the inputs provided by the user and then generate the geometry based on those inputs. Thus, the ability to assess the user inputs makes the MMG flexible, thereby supporting the design of a wide variety of configurations as shown in Figure 7.3.

8.2. ENHANCEMENT OF CAPABILITY MODULES IN MMG

The models generated by the MMG must be further processed/manipulated to support a number of key analysis tasks in SFT model design. These manipulations may include the discretization of surfaces to enable subsequent mesh generation, or directly the generation of mesh nodes, starting from the underlying geometry models. A common approach is to make use of third party meshing software, using scripts to automate their operations. Developing generalized scripts to mesh different aircraft configurations can be challenging and error-prone. Furthermore, post-processing the results of the analyses also required significant book-keeping effort to assess the design. In order to support and speed up the pre/post-processing activities in SFT model design explained in Sections 6.3.4 - 6.3.7, certain CMs of the MMG are enhanced by exploiting the meshing functionalities provided by ParaPy KBE system. In the following sections, we discuss these enhancements.

8.2.1. MESHING

ParaPy, the KBE system that powers the MMG, offers developers the possibility to automatically generate surface or volume meshes to discretize a geometry (i.e., the conceptual design generated by the initiator can be used to automatically generate geometry and then pre-process it for meshing without any manual effort). Such meshes can be used to perform aerodynamic or structural analyses. The solvers associated with surface meshes (such as VSAERO, FlightStream and NASTRAN) converge faster than solvers using volume meshes (e.g., Ansys Fluent Euler/RANS solvers). Typically, solvers based on surface meshes are called medium-fidelity tools as they are not as accurate as the high-fidelity (volume) meshes. After due trade-off of solver time vs accuracy, surface mesh based analyses are used in this dissertation (further discussed in Chapter 9). Thus, in the remainder of this section, only the automatic surface meshing capabilities of the MMG

will be discussed. In order to gather more information on automatic volume mesh generation, reader is referred to the work of Rubio Pascual [191] and Faggiano [192].

The MMG can perform surfaces meshes for a number of aerodynamic and structural analyses solvers. Depending on the best-practices manual provided by the solver vendor, different types of meshes are necessary. Irrespective of the solver, certain fundamental requirements must be satisfied by the mesh. Typically, structured (Figure 8.5), block-structured (Figure 8.6) and unstructured (Figure 8.7) meshes are used for surface meshing [193]. In the following paragraphs we discuss how the MMG produces such meshes.

Cartesian	Curvilinear
(a)	(b)
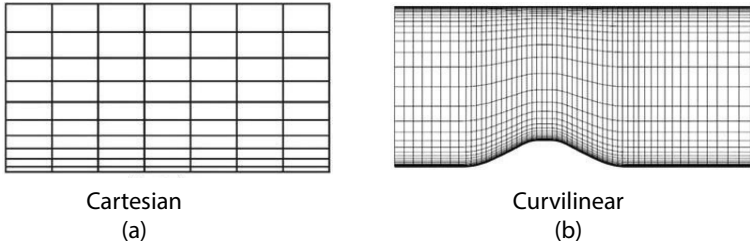
Figure 8.5: Example of structured grids generally used to discretize geometry where, (a) shows the cartesian grid and (b) shows curvilinear grid

Matching block structure	Non-matching block structure
(a)	(b)
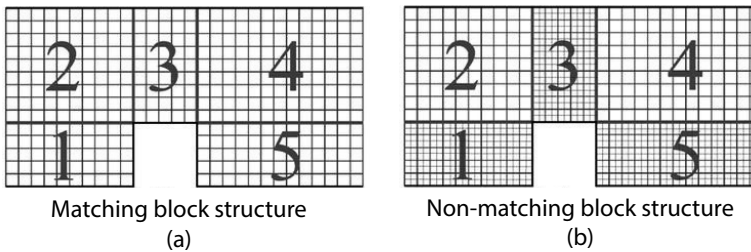
Figure 8.6: Example of block-structured grids, where, (a) shows the matching grid and (b) shows non-matching grid (adapted from [193])

8.2.2. Generation of Patches

To automate the meshing operations of configuration agnostic aircraft topology generated by the MMG, matching block-structure mesh is the preferred choice. Here, matching block grid with each block having curvilinear structured grid is used. This choice of meshing also gives developers the freedom to use unstructured meshes on some geometrical blocks (also called patches) if the solvers allow it. Thus, in order to ensure matching block-structure mesh, the MMG has to perform two main tasks:

1. Split the geometry into blocks suitable for meshing (i.e., generation of a meshable shape)
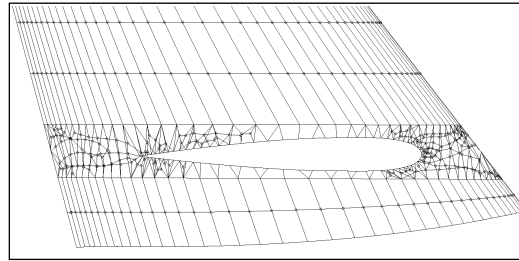
Unstructured Mesh

Figure 8.7: Example of unstructured mesh

2. Identify all the edges on which the number of mesh nodes must be equal (to ensure matching block-structure mesh)

The ability to generate meshable shape has long been there. However, this was linked to the code of geometry generation and was thus not truly configuration agnostic. In other words, the configuration agnostic mesh generation capability has been lacking. In this work, the geometry, mesh and the associated meshable shape generation have been made configuration agnostic. This increases the flexibility and applicability of the MMG and makes the SMDEE an interesting proposition in computational scaling.

To generate configuration agnostic meshable shape (see activity diagram in Figure 8.8), the MMG analyzes the geometry and groups different geometrical entities (faces, edges, vertices, etc.) based on the HLP they belong to. Next, the MMG identifies all the wing-fuselage intersection and wing-wing intersections.

When two components intersect, one of the components is called the **intersector component** and the other is the **intersected component**. Intersected components are those components that are fused first in the configuration agnostic algorithm explained in Section 8.1.3. Thus, for a conventional aircraft shown in Figure 8.4, fuselage is the intersected element in iteration 1 and the main wing and vertical tail are intersectors. However, in iteration 2, the combined solid of wing-fuselage-vertical tail will become the intersected element and the horizontal tail is intersector.

The design of wing HLP and connecting element HLP (see Appendix C) is such that the bottom and top faces are four sided, irrespective of number and location of the movables. Thus, as long as the wing is an intersector component, it is ready for block-structure meshing. Furthermore, wing is always an intersector component in wing-fuselage interesection as discussed in Section 8.1.3. Thus, for wing-fuselage intersection, splitting operations are necessary only on the fuselage. Typically, for wing-fuselage intersection, blocks are created around the intersection edges as shown in Figure 8.9 by introducing splitter curves. Similarly, vertical tail is the intersected component and horizontal tail is the intersector component in the curciform configuration. Like the wing-fuselage intersection, patches are generated by isolating the intersection edges of the vertical tail and the horizontal tail as shown in Figure 8.10.

The examples shown in Figure 8.9 and 8.10 typically require some unstructured meshes in the regions around the intersected edges. However, not all solver can function ef-
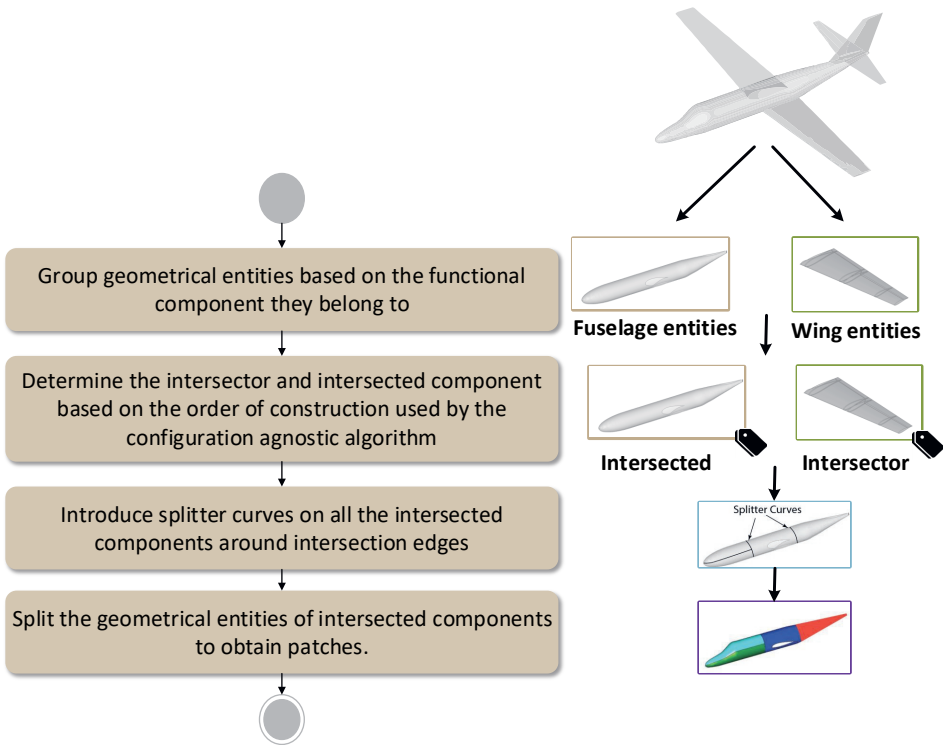
Figure 8.8: UML activity diagram of the steps involved in meshable shape generation for block structure meshing
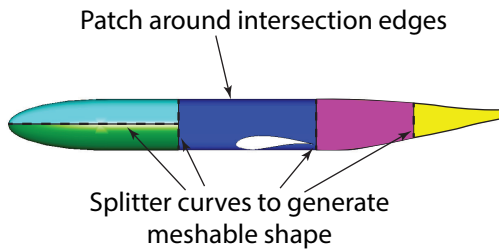
Figure 8.9: Patches generated by the MMG algorithm for block-structure meshing showing patches generated for wing-fuselage intersection

fectively with unstructured meshes. The 3D panel method solver VSAERO is one such example. In such cases, more involved splitting algorithms are necessary. The MMG has a number of in-built algorithms which can split the aircraft geometry completely into 4-sided faces as shown in Figure 8.11. Developing such an algorithm requires com-
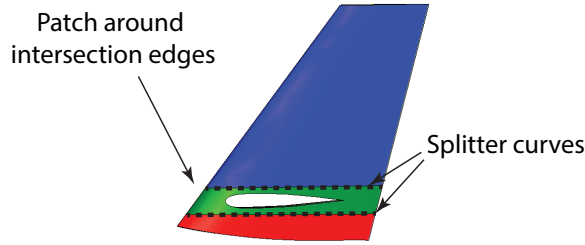
Figure 8.10: Patches generated by the MMG algorithm on the vertical tail to enable block-structure meshing

plex management of splitter curves including introduction of extra splitter-lines on the wing, propagating splitter-lines throughout the length of the aircraft and combining the splitter-lines introduced for wing-wing intersection and wing-fuselage intersection as shown in Figure 8.11.
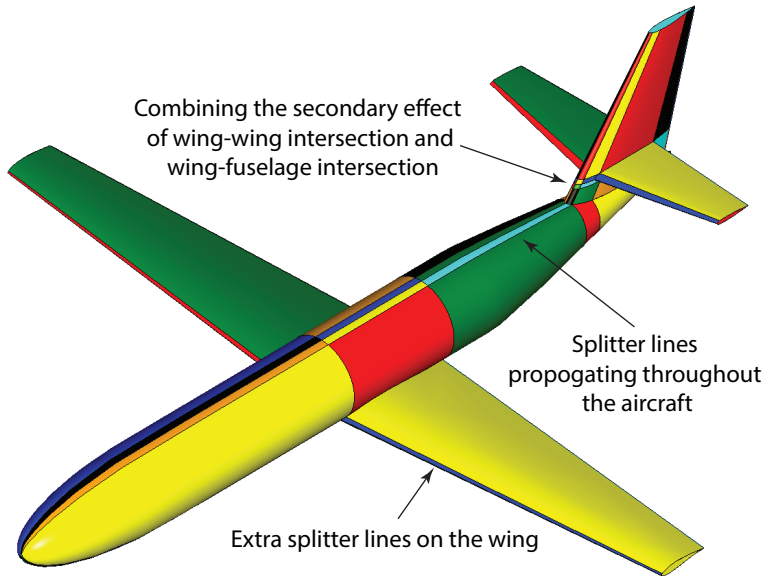
Figure 8.11: Patches generated by the MMG to ensure 4-sided faces throughout the geometry to obtain a curvilinear structured mesh

8.2.3. GENERATION OF MATCHING NODES

Generation of edge chains for block-structure meshing (i.e., list of edges which must have matching number of mesh nodes) is not used in meshing performed by third-party algorithms because there isn't enough control in the programming interface provided by most of the meshing tools. The algorithms developed in the MMG can extract connec-
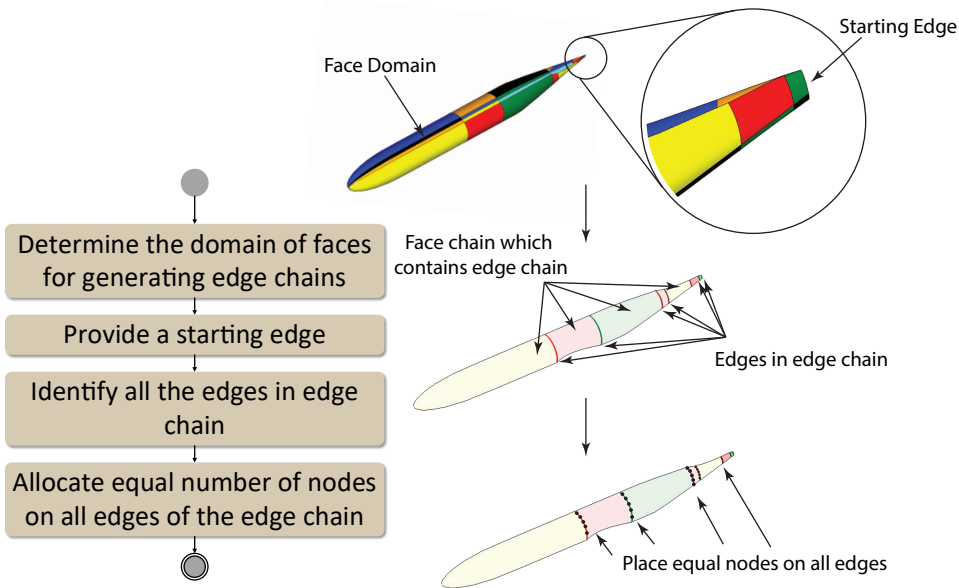
Figure 8.12: Activity diagram of steps followed by the MMG to generate edge chains and place mesh nodes

tivity information from the patches to determine the opposing edges and adjacent edges for 4 sided faces. This allows the MMG to automatically identify the edge/face chains and place equal number of nodes on all those edges. Figure 8.12 shows the activity diagram for determination of edge-chains.

When all the mesh nodes are placed on the edges, they are connected by the meshing library to generate the mesh. In case all the split faces are 4-sided, the generated mesh is block structured mesh (See Figure 8.13(a)). If there are a few faces which are not 4-sided, some unstructured patches remain as shown in Figure 8.13(b). In the MMG, unstructured meshes are only used when intersection edges must be resolved. In the absence of intersection edges (See Figure 8.13(a)(ii) and Figure 8.13(b)(ii)), a curvilinear structured mesh is generated. Importantly, all the meshes shown in Figure 8.13, are generated using the same configuration agnostic procedure for surface splitting and meshing. Thus, any change in the geometry is recognized by the MMG and the mesh is appropriately modified. This is a key enabling capability of the MMG that allows a systematic exploration of design space (by means of Design of Experiments or optimization) to maximize similitude between the model and the prototype. The application of these capability modules is discussed in Chapter 10.

8.2.4. Topology Book-Keeping for Pre/Post-processing

In order to perform pre/post-processing of models, manipulation of the geometry becomes important. For example, in order to generate a mesh, block-structure meshing
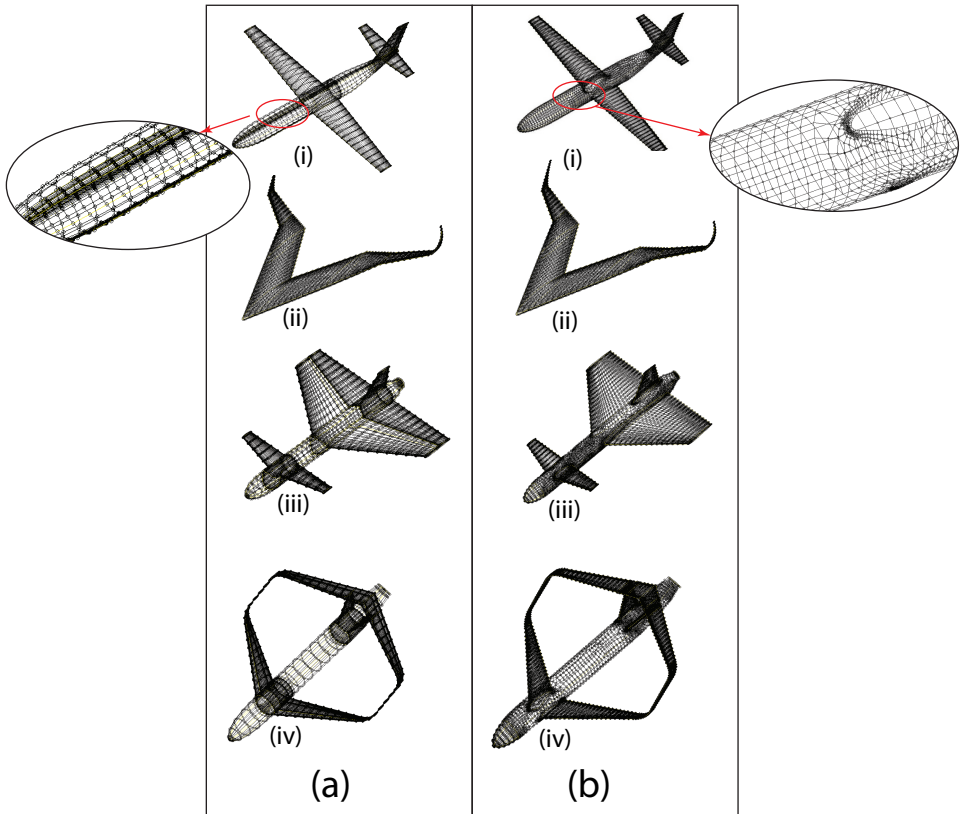
Figure 8.13: Configuration-agnostic meshes generated by the MMG, where, (a) shows all the designs meshed using block-structured mesh and (b) shows aircraft meshed using hybrid meshing approach

8

is necessary as discussed in Section 8.2.1, which in turn requires the understanding of the geometrical constitution (surfaces, lines, points) of different functional components (e.g., wing, fuselage, etc.) to split the geometry into patches.

However, the geometry of the components keeps evolving through different design steps in the MMG. An example of evolution of geometry of fuselage in configuration agnostic design process is shown in Figure 8.14. Keeping track of how individual geometrical entities transform becomes challenging.

To overcome this problem, topology[1] property (i.e., faces, edges, vertices and their connectivity) of the functional components, which are provided natively by ParaPy, is used to log the evolution of different geometrical entities.

In the example shown in Figure 8.14, *Face*#1 is tagged as the face of the fuselage. As wing components are intersected with the fuselage, this becomes *Face*#7 of the fused

---

[1]Topology is the mathematical study of the properties that are preserved through deformations, twisting and stretching of objects
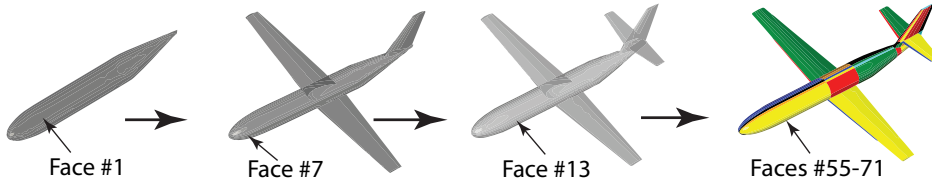
Figure 8.14: Evolution of fuselage faces from component CAD model to block-structure mesh aspect model

shell[2] and consequently *Face*#13. As the geometry is split into patches for meshing, fuselage is composed of a number of faces. The MMG tags the face of fuselage as soon as it is constructed and keeps a track of every manipulation on such face(s). In this way, irrespective of the number of operations the constituent geometrical entities can be identified by understanding the topology.
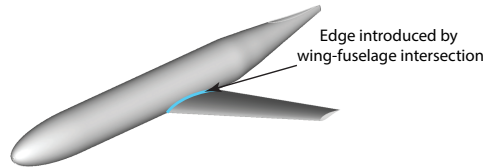
Figure 8.15: Wing-fuselage intersection edge tagged by the MMG immediately after its creation due to boolean operation

The topology book-keeping has a number of uses. In the case of SFT model design, two main benefits of topology book-keeping are:

1. **Identification of intersection edges:** As Boolean operations are performed on component, new intersection edges are introduced as shown in Figure 8.15. The MMG logs all the intersection edges and keeps track of the intersecting components that generated the intersection edge. The identification of intersection edges is important for block structure meshing as discussed in Section 8.2.1.

2. **Post-processing:** After the analyses is complete, forces and moments have to be determined at different locations. Furthermore, heresults of the analysis must be grouped per component to determine the behaviour of individual components. For example. the forces and moments acting on the fuselage are necessary size the skin panels. For this, mesh elements on each component need to be determined. This is done by collecting all the patches that constitute a component and then assembling all the elements on those patches. The MMG exercises sufficient control on the generation of patches and can provide the right mesh sub-grids for post-processing. Furthermore, in case information of mesh nodes on a specific

---

[2]typically a shell is composed of a number of faces (n) numbered from 1 to n.

edge (e.g., trailing edge for panel method to apply Neumann boundary condition) is necessary, the MMG can collect such sub-grids as well. Some examples of sub-grids generated by the MMG are shown in Figure 8.16.

Fuselage Sub-grid

Wing Sub-grid

Trailing edge Sub-grid

Vertical tail Sub-grid

Horizontal tail Sub-grid
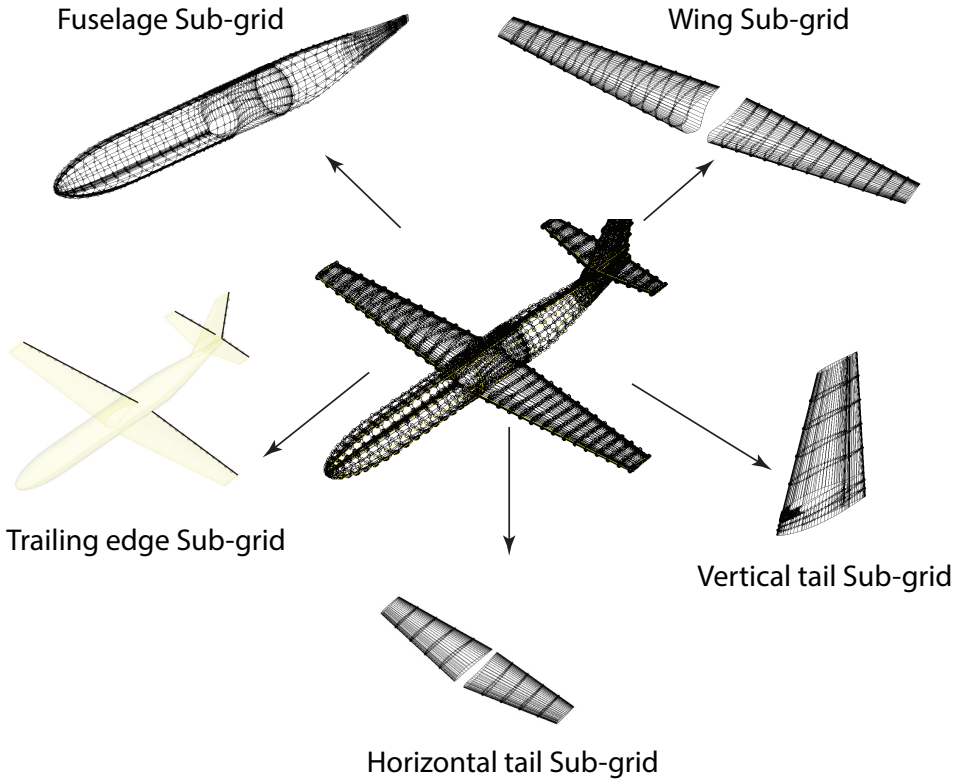
Figure 8.16: Identification of different sub-grids by the MMG to post-process analyses results

The topology book-keeping is an integral enabler of configuration agnostic approach described in Section 8.1.3.The association of functional elements to aspect model helps build a strong dependency between the geometry generation and analysis tools, which allows the transfer of information from functional components through aspect models to the individual mesh elements and back. This is beneficial in SFT model design as meshes need to be prepared on the fly for every change in the shape of the model.

8.2.5. SFT MODEL WEIGHT AND BALANCE ESTIMATION

The MMG uses a physics based approach to determine the weight and balance property of a design. To this end, the MMG determines the weight and balance properties of individual components and then uses these discrete components to determine the overall weight and balance of the complete model. The weight and balance contributors in a sub-scale model can be divided into structural W & B and COTS equipment W & B. These

will be discussed in the following paragraphs.

Structural weight & balance: Different materials might be used in structural compo-
nent design, some of the options are wood, metal (isotropic), but most modern models
are built of composites in practice. In some models the structural components have an
additional foam layer in the layup (sandwich structure) to enhance the stiffness of the
airframe. Typical material inputs for composite structural components are as follows:

1. the number of plies to be used for the component (for orthotropic plies)

2. the thickness of the ply

3. the resin mass fraction of the laminate

4. the density of the corresponding material type

5. whether or not foam material is included between ply layer and its thickness

   Based on the material data, mass of each component is estimated by using the vol-
ume of the component and the material density. The moment of inertia of every com-
ponent is estimated using the thin plate theory.

COTS weight: Most equipment available in the market have a specification sheet which
includes the mass, inertia and center of gravity location of each component. This data is
stored in the database, which is read by the MMG to determine the weight and balance
property of individual components.

Estimating system Weight and Balance: A final assembly can be created for different
scaled models, for any scale factor and with different internal structure. The CAD model
of each component is used to determine the center of gravity of the component. The
mass properties and the center of gravity locations of individual components can be
used to determine the sub-system (wings, fuselage, tails, etc.) and the system (aircraft)
center of gravity and inertia by using system of particles theory given by following equa-
tions:

$$CG_{ac} = \frac{1}{M} \sum_{i=1}^{n} m_i r_i \tag{8.1}$$

$$I_{ac} = \sum_{i=1}^{n} m_i r_i^2 \tag{8.2}$$

where, n is the number of components used in the scaled models and m_i and r_i are the
mass and the distance from the origin for the ith element respectively.
   Since the actual masses of the components and densities of structural components
are used to determine the weight and balance properties, the margin of error is small
(see discussion in Chapter 9). This CM of the MMG supports designers to quickly de-
termine the effect of adding components or moving them around in the airframe with

respect to the weight and inertia targets. Additionally, the properties assigned to individual CAD elements by the MMG for weight and balance estimation are used to automatically provide input to a finite element solver for structural analysis. This reduces the pre-processing time for FEM analysis and also reduces human-errors induced by manual repetitive tasks.

8.3. Improvements in Computational Infrastructure to support SMDEE

A key barrier in the execution of the MDAO process shown in Chapter 6 is the time needed to perform one iteration of the MDAO based similarity maximization technique. Table 8.1 enumerates the time needed to execute different tasks in one Multi-Disciplinary Analysis (MDA) shown in Figure 6.13, where, for every MDA, the geometry and the mesh must be reconstructed, the static and aerodynamic database should be generated, COTS equipment must be positioned and the flight dynamics analysis must be performed.

One MDA performed manually[3] (i.e., engineer performs each task without using the SMDEE or any other automation) takes up to 45.42 hours when the aerodynamic solvers (FlightStream) are run on one computer of 20 cores and the aerodynamic mesh has approximately 20000 panels. Furthermore, an assumption is made that the SFT model is designed using a monocoque structure and can withstand all the loads (details in Section 9.3.2).

Of the total time needed for manual process, 45% of the time goes for aerodynamic analysis. About 40% of the time is spent in generating the geometry and performing pre -processing tasks for aerodynamics and flight mechanics analysis. The remainder is spent in positioning the COTS equipment and performing the weight and balance estimation. The aerodynamic analysis takes the majority of the time because the aerodynamic solvers (FlightStream) need to be iteratively executed hundreds of times (see Section 9.4.3).

In contrast, when the SMDEE is used to perform SFT model design (with FlightStream), one MDA takes about 21 hours. In such cases, 98% of the time is spent on aerodynamic analysis as the solver needs to initialize the source and dipole matrices (necessary to solve the potential flow equations) of the model and then converge for every MDA. SMDEE's automation of geometry generation, positioning COTS equipment, estimating weight and balance properties and pre-processing tasks reduces the time needed for all other activities from 25 hours to about 20 minutes.

Despite this 55% reduction is time for one MDA, in an optimization, MDA must be performed anywhere between 200-1000 times which requires 24 - 120 weeks of optimization time (i.e., 200-1000 different designs are analyzed by the optimizer). Thus, there is a need to reduce the time to perform aerodynamic analysis.

In order to reduce the time needed for aerodynamic analysis, an improved method was implemented in FlightStream which uses the results from previous iteration of the aerodynamic analysis to initialize the source and dipole matrices. This method of reusing the results from preceding iteration is well known as a concept for a long time [194].

---

[3]This time study assumes that there is no repetition in tasks due to human-errors and the engineer executing the process manually has experience with generating meshes and geometry.

Table 8.1: Time needed for different tasks in SFT model design process on one computer of 20 cores when complete process is (a) manually executed (without SMDEE) (b) executed using SMDEE with VSAERO analysis (c) executed using SMDEE with FlightStream (FS) analysis initialized afresh for every flight condition (d) executed using SMDEE with FlightStream (FS) analysis initialized using the results of preceding execution

Task	Manual Execution[h]	VSAERO Execution[h]	FS Execution (fresh start)[h]	FS Execution (reuse results)[h]
Generation of Geometry	8	0.05	0.05	0.05
Mesh Generation	8	0.3	0.3	0.3
Positioning COTS equipment	1	0.02	0.02	0.02
W&B estimation	6	0.02	0.02	0.02
Aerodynamic data (Static clean configuration with 20000 panels)	1.2	1.2	1.2	0.2
Aerodynamic data (Dynamic data with 20000 panels)	7.2	7.2	7.2	1.2
Aerodynamic data per control surface (with 20000 panels)	2.4	2.4	2.4	0.4
PHALANX set-up	2	0.02	0.02	0.02
PHALANX Execution	0.02	0.02	0.02	0.02
Total Aerodynamic data generation (5 control surfaces)	20.4	20.4	20.4	3.4
Total Pre-processing	10	0.32	0.32	0.32
Execution: 1 iteration	45.42	20.83	20.83	3.83
Execution: 500 iterations	22,710	10,415	10,415	1,915

8

However, in practice, for most 3D panel method programs, the source and dipole matrix reuse was not implemented as the programs were not aimed at supporting MDAO processes such as the one discussed in this dissertation. The current effort to reuse results showed significant improvements in the time needed to perform aerodynamic analyses which reduced from 20.4 hours to 3.4 hours as shown in Table 8.1. Consequently, one iteration of SFT model design required 3.83 hours. Thus, for an optimization with 500 MDA, the optimization time was 12 weeks. Although a marked improvement from 60 weeks (needed for conventional initialization process), 12 weeks for optimization is too long in the SFT model design time-frame.

In order to further improve the time needed for optimization, key bottlenecks in the MMG based SFT model design process were identified as follows[4]:

1. Time needed for performing aerodynamic analysis per MDA.

2. Time overhead accrued from the instantiation and closing of processes for geometry generation and pre-processing tools

In the following sections we discuss the infrastructural improvements to improve the execution efficiency of the SMDEE framework and thereby enabling MDAO based similarity maximization.

8.3.1. Parallel Execution Environment:

The time studies shown in Table 8.1 assumed the use of one computer. However, if the same task is divided into sub-task and each sub-task is solved by a different computer, the overall time needed for aerodynamic analysis can be reduced (i.e., parallel execution).

Classically, when millions of cells/panels are used in aerodynamic analysis, the convergence of one flight condition analysis is spread on a number of computers and clusters (see Figure 8.17). This is for cases where solving one case takes hours. Thus, the overhead in sub-diving the matrix of system of equations and distributing over a number of computers and then reassembling matrix at the end of the solution is justified.

In the case of Flightstream, the solver time for every case is about 4 minutes (generally around 25000 panels), which is even lower when the source and dipole matrices are initialized using the results of previous MDA. Here, the overhead of distributing the matrix and reassembling the results is comparable to the solver time. Thus, the classical parallel execution approach (of distributing once case over many computers) is not feasible for 3DPM based aerodynamic analysis.

Nevertheless, hundreds of aerodynamic analysis cases must be run to analyze a given SFT model design (Section 9.4.3) which are independent of one another and can therefore be executed in parallel (see Figure 8.18). To this end, a parallel execution algorithm, a MATLAB-based script was developed in-house. The parallel execution algorithm runs on a master computer and controls the computations on all other computers in the network. The key tasks performed by the master computer using the parallel execution algorithm are as follows (see Figure 8.20):

---

[4]structural analysis was not considered necessary for SFT of flight dynamics provided the structure is sufficiently reinforced with composite materials and the associated analysis of load-cases was not included in the bottlenecks
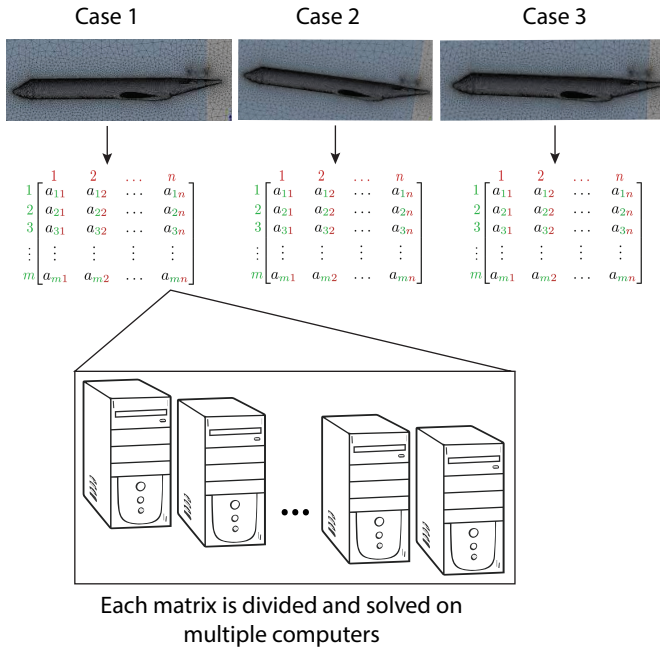
Figure 8.17: Classical parallel execution method, where, one complex case is solved over multiple high performance computers
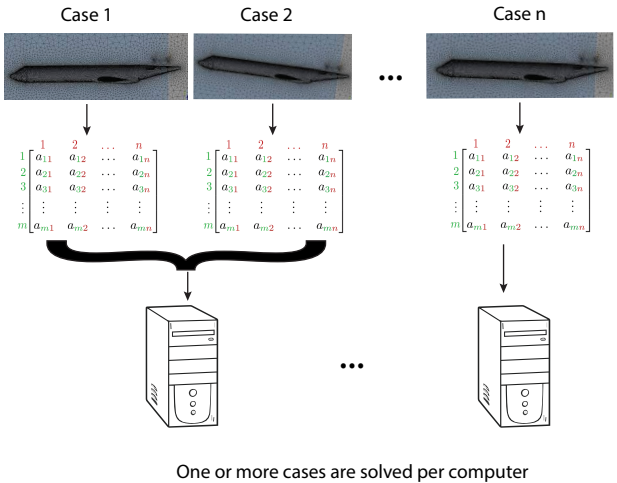
Figure 8.18: Parallel execution environment developed in the MMG to support the rapid 3DPM analysis, where, one of more cases are solved on a computer and the cases are divides over the available computational infrastructure
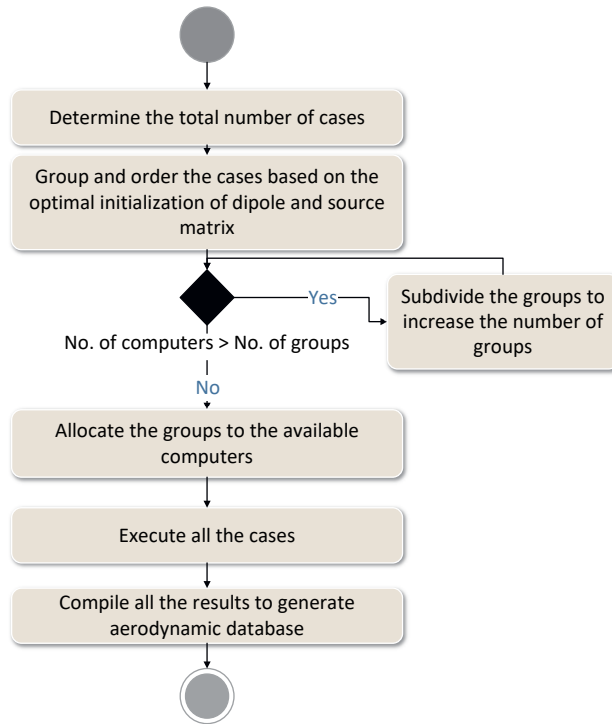
Figure 8.19: UML Activity diagram of the tasks performed by parallel execution algorithm in the MMG

1. **Estimating the number of cases:** Based on the size of the aerodynamic database expected by the user (i.e., the number of angles of attack, side-slip angles, test velocities and control-surface deflections) the algorithm determines all the cases that must be executed

2. **Grouping the analysis cases:** The algorithm then groups the cases such that analysis convergence time is fastest for a given dipole and source matrix initialization. For example, for the clean configuration, the angle of attack sweep should be grouped together and executed in ascending/descending angles of attack. This improves the speed at the which the analysis converges as the vorticity distribution of two consecutive angles of attack are quite close to one-another.

3. **Allocation of grouped cases:** Depending on the number of computers made available to the parallel execution tool, these groups are allocated to different computers. Often, the number of groups is greater than the number of computers available for parallel execution which implies multiple groups must be allocated to one computer (i.e., all the resources are optimally used). In case the number of computers is greater than the number of groups, algorithm automatically sub-divides the groups to increase the number of groups ensure that all computers are used in

parallel.

4. **Execution of the cases:** The algorithm then triggers the execution of the solvers on all the computers by generating and transferring all the script files (mesh files, information on trailing edges, scripts to run aerodynamic analysis, installation files of FlightStream etc.) to the appropriate computer over the local network. After this, appropriate software is installed (if it does not already exist). These batch scripts are run to perform the analyses. The results of the analyses are then returned back to the master computer for compilation.
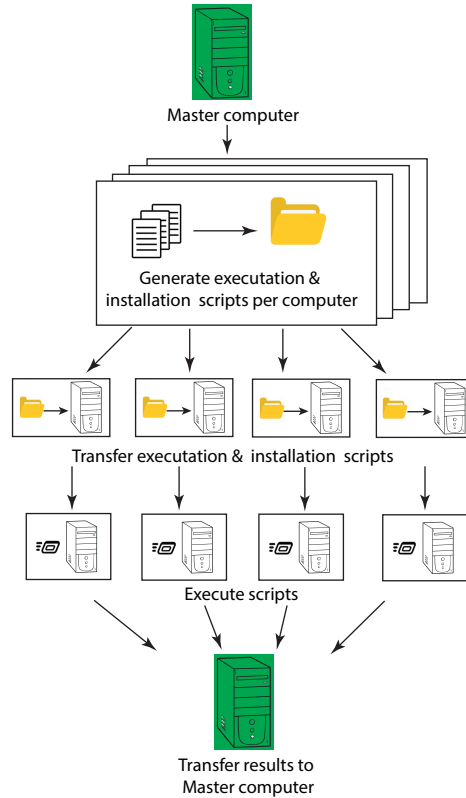
Figure 8.20: The process of executing the cases by the master computer once the grouping of cases is complete

5. **Compilation of the results:** The algorithm then tracks the progress of the analysis and waits for all the executions to be complete. At the end of the execution, all the results are compiled together to generate aerodynamic database necessary to execute PHALANX.

For this work, 9 computers (with 16 cores and 16GB RAM each) were available. Benchmark tests were performed to assess the impact of parallel execution with these 9 computers using the parallel execution algorithm. The time needed for aerodynamic data

Table 8.2: Comparison of time needed for different execution environments namely (a) One computer executing FlightStream with reuse of results (as shown in Table 8.1) (b) Nine computers executing FlightStream in parallel with reuse of results (c) Nine computers executing FlightStream in parallel and MMG deployed as web-service

Task	Single Thread[h]	Parallel Execution[h]	Parallel Execution with MMG web-service [h]
Generation of Geometry	0.05	0.05	0.01
W&B estimation	0.02	0.02	0.02
PHALANX set-up	0.02	0.02	0.02
PHALANX Execution	0.02	0.02	0.02
Aerodynamic data generation (5 control surfaces)	3.4	0.24	0.24
Pre-processing	0.32	0.32	0.02
Execution: 1 iteration	3.83	0.67	0.33
Execution: 500 iterations	1,915	335	165

generation with the use of parallel execution infrastructure reduced from 3.4 h (refer Table 8.1 to 0.24 h **(14 minutes)**. With the pre-processing time and geometry generation time being 0.32 h and 0.05 h respectively, the total execution time for 1 MDA is 0.67 h. Thus, for a complete optimization the execution takes approximately 2 weeks (approximately 14 days). The results of time benchmark studies are shown in Table 8.2.

8.3.2. MMG as a Web-Service:

The parallel execution of FlightStream reduced the optimization time significantly (by around 80%). Nevertheless, the time needed to pre-process and generate geometry exceeded the time need to perform aerodynamic analysis. Typically this indicates bottlenecks in the process as pre-processing time should be lower than the time needed by the solver.

The analysis of the SMDEE process showed that the time needed for starting/closing the MMG and initializing user/optimizer inputs during the execution of the SMDEE resulted in the long pre-processing time. Since the MMG is closed after every MDA, the native capabilities of the KBE application such as run-time caching, dependency tracking and lazy-evaluation were not being utilized between different MDAs.

To overcome this challenge, the MMG is deployed as a web-service and is instan-

tiated before the start of the SMDEE. The user/optimizer requests are then converted to URL which makes a web-request to set the user-inputs in the application. Since the MMG is instantiated and live, only those attributes that are affected by the changes due to user-inputs are re-evaluated and the results are sent back to the user/optimizer.

This deployment of the MMG as web-service reduces most overheads and speeds-up the geometry generation and the pre-processing tasks by 50% as shown in Table 8.2. This reduction ensures that one MDAO based similarity maximization optimization of 500 MDAs can be executed in a week, which is a feasible time-frame in the overall SFT model design process.

8.4. SUMMARY

The use of KBE technology by means of the MMG has shown that the generative process (what, how and why of a design) of a complex geometry product can be captured and a conceptual idea can be quickly and automatically translated into a geometry and/or aspect models. Furthermore, this automation process becomes a enabler of the SMDEE MDAO framework by providing consistent and synchronized models to the discipline specialists for their analyses.

Furthermore, the SMDEE alone cannot enable the MDAO based similarity maximization. The infrastructural improvements (i.e., parallel execution and use of the MMG as a service) speeds up the execution time of one complete MDAO with 500 design iterations from 12 weeks to 1 week. Thus, by making use of three main technological developments, namely:

- parallel computing to distribute independent design cases

- avoidance of aerodynamic matrix regeneration at each analysis within a parametric sweep

- use of KBE application as a web service to avoid multiple re-instantiation of the product model, thus, exploiting the caching and dependency tracking mechanism in the best way possible

8

the implementation of MDAO based computational scaling has been made possible. The absence of these capabilities in the past is also the reason why computational scaling, though proposed in 1990s, did not become popular. Nevertheless, MDAO based computational scaling is now a viable alternative to the geometric scaling approach discussed in Chapter 4.

III

RESULTS

9

SMDEE External Tools: Verification and Validation

In this chapter, we discuss the verification and validation of external analysis tools for four main disciplines of SFT model design, namely, aerodynamics, structures, weight & balance and flight-dynamics used in SFT model design.

Parts of this chapter have been published in AIAA SciTech conference (2019) and AIAA Aviation conference (2019) [177, 178]

9.1. AERODYNAMIC TOOL VALIDATION

As discussed in Chapter 5 and 6, aerodynamic analysis is an important step in the SFT model design process to assess the compliance with similitude and safety requirements (see Table 5.4 and Figure 6.8). A number of aerodynamic tools of varying fidelity levels are available to engineers to estimate the aerodynamic derivatives that are used to estimate the DoS and the associated constraints defined in the SFT model similarity maximization problem.

Several computational methods exist for this, such as, vortex lattice methods, 3D panel methods (3DPM), Euler equation solvers, Navier-Stokes equation solvers. Any of these methods can be selected by designers to evaluate the relevant aerodynamic coefficients. However, two important factors must be considered:

1. **Computational time**: Designers cannot study multiple SFT models in the limited design time if the aerodynamic analysis takes too long to converge.

2. **Accuracy of result:** The discrepancy between physical tests and CFD analyses can be quite high if the results are inaccurate. Consequently, establishing the extent of similarity becomes challenging as the results of physical SFT cannot be scaled up (see Chapter 4 for details).

The problem of computational error (i.e. errors due to approximation or simplification in computational method) can be resolved by validating the computational methods with appropriate wind-tunnel/flight tests as discussed in Chapter 2. In order to balance the contrasting requirements of accuracy and time, in this research work, 3D-Panel Method (3DPM) has been used to estimate the aerodynamic characteristics of the SFT model.

3DPMs are numerical schemes that solve the velocity potential equation for linear, inviscid, irrotational flow for subsonic or supersonic Mach numbers[195]. For 3-D steady subsonic flow, this equation is written as:

$$\nabla^2 \Phi = (1 - M_\infty)\Phi_{xx} + \Phi_{yy} + \Phi_{zz} \tag{9.1}$$

Where, M_∞ is the free stream Mach number and Φ is the perturbation velocity potential.

Typically, panel methods use structured geometry and wake discretization (i.e., quadrilateral panels) and apply a singularity distribution (i.e., sources, doublets, and vortex singularities) on each panel [194]. The strength of each of the singularities is calculated by applying the Neumann (for external flows such as aircraft) or Dirchlett (for internal flows such as pipes) boundary condition to Equation 9.1 [194]. The velocity potential can be used to evaluate the velocity of the flow at different locations and thereby the forces, moments and pressures acting on the body. For detailed information on panel methods, readers are referred to the work of Nathman and Erickson [194, 195].

Additional computational capabilities are often added to panel methods to account for boundary layer and compressibility effects [196] such as Prandtl-Glauert, Karman-Tsien and Lieblein-Stockman corrections [194].

The integral boundary layer calculation is provided in a viscous/potential flow coupling to calculate the boundary layer thickness. Boundary layer displacement is mod-

eled by transpiration through the body surface by iteratively using the pressure distribution from preceding iterations in succeeding potential flow solutions [194]. To study the dynamic aerodynamic derivatives, quasi-steady approach can be used [194].

These 3DPMs that correct for boundary layer thickness and compressibility effects are at best an approximation of the actual physics. Thus, it is important to determine the effect of these approximations on the SFT model design. In the following sections, we discuss the accuracy and applicability of a commercial code Flightstream[1] in the SFT model design.

9.1.1. WIND-TUNNEL TEST

To obtain validation data, a test was conducted in the Low Turbulence Tunnel (low-speed and closed return wind-tunnel) of Delft University of Technology at a Reynolds number of 300000 and 500000. The test-section has a dimension of 1.80 X 1.25m and the turbulence is less that 0.1%. The model used for the test is an aerodynamically scaled 8.8% model of Cessna Citation II 550 called Variable Geometry Model (VGM) (see Figure 9.1 for dimensions). The VGM is built of modular components which allows the lengthening/shortening fuselage and replacing the wing and the horizontal tail with other similar modular components. The rationale of using this scaled model is its availability from previous research work and its close similarity to the dimensions of Cessna Citation II, which isextensively used for the case-studies in Chapter 10. Furthermore, Cessna Citation II aircraft is co-owned by Delft University of technology, which will enable the comparison of SFT results with full-scale behaviour in the future. A photograph of the VGM setup used in the Low Turbulence Tunnel is shown in figure 9.2.

VGM was tested for angle of attack sweep from −5° to 14° with a step size of 1°. Testing beyond 14° was not possible due to physical limits of the wind-tunnel setup. For each of these test points, balance readings for forces and moments on the VGM model were acquired using an external six-component balance. The results form wind-tunnel tests are discussed in the following sections.

9.1.2. FLIGHTSTREAM VALIDATION

Flightstream is a potential flow aerodynamic solver that uses a surface grid of a geometry to analytically solve and converge influence coefficients of the vorticity of each panel [197]. Flightstream has similar methods as other panel methods to correct for the compressibility effects and account for boundary layer thickness. In addition, it also models the separation and unsteady flows (such as propellers) [197].

The key difference between Flightstream and classical panel methods is that Flightstream evaluates bound vorticity on an arbitrarily tessellated body in three dimensions by using vortex-ring elements coupled with an iterative solver and the aerodynamic loads are evaluated by the method of integrated circulation around geometry cross sections [197]. The underlying theory of Flightstream can be found in the work of Ahuja and Hartfield[197].

The benefit of Flightstream is that it allows both structured and unstructured geometry discretization because it uses vortex rings about the edges of a panel for the vorticity

---

[1]https://researchinflight.com/
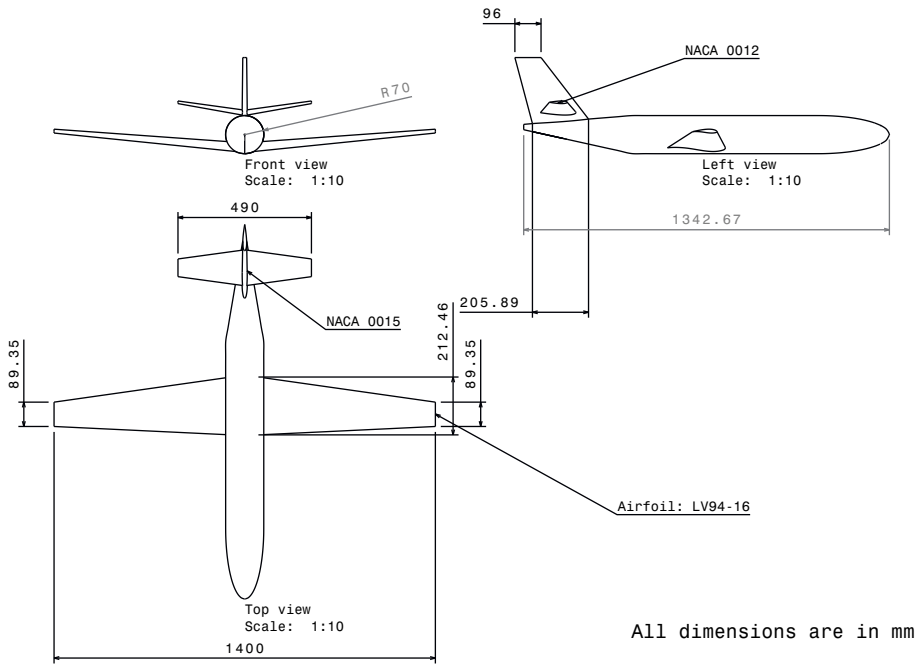
Figure 9.1: The key dimensions of the Variable Geometry Model (VGM) used for the validation of Flightstream
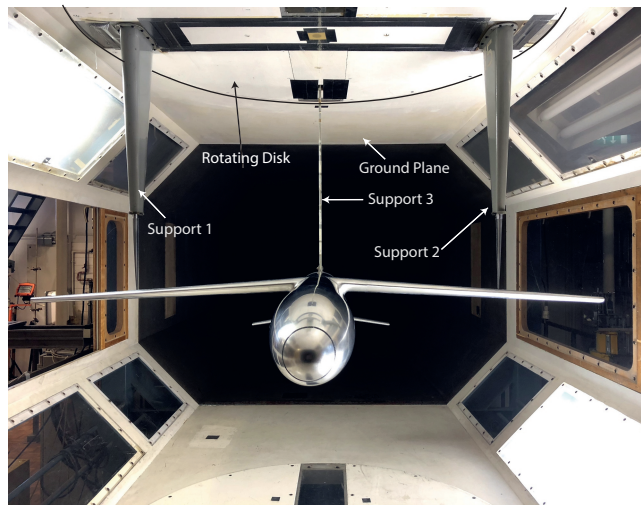
Figure 9.2: Setup of VGM in Low Turbulence Tunnel at Delft University of Technology

calculation [197] and does not depend on a structured mesh to evaluate the vorticity using collocation points as in the case of conventional panel methods (see the work done by Nathman[194] and Maskew [196] for more details).

Flightstream analysis for validation: The dimensions of VGM are fed into MMG to generate the unstructured mesh of VGM (see Figure 8.13(b) (i)). This mesh is used in Flightstream to simulate the angle of attack sweep from $-5°$ to $14°$ at Reynolds number of 500000 (as the wind-tunnel tests were performed at this Reynolds number). Flightstream was set to use potential flow solver with integral boundary layer equations and Prandtl-Glauert correction. The visualization of wake shape and pressure distribution for steady flight and pitch-up manoeuvre is shown in Figure 9.3.

| AoA = 15° M=0.13 Re = 500000 | q=4.9 rad/s M=0.13 Re = 500000 |
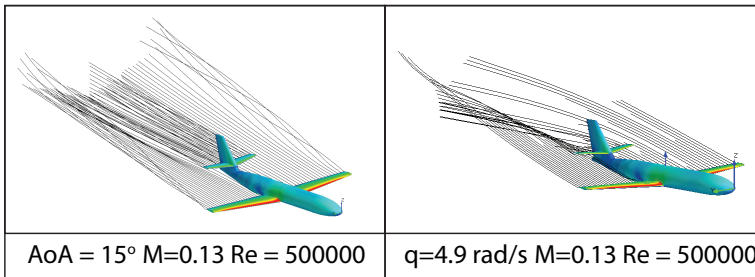
Figure 9.3: Visualization of C_p distribution and wake deformation for the VGM model flying in steady flight and pitch-up rotation simulated using Flightstream

Comparison Flightstream & Wind-tunnel test results: Figure 9.4 (a) shows the lift polar gathered from the wind tunnel test and the 3D panel code (Flightstream). This graph shows that Flightstream analysis and the wind-tunnel results have a good match up to 9° angle of attack (within 9% of one another). Beyond 9°, Flightstream shows separation (calculated using the Flightstream separation module based on the work of Swafford [198]).

However, Flightstream overestimates $C_{L_{max}}$ as compared to the wind-tunnel test results because the separation model in Flightstream is based on a simple integral analytical method that uses local values of skin friction, shape factor, and Reynolds number [198]. Nevertheless, the results are acceptable in the linear region mostly used in flight dynamics assessment. The trends of the elevator deflection are correctly represented in the Figure 9.4 (a), where, upward elevator deflection results in lower lift for a given angle of attack. Flightstream demonstrates larger elevator effectiveness as compared to wind-tunnel because its separation model is not accurate.

The drag polar is plotted in Figure 9.4 (b). The drag obtained from Flightstream analysis is lower (approximately 15% lower below 9° and 22% above 9°) than the wind-tunnel test. This is because Flightstream only implements an approximate integral boundary layer model to estimate boundary layer thickness [196, 198]. In addition, the separation model, though present, is not as accurate as the physical test, which aggravates drag
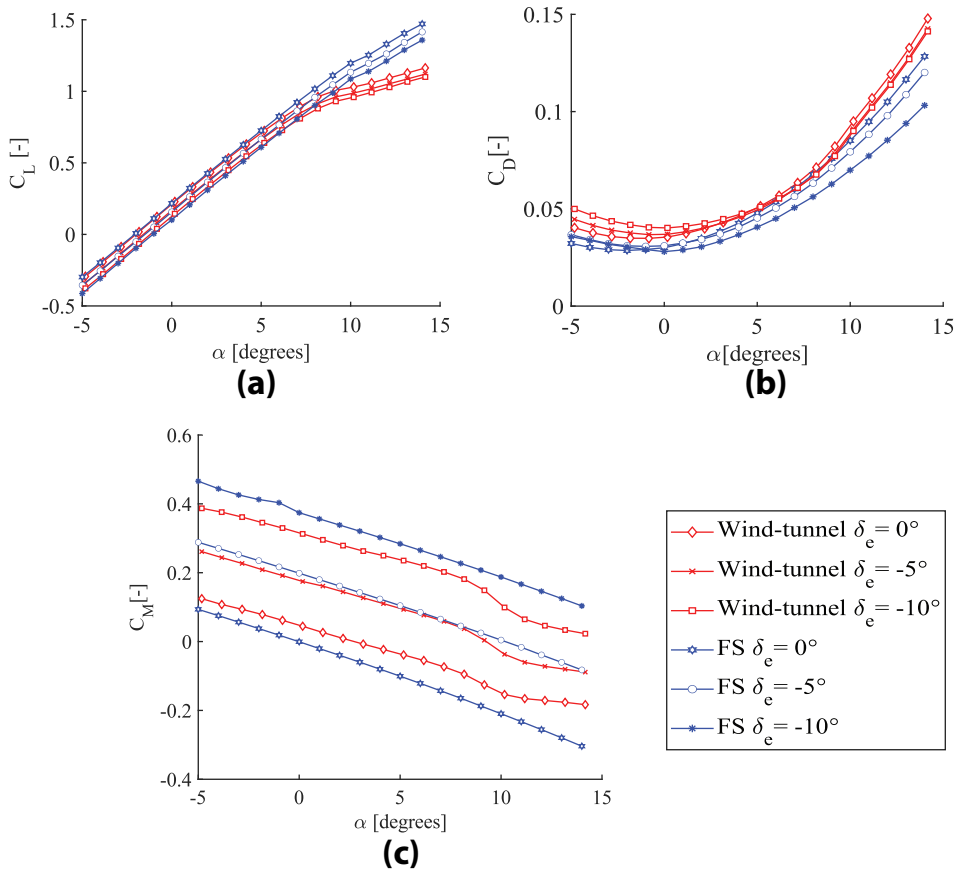
Figure 9.4: Variation of static (longitudinal) aerodynamic coefficients ((a) lift coefficient, (b) drag-coefficient and (c) moment coefficient) with angle of attack

under-prediction at higher angles of attack. Thus, the differences in the drag prediction between Flightstream and wind-tunnel test can be explained as the combination of inaccuracy in the wind-tunnel correction described in Section 9.1.1 and the uncertainties in the simplified models used for boundary layer prediction and compressibility correction.

Figure 9.4 (c) shows the moment polars. The moment estimated by Flightstream is comparable to wind-tunnel results (within 12%). While Flightstream predicts the C_{M_α} rather accurately, in general it underestimates the moments when elevators are not deflected. This is probably because Flightstream under-predicts the downwash angle. As a result, the horizontal tail is much more effective in Flightstream as compared to wind-tunnel test.

Flightstream predicts lower effectiveness of the elevator due to simplified separation modelling, which compensates for higher force generated by the tail. This is why Flight-

stream moments overlap with wind-tunnel moments at $-5°$ elevator deflection and the moments in Flightstream are larger than the moments in wind-tunnel at $-10°$ elevator deflection for all angles of attack.
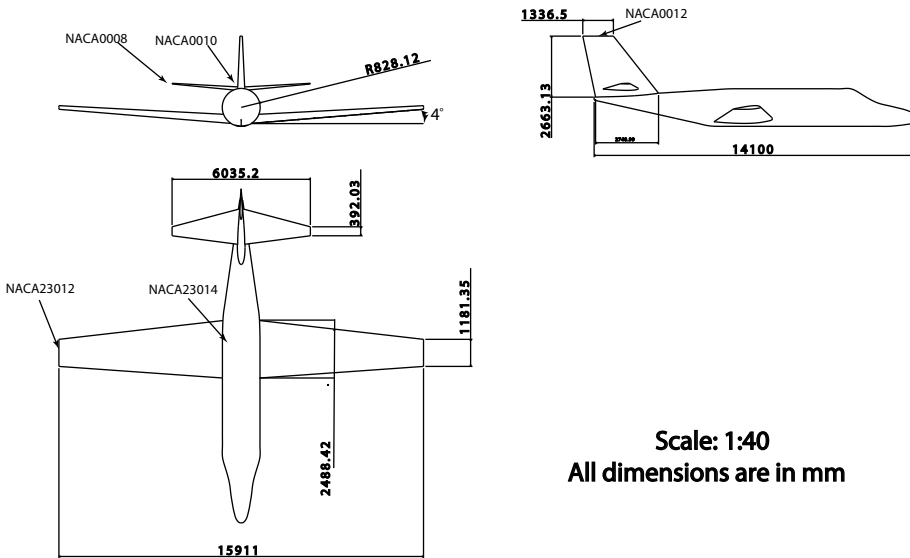
Figure 9.5: Dimensions of (the full-scale) Cessna Citation II 550 used as reference in this dissertation

Noise from the solver: For any optimizer to effectively function, the magnitude of numerical noise from a computational tool should be much smaller than the magnitude of the quantity of interest. Furthermore, the computational tool must be able to clearly demonstrate the impact of varying the inputs on the quantity of interest.

To this end, we performed a design of experiment to determine the longitudinal stability derivatives on a number of geometrically scaled models of (an approximate) Cessna Citation II 550 (see dimensions used in Figure 9.5) at different test velocities. The results of the design of experiment are plotted in Figure 9.6.

Flightstream's solver is not afflicted by noise issues primarily because Flightstream uses vortex rings for the calculation of vorticity about the edges of a panel by applying the Biot-Savart law. For detailed implementation of this method, reader is referred to the work of Ahuja and Hartfield [197]. The results appear continuous and have good correlation to the variation in the inputs, which makes the use of Flightstream suitable for MDAO based similarity maximization.
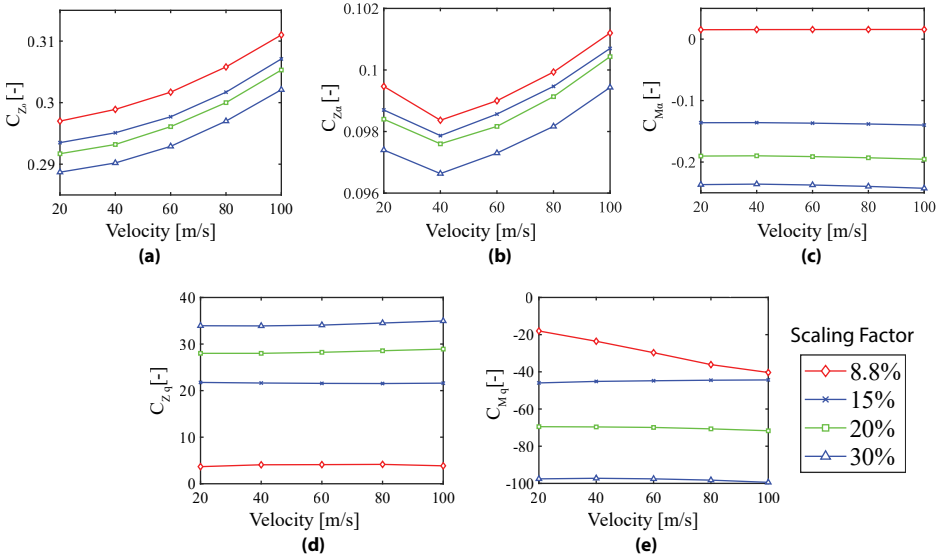
Figure 9.6: Variation of different longitudinal stability derivatives (a) C_{Z_0}, (b) C_{Z_α}, (c) C_{M_α}, (d) C_{Z_q} and(e) C_{m_q} at different test velocities and geometric scaling factors evaluated using Flightstream

9.2. WEIGHT AND BALANCE ASSESSMENT OF SFT MODEL

The weight and balance estimation approach included in SMDEE has been discussed in Section 8.2.5. In this section, we compare the weight and balance estimation provided by the SMDEE (i.e., computational method) with that of a SFT model constructed in-house at Delft University of Technology (i.e., physical model). Furthermore, SMDEE's ability to quickly determine the weight and balance characteristics of SFT models of different sizes is also demonstrated by means of a design of experiment.

9.2.1. COMPARISON OF PHYSICAL SFT MODEL WITH COMPUTATIONAL SFT MODEL

A 4.5% geometrically scaled model of Flying-V Aircraft (See Figure 9.7) was constructed at the Scaled Flight Testing Laboratory of TU Delft. In the process, the weight properties of the SFT model were measured and recorded. The physical SFT model includes the structural components and COTS components and could therefore be used to validate how well the mass and CG could be predicted by the SMDEE model (see Figure 9.8).

An overview of the equipment used in the physical and the computational method of Flying V inside SMDEE is provided in Table 9.1 and Figure 9.9. The database used for computational modelling was quite accurate. Thus, differences were negligible between the data in equipment data base and the measurement data.

Nevertheless, differences were observed in the structural mass properties estimated by the computational method and the physical measurements (see Table 9.2) even though the thicknesses and number of structural components for the physical and the computa-
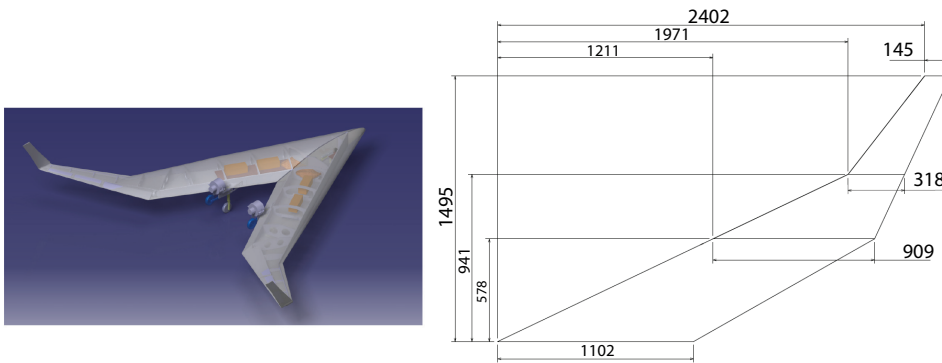
Figure 9.7: The isometric view and the planform dimensions of the Flying-V aircraft constructed at the Scaled Flight Testing Laboratory, TU Delft

(a)

(b)
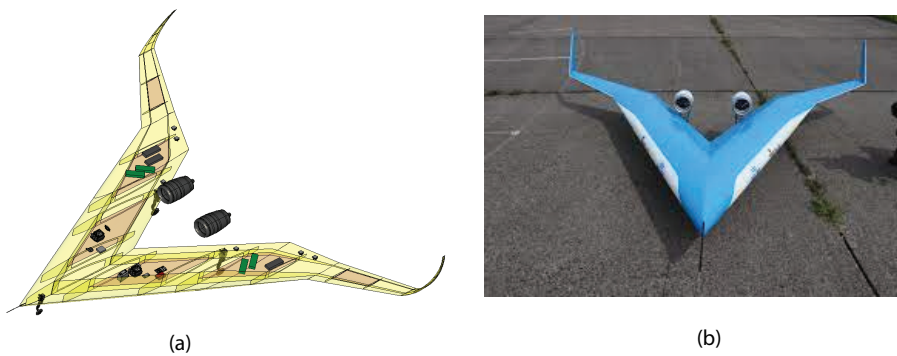
Figure 9.8: (a)The computational model generated by the MMG and (b) the physical model of Flying-V (Credits: Malcom Brown/TU Delft)

tional model were set to the same value. This is because the the computational method used standard mass properties (see Table 9.3), whereas, the fabrication of the physical model can have imperfections in the material due to the manufacturing process. Another important difference between the physics-based estimated mass and the real-built model can be the choice of resin fraction, which is set to 55% for the computational method. However, the resin fraction in the physical model is dependent on number of parameters such as lay-up process (i.e., hand-laying versus machine-laying), the skill of the person performing the lay-up, etc.

Consequently, the overall mass estimated by the computational method is 4% higher than the mass measured on the physical model (see Table 9.2). Furthermore, the center of gravity location estimated by the computational method is off by 13% as compared to the physical model (differences in y-direction are ignored as they are almost equal to zero). Although the percentage error of the center of gravity location seems large, it is only off by a few centimeters as consequence of the inaccuracies in the mass estimation

Table 9.1: Equipment mass breakdown of the Flying-V SFT model

	Component	Mass [kg]
Flight Control System	Pixhawk 4	0.033
	Receiver Rex-12	0.024
	Telemetry RF RFD868+	0.022
	Secondary Computer Raspberry Pi 3B+	0.070
	Servo D89MW/HS-5070MH	0.026
	Control power GensAce 2S 4000mAh	0.173
	GPS antenna	0.033
Scientific Instruments	Air data probe	0.013
	Air data computer	0.198
	GPS	0.094
Propulsion system	Engine	1.135
	Battery	1.47
	ESC	0.528
Landing Gear	Nose gear retract	0.335
	Nose gear leg	0.217
	Main retract	0.31
	Main leg	0.500
	Gear computer	0.048
Total Equipment mass		12.73
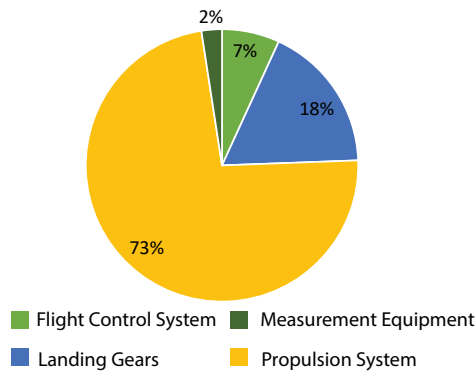
Figure 9.9: Equipment mass breakdown for Flying V SFT model

of structural components (i.e., 3 cm on a SFT model of 80 cm mean aerodynamic chord). The comparison of the moment of inertia could not be performed in this study as the moment of inertia of the physical model was not available.

Since this research work focuses on preliminary design of the SFT model, the computational method excludes the masses of fasteners, adhesives, cabling and paints in its current form. Furthermore, the masses of these components are not included in the

Table 9.2: Comparison of the weight and balance properties estimated by the computational method to those measured on the physical SFT model of Flying-V

	Physical Flying V model [kg]	Computational Method [kg]	Percentage Error [%]
wing skins	5.92	6.56	-10.8
main spars	1.87	1.95	-4.2
main ribs	0.56	0.64	-14.2
winglets	0.23	0.21	8.7
floors	1.29	1.40	-8.5
Total Structural Mass	9.87	10.76	-9.0
Total Equipment Mass	12.7	12.73	-0.2
Total Aircraft Mass	22.6	23.49	-3.9
Center of gravity [m]			
x	1.49	1.46	2.0
y	-0.003	0.001	133.3
z	0.040	0.035	12.5
Inertia [kg m2]			
I_{xx}	-	7.12	-
I_{yy}	-	5.82	-
I_{zz}	-	12.72	-

Table 9.3: Mass properties of the structural components used by the computation method for the estimation of weight and balance of Flying-V SFT model (the thickness and stacking sequence remain the same as those used for physical model)

	Material	
	orthotropic	foam
Skins		
density [kg/m2]	0.162	0.28
ply number [-]	4	-
thickness per ply [mm]	0.13	3
resin fraction [-]	0.55	-
Spars / Ribs / Floor		
density [kg/m2]	0.300	0.19
ply number [-]	4	1
thickness [mm]	0.13	5
resin fraction [-]	0.55	-

comparison shown in Table 9.2. For a 1.5 m span Flying-V model, these additional components account for 6% of the overall weight of the aircraft. Thus, in the future, these additional mass contributors should also be modelled. For the purpose of this dissertation, the computational method predicts the weight and balance properties of the SFT model within acceptable bounds of error.

9.2.2. Weight and Balance estimation Design of Experiment
The development of the weight and balance modules in SMDEE enable rapid estimation of weight and balance properties of SFT models of varying sizes and structural composition. Here, we study the impact of varying the size and the structural composition of the SFT model on the model weight and balance. Geometrically scaled models (8.8%, 12%, 16% and 20%) of an approximate Cessna Citation II 550 were used for this study (the dimensions of the full-scale aircraft are shown in Figure 9.5).

For each SFT model, the number of skin plies were varied from 2 plies to 7 plies (in a combination of 0° and 90° plies). Figure 9.10 shows the variation of the weight and balance properties with the number of skin plies (throughout the model) and the size of

the model. The mass properties of the plies are as shown in Table 9.3.
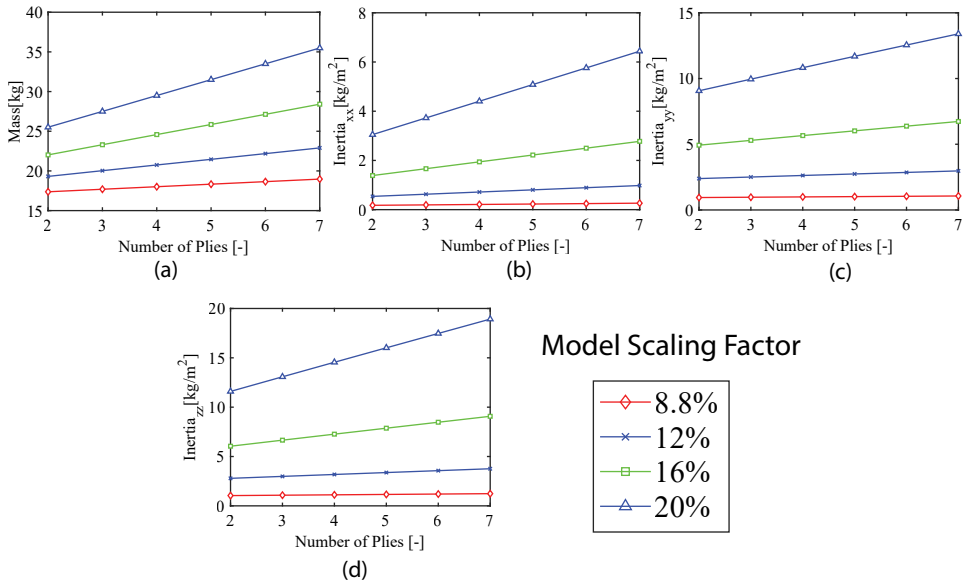
Figure 9.10: Variation of (a) Mass, (b) moment of inertia about X-axis, (c) moment of inertia about Y-axis and (d) moment of inertia about Z-axis with the number of plies and scaling Factor

The methods typically used to estimate the weight and balance are empirical and cannot accurate predict the mass and moment of inertia [190]. The design of experiment performed with the physics based weight and balance estimation developed in this work shows that the tool is sensitive to the changes in the structural design of the model. Furthermore, the variation of mass and moment of inertia with increasing number of skin plies is smooth and devoid of noise. This makes the tool suitable for optimization studies. Interestingly, the study also shows that the mass and moment of inertia properties (almost) respect the cube-squared law (i.e., mass scaled with the 3rd power of the scaling factor and the moment of inertia scales with the 5th power of the scaling factor). Of course, the actual placement of the COTS components and the variation in the structural constitution of the wings and fuselage affects the adherence to the cube-square law.

9.3. STRUCTURAL ASSESSMENT OF SFT MODEL

Depending on the type of test, a number of requirements associated with the SFT model's structural design are discussed in Chapter 5. A variety of commercial/open-source tools of varying fidelity are available for structural analyses. Some examples of these tools include ABAQUS[2], NASTRAN[3], Code Aster[4]. This is in addition to empirical methods

---

[2]https://www.3ds.com/products-services/simulia/products/abaqus/
[3]https://www.mscsoftware.com/product/msc-nastran
[4]https://www.code-aster.org/spip.php?rubrique2

[17], and finite beam element analysis methods [199] typically used during conceptual or preliminary design phase.

The trade-off between accuracy and execution time discussed in the preceding section is also applicable for structural analyses. Nevertheless, structural analysis is not as critical as the aerodynamic analyses for the study of dynamic behaviour of a rigid aircraft as long as the structural components do not fail in flight or cause significant deflections. However, structural analysis is critical and involved in the study of flexible models (i.e. models used to determine aeroelastic behaviour).

In the remainder of this dissertation, MSC Nastran is used to analyze structural behaviour. MSC Nastran supports different types of analyses such as linear static analysis (SOL 101), Buckling Analysis (SOL 105), Aeroelastic Analysis (SOL 144), Nonlinear Static and Transient Analysis (SOL 400), Structural Design Optimization (SOL 200), etc. Although SMDEE can support the pre/post-processing of most of these analyses, it has only been tested for linear static analysis in this work as the scope was limited to rigid SFT model design.

In order to perform linear static analysis, three main tasks have to performed, namely:

1. Generate a mesh suitable for structural analysis

2. Apply relevant load cases (aerodynamic loads, Equipment loads, landing gear loads etc.)

3. Generate an input file for the solver

As discussed in Chapter 7, the generation of mesh and the application of equipment loads can be done by MMG's meshing and COTS equipment modules respectively. However, transferring loads from aerodynamic analyses for structural analyses remains an open challenge. In the following sections, we discuss the aerodynamic loading module developed for structural analysis. In addition, we discuss the results of a sensitivity analyses performed using SMDEE to study the impact of structural design decisions on the SFT model design.

9.3.1. Aerodynamic Loading for Structural Analyses

The application of loads is a critical task in structural analysis. Errors in the applied loads can propagate downstream to the results of structural analysis and sizing. Thus, load envelopes experienced by SFT models such as flight maneuver loads (aerodynamic loads), propulsion loads, landing gear loads, ground handling loads and control surface loads must be determined for structural design and sizing.

Typically, the determination of loads implies identifying the locations (or surfaces) where a given load acts and applying the loads conditions at those locations. Most loads are introduced at specific points of attachment to the airframe (landing gear loads, equipment loads etc.). Notable exceptions are the aerodynamic loads and aero-propulsive loads experienced by the SFT model. Application of these loads is challenging for two reasons:

1. these loads are applicable over a large area of the aircraft and their distribution varies per load-case (i.e., flight manoeuvre)

2. these loads are not readily available, they are the result of complex simulations performed by other disciplinary analyses which must be post-processed appropriately for use in structural analysis

Consequently, a number of errors are introduced in the structural analyses tool due to inappropriate translation of forces and moments from one discipline (aerodynamics) to another (structural analyses). Figure 9.11 shows the typical differences in meshes generated for aerodynamic analyses (used by 3D panel method) and structural analysis (used by NASTRAN). The aerodynamic meshes uses cosine distribution of mesh nodes in chordwise direction and are typically sparser than the equispaced structural meshes as they do not have to account for the internal structural meshes. Furthermore, the aerodynamic meshes (used in this study) are mainly composed of quadrilateral elements whereas, structural meshes include a significant number of triangular elements. To overcome the challenge of mapping aerodynamics loads from the aerodynamic grid to the structural grid, a mapping algorithm was developed in SMDEE which probes the aerodynamic mesh to determine the forces and moments acting at different locations and appropriately applies these loads on structural mesh (see Figure 9.12). The key tasks performed by the mapping algorithm are shown in Figure 9.13.
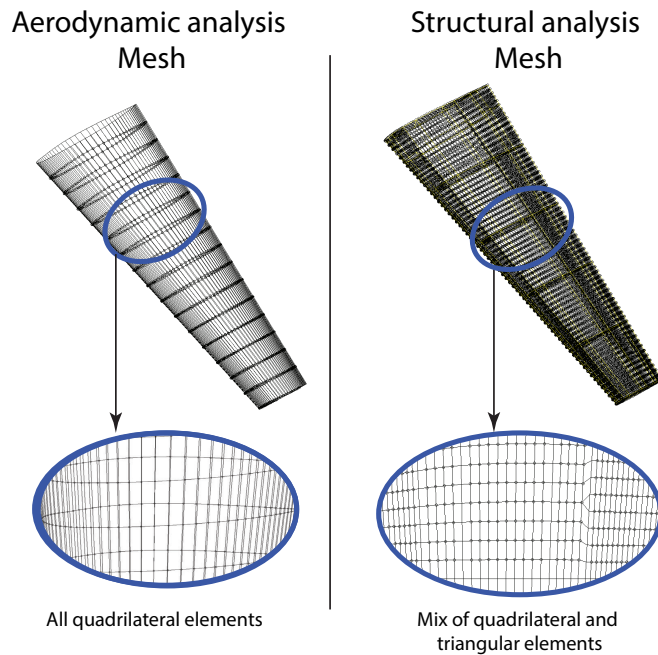
Figure 9.11: Example of the difference in the type of mesh generated for aerodynamic analysis and the structural analysis

Such transformation of forces from one type of mesh to another often leads to approximation errors as the algorithm interpolates or extrapolates forces and moments to
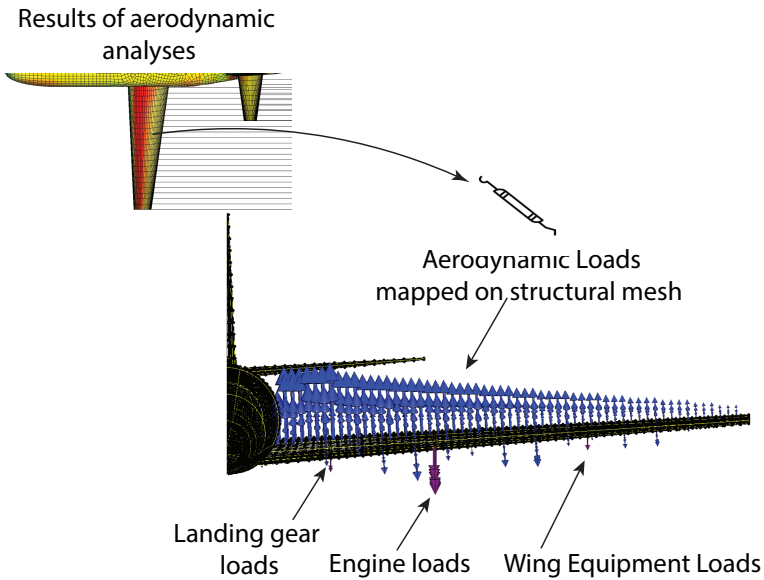
Figure 9.12: Different loads mapped on structural mesh by SMDEE to generate NASTRAN input file
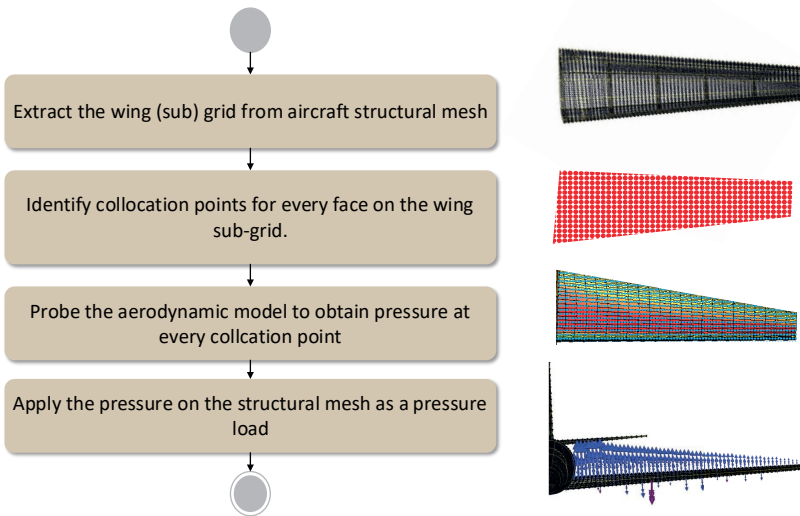
Figure 9.13: UML activity diagram of tasks performed by mapping algorithm

suit the structural mesh. Therefore, we verify whether aerodynamics loads from Flight-stream are correctly mapped to the structural mesh. Correct mapping implies that the load distribution is similar to the distribution obtained from aerodynamic analysis and

the difference between the total lift obtained from Flightstream and the lift force calculated by integrating the force distribution on the structural mesh is acceptably small (i.e., less than 5%).

Since the SFT model must handle the loads imposed during different flight manoeuvres, it must be designed for limit maneuver loads and the resulting ultimate loads. The determination of design load cases and their simulation varies per test objective and the size of the model. In this section, the verification of the load mapping is only performed for 1g steady flight condition and a 2.5g symmetric pull-up manoeuvre for an approximate model of Cessna Citation II (see full-scale aircraft dimensions in Figure 9.5) to study the applicability of the mapping algorithm. In addition, the effect of the size of the model on the accuracy of the mapping algorithm is studied by analyzing three different geometrically scaled models of 12% (1.92m span), 16% (2.56m span) and 20% (3.2m span) scaled model of Cessna Citation II (15.91m span).

Table 9.4: Comparison between the calculated lift on structural mesh and aerodynamic mesh for a 1g steady flight condition for SFT models of Cessna Citation II

Scaling Factor [-]	AoA [kg]	V_∞ [m/s]	Loadcase [$-$]	Lift from Aerodynamic mesh [N]	Lift on Structural mesh [N]	Error [%]
0.12	1	47	1g	92.3	94.3	2.12
0.16	0	47	1g	118.3	123	3.82
0.20	0	41	1g	139.5	147.8	5.62

Table 9.5: Comparison between the calculated lift on structural mesh and aerodynamic mesh for a 2.5g pull-up condition for SFT models of Cessna Citation II

Scaling Factor [-]	AoA [kg]	V_∞ [m/s]	Loadcase [$-$]	Lift from Aerodynamic mesh [N]	Lift on Structural mesh [N]	Error [%]
0.12	5	50	2.5g	224.2	235	4.59
0.16	3	47	2.5g	258.9	252	-2.73
0.20	3	41	2.5g	307	300.3	-2.23

Tables 9.4 and 9.5 detail the flight condition and the load case for models of different sizes and the associated errors introduced by mapping algorithm. Based on this design space exploration, the mapping algorithm maintains the overall lift force within 5% of aerodynamic lift. Furthermore, for 1g cases, the lift force on the structural mesh is overestimated.

For higher load cases, the mapping algorithm underestimates the lift force. For rigid aircraft tests under higher load cases (>2.5g), the lift distribution should be corrected by including a factor of safety to ensure that lift applied on structural mesh is always greater than the lift calculated by aerodynamic analyses. For both load cases, the lack or amplification of forces mainly happens near the leading edges of the wing where the pressure gradient is high and the aerodynamic mesh is refined with cosine spacing whereas the structural mesh is coarser due to equispaced meshing. As a result, the faces near the leading edge of the structural mesh that have larger area as compared to the aerodynamic mesh prevents the capture of pressure gradient leading to errors in force estimation.

In case of aeroelastic tests using SFT, the accuracy of the mapping algorithm becomes much more important. The accuracy of the mapping algorithm can be improved by scaling the pressure on the structural mesh to match the lift forces or by matching the mesh density of the aerodynamics analysis model that of structural mesh (which improves the accuracy of the mapping algorithm but increases the time needed for these analyses). Since, aeroelastic study is not the central focus of this dissertation, a detailed analyses of the implications of mapping algorithm on model flexibility is not performed as the current margins of error are acceptable for flight dynamics analysis.

9.3.2. IMPACT OF STRUCTURAL DESIGN ON MODEL DEFORMATION

In the preceding sections, we discussed the role of SMDEE in generating the structural mesh, mapping the loads onto the mesh and the accuracy of the mapping tools. In this section, we generate multiple models using the SMDEE and perform structural analyses using NASTRAN to study the impact of different types of structural designs on the deformation of the SFT model. Here, a 16% scaled model of Cessna Citation II (dimensions in Figure 9.5) wing is used to study four main structural designs as shown in Figure 9.14.

Case 1: Monocoque Structure   Case 2: 4 Ribs, 0 Spars   Case 3: 0 Ribs, 2 Spars   Case 4: 4 Ribs, 2 Spars
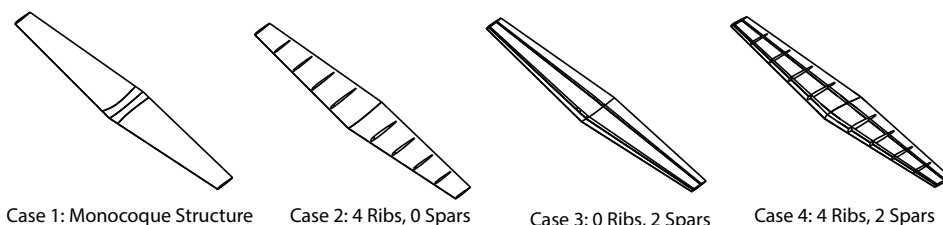
Figure 9.14: Different wing structural designs used to study the impact of structural design on model deformation
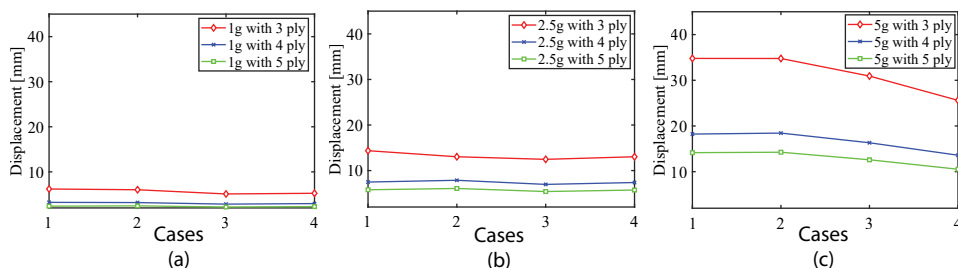
Figure 9.15: Maximum displacement for the different design cases shown in Figure 9.14 where, displacement at (a) 1g loads , (b) 2.5g loads and (c) 5g loads are shown for different number of skin plies

For each wing shown in Figure 9.14, skins with three different stacking sequences (3-ply [45°, 0°, −45°], 4-ply [90°, 0°, 90°, 0°] and 5-ply [90°, 45°, 0°, −45°, 90°]) are used. These wings are subjected to 1g, 2.5g and 3g loads. Figures 9.15, 9.16 and 9.17 show the
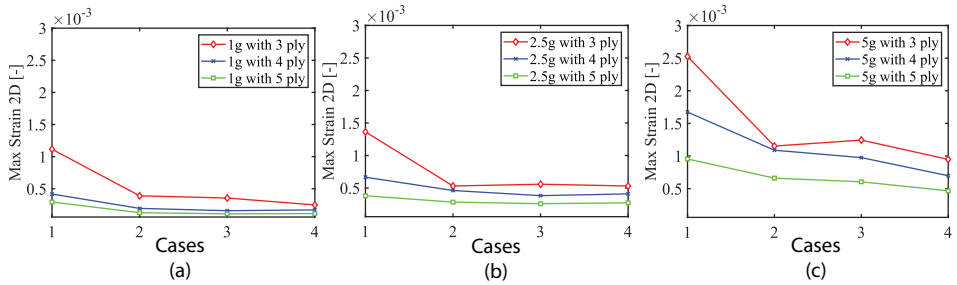
Figure 9.16: Maximum 2D strain for the different design cases shown in Figure 9.14 where, maximum 2D strain at (a) 1g loads , (b) 2.5g loads and (c) 5g loads are shown for different number of skin plies
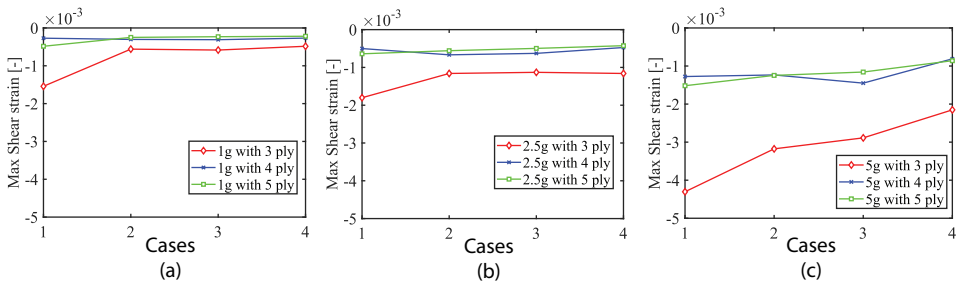
Figure 9.17: Maximum shear strain for the different design cases shown in Figure 9.14 where, shear strain at (a) 1g loads , (b) 2.5g loads and (c) 5g loads are shown for different stacking sequences

displacement, maximum 2D strain and shear strain respectively for different load cases and structural design.

Analysis of the results of this structural design study demonstrates that for 4 and 5 ply skin panels, the the monocoque structure (Case 1) is as rigid as the semi-monocoque structure (Case 2 & 3) and the conventional structure (Case 4). Thus, when rigid structures are required for SFT, a 5-ply skin panel can be used without any internal structural elements (e.g., ribs and spars). Furthermore, based on the studies performed in this dissertation, the number and position of the internal structural elements has lower impact as compared to the number of plies on the SFT model deformations.

The results of this study are in agreement with the observations made by Raymer [190] that SFT models do not really require an internal structure and a monocoque structure is generally sufficient to withstand most loads needed for rigid aircraft testing. Furthermore, since the displacement of the 5-ply conventional design (case 4) is under 10 mm irrespective of the load case, the conventional design can be used in the rigid SFT model design optimization without structural analysis in every iteration as long as the design rules shown in Table 7.1 are complied with. However, where flexible models are necessary, 3-ply or lower must be analysed at every iteration to mimic the deflection of the full-scale aircraft. In other words, when similarity requirements are associated with

structures discipline, structural analysis must be performed in every iteration of SMDEE. Otherwise, structural design initiated by SMI is sufficient to comply with the certification and safety requirements.

9.4. Flight Mechanics Assessment of SFT model

The trim conditions, the static and dynamic stability and the handling qualities of a given SFT model must comply with different requirements discussed in Chapter 5. To this end, a non-linear flight dynamics analysis tool called PHALANX (Performance, HAndling qualities and Loads ANalysis toolboX) is used. PHALANX is a data-driven, selective-fidelity, modelling and analysis toolbox developed at Delft University of Technology, which gathers data and models different aeronautical disciplines (aerodynamics, weight and balance, propulsion, etc.) to create a non-linear aircraft dynamics simulation model. This serves as a virtual flight test vehicle, and can be used to:

1. evaluate aircraft performance characteristics such as equilibrium thrust, rate of climb, cruise efficiency and maximum mission range

2. assess static and dynamic stability in different flight conditions

3. perform handling qualities assessments

4. model automatic flight control systems

5. estimate flight loads resulting from both intentional maneuvers and atmospheric disturbances.

PHALANX is developed in MATLAB/Simulink® and is centered around the SimScape™ Multibody Dynamics core for modeling and simulation of complex physical systems. This allows PHALANX to model relative motion of aircraft parts (e.g. center of gravity shift due fuel consumption, wings flexibility) and monitor local flight parameters at pre-scribed locations (e.g. angle of attack at the horizontal tail) [200]. The data from different disciplinary analyses can have different fidelity levels, which allows PHALANX to operate consistently at various design phases and also in Multi-disciplinary Design Optimization (MDO) environment [201, 202].

The following sections provide a brief insight into the working of PHALANX. Reader is referred to the work of Varriale [203] for a detailed explanation of PHALANX. Two most important algorithms in PHALANX necessary for the SFT model design are in Section 9.4.1 (trim algorithm) and Section 9.4.2 (extracting handling qualities). These algorithms are useful in assessing similitude in addition to determining the safety and certification requirements. The trim algorithm is necessary to determine the aerodynamic deriva-tives and the associated model deflections necessary to determine the DoS. The han-dling qualities extraction algorithm is necessary to populate the Behavioural Indicator Matrix which is necessary to assess similarity of flight dynamics behaviour as discussed in Chapter 6.

9

9.4.1. EQUATIONS OF MOTION AND TRIM ALGORITHM

The SFT models addressed in this study are considered rigid, with constant mass and moment of inertia. In such cases, the aircraft equations of motion reduce to the following system of coupled, non-linear, first-order ordinary differential equations:

$$\dot{x}_{\text{dynamic}} = f_{\text{dynamic}}(x_{\text{dynamic}}, x_{\text{kinematic}}, \delta) \tag{9.2}$$

$$\dot{x}_{\text{kinematic}} = f_{\text{kinematic}}(x_{\text{dynamic}}, x_{\text{kinematic}}) \tag{9.3}$$

where,

$$x_{\text{dynamic}} = \{u, v, w, p, q, r\} \tag{9.4}$$

$$x_{\text{kinematic}} = \{\psi, \theta, \phi, X_E, Y_E, Z_E\} \tag{9.5}$$

$$\delta = \{\delta_a, \delta_e, \delta_r, \delta_T\} \tag{9.6}$$

The dynamic equations can be explicitly written as,

$$\begin{Bmatrix} \dot{u} \\ \dot{v} \\ \dot{w} \end{Bmatrix} = -\begin{Bmatrix} p \\ q \\ r \end{Bmatrix} \times \begin{Bmatrix} u \\ v \\ w \end{Bmatrix} + \frac{g}{W} \begin{Bmatrix} X(\alpha, \beta, \theta, W, \delta) \\ Y(\alpha, \beta, \theta, \phi, W, \delta) \\ Z(\alpha, \beta, \theta, \phi, W, \delta) \end{Bmatrix} \tag{9.7}$$

$$\begin{Bmatrix} \dot{p} \\ \dot{q} \\ \dot{r} \end{Bmatrix} = [I]^{-1}\left(-\begin{Bmatrix} p \\ q \\ r \end{Bmatrix} \times [I] \begin{Bmatrix} p \\ q \\ r \end{Bmatrix} + \begin{Bmatrix} \mathscr{L}(\alpha, \beta, \theta, \phi, \delta) \\ \mathscr{M}(\alpha, \beta, \theta, \phi, \delta) \\ \mathscr{N}(\alpha, \beta, \theta, \phi, \delta) \end{Bmatrix}\right) \tag{9.8}$$

see Table 9.6 for details of the variables shown here.

In case the aerodynamic data is available only for the longitudinal characteristics, the system of equations (Equations 9.7 - 9.8) is reduced to equations for $\dot{u}$, $\dot{w}$ and $\dot{q}$ and the others are assumed as automatically satisfied. The only auxiliary kinematic equation simplifies to $\dot{\theta} = q$.

Trimming the aircraft means finding the combination of inputs δ and states $[x_{\text{dynamic}}, x_{\text{kinematic}}]$ that result in a steady flight, i.e. $f(x_{\text{tr}}, u_{\text{tr}}) = \dot{x}_{\text{tr}} = 0$. A subset of these parameters (i.e., states and inputs) must be assigned explicitly in the equations of motion (for example, trim speed, altitude, flight path orientation or thrust setting). The remaining parameters are called trim controls κ and have to be determined. This is obtained as a solution to an optimization problem, which is formulated as:

minimize

$$||\dot{x}_{\text{dynamic}} - f_{\text{dynamic}}(\kappa)||^2 \tag{9.9}$$

subject to the condition,

$$\kappa_{lower-bound} \leq \kappa \leq \kappa_{upper-bound} \tag{9.10}$$

where the objective function is the sum of squared residual accelerations in aircraft body axes.

Table 9.6: Description of different variables used in equations of motion in PHALANX

Symbol	Description	Units
u	velocity along x body axis	$\mathrm{m\,s^{-1}}$
v	velocity along y body axis	$\mathrm{m\,s^{-1}}$
w	velocity along z body axis	$\mathrm{m\,s^{-1}}$
p	angular velocity about x body axis	$\mathrm{rad\,s^{-1}}$
q	angular velocity about y body axis	$\mathrm{rad\,s^{-1}}$
r	angular velocity about z body axis	$\mathrm{rad\,s^{-1}}$
ψ	heading angle	rad
θ	longitudinal attitude angle	rad
ϕ	roll angle	rad
X_E	position along x Earth axis	m
Y_E	position along y Earth axis	m
Z_E	position along z Earth axis	m
δ_a	aileron deflection angle	rad
δ_e	elevator deflection angle	rad
δ_r	rudder deflection angle	rad
δ_T	normalized throttle command	-
$\dot{u}$	acceleration along x body axis	$\mathrm{m\,s^{-2}}$
$\dot{v}$	acceleration along y body axis	$\mathrm{m\,s^{-2}}$
$\dot{w}$	acceleration along z body axis	$\mathrm{m\,s^{-2}}$
W	weight of the aircraft	N
$\dot{p}$	angular acceleration about x body axis	$\mathrm{rad\,s^{-2}}$
$\dot{q}$	angular acceleration about y body axis	$\mathrm{rad\,s^{-2}}$
$\dot{r}$	angular acceleration about z body axis	$\mathrm{rad\,s^{-2}}$
ω	natuaral frequency	$\mathrm{rad\,s^{-1}}$
ζ	damping ratio	-
I	moment of inertia matrix	$\mathrm{kg\,m^2}$

9

9.4.2. HANDLING QUALITIES PREDICTION

The system of equations of motion can be numerically linearized about a trimming point by perturbing the inputs and calculating the rate of change of the states. If a set of output variables is chosen, the system can be represented with the state-space notation. The full order linearized model consists of the 12 rigid aircraft states shown in Equations 9.5 and 9.4 (of which ψ, X_E and Y_E have no effect on the dynamics), plus the actuator dynamics. The bare airframe linear model only retains the rigid body states, i.e. the ones on the left-hand side of in equations 9.7 and 9.8.

The longitudinal linearized model can be extracted from the full order linearized model by selecting the suitable states, inputs and outputs. In this study, the following longitudinal linear system is adopted:

$$\begin{Bmatrix} \dot{u} \\ \dot{w} \\ \dot{\theta} \\ \dot{q} \end{Bmatrix} = A \begin{Bmatrix} u \\ w \\ \theta \\ q \end{Bmatrix} + B\delta_e \qquad (9.11)$$

where the A and B matrices are populated by the linearization algorithm. This fourth order system is representative of the two characteristic longitudinal eigenmotions: the short period and the phugoid. The eigenvalues of the dynamic matrix are extracted and processed to obtain dynamic parameters such as damping ratio and natural frequency of the eigenmotions.

Handling qualities are used to quantify the aircraft response for the required pilot workload. HQ can be of two types, namely, predicted handling qualities (i.e., computer simulations or tests without a pilot) and assigned handling qualities (i.e., based on pilot rating).

For a full-scale aircraft, the pilot assigns a HQ rating (using the Cooper Harper rating scale [204]) which is based on the task performance (for example, trajectory tracking precision) and the piloting effort required. This process is repeated with many pilots and many different aircraft to arrive at a certain HQ metric such as Level 1/2/3. Here, each metric is aircraft size and task dependent.

For sub-scale flight testing, currently, there are no clear assigned HQ requirements because the size and task requirements of sub-scale models are different from those of full-scale aircraft. Thus, the assigned HQ criteria must be developed for sub-scale designs. However, this is beyond the scope of this work. For the remainder of this dissertation, reference to the HQ implies predicted HQ.

Within the same level of dynamic approximation (e.g. non-linear dynamics, fourth-order linearized longitudinal dynamics, second-order "coarse" short period or phugoid approximation), the fidelity of the flight mechanics simulation is tied to the fidelity of the datasets used to build the aircraft model. The HQs and S&C assessment is therefore strongly influenced by the aerodynamic dataset provided as input to the flight mechanics toolbox as discussed in the following section.

9

9.4.3. IMPACT OF AERODYNAMIC DATA ON FLIGHT DYNAMICS BEHAVIOUR

For PHALANX to provide the model trim condition, stability & control characteristics and the handling qualities, aerodynamics database (aerodynamic forces experienced by clean configuration and with movables deflected), engine database (the thrust and torque generated by the engine) and the weight and balance data (mass, moment of inertia and center of gravity location) are necessary as shown in Figure 9.18.

The generation of the aerodynamics database requires multiple simulations (e.g., 3D panel method, RANS) or an experimental test campaign (e.g., wind-tunnel test) in different flight conditions. The aerodynamic computational simulation/test campaign needs to be executed at least 18 times to generate clean static aerodynamic database, 108 times to generate the dynamic aerodynamic data and 36 times per control surface. Thus, for a 5 control surface aircraft (2 ailerons, 2 elevators and 1 rudder), the aerodynamic solver needs to be executed 306 times to generate the aerodynamic database for PHALANX
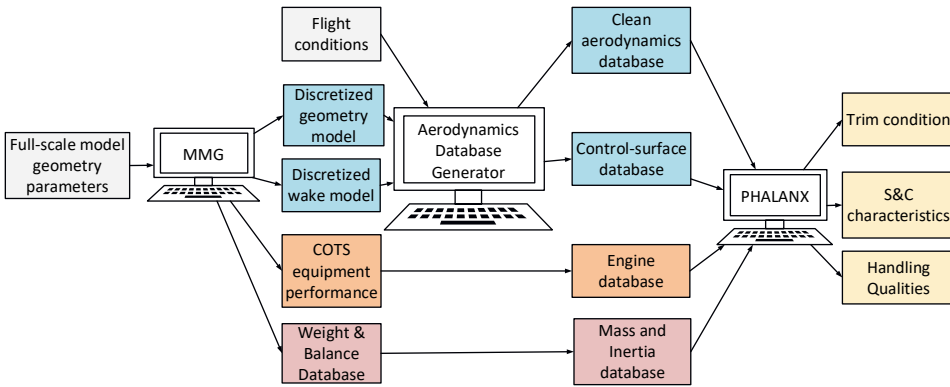
Figure 9.18: Data required to execute PHALANX produced by the MMG (exception flight conditions)

analysis.

Table 9.7: Overview of different computational simulation cases that must be run to generate the aerodynamic data for PHALANX

Condition	Case Details	Total Cases to run
Static Data (Clean Configuration)	3 × Angle of Attck 3 × Sideslip Angle 2 × Mach Number	**18**
Dynamic Data Generation (Clean Configuration)	3 × Angle of Attck 3 × Sideslip Angle 2 × Mach Number 2 × pitch rate 2 × roll rate 2 × yaw rate	**108**
Control Surface Data (per Movable Deflected)	3 × Angle of Attck 3 × Sideslip Angle 3 × Mach Number 3 × Angle of Attck 2 × Control Surface Deflection	**36**

9

Obviously, the time needed to generate such a database is quite large. Efforts made to improve the execution efficiency of the SMDEE framework are discussed in Section 8.3. Nevertheless, once the database is available, the sensitivity of the flight dynamics model to the accuracy of the database must be ascertained.

Section 9.1 compared the static aerodynamic derivatives obtained from WT and Flightstream analysis. There were differences in the aerodynamic results obtained using these two analyses. In this section, we study the impact of the differences in the aerodynamic database on the flight dynamics behaviour of the VGM aircraft (see Figure 9.1 and 9.2). To this end, we generate two sets of aerodynamic databases for VGM as shown in Figure 9.19 to study its longitudinal behaviour.

Of the two models shown in Figure 9.19 the first one is completely based on Flight-
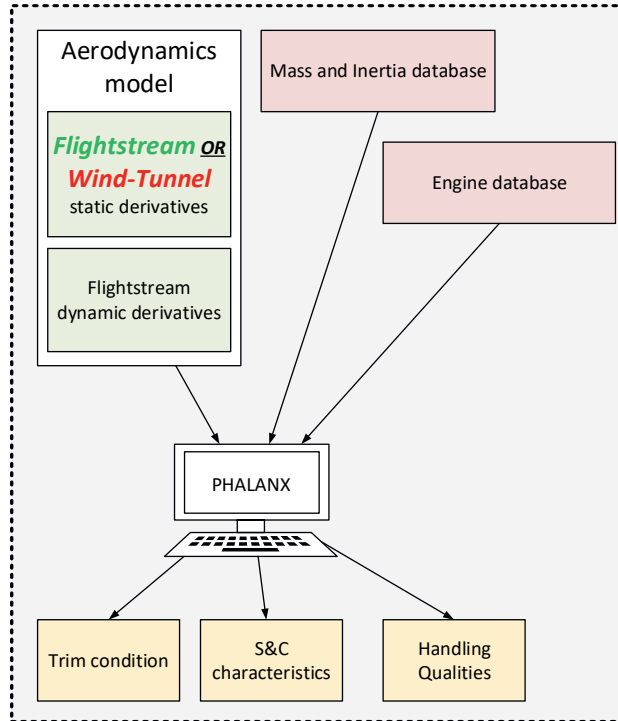
Figure 9.19: Schematic of the two flight dynamics models used in this study whose static derivatives are either obtained from Flightstream or Wind-tunnel and the dynamic derivatives from Flightstream

stream analysis the second model has a combination of wind-tunnel test results (static data) and Flightstream analysis (dynamic data). This is because dynamic derivatives could not be obtained from wind-tunnel tests. As discussed in Chapter 2 and 6, numerical methods are used to obtain the dynamic derivatives (albeit with some errors) to design a SFT model. This SFT model is then manufactured and tested to quantify the errors in the numerical method, which is accounted in the prediction of the dynamic behaviour of the full-scale aircraft. The mass and the moment of inertia values used in this study are shown in Table 9.8.

Table 9.8: Mass and moments of inertia used in this study

Quantity	Value	Units
mass	12.5	kg
I_{xx}	0.253	$\mathrm{kg\,m^2}$
I_{yy}	0.312	$\mathrm{kg\,m^2}$
I_{zz}	0.026	$\mathrm{kg\,m^2}$

Table 9.9: Neutral point of VGM aircraft execution evaluated using static aerodynamic data of different aerodynamic models shown in Figure 9.19

Aerodynamic Model	Neutral Point (wrt Fuselage Nose) [m]	Neutral Point (% of m.a.c)	CG (% of m.a.c)
FlightStream	0.705	49	6
Wind-tunnel + FlightStream	0.701	47	6

Investigations showed that both models could be trimmed. Furthermore, all the models were statically stable as the center of gravity was ahead of the neutral point as shown in Table 9.9. Since the static-stability is purely based on static aerodynamic derivatives, we directly compare the results of wind-tunnel and 3D panel method (Flightstream). The location of the neutral points computed based on different aerodynamic datasets were within 3% of one another. Assuming the wind-tunnel tests are a true depiction of reality, the results of 3D panel method analyses can be used to study the static stability of SFT models.

Table 9.10: Results of longitudinal dynamic stability analysis performed using PHALANX for different aerodynamic models (see Figure 9.19)

Aerodynamic Model	Damping Phugoid	Frequency Phugoid	Damping Short-period	Frequency Short-period
FlightStream Only	0.05	0.30	0.05	19.09
Wind-tunnel & FlightStream	0.11	0.35	0.11	24.4

PHALANX was then used to study the dynamic stability of the VGM model. All models (see Figure 9.19) were found to be dynamically stable as shown in Table 9.10. For the short period motion, the predicted handling qualities for damping and frequency criteria are shown in Figure 9.20. The short-period motion of all models exhibit similar behaviour. The differences in the magnitude of damping and frequency of the **complete 3D panel method based model (Flightstream)** and its **corresponding wind-tunnel based model** are due to the differences in C_{L_α}, C_{M_α} and C_{D_0} values of computational analysis and wind-tunnel tests as discussed in Section 9.1. Nevertheless, the results are comparable and the in-flight short-period behaviour of the SFT model is expected to be similar (see discussion in Chapter 6).

The phugoid motion HQ showed the most differences as shown in Figure 9.21. While the frequency of phugoid motion is comparable for the two models, the damping ratio is approximately 200% higher for Flightstream only as compared to Wind-tunnel + Flightstream. The main difference comes from the higher lift-to-drag ratio of pure 3DPM based models as compared to wind-tunnel test results. Since the models had similar lift forces at low angles of attack, the difference is caused by drag. Therefore, in the future, when phugoid HQ is determined using 3DPM, appropriate corrections must be made
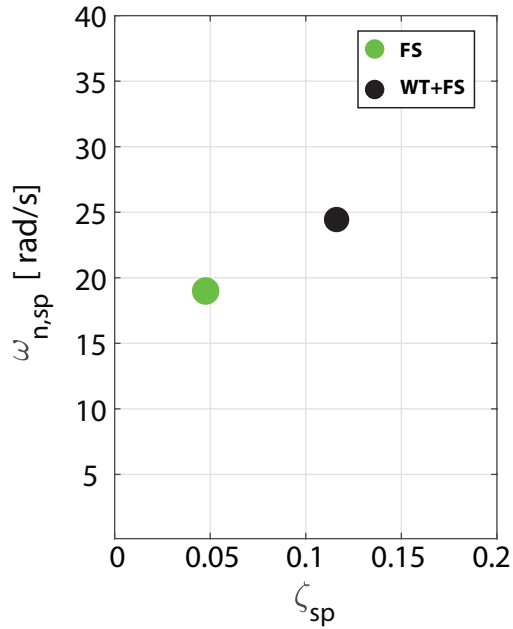
Figure 9.20: Predicted handling qualities of the short period motion, where, x-axis shows the damping of the model in short-period motion and the y-axis shows the frequency
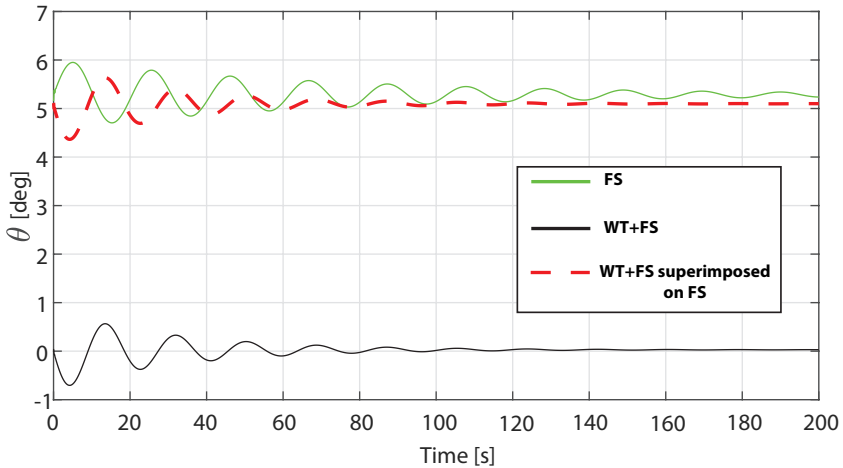
Figure 9.21: Phugoid Response to Longitudinal Step Input, where, x-axis shows the time and the y-axis shows the pitch angle at different time instances

to the predicted drag either using empirical methods or by performing higher fidelity simulations.

Furthermore, the oscillations for longitudinal step input for the Flightstream only model is around 5° whereas the Wind-tunnel + Flightstream oscillated around 0° because of the differences in the trim points of the two models. As discussed in 9.4.2, every model is perturbed from its trim condition which depends on the aerodynamics data of the clean configuration and the forces and moments generated by the control surface deflections estimated by the two models. Consequently, only the shapes of the two curves shown in Figure 9.21 can be compared (i.e., damping and frequency) and not the axis about which the oscillation occurs (i.e., trim condition).

9.5. SUMMARY

In this chapter, we discussed the disciplinary analysis tools which are external to SMDEE but a key enabler of MDAO based similarity maximization technique. Four main disciplinary analysis integral to the SFT model design, namely, aerodynamics, weight and balance, structures and flight dynamics were discussed in this chapter.

3DPM was chosen for aerodynamic analyses as it provides balance between the expected accuracy and the solver execution time. Two different 3DPMs (Flightstream and VSAERO) were investigated in this research for longitudinal behaviour. VSAERO seemed to underestimate drag significantly (see Appendix D). Furthermore, the truncation errors and approximations for warped geometry led to noisy output from VSAERO. Flightstream, although underestimating drag, was robust and could handle the analysis without any noise or discontinuity in the results. Thus, for the remainder of this dissertation, only Flightstream is used for aerodynamic analysis.

The weight and balance tool, developed in-house, to support the SFT model design performed within acceptable bounds of error for the SFT model. Therefore, it was used extensively for the case-studies performed in this research work. Structural analysis showed that sufficiently reinforced models (see best practices shown in Chapter 8) show no major displacement and can be used for the rigid SFT model testing without including structural analysis in the loop. Since this study focuses on flight-dynamic assessment of rigid model, detailed structural analysis will not be performed for every iteration. A final check will be performed after completing MDAO based similarity maximization.

Flight Dynamics analysis performed using PHALANX is sensitive to the quality of the aerodynamic database. The drag under-prediction by 3D panel method (Flightstream) significantly affects the assessment of the phenomena influenced by drag. Thus, the use of the 3D panel method with PHALANX is only recommended for phenomena where drag does not significantly affect the SFT model behaviour. For the remainder of this dissertation, short-period motion and aperiodic roll motions are studied as they are not significantly affected by model drag.

9

10

CASE-STUDIES

The results of seven case studies are reported in this chapter to demonstrate the efficacy of MDAO based similitude maximization approach as compared to the classical geometric scaling method. The first six case studies are performed using an approximate model of the Cessna Citation II 550. Here, the complexity of the problem is increased in each subsequent study by complying with more disciplinary similitude requirements and flight dynamics constraints. Such an incremental approach allows us to quantify the impact of different requirements on SFT model similitude. The last case-study is dedicated to the design of a SFT model for a box-wing aircraft to demonstrate the applicability of MDAO based similitude maximization approach to unconventional designs. All the case studies show that the SFT model designs obtained using MDAO based similitude maximization approach consistently outperform geometric scaling approach.

Although the idea of computational-scaling has been around since 1990s, the actual benefit of its use over the classical similitude theory has not been quantified. In this chapter, we perform seven case-studies to quantify the value of using computational-scaling in the SFT model design process (Table 10.1).

Table 10.1: Overview of Case-Studies performed in this chapter

Study	Nr. Variables	Aircraft	Phenomena Studied	Optimization Disciplines	Objective
1	28	Cessna Citation II	Short-Period Motion	Geometry, Aerodynamics	Aerodynamic scaling
2	11	Cessna Citation II	Short-Period Motion	Geometry, Structures, COTS Equipment, W&B	Aerodynamic scaling with CG positioning
3	20	Cessna Citation II	Short-Period Motion	Geometry, Structures, COTS Equipment, W&B	W&B scaling
4	48	Cessna Citation II	Short-Period Motion	Geometry, Structures, COTS Equipment, W&B, Aerodynamics	Aerodynmaics - W&B scaling
5	46	Cessna Citation II	Short-Period Motion	Geometry, Structures, COTS Equipment, W&B, Aerodynamics, Flight Mechanics	Aerodynmaics - W&B scaling with flight mechanics constraints
6	47	Cessna Citation II	Short-Period Motion and Roll Damping	Geometry, Structures, COTS Equipment, W&B, Aerodynamics, Flight Mechanics	Aerodynmaics - W&B scaling with flight mechanics constraints
7	25	Box-wing Aircraft	Short-Period Motion	Geometry, Structures, COTS Equipment, W&B, Aerodynamics, Flight Mechanics	Aerodynmaics - W&B scaling with flight mechanics constraints

10

In the first five studies, computationally-scaled SFT model of the Cessna Citation II aircraft is designed for short-period motion similitude. Short period motion is used in these case studies because it involves a number of dynamic derivatives that are difficult to assess using testing methods other than SFT as discussed in Chapter 2. In addition,

short period motion depends on the results of multiple disciplinary analyses (i.e., aerodynamic design, structural design, COTS equipment design and the weight & balance of the SFT model) which makes it challenging to achieve short-period motion similitude. Since SFT is a preferred testing method where multidisciplinary effects can be observed, short-period motion similitude is extensively studied in this chapter.

The motivation for the first five case studies can be summarized as follows:

1. **Case-Study 1:** The aim of this study is to design a SFT model using aerodynamic computational-scaling (i.e., changing aerodynamic design to ensure similitude of aerodynamic behaviour). This study includes a number of assumptions as it lacks the multi-disciplinary analyses necessary to design a SFT model compliant to the requirements described in Chapter 5. Nevertheless, the results of this study form a baseline for subsequent case-studies to determine the impact of the assumptions.

2. **Case-Study 2:** The aerodynamic moments used in the study of short-period motion are dependent on the center of gravity location. However, mono-disciplinary aerodynamic analysis performed in case-study 1 does not include the impact of changing center of gravity position. This study demonstrates the importance of steering the CG location to improve the short-period motion similitude between the SFT model and the prototype.

3. **Case-Study 3:** The mass and inertia characteristics of a SFT model significantly affects the short-period motion behaviour. This study aims to quantify the impact of mass and inertia computational-scaling, thereby clarifying the inadequacies of the studies that only use aerodynamic scaling for short-period motion similitude.

4. **Case-Study 4:** The case-studies 1-3 either match the weight & balance properties or the aerodynamic coefficients of the model and the prototype but not both. In this study, MDAO based computational-scaling includes the effects of aerodynamics, center of gravity position and the weight & balance properties to maximize the short-period motion similitude. This increases the design space and allows the optimizer to find a SFT model design that has better similitude to the full-scale aircraft as compared to the SFT models obtained from mono-disciplinary analyses.

5. **Case-Study 5:** In addition to the similitude requirements, SFT models must also comply with the flight mechanics requirements to guarantee the model safety in flight. This study extends the case-study 4 by including the flight mechanics discipline. Since the key SFT model design requirements are incorporated here, the results of this study are the closest to physical SFT.

10

These studies provide an in-depth analysis of using different design variables and disciplinary analyses on the model similitude for short-period motion. Nevertheless, as discussed in Chapter 2 and 4, attempts must be made to use one SFT model to study multiple phenomena to reduce costs. In **Case-study 6**, a SFT model is designed for maximum similitude with both short-period motion and roll damping. This study is a starting point for the development of a catalog of SFT models to predict full-scale aircraft behaviour.

SFT is an essential approach to mitigate the development risk of unconventional aircraft designs. Thus, the SFT model design process should be able to effectively support the unconventional SFT model design. In **Case-study 7**, a SFT model of box-wing aircraft is designed with the objective of ensuring short-period motion similitude.

10.1. Case-Study 1: Aerodynamic Scaling for Short-Period Similitude

The goal of this study is to design a SFT model with the maximum short period motion similitude to Cessna Citation II 550 (see Figure 9.5) using MDAO based aerodynamic scaling. The optimization is started with a 20% geometrically-scaled model of Cessna Citation II 550. In the subsequent iterations, new SFT models are designed by varying the scaling factor and the aerodynamic design parameters such as wing position and airfoil shapes (see Section 10.1.1). This allows the comparison of the geometrically-scaled SFT model with the aerodynamically scaled SFT model obtained at the end of the similitude optimization. This study serves as a baseline case, whose results will be used in the following case-studies to determine the impact of the assumptions made here.

Based on the aerodynamic derivatives affecting the short period motion [169], the problem statement for this study is mathematically stated as follows:

$$\text{maximize:} \qquad\qquad DoS \qquad\qquad\qquad (10.1)$$

$$\text{where,} \qquad\qquad DoS = f(C_{Z_0}, C_{Z_q}, C_{M_q}, C_{Z_\alpha}, C_{M_\alpha}) \qquad (10.2)$$

$$\text{and,} \qquad\qquad w_i = 0.2 \ (\text{for } i = 1...5) \qquad\qquad (10.3)$$

with respect to: Aerodynamic design variables (See Section 10.1.1)

here, the DoS is defined in Equation 6.12, C_{Z_0} is the force coefficient in z-direction at $0°$ angle of attack, C_{Z_α} is change of lift coefficient with changing angle of attack, C_{Z_q} is change of lift coefficient with changing pitch rate, C_{M_α} is change in moment coefficient with changing angle of attack and C_{M_q} is change in moment coefficient with changing pitch rate. In this study, all the aerodynamic coefficients are assumed to have equal influence on the short-period motion (Equation 10.3) to set a baseline for the following studies.

Research Question:

What improvements can be made to the aerodynamic design of a geometrically-scaled SFT model to enhance its (short-period motion) similarity with full-scale design?

10.1.1. Design Variables, Assumptions and Constraints

Design Variables: In order to design an aerodynamically scaled SFT model, a wide range of parameters (i.e., geometry of the model and the test conditions) can be varied to change the derivatives shown in Equation 10.2 to eventually maximize the DoS for short-period motion. In this study, 28 design variables that have an impact on the aerodynamic derivatives influencing the short-period motion of an aircraft are chosen (see Figure 10.1).
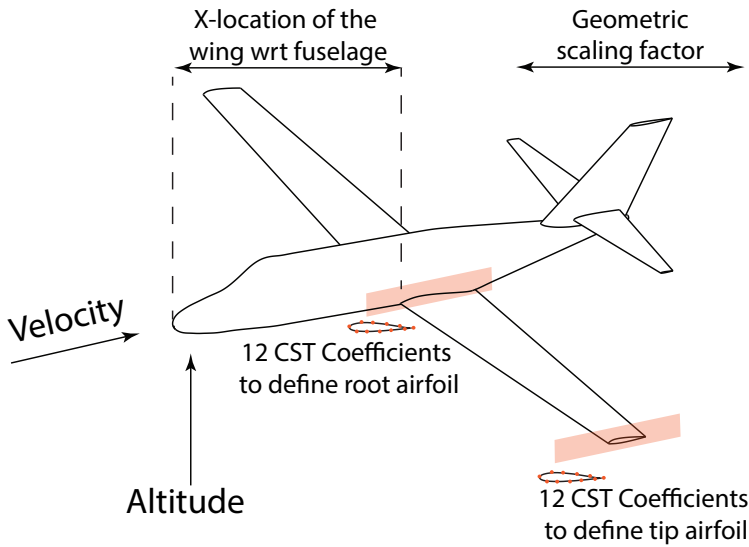
Figure 10.1: Schematic of design variables used in case-study 1 (see Appendix E (Table E.1) for initial values and bounds)

The geometric scaling factor variable controls the geometric scaling of the aircraft. The wing location and the airfoil shape variables lead to the computational-scaling (also known as aerodynamic scaling) as they directly influence the aerodynamic behaviour (by influencing C_{M_α} and C_{M_q} values) of the SFT model and makes the SFT model geometrically dissimilar to the full-scale aircraft.

Assumptions: Since this study only focuses on the aerodynamic design of SFT model, a number of assumptions are used to establish extent of similarity as follows:

1. **Interaction effects:** The aero-propulsive interaction effects are neglected because the quantification of such effects is complex and time-consuming.

2. **Propulsion System:** The same propulsion COTS equipment can cope with the different testing conditions (speed and altitude)

3. **Atmospheric effects:** SFT in open atmosphere always introduces uncertainties due to non-uniform wind, gusts, rain, etc. Owing to the complexity of modelling the atmospheric effects, they are not included in the SFT model design process

4. **Structural Design** Structure is assumed to be strong enough to ensure rigid aircraft model for the entire mission. Thus, structural analysis is not performed at every iteration. However, a check on structural analysis is performed at the end of the optimization to ensure that the model can withstand loads.

10

5. **Trim condition:** In a typical SFT, pilot trims the model and then performs the required manoeuvre. In order to determine a trim condition, a complete aerodynamic dataset coupled with weight & balance data is necessary. In this baseline case-study with only two disciplines within the optimization loop, the trim condition is assumed to be at zero angle of attack of zero and angle of side-slip.

6. **Control Power:** The tail-plane is able to guarantee stability and controllability of the aircraft within the range of possible longitudinal wing positions.

7. **Derivatives calculation:** Linearized derivatives are used in this case study

8. **Weight & Balance:** SFT model must generate lift which is equal to its weight which is not always possible at the assumed trim condition. Nevertheless, no effort is made in this study to identify a flight condition where the weight balance can be achieved.

9. **Degree of influence:** Every coefficient is assumed to have the same influence on short-period motion in this study.

10. **Mass** The mass is assumed to remain constant throughout the optimization process and is equal to 25 kg. The mass chosen in this study is generally recommended by many governmental agencies for SFT.

11. **Similarity assumption:** Since Behavioural Indicator Matrix (BIM) and virtual scaling error cannot be calculated for simplified analysis of this case-study, a higher value of the DoS implies better similitude.

12. **Center of Gravity** CG location is geometrically-scaled as is calculated as a percentage of fuselage length which remains constant throughout the optimization.

This is the simplest case study with most number of assumptions. In the following case studies, systematic effort is made to reduce the number of assumptions and quantify the impact of these assumptions and approximations.

Constraints: Only one constraint is imposed in this study, where, the optimizer assesses whether all the COTS components fit within the SFT model and do not intersect with SFT model structural components when the aerodynamic design is changed. Since this check is a Boolean operation (i.e., whether the components fit or not), a penalty "***DoS = DoS - 10***" is imposed on the DoS, when the components cannot be fit inside the SFT model.

10.1.2. Optimization Architecture and Algorithm
Architecture: The architecture used for this problem is shown in Appendix G (Figure G.1). This study requires two pre-analyses disciplines to generate the mesh/geometry and perform the aerodynamic analysis to get the derivatives of the full-scale aircraft and two disciplines within the optimization loop to generate the the mesh/geometry and perform the aerodynamic analysis to get the derivatives of the SFT model.

Algorithm: 'FMINCON' is an optimization algorithm available in MATLAB[1] optimization toolbox that can be used to solve optimization problems with constraints. This program also works well when no constraints are defined. FMINCON is the algorithm used throughout this chapter since some case-studies have constraints and some do not. The settings used for this optimization are shown in Table 10.2.

Table 10.2: The settings used to run the FMINCON optimization algorithm in MATLAB

	Values
Display	'iter-detailed'
Algorithm	'sqp'
DiffMinChange	3e-2
DiffMaxChange	2
TolCon	1e-6
TolFun	1e-6
TolX	1e-6
MaxIter	30

10.1.3. RESULTS

320 SFT models were designed during the optimization over seven iterations. The optimization started with a DoS of 66% for geometrically-scaled model and converged to a DoS of 92% (see Figure 10.2). The key aerodynamic coefficients used for the DoS calculations for initial and optimized design are shown in Table 10.3.
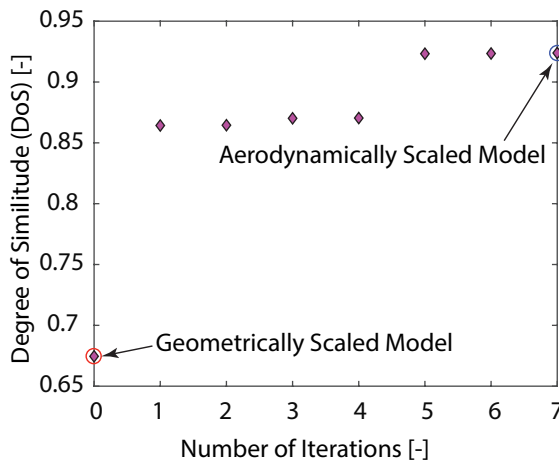
Figure 10.2: The results of aerodynamic scaling optimization performed using MATALB's 'fmincon' optimizer, where 320 SFT models were designed and analyzed

---

[1]https://nl.mathworks.com/help/optim/ug/fmincon.htmldescription

Table 10.3: The aerodynamic derivatives used for the calculation of DoS in Case-Study 1

	Full-scale Aircraft	Geometrically Scaled Model	Scaling Error Geometrically Scaled [%]	Aerodynamically Scaled Model	Scaling Error Aerodynamically Scaled [%]
C_{z_0}	0.22	0.2	13.5	0.17	22.7
C_{z_α}	5.60	5.58	0.3	5.68	-1.4
C_{m_α}	-0.42	0.11	125.0	-0.39	7.1
C_{z_q}	-7.40	-6.10	17.5	-7.40	0
C_{m_q}	- 12.30	-11.80	4.0	-12.00	2.4
DoS	1	0.66	-	0.92	-
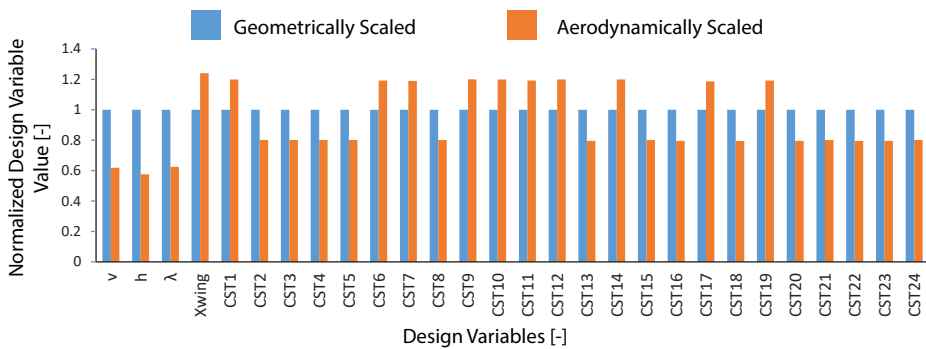
Figure 10.3: The variation of design variables for the geometrically-scaled model and the (optimized) aerodynamically scaled model (see Appendix F (Table F.1) for the values)

The key changes to the design variables are shown in Figure 10.3. After optimization, the aerodynamically scaled model has a lower test velocity as compared to the geometrically-scaled model and the wing of the aerodynamically scaled model is moved rearward with respect to the nose of the fuselage (while CG location remains constant). A consequence of these changes is the reduction in C_{m_α} and C_{m_q}, which improves the similarity of coefficients with full-scale aircraft thereby improving the DoS.

The airfoil shapes remain largely similar for the initial and the optimized design. The optimized airfoil becomes slightly thinner than the initial one (see Figure 10.4). This can be attributed to the inclusion of the simplified boundary layer model in FlightStream aerodynamic analysis due to which the optimizer reduces the airfoil thickness to ensure that the effective airfoil shape in the airflow for the full-scale aircraft and the SFT model remains the same (i.e., airfoil-thickness + boundary layer thickness is the same for model
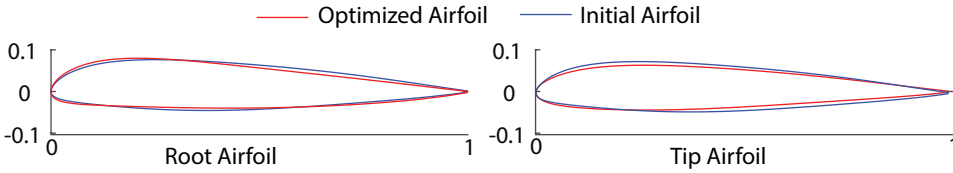
Figure 10.4: The variation of root and tip airfoils due to the aerodynamic scaling optimization

and full-scale aircraft).

10.1.4. COMPUTATIONAL (AERODYNAMIC) SCALING: MERITS AND LIMITATIONS

Aerodynamic scaling performed in this study shows promise as the DoS improves after optimization. The coefficients of the optimized design (aerodynamically scaled) have greater similarity to full-scale aircraft as compared to geometrically-scaled model (see Table 10.3). In addition, the geometrically-scaled model is unstable. Thus, not only is the geometrically-scaled model more dissimilar than the aerodynamically scaled model, but also difficult to fly for the pilot.

However, these results are based on a number of assumptions which do not depict the realistic test conditions. In particular, the change in CG location is not accounted. As a result, the calculation of aerodynamic moment derivatives is not accurate. In addition, the scale of the aerodynamically scaled model is 37.5% lower than the geometrically-scaled model which makes the assumption of constant mass incorrect. In the following studies, the assumptions will be addressed to improve the SFT model designs.

10.2. CASE-STUDY 2: EFFECT OF CG LOCATION ON SHORT-PERIOD SIMILITUDE

The aim of this case-study is to quantify the impact of the center of gravity position and the ability to control this position on the aerodynamic derivatives influencing the SFT model short-period motion. The CG position of a SFT model depends on the arrangements of its COTS equipment and structural design. An inconvenient positioning of the components by the designer might lead to sub-optimal CG location for a given DoS formulation. Systematic optimization can identify an arrangement of the COTS components (for a given aerodynamic design) that guarantees an optimal CG location to maximize the DoS. The problem formulation for this study is represented as follows:

$$\text{maximize:} \qquad DoS \qquad\qquad (10.4)$$

$$\text{where,} \qquad DoS = f(C_{Z_0}, C_{Z_q}, C_{M_q}, C_{Z_\alpha}, C_{M_\alpha}) \qquad (10.5)$$

$$\text{and,} \qquad w_i = 0.2 \ (\text{for } i = 1...5) \qquad\qquad (10.6)$$

with respect to: W&B design variables (See Section 10.2.1)

As the aim is to quantify the impact of the CG position (and not the mass and inertia

of the SFT model) on the DoS, non-dimensional mass and inertia (see Equations 6.7 and 6.6) are not included in the DoS formulation. The design variables chosen for this study are the ones that affect the CG location of the SFT model (discussed in Section 10.2.1).

To assess the improvement in the DoS obtained by steering the CG, we perform two optimization studies. In the first study, 20% geometrically-scaled model used in Case-Study 1 (Section 10.1) is used to (optimally) position the COTS equipment. In the second study, we use the aerodynamically scaled model obtained using optimization in Case-Study 1 (Section 10.1) to (optimally) position the COTS equipment. Thereafter, the results of the two optimization studies are compared to determine the effect of CG on the DoS estimation. These studies are discussed in the following sections.

To support the study, additional analysis capabilities are added as follows:

1. CG is calculated at every iteration of the optimization using physics based methods discussed in Chapters 7 and 9. Thus, no assumptions on the CG location are necessary.

2. The mass and inertia is calculated for every design point using the physics based method described in Chapter 7 (i.e., it is not assumed to be 25 kg as done in Case-study 1).

3. The BIM and virtual scaling errors are calculated to determine whether a higher DoS implies improved similarity

Research Question:

What is the impact of the center of gravity (CG) location on the (short-period motion) DoS of a given SFT model? Can we improve the DoS of a given SFT model by steering the CG position to a convenient location by rearranging COTS equipment?

10.2.1. DESIGN VARIABLES, ASSUMPTIONS AND CONSTRAINTS

Design Variables: The design variables chosen in this study are related to fuselage COTS components and landing gears as shown in Figure 10.5. A total of 11 design variables are chosen, of which, the first nine define the size and the location of the fuselage floors where the COTS components are placed (Figure 10.5). The last two design variables control the longitudinal location of the nose and the main landing gears.

10

Assumptions: Assumptions 1-9 explained in Case-Study 1 (Section 10.1.1) are applicable to this case-study too. In this study, the mass remains constant throughout the optimization as the optimizer does not change the COTS components or structural components but only modifies its position.

Constraints: The only constraint imposed is that the COTS components do not intersect with the OML and the structural components of the aircraft, in which case, a penalty function is applied as described in Case-Study 1 (Section 10.1.1).
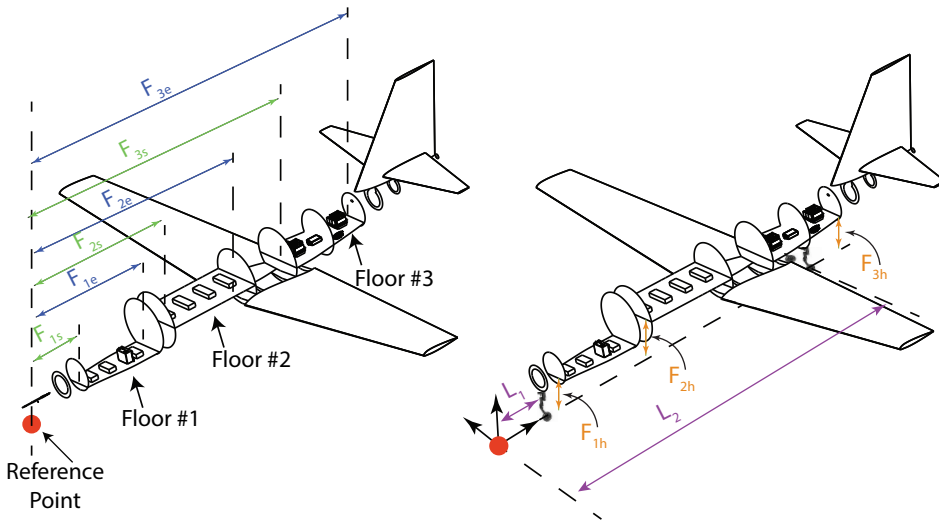
Figure 10.5: Schematic of design variables used in this study that influence the CG location of SFT model (see Appendix E (Table E.2) for initial values and bounds)

10.2.2. OPTIMIZATION ARCHITECTURE AND ALGORITHM

Architecture: The architecture of the optimization system implemented in this case study is shown in Appendix G (Figure G.2). Here, the aerodynamic behaviour of the full-scale aircraft and the SFT model is evaluated before the start of the optimization. During the optimization, only the structural and COTS components are positioned and the CG location is used to transform the aerodynamic moment derivatives from the reference point. Thus, the aerodynamic shape remains fixed throughout the optimization and changes are only made to positioning of COTS and structural components.

Algorithm: The 'fmincon' algorithm provided by MATLAB was used with the optimizer settings shown in Section 10.1.

10.2.3. RESULTS

The two aerodynamic designs from Case-Study 1 (i.e., geometrically-scaled model and aerodynamically scaled model) are used as a starting point for two COTS positioning optimization studies. The results are discussed in the following paragraphs.

geometrically-scaled model: In this optimization, 143 SFT models were analyzed by the optimizer to identify an arrangement of the COTS components with a corresponding DoS value of 0.93 (starting from a DoS of 0.43 as shown in Figure 10.6). For the optimized design, CG moved forward due to the forward positioning of the floor panels (see Figure 10.7). As a result, the moment derivatives of the optimized SFT model are almost equal to those of the full-scale aircraft (see Table 10.4).

10

Figure 10.6: The results of CG scaling optimization performed using MATLAB's 'fmincon' optimizer starting with geometrically-scaled model, where 143 SFT models were designed and analyzed
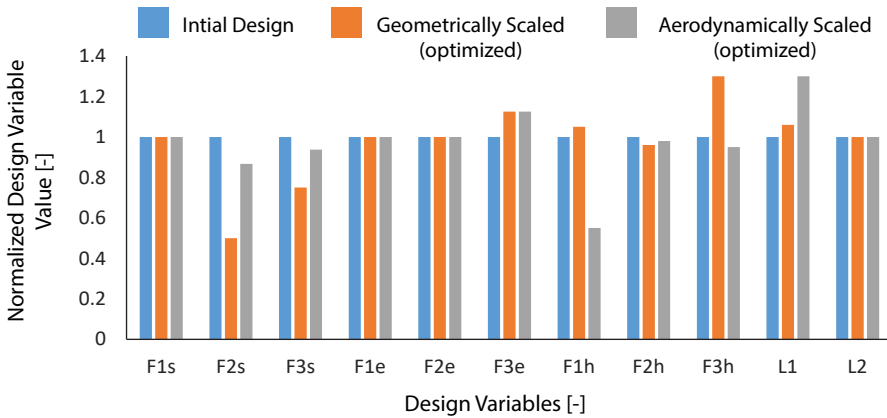
Figure 10.7: The variation of the design variables for the (optimized) geometrically-scaled model and the (optimized) aerodynamically scaled model with respect to the initial design (see Appendix F (Table F.2) for the values)

10

Aerodynamically Scaled model: The aerodynamically scaled model optimization started with a DoS of 0.77. The CG of initial COTS equipment positioning was ahead of the neutral point (at 0.923 m from the reference point of 12.5% scaled model of Citation II). After optimization, where, 186 SFT model designs were investigated, optimizer could find an arrangement of COTS components with a DoS of 0.9 (see Figure 10.8). CG moved forward marginally 0.915 m due to the forward positioning of the floors. The values of the

Table 10.4: The final values of aerodynamic coefficients obtained for the two CG optimization studies performed using geometrically scaled model and aerodynamically scaled models obtained in Case-Study 1 (See Table 10.3 for initial coefficients)

	Full-scale Aircraft	Geometrically Scaled Model (Optimized)	Scaling Error Geometrically Scaled [%]	Aerodynamically Scaled Model (Optimized)	Scaling Error Aerodynamically Scaled [%]
C_{z_0}	0.229	0.198	13.5	0.169	22.7
C_{z_α}	5.60	5.58	0.3	5.68	1.4
C_{m_α}	-0.42	-0.42	0	-0.39	7.1
C_{z_q}	-7.4	-6.1	17.5	-7.4	0
C_{m_q}	- 12.30	-12.56	2.11	-12.20	0.82
Scaling Factor (λ)	1	0.2	-	0.125	-
x_{CG} [m] (w.r.t. fuse-lage nose)	7.38*λ	7.10*λ	3.79	7.32*λ	0.80
DoS	1	0.93	-	0.90	-

design variables of the optimized design and the key coefficients affecting the DoS are shown in Figure 10.7 and Table 10.4 respectively.

The change in the CG location (before and after optimization) is much smaller for the aerodynamically scaled model (0.8%) as compared to the geometrically-scaled model (3.8%) because the moment coefficients for the aerodynamically scaled model were similar to the full-scale aircraft even before the CG optimization (see Table 10.3). Since the aerodynamic optimization in Case-Study 1 already matched the moment derivatives between the full-scale aircraft and the SFT model, the optimizer did not have much room to improve the moments for aerodynamically scaled model as the CG location change only influences the moment derivatives.

10.2.4. DISCUSSION: IMPACT OF CENTER OF GRAVITY ON THE DOS

In this section, we answer the questions posed in the Section 10.2 based on the results of the COTS equipment positioning optimization. The key inferences can be summarized as follows:
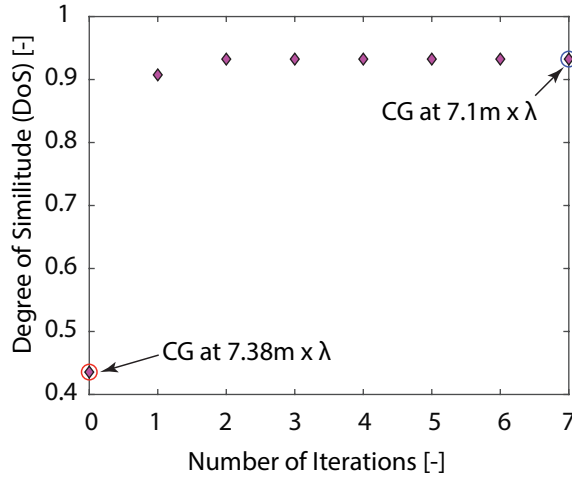
10
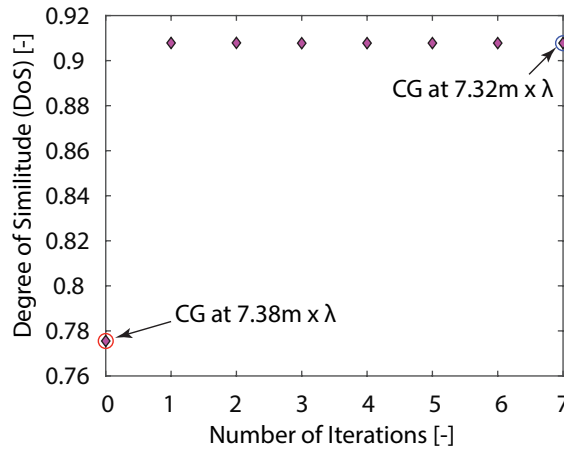
Figure 10.8: The results of CG scaling optimization performed using MATLAB's 'fmincon' optimizer starting with the aerodynamically scaled model, where 186 SFT models were designed and analyzed

1. ***Impact of CG on the DoS:*** The calculation of the CG position is indispensable for the study of the phenomena that are influenced by moment derivatives. Notably, the DoS of starting point of both the geometrically-scaled model optimization and the aerodynamically scaled model optimization (0.43 and 0.77) were lower than the DoS evaluated for the same design in case-study 1 (0.65 and 0.92 as shown in Figures 10.2, 10.6 and 10.8). Thus, the optimization of the CG location improves the similitude. The DoS calculated in Case-Study 1 is not reliable because CG does not scale geometrically. Thus, in order to accurately obtain the DoS, precise calculation of CG is imperative.

2. ***Steering CG to improve the DoS:*** The DoS of a SFT model can be improved by steering the CG. Furthermore, the impact of the CG location on the DoS is higher for those designs whose moment derivatives are principally responsible for lower a DoS. For example, in this case-study, geometrically-scaled model's DoS could be improved more (than aerodynamically scaled model) because its moment derivatives were the cause of low DoS.

10

Based on the results shown in preceding section, both geometrically-scaled model and aerodynamically scaled model have a DoS closer to 1 after COTS positioning optimization. In order to assess whether these models had short-period motion similarity with full scale aircraft, we constructed a Behavioural Indicator Matrix (BIM) composed of the real and imaginary part of the eigenvalues of short-period motion and computed their virtual scaling error (see Chapter 6 for details). Simplified equations of motions for the short-period motion as described by Nelson [169] are used to determine the eigenvalues of the full-scale aircraft and the SFT models.

The virtual scaling errors for the key design points in the optimization performed
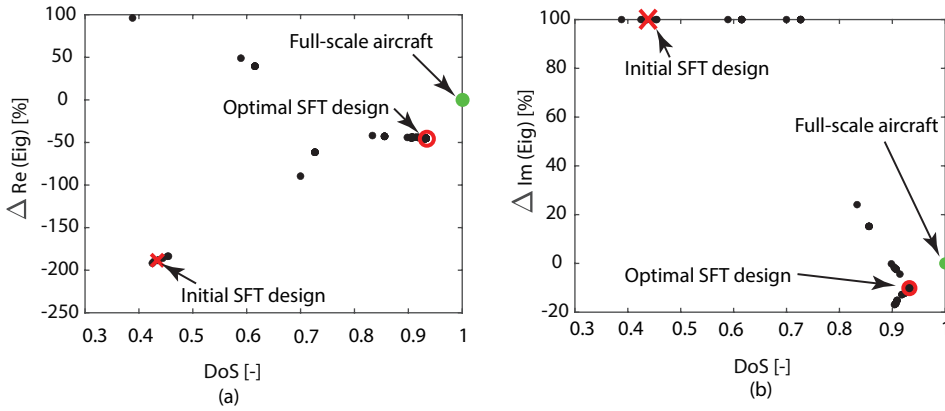
Figure 10.9: Percentage error of (a) real part and (b) imaginary part of short-period motion eigenvalues of key design points in the the optimization performed using geometrically-scaled model
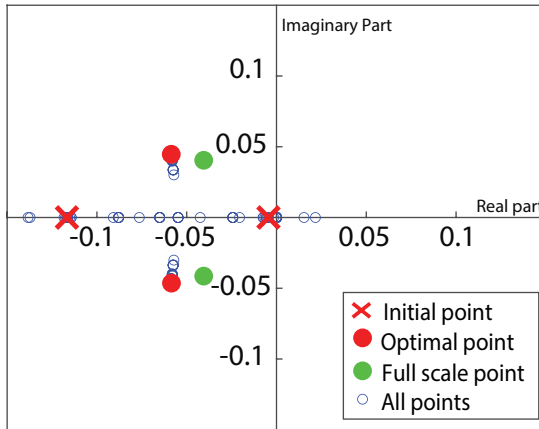
Figure 10.10: Short-period motion eigenvalues of key design points in the optimization performed using geometrically-scaled model

using geometrically-scaled model are plotted in Figure 10.9. Initial design point had a virtual scaling error of 100% and 190% for real and imaginary part of eigenvalue respectively. After the optimization, this reduced to 44% and 16% respectively. The correlation between the DoS and virtual scaling error can be clearly observed. As the DoS improves, the virtual scaling error reduced (i.e., the similarity between SFT model and the full-scale aircraft increases).

When these eigenvalues are plotted as absolute values as shown in Figure 10.10, the nature of the roots can be analysed. The initial point shows overdamped exponentially decaying motion. However, the full-scale aircraft behaviour and the optimized design have an underdamped exponentially decaying sinusoidal motion [169]. Thus, the op-

timized SFT model has similar nature of short-period motion behaviour to full-scale, albeit with different damping and frequency values. If all the assumptions made at the beginning of this section hold true, the optimized geometrically-scaled model can be used to study the short-period motion of full-scale aircraft.
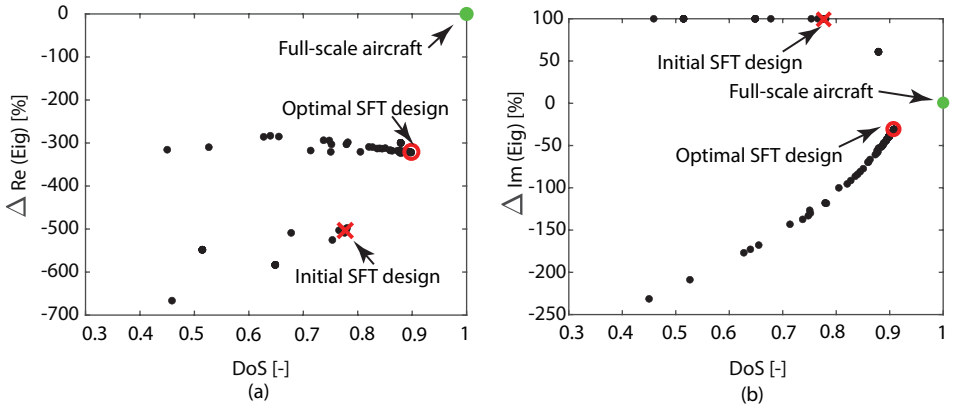
Figure 10.11: Percentage error of (a) real part and (b) imaginary part of short-period motion eigenvalues of key design points in the the optimization performed using aerodynamically scaled model
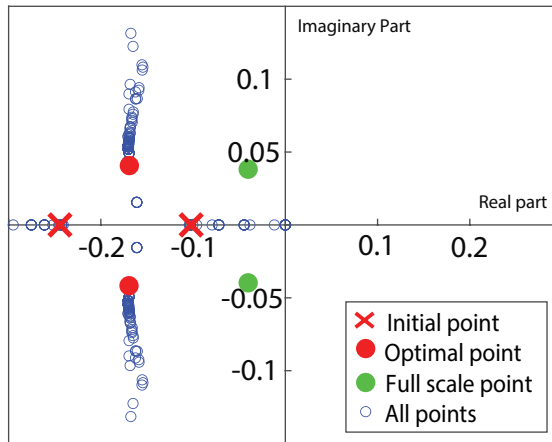
Figure 10.12: Short-period motion eigenvalues of key design points in the optimization performed using aerodynamically scaled model

Similarly, the virtual scaling errors for the key design points in the optimization performed using the aerodynamically scaled model are plotted in Figure 10.11. Before optimization, the virtual scaling error of the real and imaginary part was 530% and 100% respectively. After optimization, as the DoS improved, the virtual scaling error reduced

to 300% and 40% for real and imaginary part respectively. When the absolute eigenvalues are plotted (see Figure 10.12), like the geometrically-scaled model optimization, the initial point has overdamped exponentially decaying motion whereas the full-scale aircraft behaviour and the optimized design have an underdamped exponentially decaying sinusoidal motion. Thus, the optimization of this aerodynamically scaled model also leads to similar short-period motion behaviour provided all the assumptions of the case-study remain true.

Although optimized aerodynamically scaled model only has a 3% lower DoS as compared to optimized geometrically-scaled model, the difference in the eigenvalues is significant. This can be attributed to two main causes, namely:

1. differences in the mass of geometrically-scaled model (28 kg) and the aerodynamically scaled model (18 kg), which was not included in the DoS calculation. The difference in the masses of the two models is mainly due to the difference in the structural mass owing to the difference in the scaling factor of the two models (see Table 10.4).

2. effectiveness of the horizontal tail of the aerodynamically scaled model is increased due to the forward moment of the wing (as compared to geometrically-scaled model). As a result, the short-period motion eigenvalues of the optimized aerodynamically scaled model move further away from the origin as compared to the optimized geometrically-scaled model (see Figures 10.10 and 10.12). This tendency of eigenvalues is in agreement with the observation made by Nelson [169].

Thus, computational-scaling without considering all the relevant dimensionless coefficients (such as mass and inertia) can increase the dissimilarity of the SFT model design as demonstrated in this study. Furthermore, a number of assumptions are made in the simplified flight mechanics analysis performed to determine the eigenvalues. For example, no check is performed to determine whether the lift produced by the SFT model is sufficient to balance the weight of the model. Additionally, no analysis is performed to ascertain whether the model can be trimmed and/or controlled at zero angle of attack as assumed in this study (i.e., whether the model can be flown safely). Inclusion of these constraints/design considerations can change the nature of the SFT model short-period motion behaviour and reduce the similarity between the model and the full-scale aircraft. In the following sections, these additional similarity and safety requirements are included in the problem formulation and disciplinary analysis to reduce possible errors (and failures) during the actual SFT.

10

10.3. CASE-STUDY 3: W&B SCALING FOR SHORT PERIOD SIMILITUDE

In this study, we aim to maximize the similarity between SFT model and full-scale aircraft by including the mass and inertia characteristics in the DoS formulation. The problem statement for this study can be expressed as follows:

maximize: DoS (10.7)

where, $DoS = f(C_{Z_q}, C_{M_q}, C_{Z_\alpha}, C_{M_\alpha}, \mu_c, K_Y{}^2)$ (10.8)

and, $w_i = 0.16$ (for $i = 1...6$)   (10.9)

with respect to: W&B design variables (See Section 10.3.1)

subject to: Constraints (See Section 10.3.1)

where, μ_c and $K_Y{}^2$ are non-dimensional mass and inertia (see Equations 6.7 and 6.6) and all other variables remain the same as described in the previous studies. Notably, C_{Z_0}, which was included in the preceding studies because of its presence in governing equations, is not included in this optimization as it does not have a significant impact on the short-period motion behaviour in comparison to other parameters. Since we only assess the potential of the weight and balance scaling in this study, the aerodynamic design (i.e., outer mold line) of the SFT model is fixed. The geometrically-scaled model shown in Case-study 1 is chosen for this study for two reasons:

1. In the actual design process, engineers do not have sufficient time to perform incremental optimizations by adding one discipline at a time as done in this dissertation (if an optimization is even possible). Thus, the initial design is generally geometrically-scaled.

2. The eigenvalue comparison of short-period motion in Case-study 2 showed that geometrically-scaled model had a greater similarity to full-scale aircraft as compared to aerodynamically scaled model

The weight and balance properties of the (geometrically-scaled) SFT model are varied by the optimizer by changing the design variables (described in Section 10.3.1) to maximize the short-period motion behaviour of the SFT model and full-scale aircraft.

Research Question:

What are the implications of including mass and inertia in the DoS formulation? To what extent is the SFT model behaviour similar to the full-scale aircraft behaviour for short period motion if the weight and balance characteristics are included in the MDAO based similitude maximization for short-period motion?

10

10.3.1. Design Variables, Assumptions and Constraints

In this optimization problem, 20 design variables are used to maximize the short-period motion similitude between the geometrically-scaled SFT model of Cessna Citation II 550 (used in Case-study 1) and its full-scale counterpart. The first 11 design variables, their initial values and bounds remain the same as discussed in Case-study 2. The initial values of the design variables were not updated to the optimized values in order to simulate real design cases where sufficient time is unavailable for incremental optimization studies shown in this dissertation.

The first 11 design variables influence the CG location and the inertia of the model. However, they do not alter the mass of the SFT model significantly which prevents the optimizer from exploiting the sensitivity of the mass on the DoS. In order to study the impact of variation of mass on the DoS, optimizer should be able to vary the mass (sufficiently) by adjusting the design variables. Thus, additional ballast masses were added to design variables whose mass and location could be set by the optimizer (see Figure 10.13).
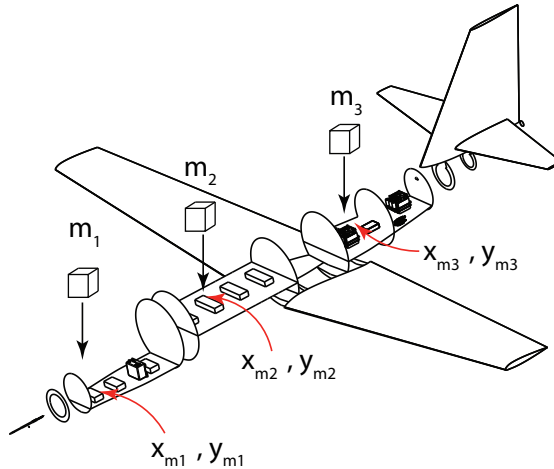
Figure 10.13: Additional design variables (i.e., ballast masses and their location on fuselage floors) to allow optimizer to vary the mass and COTS equipment location of the SFT model (see Appendix E (Table E.3) for initial values and bounds)

Assumptions: Assumptions 1-9 explained in Case-Study 1 (Section 10.1.1) are applicable to this case-study too. However, the optimization of ballast masses and COTS equipment includes the calculation of the CG, mass and inertia at every iteration. Furthermore, the aerodynamic design of the SFT model remains fixed throughout the optimization. Only the aerodynamic moment derivatives are updated at every iteration by accounting for the changes in the CG location. Finally, the COTS equipment remain the same same throughout the optimization which results in constant COTS equipment mass.

Constraints: The constraints for this study remain the same as discussed in Case-Study 2.

10.3.2. OPTIMIZATION ARCHITECTURE AND ALGORITHM
Architecture: The architecture used for this optimization problem is shown in Appendix G (Figure G.2). Here, the aerodynamic shape remains fixed throughout the optimization and changes are only made to the positioning of COTS and structural compo-

nents.

Algorithm: The 'fmincon' algorithm provided by MATLAB was used with the optimizer settings shown in Section 10.1.

10.3.3. RESULTS

A total of 995 SFT model designs were assessed in this optimization study. The optimization started at a DoS of 0.64 (see Figure 10.14). Since the non-dimensional mass and inertia parameters were included in the DoS formulation, the DoS of starting point of this study was higher than the DoS (0.44) calculated in Case-Study 2. At the end of the optimization, a SFT model with a DoS of 0.86 was found.
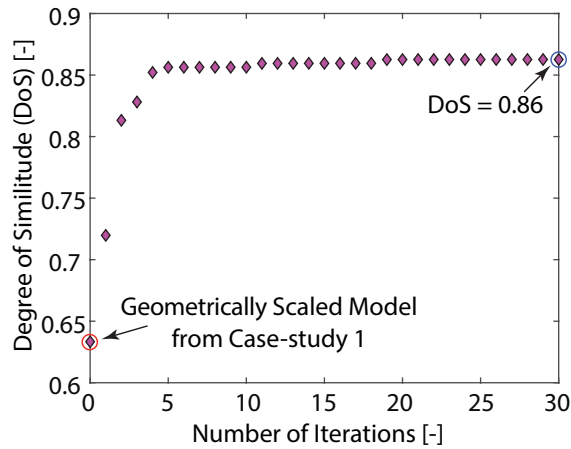
Figure 10.14: The results of weight and balance scaling optimization performed using MATLAB's 'fmincon' optimizer starting with the geometrically-scaled model, where 995 SFT models were designed and analyzed

The final design variable values of the optimized design are shown in Figure 10.14. The key changes in the optimized SFT model as compared to the initial geometrically-scaled model design were:

1. The Floor #2 was made larger to move the CG forward by positioning COTS equipment closer to the nose of the fuselage (see variable F2s in Figure 10.14).

2. The ballast masses were lowered from 7.5 kg to 6.5 kg.

3. All the ballast masses were moved closer to the CG location. The ballast masses on Floor #1 and Floor #2 were moved rearwards and the mass on Floor #3 was moved forward (see variables X1, X2 and X3 in Figure 10.14).

As a consequence of changes made by the optimizer to the design variables to optimize the SFT model design, following results could be observed:
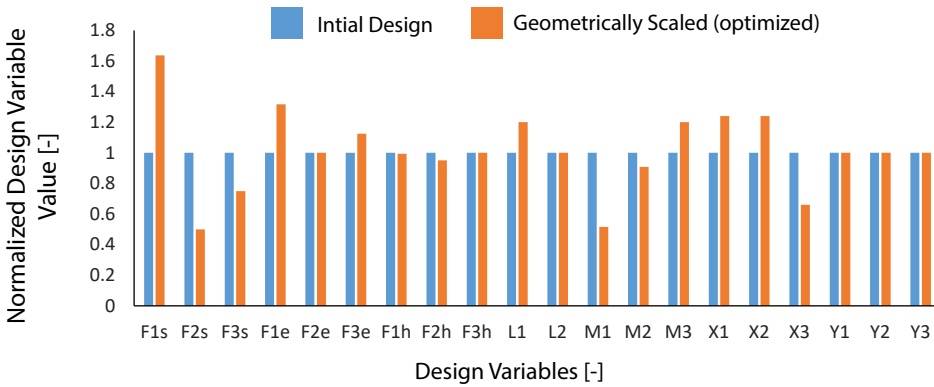
Figure 10.15: The variation of the design variables for the (optimized) geometrically-scaled model with respect to the initial design (see Appendix F (Table F.3) for the values)

Table 10.5: Key performance indicators of the SFT model obtained from W&B scaling optimization

	Full-scale Aircraft	Initial Values	Optimized Values	Optimized Design Scaling Error[%]
C_{z_α}	5.60	5.58	5.58	0.33
C_{m_α}	-0.42	0.11	-0.42	0
C_{z_q}	-7.4	-6.1	-6.1	17.5
C_{m_q}	- 12.30	-11.80	-12.56	2.11
Scaling Factor (λ)	1	0.2	0.2	-
μ_c	88.39	61.00	60.10	32.10
$K_Y{}^2$	2.08	2.02	1.82	12.50
x_{CG} (w.r.t. fuselage nose) [m]	7.38*λ	7.10*λ	7.10*λ	3.79
DoS	1	0.64	0.86	-

1. The location of the CG position in both Case-Study 2 and 3 remained the same despite different DoS formulations.

2. The displacement of masses towards the CG coupled with the overall reduction in ballast masses reduced $K_Y{}^2$ from 2.02 (initial design) to 1.82 (optimized design) (see Table 10.5 for comparison with full-scale aircraft data)

3. Because of the reduction in he SFT model mass, μ_c value reduced slightly (61 to 60.1), which resulted in a 32% difference in the μ_c values of the optimized SFT model and the full-scale aircraft (see Table 10.5)

10.3.4. DISCUSSION: W&B SCALING

Based on the results of the W&B scaling optimization study, we answer the questions posed at the beginning of the study.

Implication of mass and inertia on the DoS: The optimization led to a SFT model whose positioning of COTS components and CG location was exactly the same as in case-study 2. Nevertheless, the DoS of optimized SFT model was lower than the optimized DoS obtained from Case-Study 2 because of the inclusion of mass and inertia parameters in the DoS formulation in case-study 3.

Due to the problem formulation chosen in this study, where, all the coefficients had equal degree of influence of 0.16, the optimizer deduced improved exploitation potential in enhancing similarity of aerodynamic derivatives as they contributed to 67% of the DoS formulation. Thus, the optimizer first tried to find an ideal CG location which matched the moment coefficients.

The inclusion of mass and inertia in the DoS formulation typically reduces the DoS of the SFT model (as compared to the case where mass and inertia are not included) because additional similarity requirements have to be satisfied by the optimized SFT model design. The effect of inclusion of mass and inertia in the DoS formulation for the short-period motion similarity is discussed in the following paragraphs.
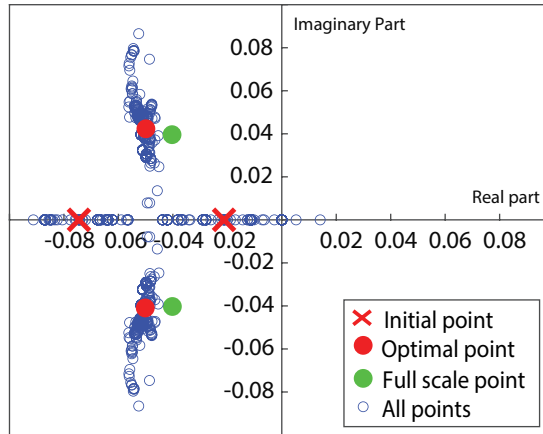
Figure 10.16: Short-period motion eigenvalues of key design points in weight and balance scaling optimization

Impact of including mass and inertia in the DoS on the Eigenvalues: The simplified equations of motion proposed by Nelson[169] are used to calculate the eigenvalues of
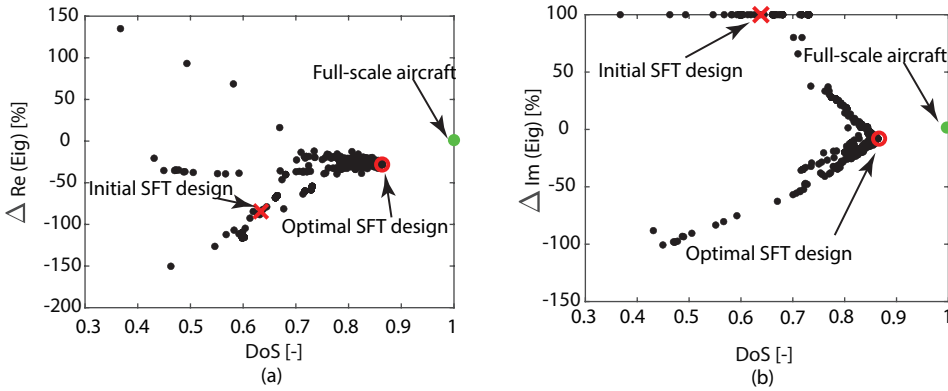
Figure 10.17: Percentage error of (a) real part and (b) imaginary part of short-period motion eigenvalues of key design points in the W&B scaling optimization performed using geometrically-scaled model

all the designs assessed in this optimization (see Figure 10.16). Like in Case-Study 2, the initial point has overdamped exponentially decaying motion whereas the full-scale aircraft and the optimized design have an underdamped exponentially decaying sinusoidal motion. Furthermore, when the virtual scaling errors (see Equation 6.20) are calculated for the real and the imaginary part of eigenvalues (see Figure 10.17), the initial scaling error is 90% and 100% for real and imaginary part respectively. After optimization, these scaling errors reduced to 29% and 8% respectively.

Since the DoS formulation for Case-study 2 and Case-study 3 are different, they cannot be compared directly. However, the constituents of the Behaviour Indicator Matrix (i.e., eigenvalues) can be compared as it quantifies the intrinsic behaviour of a SFT model and is not subject to change due to the DoS formulation. Clearly, the virtual scaling errors of optimized design in Case-study 3 (29% and 8%) are lower than the virtual scaling errors of optimized design in Case-study 2 (44% and 16%). Thus, the inclusion of mass and scaling parameters in the DoS improves the similarity between the optimized SFT model and the full-scale aircraft irrespective of the actual values of the DoS. As discussed in the previous case-studies, these results are only valid if all the assumptions made for the case-study hold true. Thus, in the following case-studies, the assumptions will be further reduced and appropriate analysis will be used improve the accuracy of SFT model similarity prediction.

10.3.5. NATURE OF MDAO BASED SIMILARITY MAXIMIZATION PROBLEM

To study the nature of MDAO based similarity maximization problem, a multi-start optimization was performed to check whether the obtained optima were local or global. In this study, the initial value of design variables 12-14 (see Table E.3) was set to 1.5 kg. All other details such as variables, assumptions, architecture and problem formulation are kept the same. The results of this optimization are shown in Figure 10.18. This optimization resulted in a SFT model that was different from the SFT model obtained from

previous study. The DoS of the design obtained with 1.5 kg starting ballast mass is 0.82, which is lower than the design obtained from optimization performed using 2.5 kg starting ballast masses.
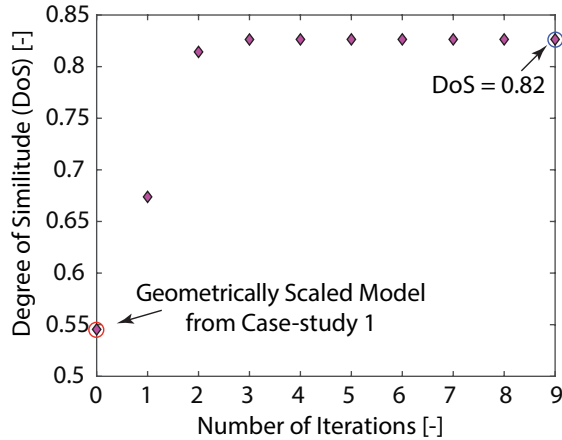
Figure 10.18: The results of weight and balance scaling optimization performed using MATLAB's 'fmincon' optimizer starting with geometrically-scaled model and each ballast mass weighing 1.5 kg, where 326 SFT models were designed and analyzed

Interestingly, the CG location and the aerodynamic derivatives remained the same as for 1.5 kg start point and 2.5 kg start point. The μ_c and K_Y^2 values of the 1.5 kg start point optimization are 51.09 and 1.98 respectively. The μ_c and K_Y^2 values of the optimized design are 54.3 and 2.09 respectively. Clearly, the virtual scaling errors are higher (compared to 2.5 kg starting point) which results in a lower DoS. Since multi-start optimization leads to different optimal designs, MDAO based similarity maximization problem is a multi-modal problem. This multi-start study was performed to understand the nature of the optimization problem. Since it is challenging and time-consuming to find a global optima, no attempts will be made to find the global optima in this dissertation.

10.4. CASE-STUDY 4: AERODYNAMICS - W&B SCALING

In this study, we perform MDAO based similitude maximization, where, the optimizer can modify the model flight condition (i.e., velocity and altitude), aerodynamic design (i.e., scaling factor, airfoil shape and wing location), structural design (i.e., floor location and size), ballast masses and the positioning of COTS equipment. This study aims to ascertain whether SFT model designs can be found that have better short-period motion similarity to full-scale aircraft than models obtained using single-discipline computational-scaling. Mathematically, the problem can be represented as follows:

maximize: DoS (see Equation 6.12)   (10.10)

where, $DoS = f(C_{Z_q}, C_{M_q}, C_{Z_\alpha}, C_{M_\alpha}, \mu_c, K_Y{}^2)$

(10.11)

and, w_i (tabulated in Section 10.4.1)   (10.12)

with respect to: Aero-W&B design variables (See Section 10.4.2)

subject to: Constraints (See Section 10.4.2)

where, all the coefficients remain the same as done in Case-Study 3.

To prevent excessive influence of the aerodynamic derivatives (4 parameters) on the DoS as compared to the mass and inertia derivatives (2 parameters) when equal degree of influence (w_i) is used, a systematic sensitivity analysis is performed to determine the degree of influence based on the quantitative impact of different parameters used in the DoS for short-period motion behaviour (see Section 10.4.1).

In this study, we perform an MDAO based similarity optimization starting from geometrically-scaled model of Cessna Citation II shown in Case-Study 1 to find a SFT model whose short period motion is similar to full-scale aircraft. The degree of influence used in the problem formulation, design variables, assumptions, constraints and study results are discussed in the following sections.

Research Question:

To what extent can the short-period motion similarity of SFT model be improved by performing multi-disciplinary computational-scaling (i.e., aerodynamics and weight & balance scaling together)?

10.4.1. Degree of Influence Parameters

As discussed in Chapter 6, the degree of influence (DoI) provides a rank-list of different similitude requirements to the DoS based on their relative importance in the phenomenon being tested. In order to rank the different similitude requirements for this case-study, sensitivity index (see Equation 6.15) as described in Section 6.2.4 is used.

Coefficients of full-scale aircraft shown in Table 10.5 are used to determine the real and imaginary part of the short-period motion eigenvalues. After this, each coefficient is varied by ±50% to determine the eigenvalues with perturbed coefficients to obtain D_{max} and D_{min} in Equation 6.15. These sensitivity indices are normalized to obtain the degree of influence as shown in Equations 10.13 and 10.14.

10

$$SI_{total} = \sum SI_i$$ (10.13)

where, i= 1...n (n = number of parameters in DoS formulation)

$$w_i = \frac{SI_i}{SI_{total}}$$ (10.14)

Table 10.6: Degree of Influence values for different parameters used in this Case-Study

Coefficients	Degree of Influence
C_{z_α}	0.0937
C_{m_α}	0.1489
C_{z_q}	0.0045
C_{m_q}	0.1721
μ_c	0.3847
$K_Y{}^2$	0.1962

Based on the calculations shown above, the DoI for the parameters used in the DoS formulation of this Case-Study are tabulated in Table 10.6. Contrary to the assumptions on the degree of influence in Case-study 3, the mass and inertia parameters have the largest influence (60%) on the short-period motion eigenvalues. The moment derivatives have 30% influence and the remaining parameters 10%. Thus, the optimizer should prioritize matching mass and inertia values over aerodynamic coefficients in this problem.

10.4.2. DESIGN VARIABLES, ASSUMPTIONS AND CONSTRAINTS

Design Variables: 48 design variables are used in this study. Of these, 28 pertain to aerodynamic design as shown in Figure 10.1. The initial values and the bounds for this study remain the same. 20 design variables are used for weight and balance scaling as shown in Figure 10.5 and 10.13.

Assumptions: Assumptions 1-8 explained in Case-Study 1 (Section 10.1.1) are applicable to this case-study too. However, additional analysis capabilities are added in this study as follows:

1. CG is calculated at every iteration of the optimization using physics based methods.

2. The mass and inertia is calculated for every design point using physics based method.

3. The degree of influence of different parameters is no longer considered equal for all parameters. The sensitivity index is used to calculate the degree of influence as discussed in Section 10.4.1.

4. Unlike Case-study 2 & 3, the aerodynamic design and the scaling factor is not fixed throughout the optimization and varies per iteration of the optimization process.

10

Constraints: The constraints for this case study remain the same as those for Case-Study 2.

10.4.3. OPTIMIZATION ARCHITECTURE AND ALGORITHM

Architecture: The architecture used for this optimization problem is shown in Figure G.3. Here, the aerodynamic analysis is performed for every iteration inside the optimization loop thereby changing the aerodynamic shape. This is in addition to the weight and balance optimization discussed in Case-Study 3.

Algorithm: The 'fmincon' algorithm provided by MATLAB was used with the optimizer settings shown in Section 10.1.

10.4.4. RESULTS

In this optimization, 286 SFT models were synthesized and assessed to identify the design with best short-period motion similarity. The optimization started with a DoS of 0.58 and ended at 0.84 as shown in Figure 10.19. Note, the DoS of optimization start point is lower than the start-point the DoS of Case-Study 3 because of use of sensitivity based degree of influence in this case study.
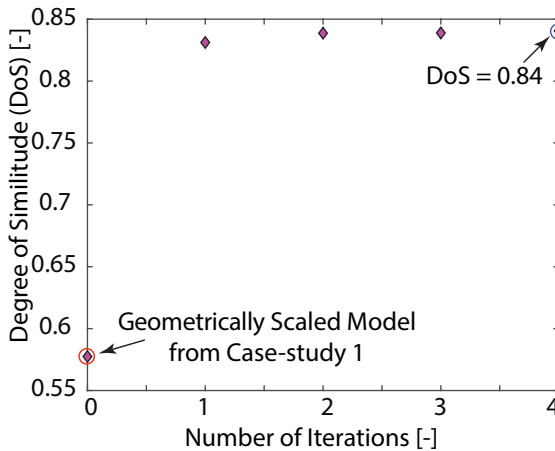
Figure 10.19: The results of aerodynamics - W&B scaling optimization performed using MATLAB's 'fmincon' optimizer starting with geometrically-scaled model, where 286 SFT models were designed and analyzed

10

The key changes to the initial design variables by the optimizer can be summarized as follows (see Figure 10.20 and 10.21 for detailed information):

1. The floor panels were moved closer to the nose of the fuselage and made larger in size. Since the ballast masses are a function of floor location, they also moved towards the nose of the fuselage (Figure 10.21)

2. The scaling factor of the model was reduced (Figure 10.20)

3. The wing (with its structural components and COTS equipment) was moved farther away from the nose of the fuselage (Figure 10.20)
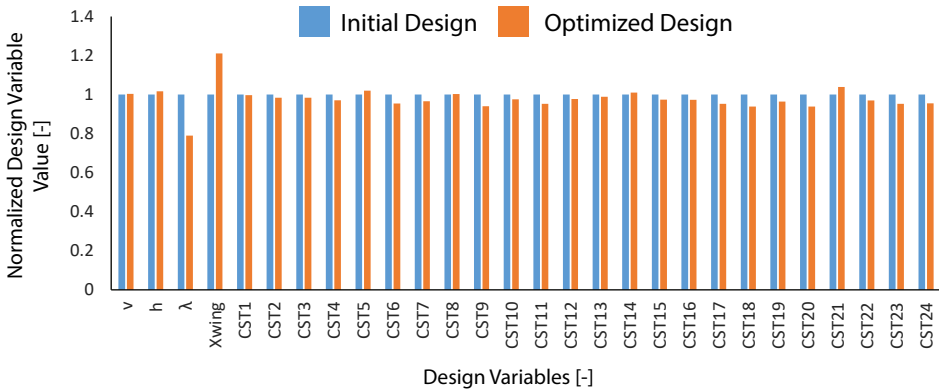
Figure 10.20: The variation of the design variables for the optimized SFT model with respect to the initial design (see Appendix F (Table F.4) for the values)
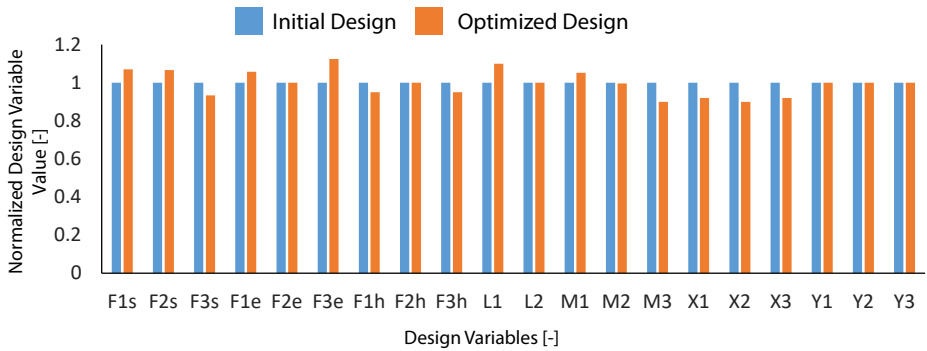
Figure 10.21: The variation of the design variables for the optimized SFT model with respect to the initial design (see Appendix F (Table F.5) for the values)

10

All other design variables remained almost similar to the initial values. The consequences of the changes in design variables on the overall SFT model performance is as follows:

1. The movement of the floor towards the fuselage nose is less than the movement of the wing away from the fuselage nose. As a result, the CG has moved back (w.r.t starting point of optimization) and coincides with the full-scale aircraft CG when scaled geometrically (see Table 10.7).

2. The rearward positioning of the main wing has increased the pitch down moment and improved the similitude of moment derivatives with full-scale aircraft

3. Although the scaling factor of the model is reduced, the ballast masses remain the same. As a result, the μ_c values increase (see Table 10.7) which reduces the virtual scaling error due to non-dimensional mass from 32% (at the start of the optimization) to 20% after optimization

4. Another impact of the reduced scaling factor is the reduction in the mean aerodynamic chord. This results in lower reduced frequency ($qc/2V$) when the velocity remains constant. Consequently, the value of C_{Z_q} increases as seen in Table 10.7

5. As the wing moves closer to the CG, the moment of inertia of the model reduces to 1.86 (from 2.02 at the starting point) thereby increasing inertia scaling error.

Table 10.7: Key performance indicators of the SFT model obtained from Aerodynamic-W&B scaling optimization

	Full-scale Aircraft	Initial Values	Optimized Values	Optimized Design Scaling Error[%]
C_{z_α}	5.60	5.58	5.55	0.89
C_{m_α}	-0.42	0.11	-0.39	7.14
C_{z_q}	-7.4	-6.1	-7.7	4.1
C_{m_q}	- 12.30	-11.80	-12.50	1.62
Scaling Factor (λ)	1	0.2	0.159	-
μ_c	88.39	61.00	106.11	20.04
$K_Y{}^2$	2.08	2.02	1.86	10.57
x_{CG} (w.r.t. fuselage nose)[m]	7.38*λ	7.10*λ	7.38*λ	0
DoS	1	0.58	0.84	-

10

10.4.5. Discussion: Aerodynamics - W&B scaling

With the sensitivity based quantification of degree of influence, the tendency of only improving aerodynamic coefficients is reduced. Furthermore, optimizer makes most effort in reducing the virtual scaling errors associated with mass and inertia parameters as they account for 60% influence on short-period motion.
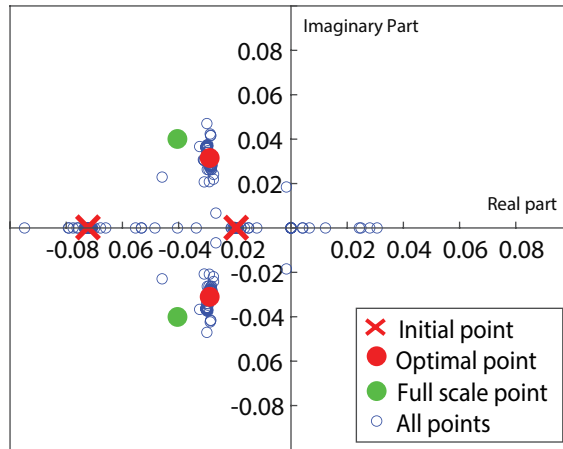
Figure 10.22: Short-period motion eigenvalues of key design points in the aerodynamic-W&B optimization

When the eigenvalues of different designs in the optimization are plotted using simplified equations of motion (see Figure 10.22), trends similar to the preceding case-studies are observed. The initial point has overdamped exponentially decaying motion whereas the full-scale aircraft and the optimized design have an underdamped exponentially decaying sinusoidal motion. Thus, the short-period motion of optimized SFT model is similar to that of full-scale aircraft.
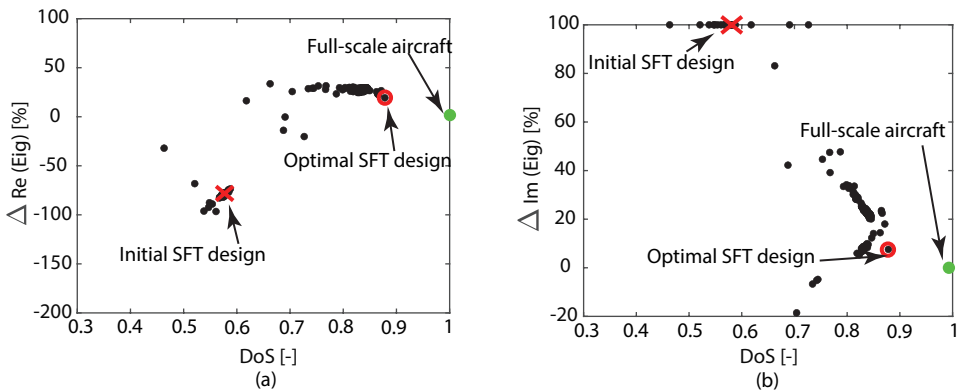
Figure 10.23: Percentage error of (a) real part and (b) imaginary part of short-period motion eigenvalues of key design points in the optimization

In addition, due to the combined effect of multidisciplinary scaling and the use of appropriate degree of influence, the eigenvalue virtual scaling errors of the SFT model are also lower than previous case-studies (see Figure 10.23). The real part has a scaling error of 19% and the imaginary part has a scaling error of 7%.

Thus, if all the assumptions made in this study are true, not only is the nature of the motion similar but the actual values of the damping and frequency of the short period motion are comparable to that of full-scale aircraft. However, in practice, the case-study assumptions introduce serious differences in the model and prototype behaviour. In particular, the constraints related to dynamic and static stability, trimmability of the SFT model, differences in trim conditions of SFT model and the full-scale aircraft, etc. can lead to severe limitations in achieving similar behaviour. The impact of including these constraints is discussed in the following case-study.

10.5. CASE-STUDY 5: AERODYNAMICS - W&B SCALING WITH FLIGHT MECHANICS constraints

The goal of this study is to identify a SFT model whose short-period motion is similar to that of full-scale Cessna Citation II 550 in realistic test condition. This involves the simulation of the flight dynamics behaviour to determine the trim condition, available control power and static and dynamic stability. Since the similitude requirements do not change, the mathematical description of the problem statement for this case study is as follows:

$$\text{maximize:} \qquad DoS \text{ (see Equation 6.12)} \qquad (10.15)$$
$$\text{where,} \qquad DoS = f(C_{Z_q}, C_{M_q}, C_{Z_\alpha}, C_{M_\alpha}, \mu_c, K_Y{}^2)$$
$$(10.16)$$
$$\text{and,} \qquad w_i \text{ (tabulated in Section 10.4.1)} \qquad (10.17)$$
$$\text{with respect to:} \qquad \text{Aero-W\&B design variables (See Section 10.5.1)}$$
$$\text{subject to:} \qquad \text{Constraints (See Section 10.5.1)}$$

where, all the coefficients remain the same as done in Case-Study 3.

In this study, we perform an MDAO based similarity optimization starting from geometrically-scaled model of Cessna Citation II shown in Case-Study 1 to find a SFT model whose short period motion is similar to the full-scale aircraft while including the flight dynamics constraints (details in Section 10.5.1).

Research Question:

> ***How is the similitude of a SFT model influenced by the inclusion of SFT flight mechanics constraints in SFT model design?***

10

10.5.1. DESIGN VARIABLES, ASSUMPTIONS AND CONSTRAINTS

Design Variables: 46 design variables are used in this study. Of these, 28 pertain to aerodynamic design as shown in Table E.1. 18 design variables are used for weight and balance scaling as shown in Tables E.2 and E.3. Design variables 10 and 11 in Table E.2, which indicate the landing gear locations, are left out as the optimizer does not change its position in any of the preceding case studies.

Assumptions: The assumptions 1-4 shown in Case-Study 1 are applicable to this study. Since flight dynamics analysis is performed at every iteration, the actual trim-conditions are evaluated for a given design. Thus, the remaining assumptions are not applicable here. This study comes closest to the simulation of physical SFT as all the flight mechanics requirements are incorporated in the determination of derivatives used in the DoS calculation.

Constraints: Two types of constraints are used in this optimization problem. In cases where the constraint violation analysis results in a Boolean result (i.e., whether the constraint is violated or not), penalty is added to objective function to account for non-compliance of a design. Penalty function is used to account for two main scenarios:

1. To check whether all the COTS equipment fit inside the outer mold line of the SFT model

2. To ascertain whether the SFT model can be trimmed for the given design and test condition. The trim algorithm within PHALANX in its current version (see Chapter 9) only provides a Boolean response (i.e., whether the model can be trimmed or not) and does not provide a figure of merit to estimate the extent of trim. Thus, when the SFT model cannot be trimmed a penalty is added to the DoS (***DoS = DoS - 10***) to indicate the lack of feasibility of the SFT model design.

In addition to the penalty function, the classical equality and inequality constraints are used to determine the static stability of the model. This is mathematically represented as follows:

Equality constraint:

$$\text{Lift} - \text{Weight} = 0 \tag{10.18}$$

Inequality constraint:

$$X_{CG} - X_{neutral-point} < 0 \tag{10.19}$$

The equality constraint shown in Equation 10.18, guarantees that the weight of the model is balanced by the lift forces generated by the aircraft. The inequality constraint shown in Equation 10.19 is used to assess the static stability of a given SFT model by verifying whether the neutral point is behind the center of gravity of the SFT model.

10.5.2. OPTIMIZATION ARCHITECTURE AND ALGORITHM
Architecture: The architecture used for this optimization problem is shown in Figure G.4. Here, the flight mechanics discipline is added to evaluate the static and dynamic stability, trim conditions and the available control power.

Algorithm: The 'fmincon' algorithm provided by MATLAB was used with the optimizer settings shown in Section 10.1.

10.5.3. Results

In this optimzation, 283 SFT models were designed and assessed to obtain a SFT model with most short-period motion similarity with full-scale aircraft. The optimization started at a DoS of 0.63 and ended with a DoS of 0.81 with four iterations. The results of the optimization per iteration are shown in Figure 10.24.
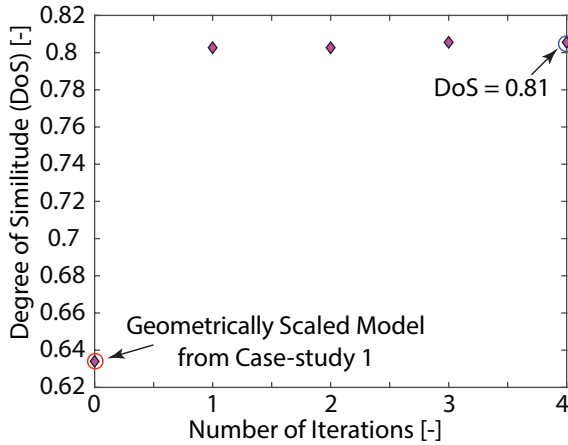
Figure 10.24: The results of aerodynamics - W&B scaling optimization with flight mechanics constraints performed using MATLAB's 'fmincon' optimizer starting with geometrically-scaled model, where 283 SFT models were designed and analyzed

Table 10.8: The trim condition at which different coefficients of DoS are calculated for full-scale aircraft, the initial geometrically scaled SFT model and the optimized SFT model

	Full-scale Aircraft	Initial Values	Optimized Values
$\delta_{elevator}$	3.16	5.12	4.19
$\delta_{aileron}$	-0.073	0.029	-0.79
δ_{rudder}	0	0	0
α	-0.02	-1.19	-1.5
β	0	0	0

The key addition in this study is the inclusion of flight dynamics analysis which is used to determine the trim condition and to assess the static and dynamic stability the available control power. For each SFT model design proposed by the optimizer, a detailed aerodynamic database, weight and balance parameters and the engine performance parameters are provided to PHALANX as input (discussed in Chapter 9). This information is used by PHALANX to determine the trim condition (i.e., the angle of attack,

side-slip angle and the control surface deflections). Since the testing for most phenomena only starts after the pilot is able to trim the model, the coefficients used to determine the DoS must also be evaluated at the trim condition. The trim conditions for the full-scale aircraft, the initial geometrically-scaled SFT model and the optimized SFT model are shown in Table 10.8.

Table 10.9: Key performance indicators of the SFT model obtained from Aerodynamic-W&B scaling optimization with flight mechanics constraints

	Full-scale Aircraft	Initial Values	Optimized Values	Optimized Design Scaling Error[%]
C_{z_α}	6.36	5.78	7.79	22.4
C_{m_α}	-1.91	0.35	-0.37	80.62
C_{z_q}	-11.41	-6.49	-11.35	0.52
C_{m_q}	-19.80	-14.19	-14.82	25.15
Scaling Factor (λ)	1	0.2	0.1735	-
μ_c	88.39	60.95	89.19	0.90
$K_Y{}^2$	2.08	2.19	2.03	2.4
x_{CG} (w.r.t. fuselage nose) [m]	7.38*λ	7.00*λ	6.97*λ	5.55
$x_{neutral-point}$ (w.r.t. fuselage nose) [m]	7.42*λ	6.85*λ	7.03*λ	5.25
DoS	1	0.63	0.81	-

The coefficients are calculated at the trim condition as shown in Table 10.9. The values of the optimized aerodynamic and weight & balance design variables are shown in Figure 10.25 and 10.26 respectively. The key changes made to the design variables by the optimizer can be summarized as follows (see Figure 10.27):

10

1. The ballast mass on Floor #1 is reduced from 2.5 kg to 2.06 kg

2. The ballast mass on Floor #2 was moved ahead by 45% of the floor length

3. The ballast mass on Floor #3 was moved ahead by 40% of the floor length

4. Floor #2 was shortened and moved ahead towards the nose of the fuselage

5. The scaling factor of the complete model was reduced from 20% to 17.3%
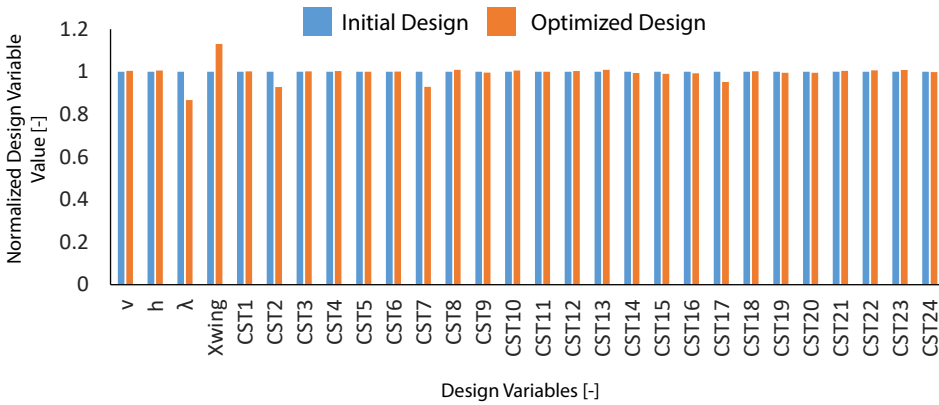
Figure 10.25: The variation of the design variables for the optimized SFT model with respect to the initial design (see Appendix F (Table F.6) for the values)
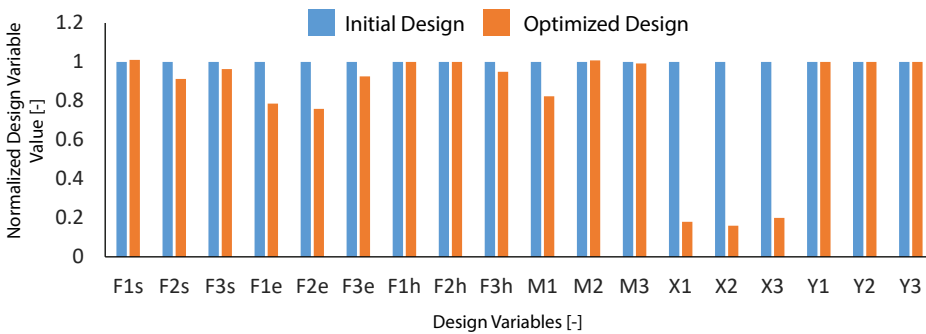
Figure 10.26: The variation of the design variables for the optimized SFT model with respect to the initial design (see Appendix F (Table F.7) for the values)

6. The wing was moved rearward by 13% of the fuselage length

 The consequence of these design changes on the non-dimensional coefficients and the DoS are summarized as follows (see Table 10.9 for the values of the coefficients):

1. The forward positioning of the ballast masses results in the forward center of gravity location

2. The rearward positioning of the wing with respect to the fuselage pushes the aerodynamic center rearward.

3. The combined effect of the above modifications results in a statically stable aircraft (which was unstable initially). Since statically stable SFT model was a strict

10
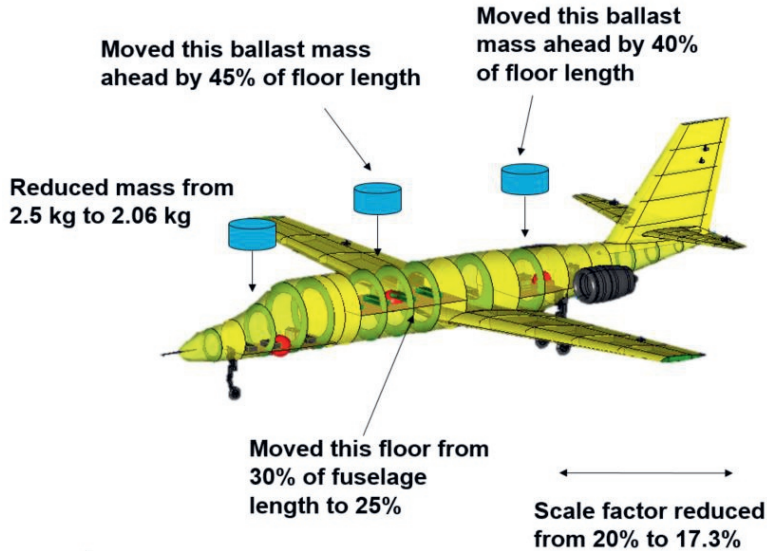
Figure 10.27: Summary of the key changes made by the optimizer to arrive at the optimal SFT model

requirement for this study, the initial design was non-compliant to flight mechanics requirement whereas the optimizer could identify a compliant SFT model design. This change in static stability can also be observed from the change in the C_{m_α} values shown in Table 10.9.

4. Although the scaling factor was reduced, the mass of the model largely remained constant. This increased the non-dimensional mass of the optimized SFT model (from 60.95 for initial design to 89.19 for optimized design) practically matching its non-dimensional mass with that of the full-scale aircraft.

5. The clustering of the floor panels and the ballast masses near the center of gravity location reduced the radius of gyration of the optimized SFT model thus making it similar to that of full-scale aircraft

6. The reduction of mass on Floor #1 reduces the moment arm due to the ballast mass and reduces the moment required from the horizontal tail

10

10.5.4. DISCUSSION: EFFECT OF FLIGHT MECHANICS CONSTRAINT ON SIMILITUDE

The goal of this study was to determine the impact of including flight mechanics constraints with aerodynamics and weight & balance similitude requirements on SFT model's short period motion similitude. Inclusion of flight mechanics constraints in the optimization process has three main implications as follows:

1. The 'Lift = Weight' constraint drives the optimizer to choose a smaller model (λ =

0.173) while keeping the weight intact because the lift generated by the model at
$\lambda = 0.2$ was greater than the weight of the model. The reduction in size reduces
the lift force generated by model while guaranteeing that the weight of the model
is balanced by the lift force. Furthermore, The use of dimensionless coefficients
at trim conditions (as against at $\alpha = 0$ & $\beta = 0$ done in previous studies) also af-
fects the aerodynamic coefficients. Consequently, the aerodynamic derivatives are
much more sensitive to changes in design variables in this study as compared to
preceding case studies.

2. The static stability constraint drives the center of gravity location of the SFT model
   forward for the optimal design (w.r.t initial design) and the neutral point backward.
   This is done by rearranging the locations of the main wing and the ballast masses
   in the model.

3. The weight and balance coefficients have higher degree of influence. Hence, opti-
   mizer chooses designs with similar weight and balance coefficients (μ_c and $K_Y{}^2$)
   to full-scale aircraft. In addition, the inclusion of trim analysis and flight mechan-
   ics constraints improves the weight & balance similitude as compared to the op-
   timization performed without flight mechanics constraints (see Case Study 4 for
   comparison).

In order to assess the effect of optimizer design decisions on short period motion of
the SFT model, the eigenvalues of key design points in the optimization are plotted in
Figure 10.28. The initial geometrically-scaled model showed overdamped exponentially
decaying motion whereas the full-scale aircraft demonstrated an underdamped expo-
nentially decaying sinusoidal motion. Thus, the initial design's short period motion was
dissimilar to that of full scale aircraft. After optimization, the final design showed under-
damped exponentially decaying sinusoidal motion like the full-scale aircraft as shown
in Figure 10.28. It is important to note that the eigenvalues plotted in Figure 10.28 are
based on flight mechanics analysis performed by PHALANX as discussed in Section 9.4
unlike the use of simplified equations of motion in the preceding case-studies.

The virtual scaling error of the real and imaginary part of the eigenvalues are also
computed and plotted in Figure 10.29. The real part of initial design point has an error
of 554% whereas the final design point is off by 112%. The imaginary part of the initial
design has an error of 100% (as it has no imaginary part) and the optimized design has
an error of 25%. The key reason for the large virtual scaling error is due to the differences
in aerodynamic moment coefficients (see Table 10.9). The aerodynamic moment coeffi-
cients are different due to the different trim conditions of the initial and optimized SFT
model as compared to the trim conditions of the full-scale aircraft (see Table 10.8).

Although the virtual scaling error of the real part of the eigenvalues is high in the op-
timized SFT model design (112%) in absolute numbers, the behaviour of the optimized
design is similar to the full-scale aircraft. Furthermore, the optimizer is able to find a fea-
sible (statically stable) design point starting from an infeasible design point (which was
not assessed in the preceding case-studies). The optimized design can be used to per-
form SFT and the results of the SFT can be used to validate the computational methods
used in this study.
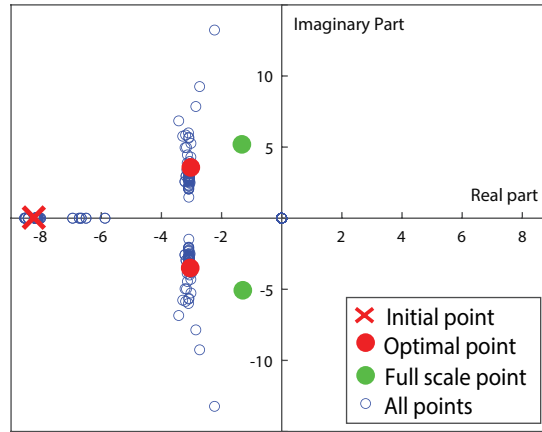
Figure 10.28: Short-period motion eigenvalues of key design points in the aerodynamic-W&B optimization with flight mechanics constraints
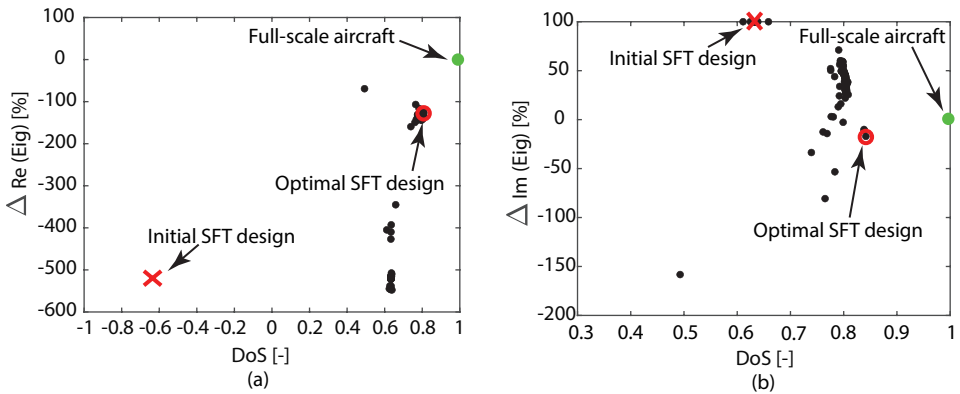
Figure 10.29: Percentage error of (a) real part and (b) imaginary part of short-period motion eigenvalues of key design points in the optimization

10

The results of this study come closest to the simulation of the reality as a detailed flight mechanics analysis is performed in this study which was absent in preceding studies. The results of this study also clarify that the consideration of flight mechanics analysis, particularly the trim analysis, is very important for the determination of the DoS because every design can have a different trim condition. Consequently, the constituent aerodynamic coefficients of the DoS are (significantly) different at every design point.

10.6. Case-Study 6: Aerodynamic - W&B scaling with Flight Mechanics constraints for Short Period and Roll Damping Motion

In all the preceding studies, optimization was performed to test only one phenomenon (i.e., short period motion). However, as discussed in Chapter 4, designing, manufacturing and testing only one model per phenomenon has an undesirable consequence of significantly driving up the cost of SFT. Thus, designing a SFT model which can be used to study multiple aspects of full-scale aircraft can be beneficial. In this study, MDAO based similarity maximization is used to identify a SFT model whose short-period motion and roll damping behaviour is similar to that of full-scale Cessna Citation II 550 in realistic test condition. These two motions are chosen because the parameters affecting the two motions are independent of one another. The mathematical description of the problem statement for this case study is as follows:

$$\text{maximize:} \qquad DoS \text{ (see Equation 6.12)} \qquad (10.20)$$

$$\text{where,} \qquad DoS = f(C_{Z_q}, C_{M_q}, C_{Z_\alpha}, C_{M_\alpha}, \mu_c, K_Y{}^2, C_{L_P}, \mu_b, K_X{}^2) \qquad (10.21)$$

$$\text{and,} \qquad w_i \text{ (Table 10.10)} \qquad (10.22)$$

$$\text{with respect to:} \qquad \text{Design variables (Section 10.6.1)}$$

$$\text{subject to:} \qquad \text{Constraints (Section 10.6.1)}$$

where, C_{L_P} is rate of change of moment about x-axis w.r.t roll rate, μ_b is non - dimensional mass using aircraft span, and $K_X{}^2$ is the radius of gyration about x-axis. All other coefficients remain the same as in Case-Study 3. The degree of influence of the different coefficients used in the DoS formulation is shown in Table 10.10. Here, the degree of influence for each phenomenon is calculated individually using the sensitivity index (see Equation 6.15). Thereafter, the DoIs of all the coefficients are multiplied by 0.5 to ensure that the equal weightage is provided to roll-damping and short-period motion coefficients.

In this study, we perform an MDAO based similarity optimization starting from geometrically scaled model of Cessna Citation II shown in Case-Study 1 to find a SFT model whose short period motion and roll damping behaviour have maximum similarity to full-scale aircraft while including the flight dynamics constraints (details in Section 10.6.1).

10

Research Question:

> *How is the similarity of SFT model affected when one model is used to simulate multiple aspects (phenomena) of full-scale aircraft behaviour?*

10.6.1. Design Variables, Assumptions and Constraints
Design Variables: 47 design variables are used in this study. the first 46 design variables remain the same as discussed in Case-Study 5. However, all those design variables

Table 10.10: Degree of Influence values for different parameters used in this Case-Study

Coefficients	Degree of Influence
C_{z_α}	0.04685
C_{m_α}	0.07445
C_{z_q}	0.00225
C_{m_q}	0.08605
μ_c	0.19235
$K_Y{}^2$	0.0981
C_{L_p}	0.15
μ_b	0.2
$K_X{}^2$	0.15

mainly influence the short-period motion and not roll damping. Typically wing dimensions affect the roll damping characteristics [205].

Thus, an additional design variable, the ***wing scaling factor (λ_{wing})***, is introduced that influences the roll damping motion. This variable allows the scaling of the wing independently from the scaling factor of the SFT model (λ) thereby changing the relative dimensions of the wing and model (see Table E.4 for intial values and bounds).

Assumptions: The assumptions used in this study remain the same as discussed in Section 10.5.1.

Constraints: The constraints used in this study remain the same as discussed in Section 10.5.1.

10.6.2. OPTIMIZATION ARCHITECTURE AND ALGORITHM
The optimization algorithm and the architecture remain the same as shown in Case-study 5.

10.6.3. RESULTS
A total of 513 SFT models were designed in this study. The optimization process started with the geometrically-scaled model shown in Case-Study 1 whose DoS is 0.64 and the final optimized design has a DoS of 0.89 (see Figure 10.30). As discussed in Case-Study

5, the DoS was calculated at the trim condition as the pilot generally starts the test af-
ter trimming the model. The trim conditions of the full-scale aircraft, the initial design
and the optimized design and the dimensionless coefficients at the trim condition are
tabulated in Tables 10.11 and 10.12 respectively.
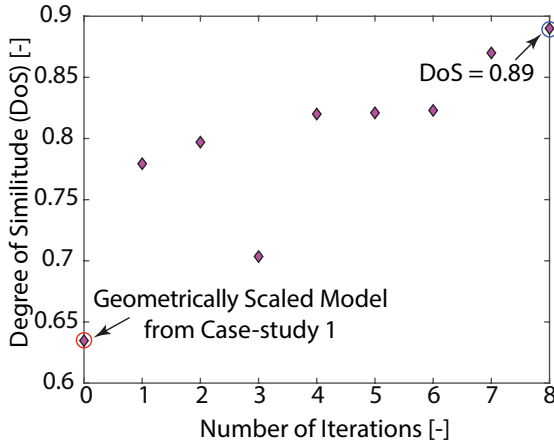
Figure 10.30: The results of aerodynamics - W&B scaling optimization with flight mechanics con-
straints performed using MATLAB's 'fmincon' optimizer starting with geometrically-scaled model,
where 513 SFT models were designed and analyzed

Table 10.11: The trim condition at which different coefficients of DoS are calculated for full-scale
aircraft, the initial geometrically scaled SFT model and the optimized SFT model

	Full-scale Aircraft	Initial Values	Optimized Values
$\delta_{elevator}$	3.16	5.12	1.36
$\delta_{aileron}$	-0.073	0.029	-0.001
δ_{rudder}	0	0	0
α	-0.02	-1.19	-0.233
β	0	0	0

10

The values of the optimized design variables are shown in Figure 10.32 (Aerodynamic
design variables) and 10.33 (Weight & balance design variables). The key changes made
by the optimizer can be summarized as follows (see Figure 10.31):

1. The ballast masses were moved closer to the nose of the fuselage (by 40% of floor
   length for mass #1, 43% of floor length for mass #2 and 40% of floor length for mass
   #3)

Table 10.12: Key performance indicators of the SFT model obtained from Aerodynamic-W&B scaling optimization

	Full-scale Aircraft	Initial Values	Optimized Values	Optimized Design Scaling Error[%]
C_{z_α}	6.36	5.78	5.67	10.84
C_{m_α}	-1.91	0.35	-1.71	10.47
C_{z_q}	-11.41	-6.49	-10.26	10.07
C_{m_q}	-19.80	-14.19	-16.07	18.83
C_{l_p}	-5.10	-4.53	-4.68	8.23
Scaling Factor (λ)	1	0.2	0.165	-
μ_c	88.39	60.95	89.19	0.90
μ_b	11.36	7.87	12.4	9.15
$K_Y{}^2$	2.08	2.19	2.03	2.41
$K_X{}^2$	0.012	0.013	0.0104	13.34
x_{CG} [m] (w.r.t. fuselage nose)	7.38*λ	7.00*λ	6.77*λ	8.26
$x_{neutral-point}$ (w.r.t. fuselage nose) [m]	7.42*λ	6.85*λ	7.39*λ	0.40
DoS	1	0.64	0.89	-

10

2. The ballast mass on Floor #1 was reduced to 2.13 kg (from 2.5 kg)

3. Scaling factor of the optimized model was lowered to 16.5% (from 20%)

4. Since the wing is scaled independently of the aircraft, the wing scaling factor of the optimized SFT model was lowered to 16.2% (from 20%). Interestingly, the size of the wing is scaled down commensurately with the scale of the aircraft although the scaling factor of the wing and the aircraft are independently controlled by the
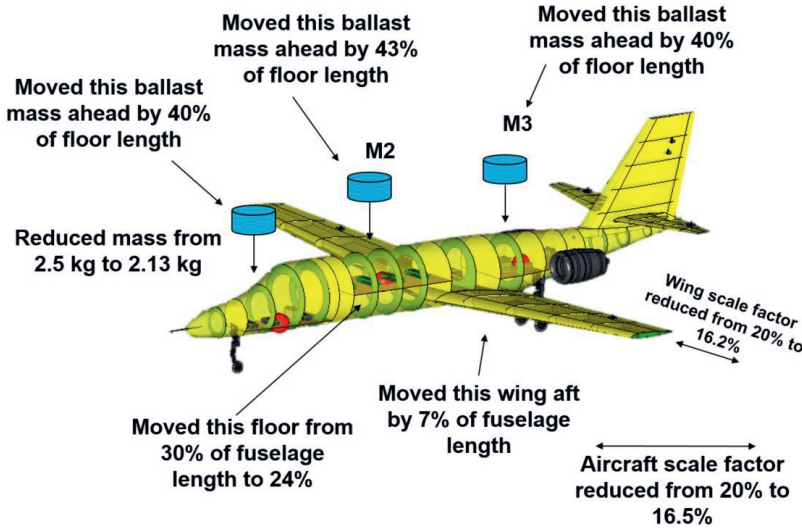
Figure 10.31: Summary of the key changes made by the optimizer to arrive at the optimal SFT model
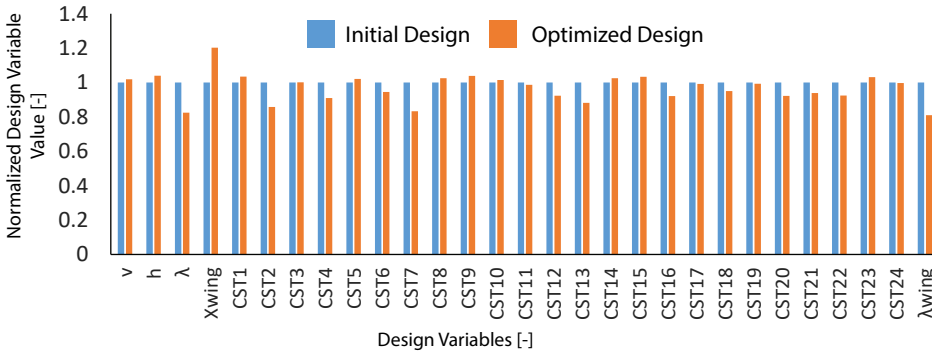
Figure 10.32: The variation of the design variables for the optimized SFT model with respect to the initial design (see Appendix F (Table F.8) for the values)

optimizer

5. Floor #2 was moved closer to the nose of the fuselage which helps in moving the center of gravity forward

The changes made by the optimizer in this case study have similar impact on the non-dimensional coefficients and the DoS as observed in the previous study. The center of gravity of the model was moved forward and the aerodynamic center of the model was moved rearward (see Table 10.12). Consequently, the optimized SFT model design is statically stable (initial design is statically unstable).

10
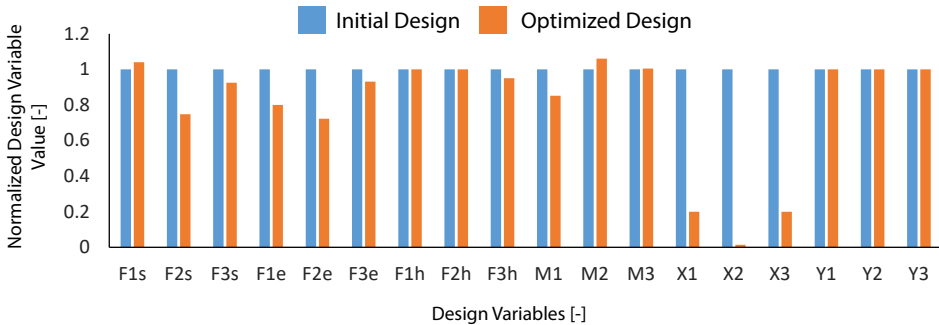
Figure 10.33: The variation of the design variables for the optimized SFT model with respect to the initial design (see Appendix F (Table F.9) for the values)

The additional impact on the coefficients was observed due to the scaling of wing independently of the aircraft scaling, which increased the C_{l_p} and μ_b (non-dimensional mass normalised using model span) and reduced the radius of gyration about X-axis. The optimizer reduced wing scaling factor a little more than the aircraft scaling factor because the lift forces produced by the main wing of the geometrically-scaled SFT model (initial design) required large elevator control surface deflection that reduced the available control power and made model trimming challenging (see Table 10.11).

10.6.4. DISCUSSION: ONE MODEL TO TEST MULTIPLE PHENOMENA

The goal of this study was to determine whether the proposed computational-scaling approach can be used to study multiple phenomena using one SFT model without significantly compromising the similitude between the SFT model and the full-scale aircraft. Two flight dynamics phenomena, namely short-period motion and roll damping were chosen for this study.

Since the eigenvalues of the two phenomena are the behavioural indicators of similitude, the eigenvalues of short-period motion and roll damping of key design points in the optimization are plotted in Figure 10.34 and 10.35 respectively.

For short-period motion, the initial geometrically-scaled model showed overdamped exponentially decaying motion whereas the full-scale aircraft and the optimized SFT model demonstrated an underdamped exponentially decaying sinusoidal motion. Thus, through the course of the optimization, similarity of behaviour was obtained. Furthermore, when the virtual scaling errors were assessed (see Figure 10.36) for short period motion, both the real and imaginary part showed an error of 34% and 37% respectively. This virtual scaling error is lower than for the design obtained in Case-Study 5 where the SFT model design was specifically optimized for short-period motion.

The key difference between Case-Study 5 and 6 is the inclusion of an addition wing scaling factor (λ_{wing}) design variable. Although λ_{wing} was included to alter the roll behaviour, its beneficial impact could be observed in short-period motion behaviour of the optimized design. The reduction in wing-size reduced the lift force generated by the wing, consequently reducing the balancing force from the horizontal tail. This change
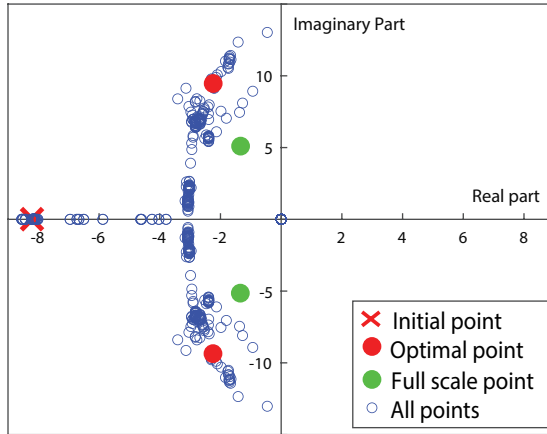
Figure 10.34: Short-period motion eigenvalues of key design points in the aerodynamic-W&B optimization with flight mechanics constraints
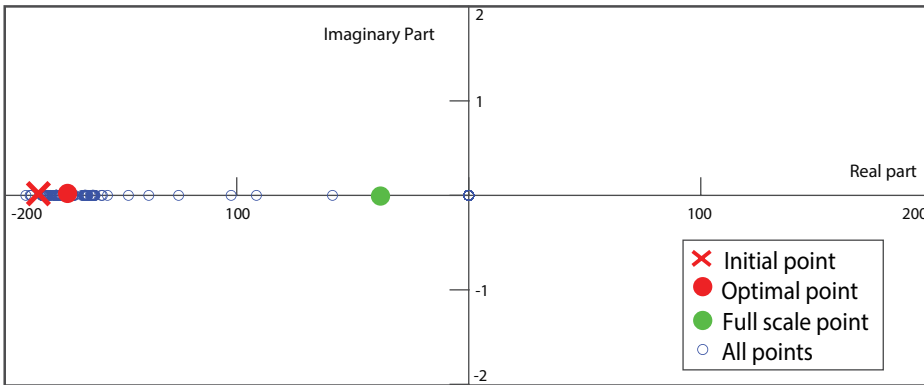
Figure 10.35: Roll-damping eigenvalues of key design points in the aerodynamic-W&B optimization with flight mechanics constraints

improved the similitude of aerodynamic lift and moment coefficients of the optimized SFT model of Case-Study 6 with full-scale aircraft as compared to the optimized SFT model obtained in Case-Study 5 (see Tables 10.9 and 10.12 for details).

As for roll-damping, the initial design, the optimized design and the full-scale aircraft have similarity of behaviour. Although the optimized design showed better similarity to full-scale aircraft as compared to initial design, the virtual scaling error for both the initial design (365%) and the optimized design (334%) was quite high. The key reason for high virtual scaling error can be attributed to insufficient number of design variables that could alter the weight and balance properties in lateral direction (such as ballast masses on the wing, engine positioning, batteries on the wing, etc.). Nevertheless, the initial
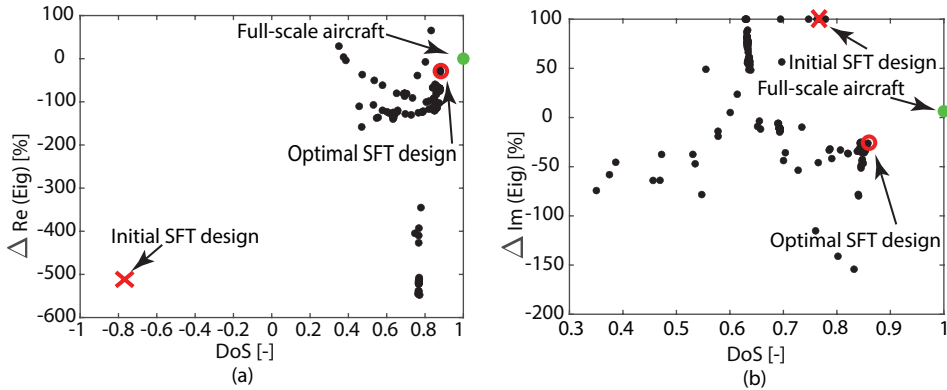
Figure 10.36: Percentage error of (a) real part and (b) imaginary part of short-period motion eigen-values of key design points in the optimization

results for this study indicates that the roll damping behaviour can be further improved by increasing the relevant design variables in the optimization. However, the detailed investigation with increased number of design variables and its impact of roll damping behaviour is beyond the scope of this dissertation.

Based on the results of this study, it appears that multiple independent phenomena can be tested using one SFT model. However, the design variables must be carefully selected to offer sufficient freedom to the optimizer to find a SFT model design whose behaviour is similar to full-scale aircraft for all the phenomena being tested.

10.7. CASE-STUDY 7: AERODYNAMIC AND W&B SCALING WITH FLIGHT MECHANICS CONSTRAINTS FOR SHORT PERIOD MOTION OF AN UNCONVENTIONAL AIRCRAFT

10

The goal of this study is to demonstrate the application of the MDAO based similarity maximization approach for unconventional designs. In this study, a SFT model of a box-wing aircraft configuration is designed to mimic its short-period motion behaviour. The key dimensions of the full-scale aircraft used in this study are shown in Figure 10.37

Since the similitude requirements do not change, the mathematical description of the problem statement for this case study is as follows:
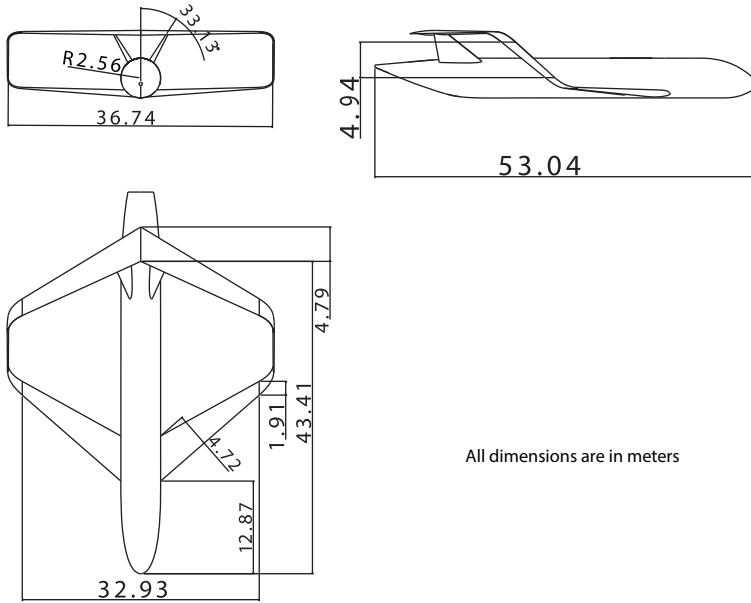
Figure 10.37: Key dimensions of the unconventional box-wing aircraft configuration used in this study

$$\text{maximize:} \qquad DoS \text{ (see Equation 6.12)} \qquad (10.23)$$

$$\text{where,} \qquad DoS = f(C_{Z_q}, C_{M_q}, C_{Z_\alpha}, C_{M_\alpha}, \mu_c, K_Y^2) \qquad (10.24)$$

$$\text{and,} \qquad w_i \text{ (tabulated in Section 10.4.1)} \qquad (10.25)$$

with respect to: Aero-W&B design variables (See Section 10.7.1)

subject to: Constraints (See Section 10.7.1)

All coefficients remain the same as in Case-Study 3. The degree of influence of the different coefficients used in the DoS formulation remain the same as shown in Table 10.6. Here, we perform an MDAO based similarity optimization starting from 5.6% geometrically-scaled model of a box-wing aircraft to find a SFT model whose short period motion behaviour has the maximum similarity to full-scale aircraft while including the flight dynamics constraints (details in Section 10.7.1). 5.6% geometrically-scaled model is chosen because it results in a span of 2 m and mass of 23 kg which is in the typical size and weight of the model generally used for SFT.

Research Question:

Can the proposed MDAO based similarity maximization approach be used to

augment similitude of SFT model for unconventional aircraft designs?

10.7.1. DESIGN VARIABLES, ASSUMPTIONS AND CONSTRAINTS

Design Variables: 25 design variables are used in this study. Of these, 7 design variables influence the aerodynamic design as shown in Figure 10.38. The CST coefficients used in the preceding studies are not used in this study as the airfoil shape did not have a significant impact on the short-period motion behaviour of the SFT model. Instead, airfoil thicknesses are used to limit the number of design variables while still allowing the optimizer to alter the force and moment coefficients used in the DoS formulation. The weight and balance design variables remain the same as used in Case-Study 5. However, their initial values and bounds were modified (see Appendix E (Table E.6)).
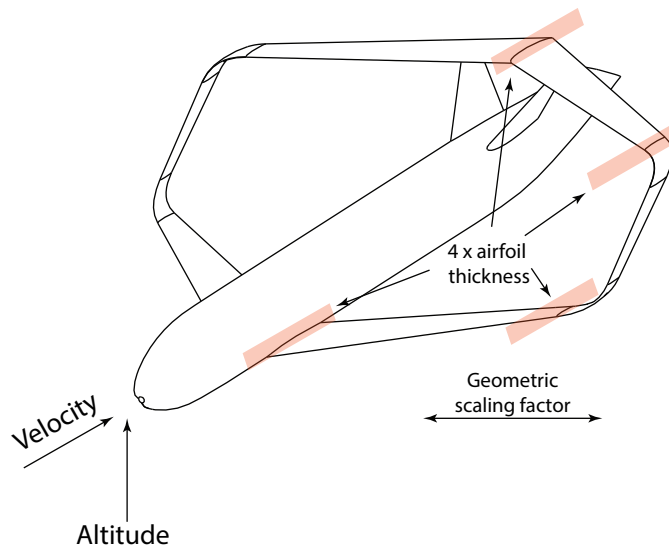
Figure 10.38: Schematic of design variables used in this study that influence the aerodynamic behaviour (consequently flight dynamics) of SFT model (see Appendix E (Table E.5 for initial values and bounds)

10

10.7.2. OPTIMIZATION ARCHITECTURE AND ALGORITHM

The optimization algorithm and architecture used in this study remains the same as used in Case-Study 5 as the problem formulation and the underlying disciplines remain the same. Only airfoil thicknesses are used instead on CST coefficients.

10.7.3. RESULTS

A total of 464 designs were investigated in this optimization study. The initial geometrically-scaled model had a DoS of 0.66 and the optimized SFT model of the box-wing aircraft has a DoS of 0.87 (see Figure 10.39). The trim condition of the full-scale aircraft, the

initial model and the optimized SFT model design are shown in Table 10.13. The non-dimensional coefficients used for the DoS calculation are shown in Table 10.14.
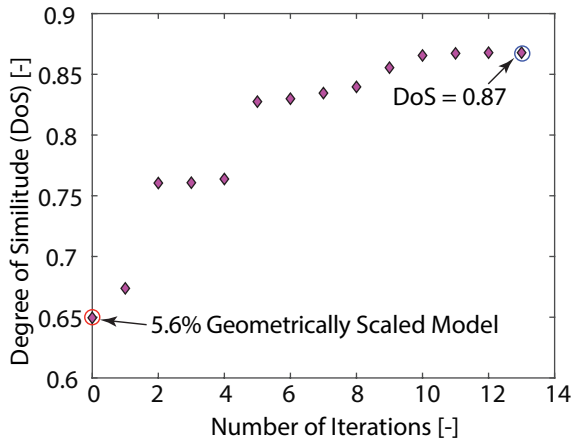
Figure 10.39: The results of aerodynamics - W&B scaling optimization with flight mechanics constraints performed using MATLAB's 'fmincon' optimizer starting with geometrically-scaled model, where 464 SFT models were designed and analyzed

Table 10.13: The trim condition at which different coefficients of DoS are calculated for full-scale aircraft, the initial geometrically scaled SFT model and the optimized SFT model

	Full-scale Aircraft	Initial Values	Optimized Values
$\delta_{elevator}$ x 4 (2 on front wing & 2 on rear wing)	-3.56	3.23	4.39
δ_{rudder}	0	0	0
α	0.87	-5.06	-3.19
β	0	0	0

In order to trim the model and to obtain an optimized DoS, following changes were made to the SFT model design by the optimizer (see Figure 10.40 and 10.41):

1. The scaling factor of the aircraft is reduced from 5.6% to 4%

2. Thickness of the root airfoil is increased by 25%

3. The ballast mass in Floor #1 is reduced from 3 kg to 2.29 kg. All other ballast masses are reduced to zero.

4. Floor #1 is moved rearwards closer to the center of gravity by 12% of fuselage length

10

Table 10.14: Key performance indicators of the SFT model obtained from Aerodynamic-W&B scaling optimization

	Full-scale Aircraft	Initial Values	Optimized Values	Optimized Design Scaling Error[%]
C_{z_α}	4.70	4.02	4.04	14.04
C_{m_α}	-4.46	-4.77	-4.49	0.67
C_{z_q}	-15.67	-14.16	-14.17	9.57
C_{m_q}	-91.41	-77.56	-78.67	13.93
Scaling Factor (λ)	1	0.056	0.04	-
μ_c	220.14	91.61	182.10	17.32
$K_Y{}^2$	5.70	7.89	6.52	14.38
x_{CG} [m] (w.r.t. fuselage nose)	22.48*λ	22.67*λ	22.75*λ	1.20
$x_{neutral-point}$ (w.r.t. fuselage nose)	27.39*λ	27.37*λ	27.53*λ	0.51
DoS	1	0.66	0.87	-

All other aerodynamics and weight & balance variables remain largely constant throughout the optimization. The key consequence of the changes to the design variables can be summarized as follows:

1. The reduction in the scaling factor lowered the model radius of gyration and increased the non-dimensional mass as all the COTS equipment remained the same while the model size decreased.

2. The CG location and the neutral point of the full-scale aircraft, the geometrically-scaled model and the optimized SFT model were statically stable and did not change much throughout the optimization.

3. The rearward positioning of Floor #1 further helps in reducing the radius of gyration.

10
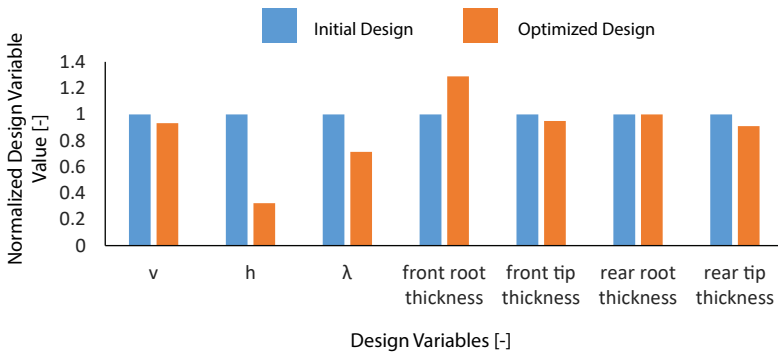
Figure 10.40: The variation of the design variables for the optimized SFT model with respect to the initial design (see Appendix F (Table F.10) for the values)
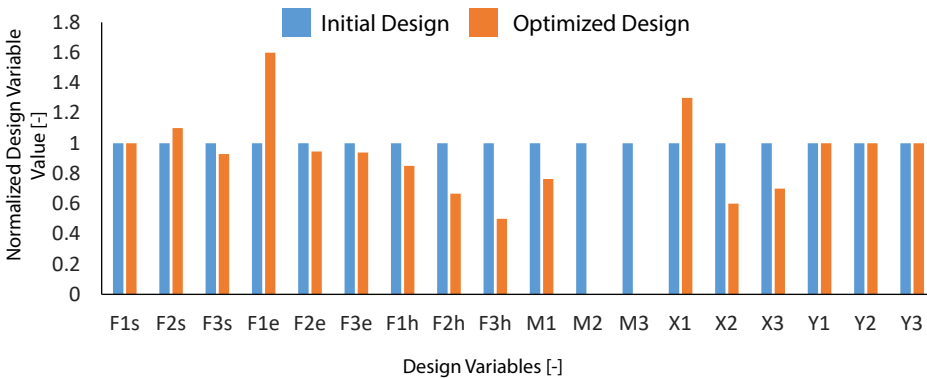
Figure 10.41: The variation of the design variables for the optimized SFT model with respect to the initial design (see Appendix F (Table F.11) for the values)

10.7.4. DISCUSSION: DESIGNING UNCONVENTIONAL AIRCRAFT SFT MODELS

The study results demonstrate that MDAO based similarity maximization can significantly improve the DoS of unconventional aircraft. To verify whether the improvement in the DoS translates into improved similitude, the short-period behavioural indicators (i.e., eigenvalues) are plotted in Figure 10.42. The full-scale aircraft, the initial geometrically-scaled model and the optimized SFT model demonstrate an under-damped exponentially decaying sinusoidal motion. Thus, the initial and optimized SFT models have similar short-period motion behaviour of the full-scale aircraft.

Furthermore, to determine the improvements from the optimization process, the virtual scaling errors of the real and imaginary part of the eigenvalues are plotted in Figure 10.43. A significant improvement can be seen in the real part of the optimized design as compared to the initial design (improvement of 300%). Whereas the virtual scaling er-
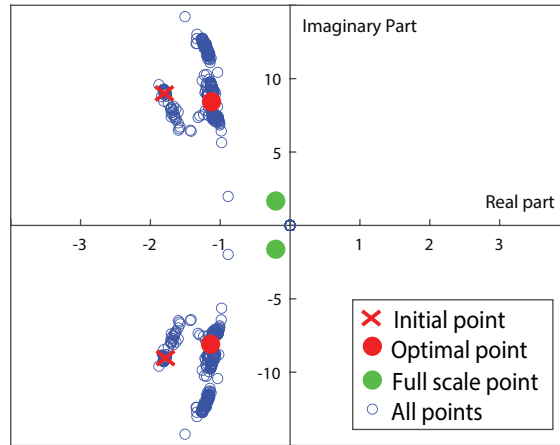
Figure 10.42: Short-period motion eigenvalues of key design points in the aerodynamic-W&B optimization with flight mechanics constraints

ror of the imaginary part remains constant for the initial and the optimized design. This can be explained by the greater influence of aerodynamic coefficients on imaginary part which does not change significantly throughout the optimization. Whereas the real part is influenced by weight & balance parameters that change considerably throughout the optimization (see Table 10.14).
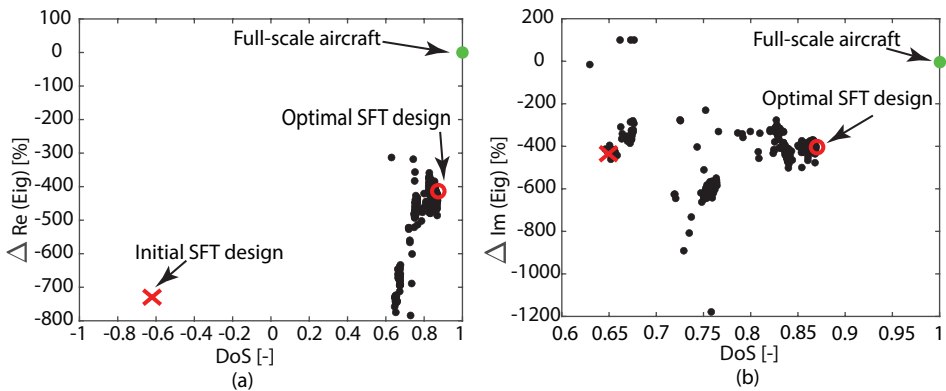
Figure 10.43: Percentage error of (a) real part and (b) imaginary part of short-period motion eigenvalues of key design points in the optimization

The higher virtual scaling error of the box-wing aircraft compared to preceding studies using Cessna Citation II can be attributed to larger difference in the size and weight of the full-scale aircraft and the SFT model in the case of box-wing aircraft. In addition, the starting point chosen for this optimization (i.e., 5.6% scaled model) could have forced the optimizer into local optima.

Moreover, the scaling factor of the optimal design is at the bounds of the design variable (see Tables E.5 and F.10). Typically, when the bounds are reached, another optimization must be performed with relaxed bounds to see the progress of optimization. Since the goal of this study to demonstrate the applicability of the proposed method to unconventional aircraft SFT model design was fulfilled, further detailed studies are not continued in this dissertation. However, detailed studies with larger bounds of optimization and more design variables relevant to the phenomenon being tested must be performed before e manufacturing the box-wing SFT model.

10.8. LESSONS LEARNT FROM THE CASE-STUDIES

A number of case-studies with increasing complexity (i.e., more disciplinary analyses and constraints) were performed in this chapter. In this section, we summarize the key lessons learnt from these case studies that are applicable to future MDAO based similarity maximization problems as follows:

1. For all case-studies, the use of MDAO based similarity maximization helped in identifying designs with improved similarity as compared to geometrically-scaled initial point. Thus, for correctly formulated problem, **computationally-scaled models consistently performed better than purely geometrically-scaled models**.

2. For a given test, a higher DoS implies lower virtual scaling error and therefore better similarity with full-scale aircraft.

3. The nature of the design space in MDAO similarity maximization problem is multimodal. Thus, the starting values of the design variables has a significant impact on the optimal design that can be identified by the optimizer.

4. The similarity obtained from the DoS is sensitive to the disciplinary analysis and constraints and is only valid for specific test condition(s) included in the problem formulation and not a general purpose solution.

5. Of all the studies, the inclusion of trim constraints significantly affected the DoS and the behavioural indicator matrix. Thus, similitude obtained from methods that do not include flight mechanics constraints might lead to errors in realistic SFT conditions.

6. The proposed method is configuration agnostic and shows promise in the design of SFT model for varied phenomena.

7. Based on the preliminary results of Case-Study 6, MDAO based similitude maximization approach can help in developing one SFT model that could be used to study multiple phenomena thereby reducing the size of the catalog of SFT model designs necessary to study the full-scale aircraft behaviour.

10

IV

CONCLUSIONS

11

CONCLUSIONS AND RECOMMENDATIONS

In this dissertation, Sub-scale Flight Testing (SFT) has been discussed in parallel to other testing techniques such as computational simulation and ground based testing methods such as wind tunnel testing. SFT is often viewed as a competitor to the ground-based testing methods. However, this apprehension is not well-founded as SFT is only utilized in those dynamic test cases where the ground-based testing infrastructure cannot adequately recreate the flight-conditions necessary to replicate the prototype behaviour.

Furthermore, due to the improvements and availability of miniature electronics and components, SFT can be used in all types of tests (demonstrator, phenomenological and simulation tests). This is not always possible with other ground-based testing methods or computer simulation. Majority of the SFTs addressed in the literature are used as concept demonstrators (52%) as they adequately arouse the interest of the scientific community and industry without requiring a cumbersome design approach to establish similitude with the prototype. So far, less than 30% of the total tests used in the literature actually simulate prototype behaviour.

The author believes that using SFT models for the sole purpose of demonstration is a major under-utilization of SFT's potential. Emphasis on simulation and phenomenological tests will not only enhance confidence on unconventional configurations but also reduce development cost and lead times, thereby making SFT a viable and attractive testing method in early stages of design. To this end, the **methodology proposed in this dissertation for maximizing the sub-scaled model similarity** provides an answer to the most urgent challenge that must be overcome to make SFT a powerful assessment method for aircraft designs.

The evolution and developments in SFT model design approaches brings to light three main methods, namely, (1) classical similitude theory, (2) similitude theory with governing equations and approximation theory, and (3) computational similitude theory. The survey of past SFTs reveals that in cases where a formal design approach was considered, 75% of sub-scale models were geometrically-scaled (based on classical simil-

itude theory) because its application is simple and time-efficient. The state-of-the-art computational-scaling approach, which shows most promise in accurately scaling up SFT results, has only been used in 16% of all SFT models.

Although computational similitude theory shows significant promise in the design of similar sub-scale models, its widespread use is limited because of the **inherent complexity and computational expense** associated with its application. In addition, the **actual value and improvements offered by computational-scaling** over the widely used geometric-scaling approach remains unclear. In order to address these challenges, this work answered the following research question:

> *To what extent can the value and applicability of SFT be improved by using the MDAO based computational-scaling approach in the SFT model design process?*

In the following sections, the scientific contributions and technical developments that enable the adoption of computational-scaling are discussed.

11.1. SCIENTIFIC CONTRIBUTIONS

11.1.1. MDAO BASED SIMILITUDE MAXIMIZATION APPROACH

This dissertation proposed the use of an iterative computational-scaling approach that uses MDAO to maximize the extent of similitude between a SFT model and the full-scale aircraft (Chapter 6). In the past, a generalized figure of merit to quantify the extent of similitude was missing. Therefore, in this dissertation, a novel figure of merit called the **Degree of Similitude (DoS)** (Equation 6.12) was proposed to quantify the extent of similitude thereby enabling its exploitation by means of numerical optimization. At the same time, the translation of the SFT model design process into a formal optimization problem enables the inclusion of SFT model design requirements (such as control-power, static and dynamic stability of the model and the trim conditions) by means of constraints which are often neglected in the state of practice . The DoS accounts for the virtual scaling error to determine the similarity of model and the prototype behaviour for a given test objective.

In addition, the figures of merit **Behavioural Indicator Matrix (BIM)** and **Allowable Scaling Error (ASE)** were proposed in Chapter 6 to assess the suitability of the optimized SFT model (i.e., the model with largest DoS) for the phenomenon being tested. These support designers in deciding whether or not meaningful results can be gathered from SFT performed using a model having DoS < 1. Thus, this addresses the challenge of comparing different SFT models to identify a SFT model with maximum similitude to full-scale aircraft for the given test objective.

11.1.2. COMPUTATIONAL-SCALING: VALUE AND ADOPTION

Although computational-scaling has been used in past studies (see Chapter 4) as an improvement over classical similitude theory and geometric-scaling approach, till date, no study has been performed to systematically quantify the value of using computational-scaling. To fill this gap and to verify and validate the methodology proposed in this dissertation, an extensive design campaign was carried out to compare geometrically-scaled SFT models to computationally-scaled SFT models for varying test objectives and

11

design constraints. The results of the campaign are reported Chapter 10 in the form of seven case studies.
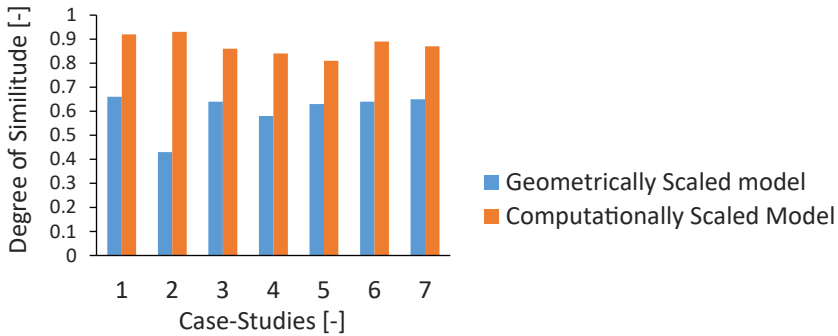
Figure 11.1: A comparison between DoS of geometrically-scaled model and similarity maximized computationally-scaled models for different case studies shown in Chapter 10
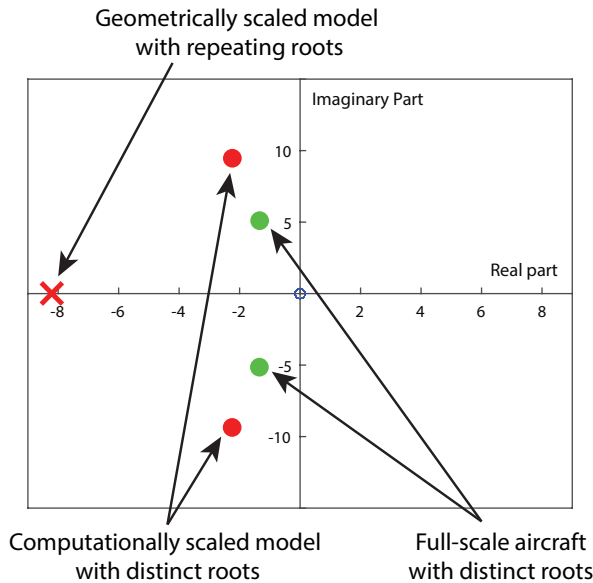
Figure 11.2: Differences in the short-period motion behavioural indicators (i.e., eigenvalues) of the geometrically-scaled model and computationally-scaled model for case study 6 in Chapter 10

11

In all the case-studies, the MDAO based similarity maximization process was started from a geometrically-scaled model to arrive at a design whose similarity was maximized for the given test objective. In every study, the optimizer found a computationally-scaled

SFT model design which showed better DoS as compared to geometrically-scaled model (see Figure 11.1). Furthermore, for each study, computationally-scaled model showed better match with the full-scale aircraft eigenvalues as compared to the geometrically-scaled model, which shows that **higher DoS implies better similitude** with full-scale aircraft.

In case DoS < 1 (i.e., all the cases in Figure 11.1), two models can have comparable DoS but completely different behaviour as compared to the full-scale aircraft. Thus, in cases where DoS<1, behaviour indicators must be used. For example, in case-study 6, the DoS of the geometrically-scaled model is only slightly lower than the computationally-scaled model but the behavioural indicators (i.e., eigenvalues in the case of short period motion) are markedly different as shown in Figure 11.2. Thus, the DoS calculation must be used in conjunction with the behavioural indicators to effectively use the MDAO based computational-scaling approach. Based on these studies, we can conclude that the methodology proposed in this dissertation is effective and important recommendations can be provided to the scientific community to improve the similitude of SFT model designs.

Many experimenters who have expertise in phenomenological testing often have a psychological reliance on geometric-scaling. In fact, this is not just encountered in SFT but is often seen in other sub-scale model tests where scale effects are prominent. Nevertheless, the results shown in the case-studies prove that the psychological reliance on geometrically-scaled models is unfounded and computationally-scaled models are better suited for phenomenological and simulation studies. Thus, we can validate Szücs's observation that geometric similarity is neither necessary nor sufficient condition to prove similitude [147].

11.2. TECHNICAL DEVELOPMENTS

SFT model design is an involved and meticulous process which requires several considerations as discussed in Chapter 5. Despite the importance of designing similar model, only a small portion of the available time is allocated to design because engineers have to dedicate larger share of the lead time to overcome practical challenges such as manufacturing, pilot training and development of auto-pilot.

Furthermore, a dedicated SFT model design team is often not available. A small team of engineers is entrusted with the responsibility of designing, manufacturing, testing and analysing the results without much help from disciplinary experts. Insufficient resources coupled with limited time for available for SFT creates tremendous pressure on small teams to "fly" the model without systematically exploring the design space. Consequently, the model cannot adequately simulate the prototype behaviour.

These barriers in the use of computational-scaling can be lowered by strengthening the interaction between the different disciplinary analyses by using design automation technologies such as KBE and MDAO. These advanced design methods are key enablers in the application of computational similitude theory to improve the quality and applicability of SFT. To this end, two major developments were presented in this dissertation. These developments are the fundamental building-blocks that enable computational-scaling and are summarized as follows:

1. **Scaled Model Design and Engineering Engine (SMDEE):** To enable the MDAO based similarity maximization approach, the technical challenge of automating the complete modeling and multidisciplinary analysis must be solved. This is achieved through the implementation of the SMDEE, the computational design and optimization framework presented in Chapter 7 and based on the DEE concept from La Rocca [185]. The core of the SMDEE is the Multi-Model Generator (MMG), a KBE tool, that supports designers in quickly and automatically generating the geometry of the scaled models (both isotropic & anisotropic), aspect models (for pre/post-processing) and weight & balance data to support MDAO similarity maximization. MMG is the key technology that enables the SMDEE framework to perform configuration agnostic geometry-in-the loop optimization, using a flexible suite of physics based disciplinary tools, which is necessary to adequately account for all the design constraints (including those typically not included in the SM design process) and to address unconventional aircraft configurations as demonstrated in Chapter 7.

2. **Parallel Execution Environment:** The SMDEE relies on dedicated disciplinary tools to assess a SFT model design (i.e., compliance with various requirements). The time taken by SMDEE to synthesize and assess a design mainly depends on the time required by external disciplinary tools (up to 90% of SFT model design time). In order to speed up the SMDEE iteration, a distributed computational system has been developed, called Parallel Execution Environment, that uses an algorithm specifically devised in this research, to distribute analysis tasks to computers that are free and available on the local network to speed up the SFT model design process (see Chapter 8 for details). The benchmark studies performed in this dissertation show that the parallel execution environment speeds up the execution time of one complete MDAO with 500 design iterations from 12 weeks to 1 week which has allowed the design and analyses of over 2500 SFT models reported in Chapter 10.

Thus, the combined use of SMDEE and the parallel execution environment enable the MDAO based computational-scaling approach by reducing the need for large teams and making the SFT model design process compatible with the limited time available.

11.3. RECOMMENDATION FOR FUTURE WORK

The work done in this dissertation on the SFT model design can be further expanded with additional research. This section provides an overview of future work that can improve the state of SFT and aid in the analysis of future aircraft designs.

11.3.1. QUANTIFICATION OF COMPUTATIONAL ERRORS

As discussed in Chapter 6, the full-scale aircraft behaviour can be predicted by combining SFT results, virtual scaling error, experimental errors and computational errors (see Equation 11.1 and Figure 11.3). A large part of this dissertation has been dedicated to the estimation and minimization of virtual scaling errors which have been computed using medium fidelity tools such as 3D panel methods. Such medium fidelity tools are subject to computational errors which must be quantified to predict the full-scale aircraft

11

behaviour. Although some computational errors of static derivatives have been quantified in Chapter 9 based on the comparison with ground-based tests, the computational errors of dynamic derivatives have not been quantified.

$$Q_p = Q_m \pm \epsilon_v \pm \epsilon_c \pm \epsilon_e \text{ (see Equation 6.11 for details)} \tag{11.1}$$
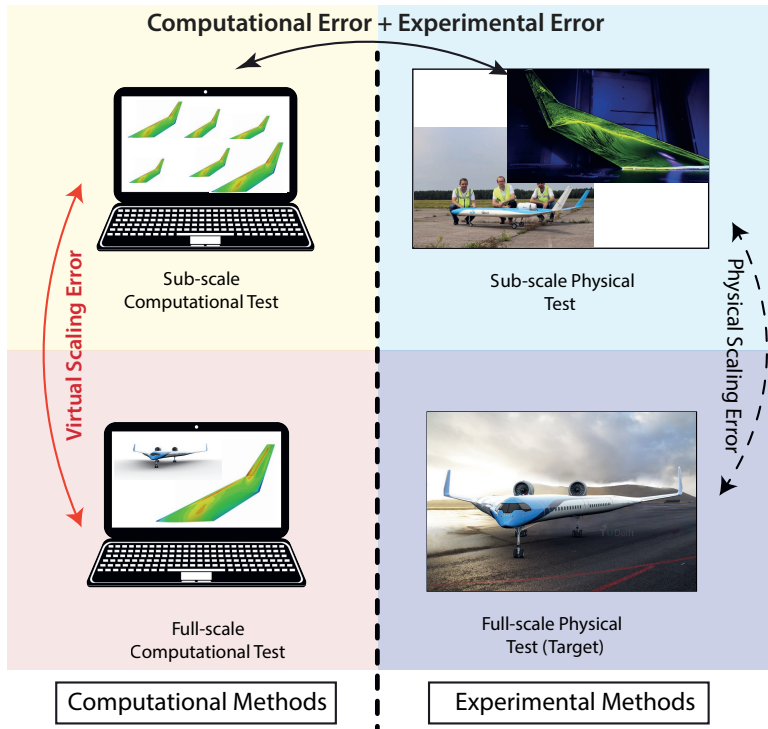
Figure 11.3: Schematic representation of scaling errors

Furthermore, the results from the ground based tests are prone to errors due to supporting stings and strings as discussed in Chapter 2. Thus, an appropriate method of quantifying the computational errors is to perform the (physical) SFT of a computationally-scaled model and then compare the results with SFT model behaviour obtained from computational methods (i.e, virtual test).

Consequently, manufacturing and sub-scale flight testing of a computationally-scaled SFT model for different phenomena to quantify the computational errors is recommended for follow-up research. This quantification must be performed in two steps. In the first step, computationally-scaled SFT model of conventional aircraft must be designed and tested to determine the applicability of Equation 6.11. This validation step can be succeeded by design and testing of unconventional aircraft SFT models.

11.3.2. DEVELOPMENT OF DATA-DRIVEN GENERALIZED SCALING LAWS

A major reason for the popularity of geometric-scaling and classical similitude theory is its ease of implementation without requiring rigorous mathematical and computational effort. computational-scaling requires efforts in problem formulation, development of design automation tools and implementation within an MDAO framework. These steps, although streamlined and formalized in this dissertation remain laborious and time-consuming.

In the future, after designing hundreds of computationally-scaled models for diverse test objectives, a sufficiently large database of SFT model designs, their degrees of similitude and the MDAO design variables and constraints can be generated. This database can be used in conjunction with regression models and machine learning algorithms such as artificial neural networks to develop simplified scaling laws that propose tailored polynomial functions to determine the size, shape and test conditions of SFT models as a function of full-scale aircraft design parameters (e.g., sweep, span, taper, tail volume, etc.) and the test objective (e.g., short-period motion, phugoid motion, etc.). This eliminates the need to calculate the non-dimensional coefficients of the SFT models and the full-scale aircraft, the most laborious and time consuming activity in computational-scaling, thereby lowering the barriers in the computational-scaling approach further.

11.3.3. METHODOLOGY TO GENERATE A CATALOG OF SFT MODELS

A close examination of the literature exposes the classical notion of using one sub-scale model to predict the complete flight behavior of the prototype which can lead to overloading the SFT model as discussed in Chapter 4. To overcome this, we propose the development of a catalog of sub-scale models, whose individual responses can be superimposed to predict the overall prototype behavior.

The development of such a catalog of designs, testing all designs economically, and then combining the results of all the tests remains an open challenge. Furthermore, number of SFT models in the catalog can significantly drive-up the cost of SFT to the point of making it economically unviable. Thus, follow-up research work must develop a methodology to reduce the size of the catalog without overloading the SFT model. The initial study of SFT model design for short-period motion and roll damping similarity using MDAO based similarity maximization approach shows promising results in the development of such a catalog of designs (see Case-Study 6 in Chapter 10).

The MDAO based computational-scaling approach proposed in this dissertation must be extended by developing a systematic approach for the selection of design variables to account for the modularity in SFT model design. Such an approach allows he reuse of SFT model for a completely different phenomenon with minor modification to the design while still guaranteeing sufficient similitude. The use of modularity in the catalog of SFT models is similar to the design of family of full-scale aircraft which is often used by aircraft manufacturers to save on overall development cost. A generalized solution to the SFT model catalog which includes the rules and methods to optimize the number of SFT models and the associated costs will be the next breakthrough in the field of sub-scale flight testing.

11

11.3.4. MODELLING UNCERTAINTIES IN SFT

SFTs are performed in open atmosphere. As discussed in Chapter 5, the uncertainties in the atmospheric conditions such as turbulence and gusts can introduce significant errors in the results of SFT and consequent prediction of full-scale aircraft behaviour. A classical solution to this problem is to repeat SFT multiple times (often 50-100 times) to get consistent SFT results. This significantly drives up the cost and the time needed to get reliable results.

To mitigate this challenge, in the future, the SFT model design process can be enriched by including a disciplinary analysis that models atmospheric effects (e.g., work of Van Staveren [170]), which can be used to simulate atmospheric uncertainties. Such an analysis can be used to computationally simulate the expected errors in SFT and quantify the atmospheric uncertainties to reduce the time and effort needed in performing such tests physically.

Similar uncertainty modelling techniques are also useful to account for the uncertainties introduced by the SFT model manufacturing process. In addition, the COTS equipment used for measurement are prone to noise. Significant time and effort is spent on post-processing SFT results which can be streamlined by developing models for uncertainty quantification in measurements.

11.3.5. IMPROVEMENTS IN PROBLEM FORMULATION AND SOLUTION STRATEGY

The case-studies performed in Chapter 10 used the same (subset of) continuous design variables for all case-studies. These design variables were kept consistent to study the impact of changing the test objective (i.e., DoS formulation). However, more studies must be performed in the future with a larger set of design variables to identify the key design variables that affect a given test objective. However, larger set of design variables implies longer optimization time. To speed up the process, after a few iterations of MDA, a surrogate model of all the disciplinary analysis can be constructed and used for MDAO based computational-scaling. A recurring challenge in the use of surrogate model is their accuracy which can be overcome by using appropriate response correction methods (see the work of Koziel and Leifsson [206]). Furthermore, a data table linking the key design variables with most impact on a given test-objective must be created, which can be used for all future MDAO based computational-scaling problems.

11

V

APPENDIX

A

EXAMPLE OF CLASSICAL SIMILITUDE THEORY APPLICATION

A.1. EXAMPLE

A sub-scale model must be used to study the short period motion of a full-scale aircraft with 34 m span (b), 4.2 m mean aerodynamic chord (c) and 73 000 kg mass ($W_{full-Scale}$) flying at a velocity ($V_{full-scale}$) of 472 km/h and an altitude ($h_{full-scale}$) of 2300m. Two certification constraints [1] are considered in the design of sub-scale model as follows:

1. model must fly at an altitude (h_{model}) of 4000 m[2]

2. model mass (W_{model}) should not exceed 100 kg

Based on this information, the test conditions (i.e., speed (V_{model})) and the size of the sub-scale model (i.e., mean aerodynamic chord (c_{model}) and the mass (W_{model})) must be determined.

A.2. STEP 1: SELECTION OF RELEVANT PARAMETERS IN SIMILITUDE

Full-scale aircraft parameters are defined as follows:

$$W_{full-scale}, \qquad V_{full-scale}, \qquad c_{full-scale}, \qquad h_{full-scale} \qquad \text{(A.1)}$$

---

[1] For this example, a representative value 100kg is chosen, which is either a certified or specified category model depending on its span as per the categorization provided by the Dutch Government (Section 2.1.2) [83, 84, 207]. Certification authorities also require safe model operation proof [83, 84, 207], which is beyond the scope of classical similitude theory.

[2] Note that the model test altitude is higher than the full-scale aircraft altitude. This allows model operations at lower density thereby allowing for lowing model mass as shown in Equation A.3

A

model parameters:

$$W_{model}, \qquad V_{model}, \qquad c_{model} \qquad h_{model} \qquad \text{(A.2)}$$

A.3. STEP 2: SELECTION AND APPLICATION OF SCALING LAWS

Applying mass scaling and correcting for densities due to difference in test altitude [42] gives the scaling factor λ:

$$\lambda^3 \frac{W_{full-scale}}{\rho_{full-scale}} = \frac{W_{model}}{\rho_{model}} \implies \lambda = 0.1176 \qquad \text{(A.3)}$$

Applying geometric scaling gives the mean aerodynamic chord of the model:

$$c_{model} = \lambda * c_{full-scale} \implies c_{model} = 0.5m \qquad \text{(A.4)}$$

A.4. STEP 3: SELECTION AND APPLICATION OF MODEL LAWS

Applying Froude number scaling to ascertain the ratio of gravity forces to inertia forces of the model and prototype are similar [42]:

$$Fr_{model} = K_{Fr} * Fr_{full-scale} \qquad \text{(A.5)}$$

where $K_{Fr} = 1$ (to ensure Froude number scaling) and

$$Fr = \frac{V}{\sqrt{gL}} \implies V_{model} = 44.44 m/s \qquad \text{(A.6)}$$

With the available capabilities of COTS components, 150 kg models have been flown at 50 m/s [74, 134]. Thus, 44 m/s is a reasonable test velocity, provided the flight box is sufficiently large.

In addition, for short period motion, Reynolds number scaling must also be satisfied [42] which is defined as

$$Re_{model} = K_{Re} * Re_{full-scale} \qquad \text{(A.7)}$$

where, Reynolds number is given by formula

$$Re = \frac{\rho V L}{\mu} \qquad \text{(A.8)}$$

Since all the variables in Equation A.8 are known, it is not possible to impose the condition $K_{Re} = 1$. By combining Equations A.4, A.6, and A.8, we get:

$$K_{Re} = 0.035 \qquad \text{(A.9)}$$

Thus, Reynolds number scaling is not possible. Conversely, if we want to impose Reynolds scaling, the Froude number scaling that cannot be achieved, as shown below

$$K_{Re} = 1, \tag{A.10}$$

$$k_{Fr} = 28.90 \tag{A.11}$$

A.5. STEP 4: EVALUATION

Clearly, Froude and Reynolds number similarity cannot be achieved simultaneously when used in conjunction with the certification requirements because the problem is over constrained. In such cases, engineers typically choose to match a sub-set of original similitude criteria and attribute variations of results with respect to full-scale aircraft to those criteria for which similitude could not be matched.
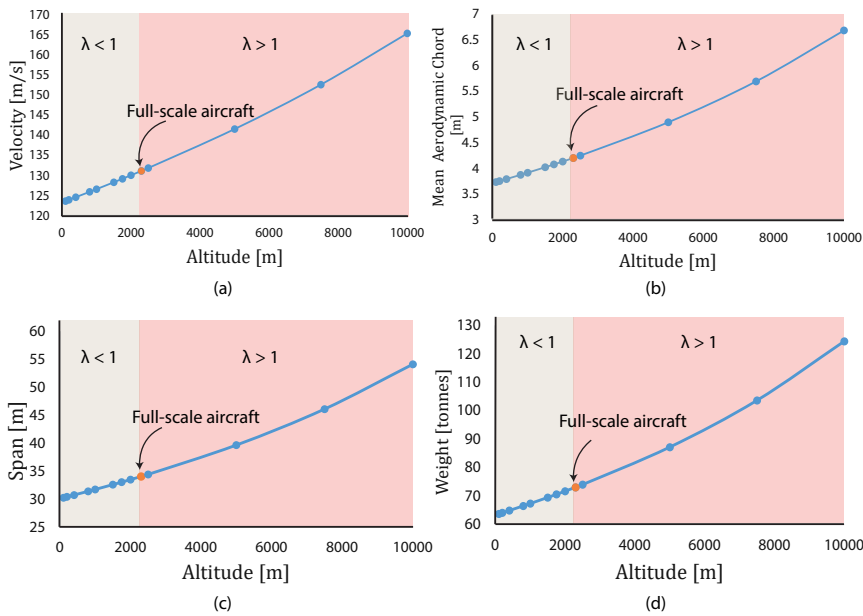
Figure A.1: The (a) velocity, (b) mean aerodynamic chord, (c) span and (d) weight of the model at different test altitudes for geometrically scaled models, determined using classical similitude theory without any certification constraints, where, $\lambda < 1$ implies model smaller than the full-scale aircraft (i.e., sub-scale model) and $\lambda > 1$ implies model larger than the full-scale aircraft (i.e., super-scaled model).

In case no certification requirements are imposed, both Froude and Reynolds number similarity can be achieved by solving Equations A.5-A.8. However, this does not mean that building a similar SFT model is a viable option. As illustrated in **Figure A.1**, the size (i.e., mean aerodynamic chord and span as shown Figure A.1 (b) & (c)) and weight (Figure A.1 (d)) of the sub/superscaled model ranges from 70-130% and 83-236% respectively of the full-scale aircraft at varying altitudes. Such large models could be as expensive as the

A

full-scale aircraft, which defeats the purpose of using SFT (i.e., cost-effectiveness). Thus, even when no certification constraints are imposed, engineers limit the model weight and size to ensure that the cost of the test remains low.

B

EXAMPLE OF GOVERNING EQUATIONS BASED SIMILITUDE THEORY APPLICATION

B.1. EXAMPLE

A sub-scale model must be designed such that its pressure distribution is similar to a 2-dimensional full-scale model, using governing equations. Where, the full-scale model has a span of length L and operates at Mach number 0.65. Furthermore, the sub-scale model must be tested at 0.3 Mach number. Unsteady effects and viscous effects may be ignored to ensure similitude.

B.2. ITERATION 1

Since, similitude is established by matching the governing equations, the actual values of the flight conditions and the size of the model and the prototype are not important, as long as the governing equations used to establish similitude are the same for model and prototype. The equations shown in the remainder of the section are assumed to apply to both model and prototype.

Step 1: Selection of governing equation:

This problem can be best solved using Navier-Stokes equation. This equation is represented as follows:

x-momentum equation:

$$\rho u \frac{\partial u}{\partial x} + \rho v \frac{\partial u}{\partial y} = -\frac{\partial p}{\partial x} + \frac{\partial}{\partial y}\left(\mu\left(\frac{\partial v}{\partial x} + \frac{\partial u}{\partial y}\right)\right) \tag{B.1}$$

y-momentum equation:

$$\rho u \frac{\partial v}{\partial x} + \rho v \frac{\partial v}{\partial y} = -\frac{\partial p}{\partial x} + \frac{\partial}{\partial x}\left(\mu\left(\frac{\partial v}{\partial x} + \frac{\partial u}{\partial y}\right)\right) \tag{B.2}$$

B

where, x is the x-coordinate, y is the y-coordinate, u is the x-component of the velocity, v is the y-component of the velocity, μ is the dynamic viscosity, ρ is the density, and p is the pressure.

Step 2: Normalization of governing equation:

The process of normalizing Navier-Stokes equation is shown in Equation 4.8 and 4.9. In order to ensure similitude between the model and the prototype, the coefficients of these equations must be equal for the model and the prototype (i.e., all three π-terms shown in Equation 4.11).

Step 3: Comparison of coefficients

Both Reynolds number and coefficient of pressure cannot be matched owing to differences in operating conditions.

Step 4: Transformation of the model

With the governing equation shown in Equation 4.8 and 4.9, transformation is not possible as long as viscous effects are a part of the equations (as shown in the example in Figure 4.1). In other words, just changing the shape of the model will not be sufficient to make the coefficients of model and prototype equal.

Step 5: Application of approximation theory

Since the model cannot simultaneously match Reynolds number and the coefficient of pressure, the viscous effects are ignored to simplify the governing equations and to enable transformation.

B.3. ITERATION 2

Step 1: Selection of governing equation

The simplifications lead to new governing equation as follows:

$$\frac{\partial^2 \phi}{\partial x^2} + \frac{1}{1-M^2}\frac{\partial^2 \phi}{\partial y^2} = 0 \tag{B.3}$$

the boundary condition at $y = 0$:

$$\frac{\partial \phi}{\partial y} = U_1 \frac{\partial y}{\partial x} \tag{B.4}$$

the boundary condition at ∞:

$$\frac{\partial \phi}{\partial x} = \frac{\partial \phi}{\partial y} = 0 \tag{B.5}$$

$$(c_p)_{body} = -\frac{2}{U_1} \frac{\partial \phi}{\partial x} \tag{B.6}$$

where, ϕ is the velocity potential, M is the Mach number, U_1 is the component of the velocity tangential to the body, C_p is the coefficient of pressure on the body and the remaining terms remain the same as described in Iteration 1.

Step 2: Normalization of governing equations
These governing equations are normalized as follows

$$\overline{\phi} = \frac{\phi}{U_1 L}, \qquad \overline{x} = \frac{x}{L}, \qquad \overline{y} = \frac{y}{L} \tag{B.7}$$

This keeps the governing equation the same:

$$\frac{\partial^2 \overline{\phi}}{\partial \overline{x}^2} + \frac{1}{1 - M^2} \frac{\partial^2 \overline{\phi}}{\partial \overline{y}^2} = 0 \tag{B.8}$$

and the C_p value changes to

$$(c_p)_{body} = -2\frac{\partial \overline{\phi}}{\partial \overline{x}} \tag{B.9}$$

However the boundary condition changes to:

$$\frac{\partial \overline{\phi}}{\partial \overline{y}} = \frac{\partial y}{\partial x} \tag{B.10}$$

Step 3: Comparison of coefficients
Due to the differences in the Mach numbers of the model and the prototype, the coefficients of governing equation (i.e., Equation (B.8)) cannot be matched. Thus, similitude cannot be established with the equations shown in Step 2.

Step 4: Transformation of the model
In order to absorb the Mach number terms into the governing equations, the y-axis can be transformed as follows:

$$y_1 = \overline{y}\sqrt{1 - M^2} \tag{B.11}$$

B

this makes the governing equation

$$\frac{\partial^2 \overline{\phi}}{\partial \overline{x}^2} + \frac{\partial^2 \overline{\phi}}{\partial y_1{}^2} = 0 \tag{B.12}$$

which makes the boundary condition as follows

$$\frac{\partial \overline{\phi}}{\partial y_1} = \frac{1}{\sqrt{1 - M^2}} \frac{\partial y}{\partial x} \tag{B.13}$$

assuming the dimensions of the model in y direction can be defined as a product of an arbitrary function f and a thickness scaling factor t, it is given as

$$\overline{y} = t f(\overline{x}) \implies \frac{\partial y}{\partial x} = t f'(\overline{x}) \tag{B.14}$$

this changes the boundary conditions to

$$\frac{\partial \overline{\phi}}{\partial y_1} = \frac{t}{\sqrt{1 - M^2}} f'(x) \tag{B.15}$$

Since $f(\overline{x})$ is purely a function of the shape the model, Equations (B.12) and (B.15) can be used to establish similitude (Section B.4). Furthermore, since the transformation is performed on y axis alone, it has no effect on $(c_p)_{body}$.

B.4. Iteration 3

Step 3: Comparison of coefficients

It is clear from Equation (B.12) that the coefficients of the governing equations will always be equal because they are always equal to 1. However, at different operating Mach number, the coefficients in the boundary conditions shown in Equation (B.15) will be
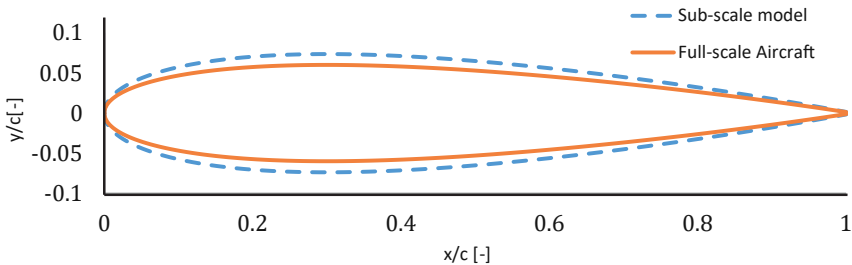
Figure B.1: The transformation of airfoil shape necessary to maintain similar pressure distribution in inviscid flow between a sub-scale model tested at 0.3 Mach and the full-scale aircraft tested at 0.65 Mach

different. If these coefficients can be matched, the model and the prototype will be similar to one another. Thus the following conditions should be satisfied:

$$\frac{t_{Model}}{\sqrt{1 - M_{Model}^2}} = \frac{t_{full-scale}}{\sqrt{1 - M_{full-scale}^2}} \tag{B.16}$$

B

Step 6: Selection of model scaling

Substituting the values of the model and the full-scale flight speed from the example in Equation (B.16), the thickness scaling factor of the model (t_{Model}) is 1.255. This is shown using a normalized airfoil in Figure B.1.Thus, when the model is scaled geometrically, by a scaling factor (SF) in x-direction, it must be distorted in y-direction by a factor 1.255(SF) to ensure that the pressure distributions are the same for model and prototype. It is important to note that the relations shown in this example are not applicable to transonic flows because of singularity in Equation B.16. However, similar mathematical effort can be performed to develop scaling laws for inviscid flow in transonic conditions as shown by Kline [145].

C

HIGH-LEVEL PRIMITIVES: IMPLEMENTATION IN MMG

The Multi Model Generator (MMG) has been in continuous development at TU Delft since 2005. It has been (re-)implemented with suitable modification using different KBE systems namely ICAD, Genworks GDL and ParaPy. In this chapter, the current implementation in ParaPy KBE system is discussed.

The aircraft MMG is composed of seven HLPs as shown in Figure C.1. A number of these primitives of MMG were discussed in Chapter 8. Of these, the wing, fuselage, connecting element and engine modules are OML HLPs and the structures module is internal HLP. In the following sections, the wing, the fuselage and the connecting element HLPs are discussed as these HLPs have been modified/extended by the author to support SFT model design. The detailed description of the other primitives can be found in the work of Pieter-Jan Proesmans (Engine HLP) [208], Roy Groot (ConnectingElement HLP) [209] and Luc de Ruiter (Structure HLP) [210].

C.1. WINGMOVABLEFROMRAILS PRIMITIVE

The WingMovableFromRails primitive[1] is used to generate wing and multiple movables on the wing. The generative modelling of wing is an extensively studied problem with numerous ways of parametrization [211, 212]. In MMG, WingMovableFromRails primitive is composed of one or more trapezoidal wing sections called wing trunks. These trunks are suitably modified, positioned and fused to obtain a lifting surface. An example of a wing trunk implementation is shown in Figure C.2.

The generation of a wing in MMG involves four main tasks as shown in Figure C.3. The first step is the generation of a clean wing (i.e., without any movables). The second step involves the generation of the movable(s) from the wing. In the third step, the movables and the fixed part of the wing are fused together to obtain a wing. Finally, the wing

---

[1] read as: wing and movables generated from rails
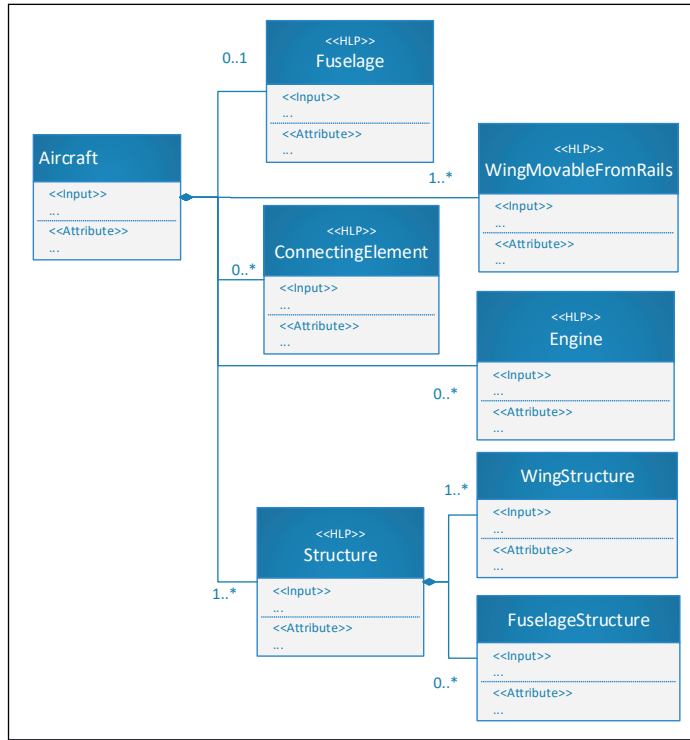
Figure C.1: UML class diagram of aircraft composed of five High Level Primitives (i.e., Fuselage, WingMovableFromRails, ConnectingElement, Engine and Structure) in MMG as per current implementation

is positioned with respect to other aircraft components. All these activities are accomplished by the HLP WingMovableFromRails as shown in Figure C.4. These activities are performed by classes WingFromRails (for clean wing), CutShapes (for movable generation) and WingModel (to generate wing geometry and positioning) as shown in Figure C.4 and are discussed further in the following sections.

The MMG reads the wing user inputs from a JSON data file. In addition, in-house plugins are available to support the conversion of Common Aircraft Parametric Configuration Schema (CPACS) file (.XML) or Initiator (.MAT) output file to MMG compatible JSON file. These JSON files contain a node for each wing as shown in Figure C.5. User can add or remove a wing by simply adding or removing a node. Each wing node contains five sub-nodes (See Figure C.5) as follows:

1. ***is_mirrored:*** is a boolean parameter used to mirror a wing about the axis of the wing without user having to repeatedly provide similar inputs. For example, this parameter is typically set to true for main wing and horizontal tail of a conventional tube-and-wing aircraft.

2. ***rails:*** contains elements that can be used to model the planform of the wing (dis-
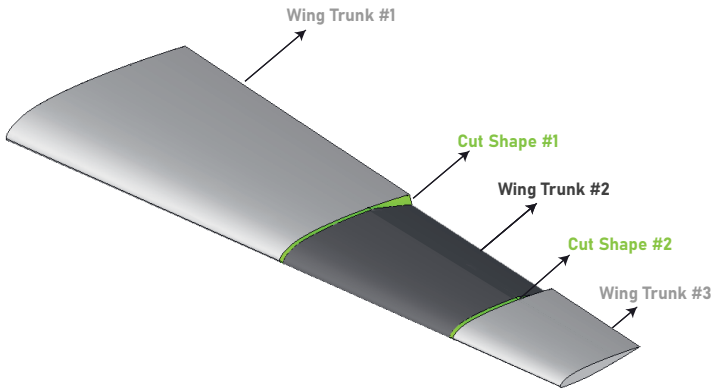
Figure C.2: Example wing composed of 3 (trapezoidal) wing trunks and two specialized lofted surfaces (called cut-shapes) used to connect movable wing trunk (#2) and fixed wing trunks (#1 and #3)
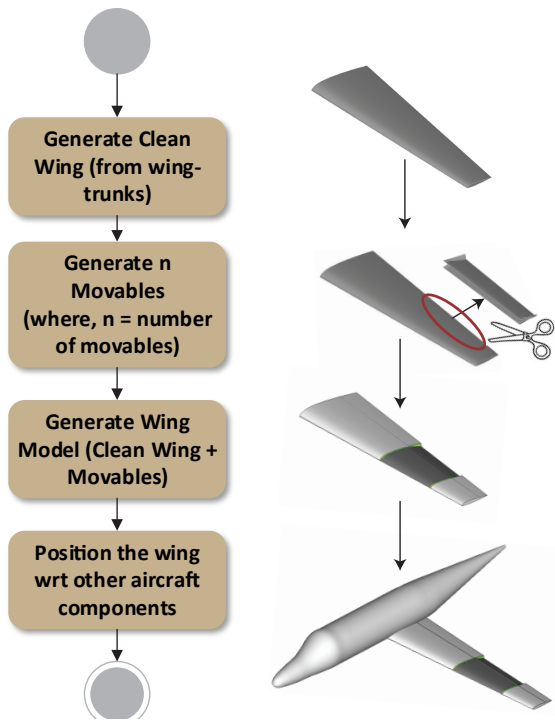
Figure C.3: UML activity diagram of generative wing modelling implemented in MMG

cussed in Section C.1.1).
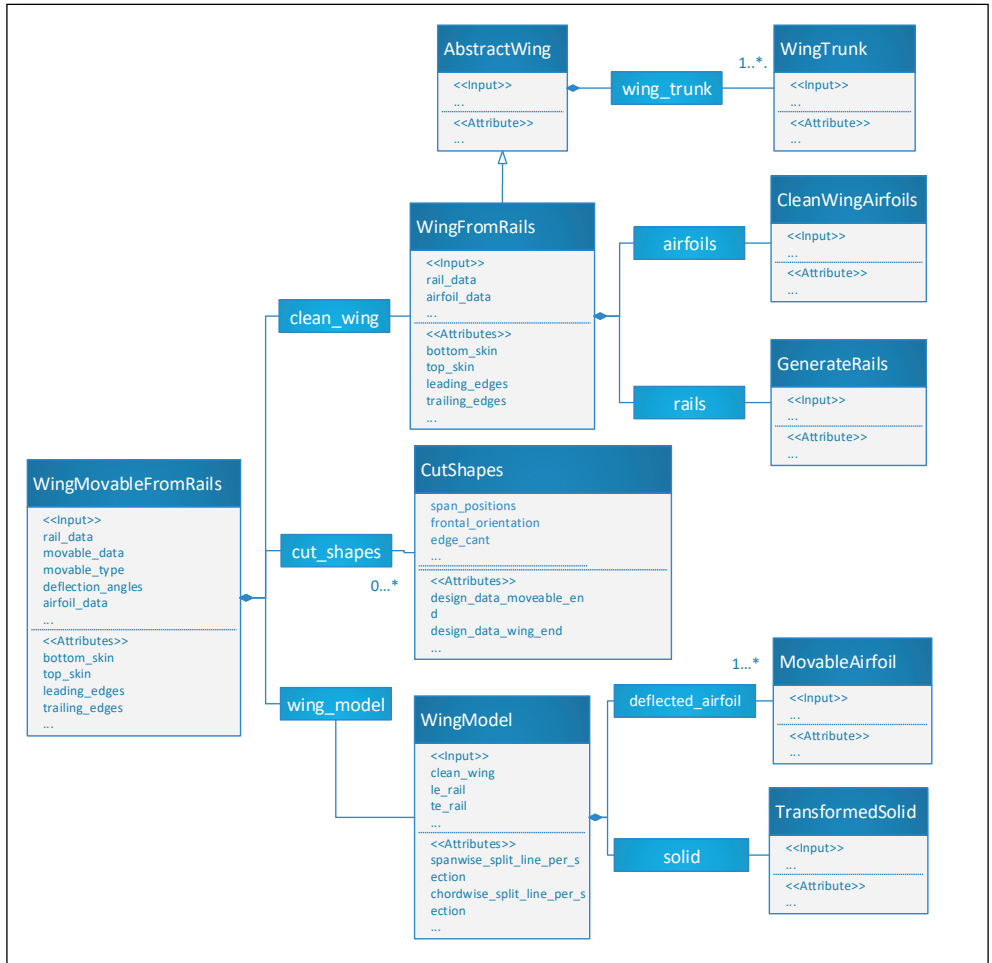
Figure C.4: Modified UML class diagram of WingMovableFromRails HLP including the names of the instances used in the code

3. *parameters (airfoil):* contains elements based on which MMG reads the relevant airfoils from the database and then scales and positions them on the rails (discussed in Section C.1.1).

4. *movable_parameters:* contains elements that are used by MMG to model the movables on the wing (discussed in Section C.1.2).

5. *position:* contains data to position the wing with respect to the aircraft (discussed further in Section C.1.3).
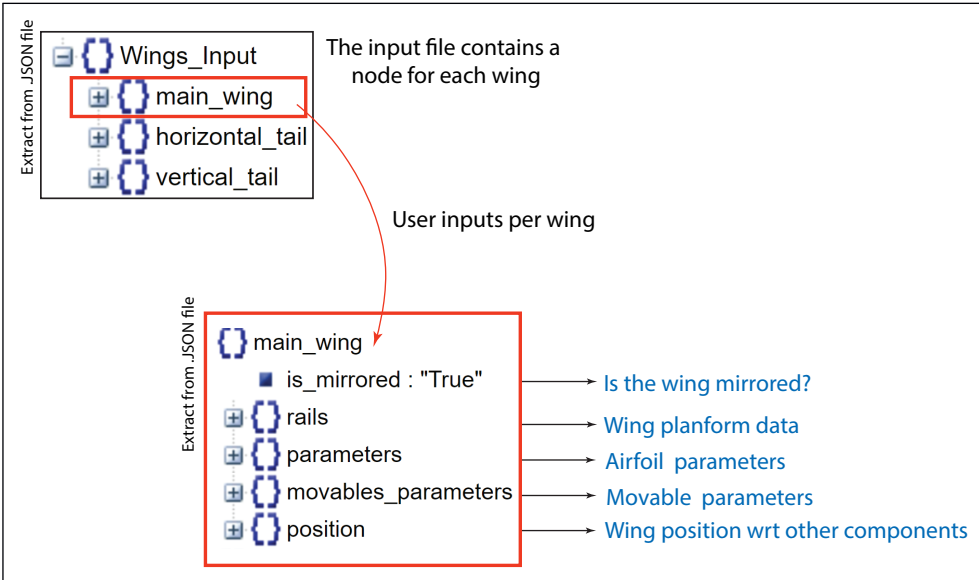
Figure C.5: Extract from an MMG input file showing the main inputs per wing

C.1.1. WINGFROMRAILS

WingFromRails generates a clean wing by lofting a smooth surface across a skeleton of wing sections (i.e., airfoils) as shown in Figure C.6. The GenerateRails class determines the wing planform by positioning leading edge and trailing edge of the wing by including sweep, twist and dihedral, which is used by CleanWingAirfoils class to read (from database), scale and position the airfoils. Both these classes are children of WingFromRails as shown in Figure C.4.

WingFromRails needs at least two airfoils, one at the root and one at the tip section. However, unlimited airfoils that can be used to define a wing. Two instantiations of WingFromRails are shown in Figure C.6. One is generated using two airfoils, the other using three. In both cases, the implementation of WingsFromRail produces a (family of) single-curvature surface loft(s) (with 3 airfoils, two single curvature surfaces (from airfoil 1 to 2 and airfoil 2 to 3)) are produced. Thus, if more than one airfoil used, only linear interpolation is performed between adjacent airfoils. This implementation of WingsFromRail has been used throughout this dissertation.

PLANFORM DEFINITION WITH GENERATERAILS CLASS

The GenerateRails class is used to model the planform, in particular, the leading and trailing edges of the wing taking into account the twist, dihedral and sweep of the wing. To generate the planform, MMG first generates flat leading and trailing edges (i.e., in x-y plane) as shown in Figure C.7. The sweep of the wing is included in this step and the planar planform of the wing is available.

The leading and trailing edge rails are constructed using the user defined inputs leading and trailing edge points as shown in Figure C.7 and described in Table C.1. In order
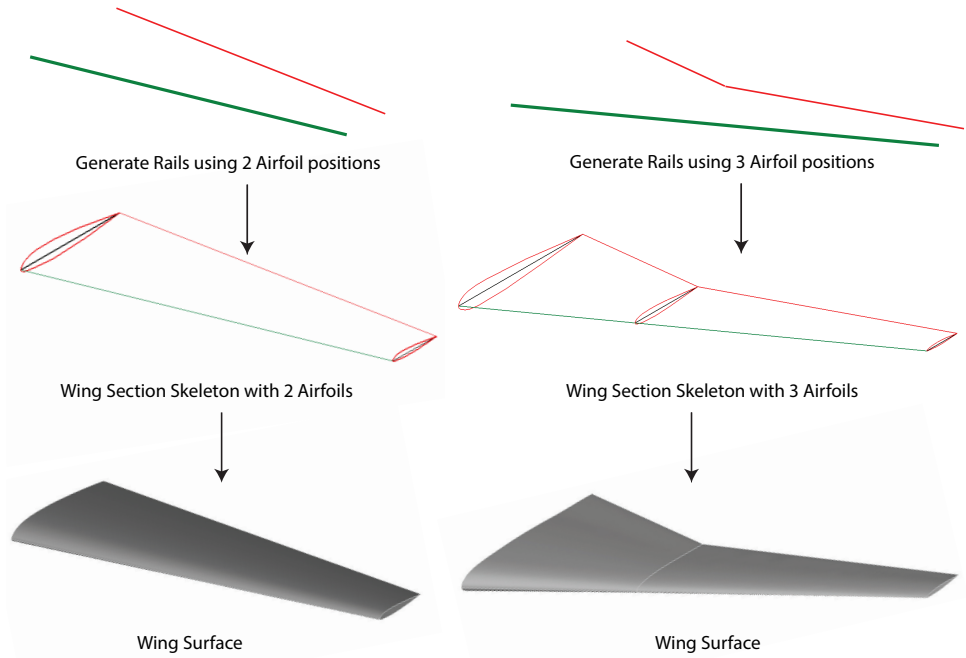
Figure C.6: Wing section skeleton across which MMG performs lofting operation to generate clean wing geometry

to generate a wing, at least two leading and trailing edge points are necessary. User can choose to add more points depending on the shape of the wing to be modelled. MMG requires the user to provide consistent data for every planform section. The example shown in Table C.1 shows the data required for a planform with three sections.

Similarly, the twist axis is modelled using the twist axis points. In order to apply the dihedral to the wing, a dihedral curve is necessary which determines how the planform is rotated. The curve is based on dihedral points which are calculated by rotating the leading edge points around the local x-axis of the wing (discussed in Section C.1.3) by an angle desired by the user. This gives the leading edge rail with the dihedral. The input format for dihedral is shown in Table C.1. Similarly, trailing edge and the twist axis are rotated (Figure C.7). Positive dihedral angles lead to dihedral wings and negative dihedral angles lead to anhedral wings.

Once the rails are rotated to include the dihedral angle, the chords at different wing sections are identified and rotated at the twist points about the twist axis (see Figure C.7). The magnitude of twist is based on user input *twist_point_list* as shown in Table C.1. Based on the twisted chords, new rails are modelled which is used by CleanWingAirfoils to position the airfoils. The operations on different rails are performed by GenerateWingRails class in MMG (see class diagram in Figure C.8).

Table C.1: Inputs to model the wing planform

Input keyword	Input Type	Example	Description
le_point_list	coordinates list	[[0,0,0], [0,20,0], [20,100,0]]	list of coordinates on which the planar leading edge lies (i.e., the z value of every point is 0)
te_point_list	coordinates list	[[100,0,0], [100,20,0], [70,100,0]]	list of coordinates on which the planar trailing edge lies (i.e., the z value of every point is 0)
dihedral_point_list	list	[[0,0,0], [0,20,5], [20,100,10]]	**[[x-coordinate of point on leading edge, y-value of point on leading edge, dihedral angle in degrees]]**
twist_axis_point_list	coordinates list	[[50,0,0], [50,20,0], [45, 100, 0]]	list of coordinates on which the planar twist axis lies (i.e., the z value of every point is 0)
twist_point_list	list	[[50,0,0], [50,20,-2], [45,100,5]]	**[[x-coordinate of twist axis point, y-value of of twist axis point, twist angle in degrees]]**

AIRFOIL DEFINITION WITH CLEANWINGAIRFOILS CLASS

Once the planform model is ready, MMG reads, scales and positions the airfoils at different wing-sections for lofting with CleanWingAirfoils class. The associated class diagram is shown in Figure C.9. The key tasks performed by CleanWingAirfoils class are shown in Figure C.10.

Reading the airfoil: This class is a capability module (see Chapter 7) within the Clean-WingAirfoils class. The key task of this class is to read the airfoil data points from a central airfoil database. User defined airfoils are read by this class. User must define at least two airfoil (filenames) using **"airfoils"** parameter as shown in Table C.2. For complex wing geometries such as kinked wings, more wing sections and corresponding inputs must be provided.

The user can either provide a data filename that matches with the name of a corresponding file in a predefined "airfoil library". These files are plain ASCII files, each containing a list of point coordinates (see example in Figure C.11). The user can expand the airfoil library by adding files containing new airfoil definitions. MMG reads the airfoil definition from the files in the class TUDReader as shown in Figure C.9, provided:

1. the coordinates of the points are specified in a 2D reference system

2. the coordinates are normalized with respect to the chord length
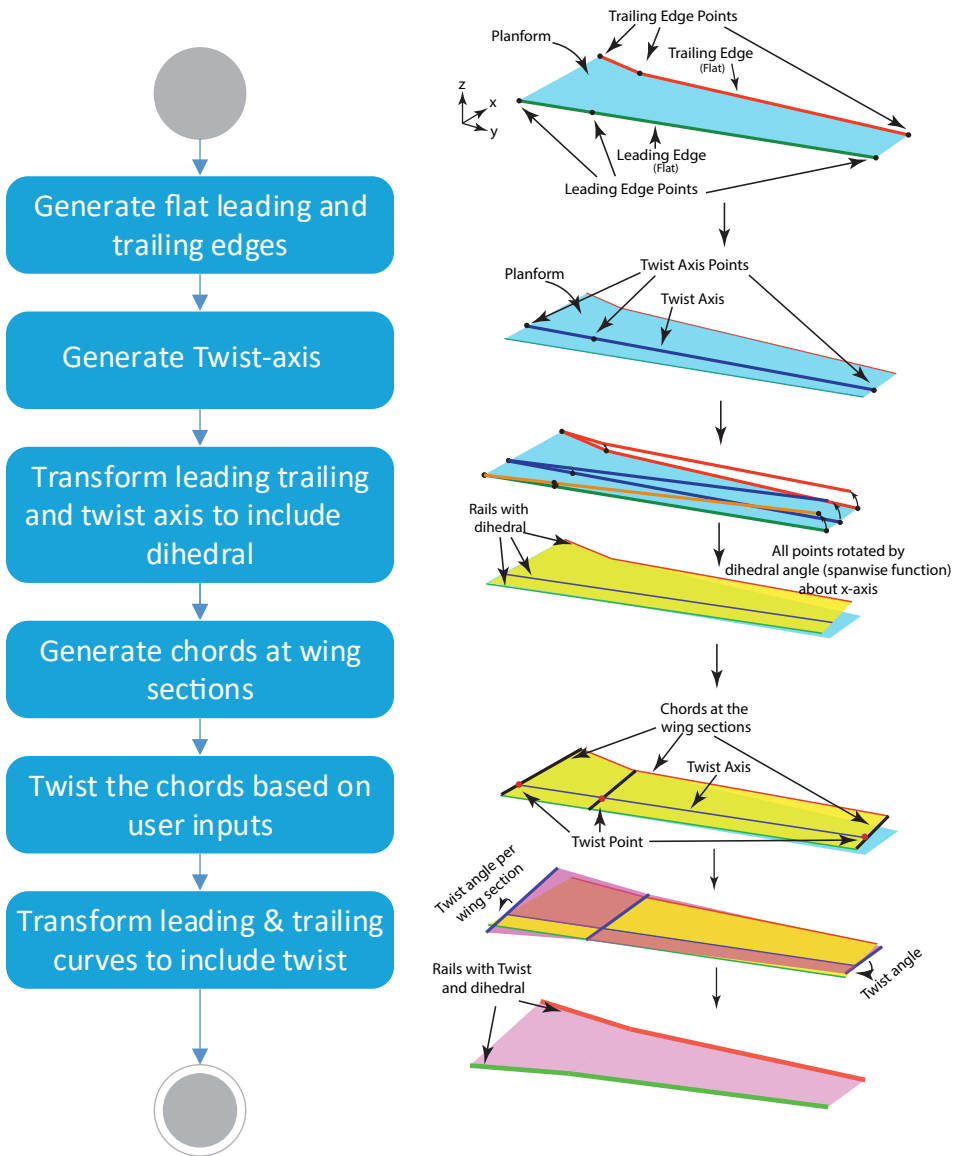
Figure C.7: UML activity diagram showing the sequence of tasks performed by MMG to generate the wing leading and trailing edges

3. the points are provided in sequence (counter-clockwise starting at trailing edge) as shown in Figure C.11
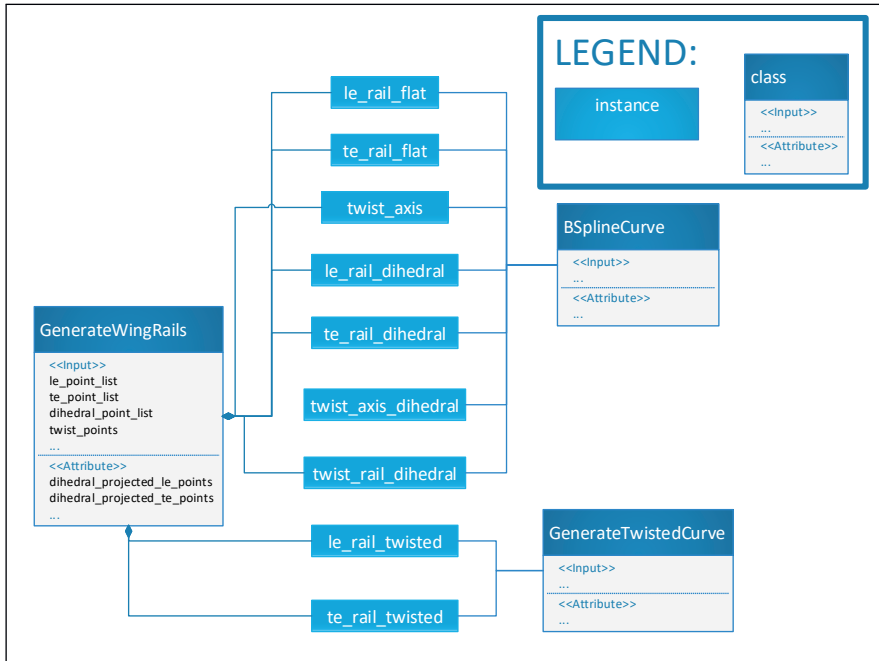
Figure C.8: Modified UML class diagram of GenerateWingRails including the names of the instances used in the code with color coding to indicate the significance of each instance in the planform generation process

4. the leading edge and trailing edge point must be included in file

Alternatively, the user can also provide the names of airfoil exactly as provided in UIUC airfoil database[2], which can be read by MMG. This is done by the class UIUCReader (see Figure C.9).

Once the coordinates are read, the Reader class generates the points and interpolates a curve passing through these airfoil coordinate points using the ParaPy primitive FittedCurve. This airfoil curve is further split into of two parts, namely, the bottom airfoil curve and the top airfoil curve as shown in Figure C.12. Such a split in the curve automatically generates a leading and trailing edge on the wing. Furthermore, it helps in the identification of faces that become skin panels.

The coordinate based airfoil definition is simple and supports common conceptual and preliminary design process. Furthermore, it enables easy modification/extensions of the airfoil database. However, the coordinates-based airfoil definition is not best suited method in aerodynamic shape optimization.

A better way to support the optimization of airfoils and aerodynamic surfaces in general would require an analytical definition of airfoils and surfaces, such as the CST method proposed by Kulfan [213], based on Bernstein polynomials. Very large design

---

[2]https://m-selig.ae.illinois.edu/ads.html
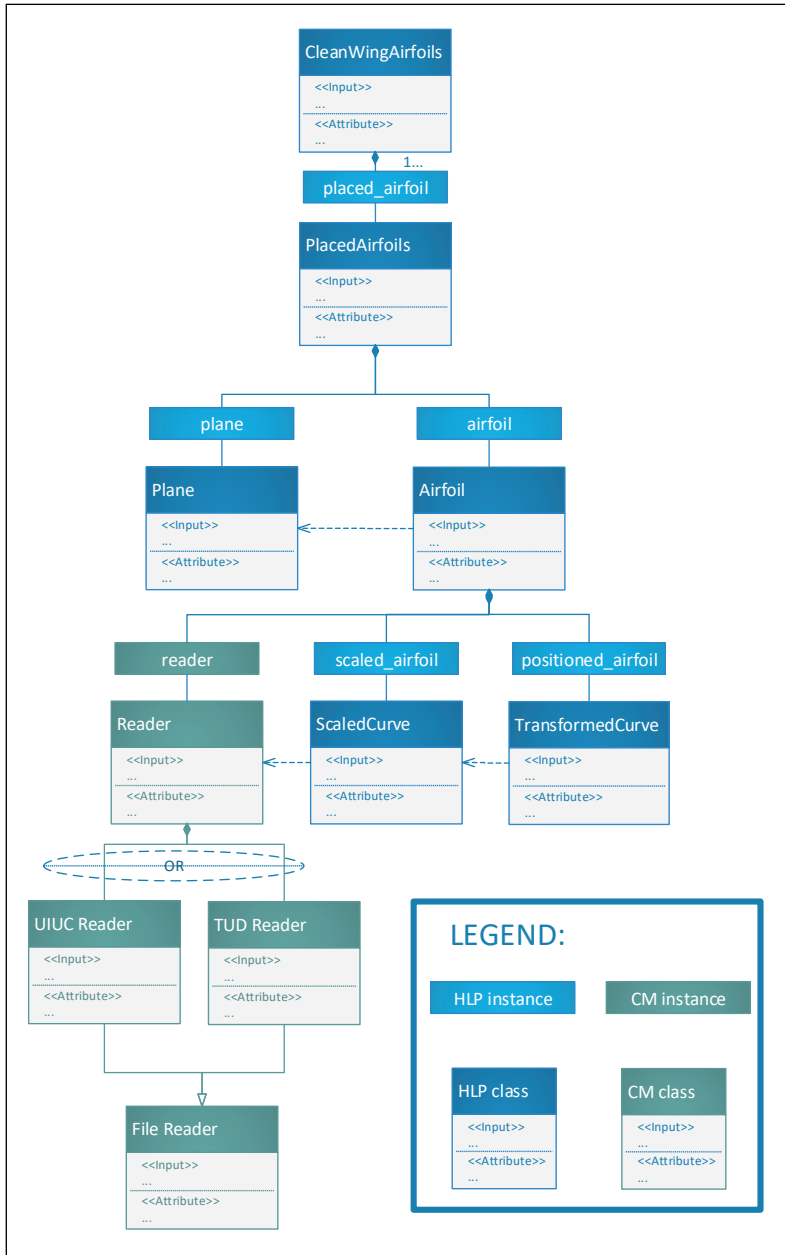
Figure C.9: Modified UML class diagram of CleanWingAirfoils including the instance names used in the code and the capability module to read the airfoil data

space can be covered using a few design variables. To this end, functions have been added to MMG which automatically converts CST coefficients into an airfoil data file
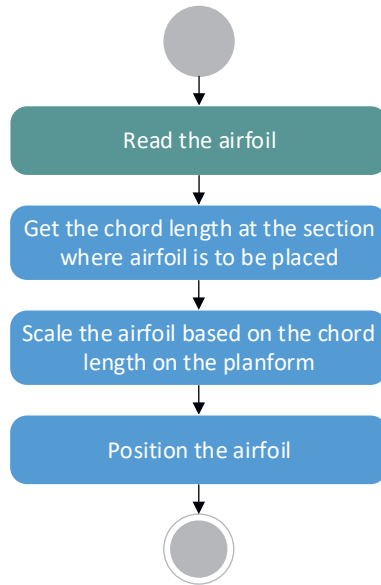
Figure C.10: UML activity diagram showing the sequence of tasks performed by MMG to generate the wing airfoils

Figure C.11: Schematic showing how the airfoil is read by MMG and the order in which airfoil coordinates must be noted (counter-clockwise starting at trailing edge) in the data file

Table C.2: Inputs to model and position the airfoils

Input keyword	Input Type	Example	Description
airfoils	string list	['file1.dat', 'file2.dat']	indicate the file names in database containing airfoil coordinates. The list length determines the number of airfoils created
span_positions	integer list	[0, 1]	list of normalized Y-coordinates (y-coordinate /span) ranging from 0 to 1 that determines the position of the airfoil curves along the span
airfoil_thickness	float list	[100, 100]	list of thickness to chord ratio with respect to original airfoil in percentage at each section (example shown in Figure C.16)
airfoil_cant	string list	["streamwise", "streamwise"]	list of orientation of the airfoil with respect to x-axis at each section (user can possibly use four different settings as shown in Figure C.14)
follow_dihedral	integer list	[1, 1]	list of orientation of the airfoil with respect to z-axis at each section (user can possibly use two different settings (0 & 1) as shown in Figure C.15)
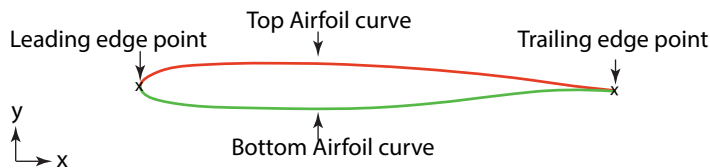
Figure C.12: Airfoil curve split into top and bottom curves to generate leading edge in the loft

(called CST Reader), while adhering to all the airfoil data file requirements. This allows engineers to update the airfoils in MMG airfoil library during aerodynamic shape opti-

mization. This feature has been extensively used in this work for similitude maximization as demonstrated in Chapter 10.

The airfoil generated by the CST reader is a unit airfoil (i.e., normalized with respect to chord length). It must be scaled to the chord length of the spanwise location of wing-section where the airfoil must be placed. Typically, the locations where the airfoils must be placed must be set by the user using the ***"span_positions"*** parameter as shown in Table C.2. Based on the inputs, planes are placed at the normalized span locations. and intersected with planform to determine the chord at a given wing section as shown in Figure C.13. The selection of the span_positions does not necessarily need to be at the same location as the leading_edge_points used in rail generation.
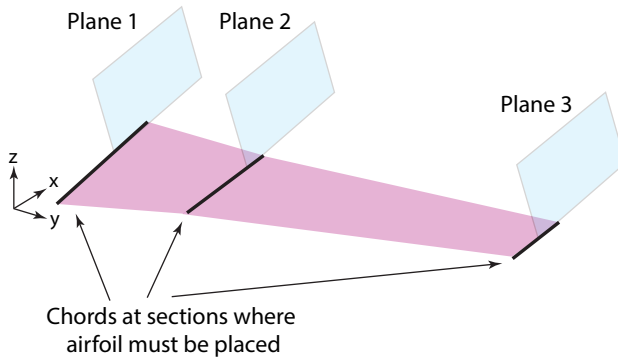
Figure C.13: Airfoil chord length estimation at different user-defined location

The orientation of the planes are based on two user-input parameters ***airfoil_cant*** and ***follow_dihedral***. The airfoil_cant determines the orientation of the intersection plane with respect to x-axis. User can select one of four possible options for the orientation of the plane as shown in Figure C.14. The follow_dihedral parameter determines the plane's orientation with respect to the vertical. User can select one of two possible settings as shown in Figure C.15 and described in Table C.2.

The planes for the determination of the chords lengths at different sections are constructed in the Plane class as shown in Figure C.9. The intersection with the planform is performed in PlacedAirfoil class. The scaling of the airfoils and the positioning of the airfoil is done in Airfoil class (see Figure C.9).

The chord length determines the x-axis scaling of the airfoil (see Figure C.12). However, for certain optimizations and parametric studies, scaling in y-direction might also be interesting to the engineer. To facilitate this, the thickness of the airfoil can be scaled using the ***airfoil_thickness*** parameter shown in Table C.2. An example of airfoil thickness scaling is shown in Figure C.16. These scaled airfoils are placed along the chords obtained from the intersection to construct wing trunks and eventually clean wing as shown in Figure C.6.

WING TRUNKS AND TOPOLOGY
Once the airfoils are placed appropriately, adjacent airfoils are lofted to generate wing trunks (Figure C.17). Thus, the number of wing-trunks is one less than the number of
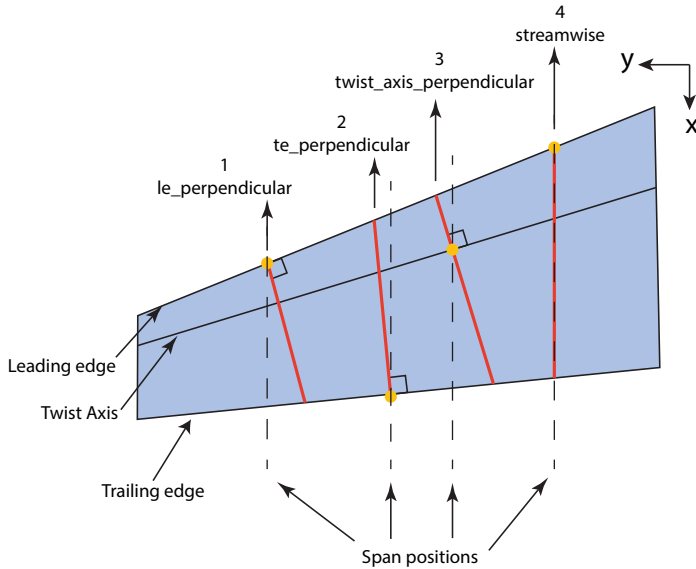
Figure C.14: Different options available to the user to orient the airfoil with respect to x-axis
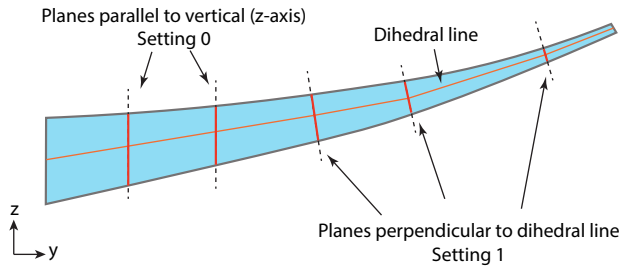
Figure C.15: Different options available to the user to orient the airfoil with respect to the vertical (z-axis). Note, ***Setting 0*** affects the thickness of the airfoils. Thus high dihedral implies very thin wing.

airfoils provided as an input. The grouping of airfoils and the eventual generation of trunks is shown in Figure C.17.

Once the trunks are modelled, the lofted surfaces are sewn together to generate the clean wing Solid. These tasks are performed in the AbstractWing class as shown in Figure C.4. AbstractWing is a generalized class which is inherited by WingFromRails to generate the wings.

In addition to generating the trunks, AbstractWing class also links different geometrical entities to the product definition to generate a topology table. For example, some faces (Faces #1 and #2 in Figure C.18) of the wing geometry constitute the top skin of the wing. MMG identifies these faces and stores them in the topology table. As a result, any capability module can perform actions on the product instead of their composing faces.
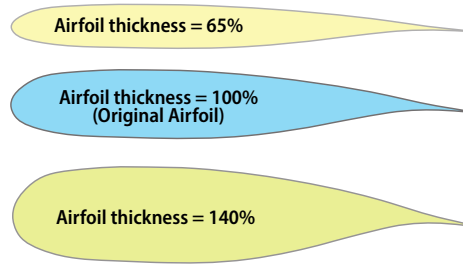
Figure C.16: Airfoil shaped when different percentages of thickness to chord ratio with respect to original airfoil are chosen
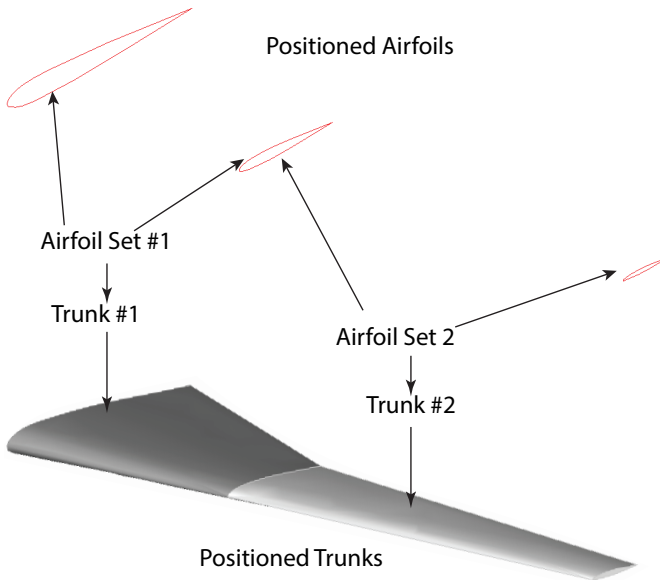
Figure C.17: Construction of wing trunks by pairing adjacent airfoils

For example, MMG can collect and group all the mesh elements and the associated forces and moments of the top-skin by using the information in the topology table. This eliminated the manual intervention of the user to identify the geometrical features such as edges and faces. The topology table is constructed automatically by AbstractWing class. For this, algorithms have been implemented that utilize product knowledge.

For example, root and tip curves are identified by intersecting a plane with the wing at 0 and 100% of the span respectively. Edges coincident with the leading and trailing edge rails discussed in rail generation section are selected as leading and trailing edges as shown in Figure C.18. The top skin faces are identified using the following algorithm:
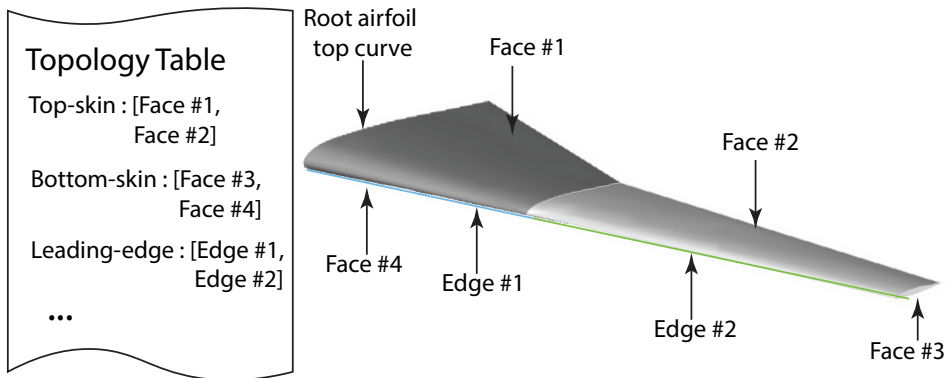
Figure C.18: Construction of wing wing topology table using function identification algorithms

1. **Identify root adjacent face:** iterate through all the faces and identify the face whose edges are (a part of) root airfoil top curve, leading edges and trailing edges (Face #1 in Figure C.18)

2. **Populate top skin faces list:** Add root adjacent face to the list containing top skin faces

3. **Identify root and tip faces (end faces):** identify faces whose edges are both bottom and top curves of root or tip airfoil

4. **Generate face list without end faces (top-bottom faces)** collect all faces except the end faces

5. **Identify the neighbour of root adjacent faces:** identify the face in top-bottom faces which shares an edge other than leading or trailing edge with root adjacent face (Face #2 in Figure C.18)

6. **Populate top skin faces list:** Add root adjacent face neighbour to the list containing top skin faces

7. **Reassign root adjacent face:** set root adjacent face neighbour as root adjacent face

8. **Iterate:** Iterate Steps 5-8 until no root adjacent face neighbour can be found

Similar algorithm can be used to identify bottom faces. Implementation of such algorithms and the generation of topology tables enables numerous capability modules discussed in Chapter 7 and opens up the possibility of computational scaling by automating complex analysis steps.

C.1.2. MOVABLE DEFINITION

For most aerospace applications, a wing movable is necessary to control the aircraft. The topology information and the clean wing geometry are used to generate the movables.

The activity diagram of the tasks performed by wing movable is shown in Figure C.19. The movable modelling and its fusion with the wing is performed by classes CutShapes and WingModel as shown in Figure C.4. In the version of MMG used for this work, control surfaces are built using the same approach used to model simple flaps. Furthermore, the wing and the movables have a 'C0' continuous surface and no slots are modelled.

C
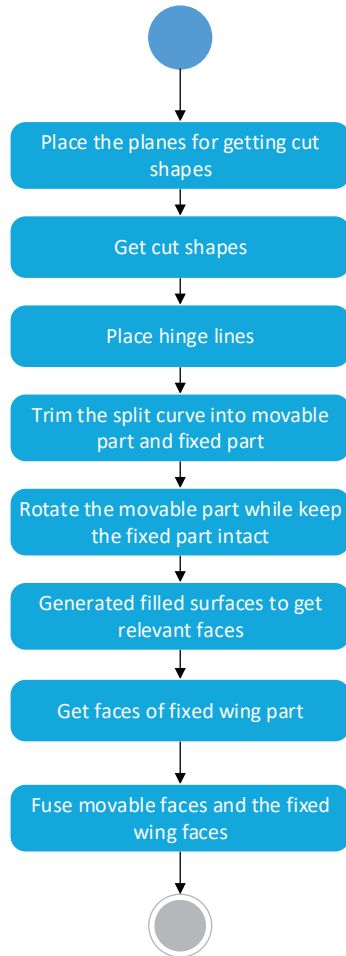
Figure C.19: UML activity diagram of the tasks performed by MMG to model the wing movable

The movable design is started with the definition of the movable location along the span. This is done using the user-defined input parameter ***span_positions*** as shown in Table C.3. This parameter includes the start and end positions of every movable as a fraction of the normalized span, which is used by MMG to place the planes for wing intersection as shown in Figure C.20

The position of the planes is given by span_positions and the orientation is pro-
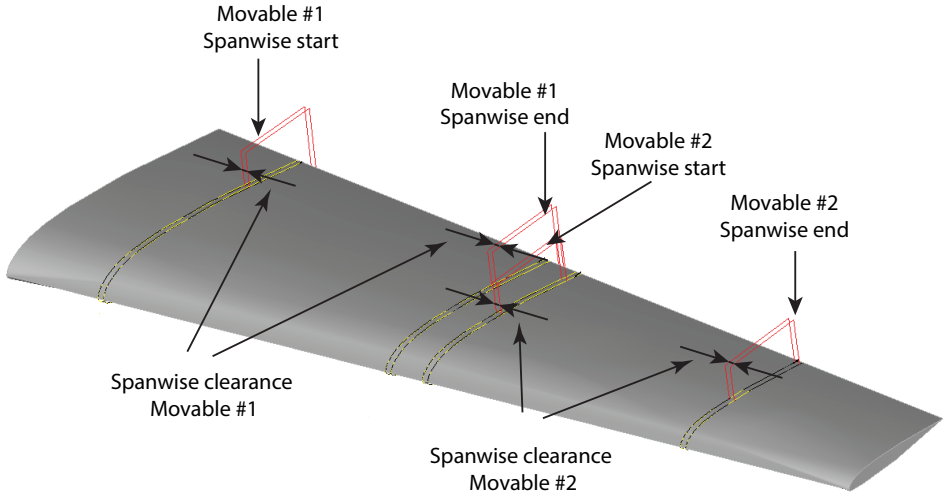
Figure C.20: Locations of the planes used to determine the span-wise location of the movables

vided by ***edge_cant*** and ***frontal_orientation***. Each of these parameters apply to each end of the movable as explained in Table C.3. The orientation options remain the same as shown in Figure C.14 (for edge_cant) and Figure C.15 (for frontal_orientation).

For the movables to rotate freely, they require some clearance from the fixed part of the wing. The ***spanwise_clearance*** parameter defined by the user is used to determine the clearance. This clearance is used to place internal planes parallel to the start and end planes as shown in Figure C.20. The planes are intersected with the wing to obtain the airfoils of movable and wing side (Figure C.21). These are called the cut shapes and performed by the class CutShapes as shown in Figure C.4.
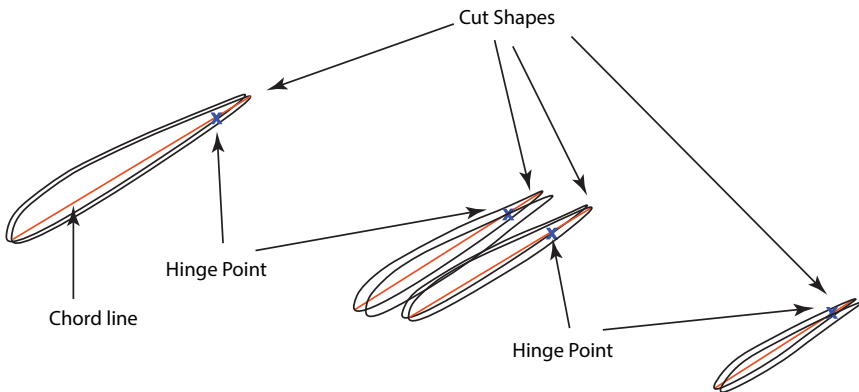
Figure C.21: Cut shapes obtained by intersecting span-wise planes with the clean wing

Table C.3: Inputs to generate movables

Input keyword	Input Type	Example	Description
span_positions	string list	[[0.1, 0.35], [0.4, 0.85]]	
frontal_orientation	integer list	[[0, 0], [0, 0]]	the orientation of cut-shapes with z-axis (Figure C.15) for every cut shape
edge_cant	float list	[['streamwise', 'streamwise] ['streamwise', 'streamwise]]	the orientation of cut-shapes with z-axis (Figure C.14) for every cut shape
hinge_chord_ratios	string list	[[0.3, 0.32], [0.3, 0.35]]	ratio of the movable length on the chord to the chord length at every cut-shape associated with the movable
deflection_angles	string list	[10, 10]	angle in degrees by which each movable must be deflected
clearance_chordwise	string list	[20, 20]	
clearance_spanwise	string list	[50, 50]	

Once the cut-shapes are available, they are used by WingModelling class to generate the exact shape of movable. This is done by placing the hinge lines on the chords of the cut-shapes. The hinge point is obtained by using the user-defined input ***hinge_chord _ratios*** (see Table C.3) at every section associated with the movable as shown in Figure C.21.

The hinge point is projected on the top and bottom curves of every cut-shape to obtain trimming points. These trimming points are used to trim the cut shapes as shown in Figure C.22. After splitting, the curves associated with the wing and the movable identified and the movable curves are rotated by an angle defined by the user input ***deflection_angles*** per movable. This splitting operation only happens on the inner cut-shapes (i.e., shapes associated with the movables).

After the split, the movables are sometimes moved in chord-wise direction by a user defined input ***clearance_spanwise***. This models the gap between the movable and the fixed part of the wing to provide the clearance for free rotation. Faces are created us-
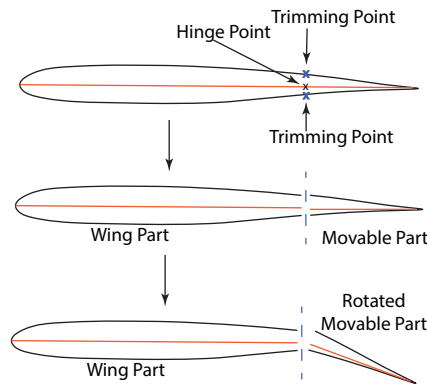
Figure C.22: Trimming operation on the cut-shape and the rotation of the trimmed curves to obtain movable deflection

ing the different airfoil curves and tagged with their topological properties such as wing (fixed part) faces, movable faces, trailing edge, leading edges etc.

C.1.3. WING POSITIONING

The positioning of the wing happens with respect to the forward-most point (global origin) on the aircraft (Figure C.23). For an aircraft with fuselage, the global origin is the tip of fuselage nose and for a wing-only aircraft the global origin is the leading edge point of the forward-most wing. Typically most wings are oriented about x-y plane of the global coordinate system except the vertical tails, which are positioned in x-z plane. All other points used to define the wing planform described in Table C.1 are done with respect to the local coordinate system (i.e., about the root chord leading edge point).

C.2. CONNECTING ELEMENT PRIMITIVE

The current definition of dihedral rail used in WingMovablesFromRails does not allow a dihedral angle greater than 90° which prevents the construction of winglets and box-wing-configurations. Groot [209] added a connecting element primitive to support the geometry generation of box-wing aircraft and winglets.

For a box-wing aircraft, the process of generating the wings by using the offset plane is shown in Figure C.24. Four input parameters are necessary to define the connecting elements for a box wing aircraft (shown by d_1, d_2, h_1 and h_2 in Figure C.24). For the winglet generation, only two input parameters are necessary (shown by d_1 and in Figure C.24). The detailed treatment of connecting elements can be found in the work of Groot [209].
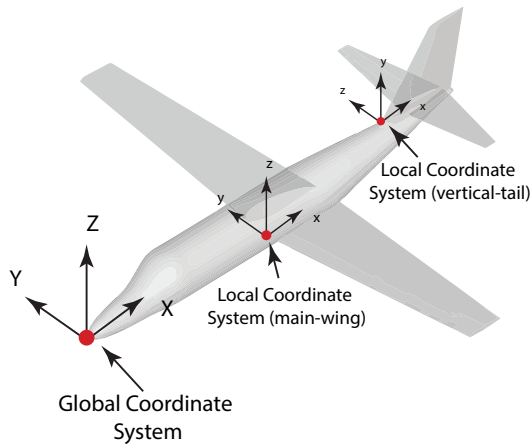
Figure C.23: The coordinate systems used for wing-positioning.

C.3. NOTE ON CURVED LEADING AND TRAILING EDGES

The current WingMovablesFromRail uses five rails to define the planform of the wing. These rails are the leading edge, trailing edge, twist axis, dihedral rail, and twist rail as discussed in Section C.1.1. The rails are built using a set of points. The airfoils of the wing are provided by the user and are placed on the rails to form a wire frame of the wing. This wire frame is used for the lofting operation to generate wing solid. These inputs to create these rails are points that define a connected sequence of line-segments. Such a wing generation approach results in two main drawbacks:

1. commonly used intuitive wing properties such as dihedral, sweep angle, twist etc. are implicitly defined with the rail points which makes it difficult for engineers modify the wing geometry

2. piecewise linear rails used to construct the wings often result in linear loft per segment of the rail. These lofted surfaces do not respect tangency conditions with one another resulting in discontinuos wings

To overcome these limitations, a new wing primitive definition was necessary that satisfies the following requirements:

1. The parameterization should be based on intuitive geometrical characteristics such as dihedral angle, sweep angle, and chord length instead of geometry rails.

2. The primitive should support continuous rails.

3. The primitive should not impose any limit on the dihedral angle

Heimans [214] developed a new wing-parametrization in the MMG that complies with the aforementioned requirements. This primitive is based on the parametrisation described by Sóbester and Forrester [211]. An example of a wing generated using the new

C
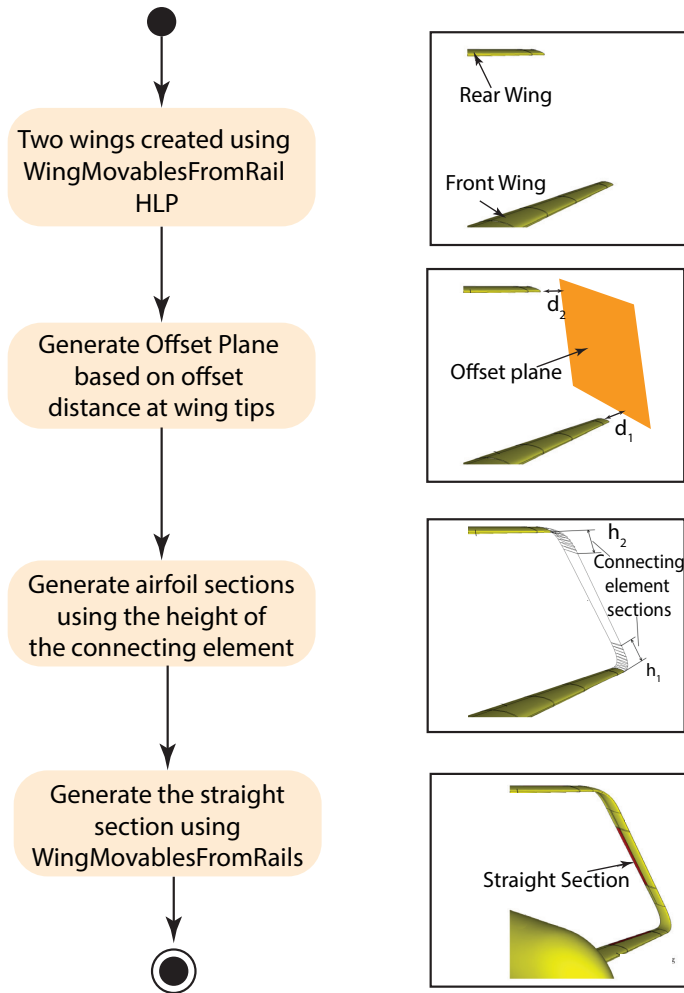
Figure C.24: Activity diagram showing the generation of connecting element

primitive is shown in Figure C.25. For detailed information on the parameterization and the inputs necessary to use this application, reader is referred to the work of Heimans [214].

C.4. Fuselage Primitive

In this section, the basic characteristics and functionalities of the Fuselage primitive are briefly illustrated. Details of the technical implementation using the ParaPy KBE software can be found in the work of Wei [215]. Like the Wing-part, the Fuselage HLP has a modular architecture, where separate classes have been defined to model the outer

Curved rails used in ParaWing with each
rail made from one fitted curve

Wing surface generated from
single lofting operation using the rails
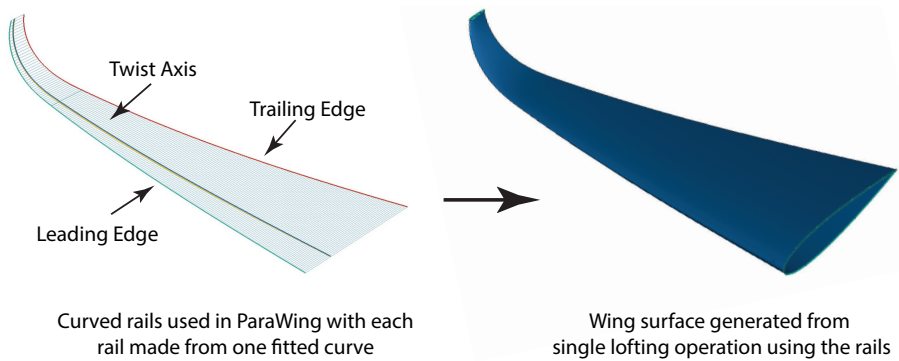
Figure C.25: Example of a wing generated using new wing parameterization approach to support curved rails

surface (see class diagram in Figure C.26).

The modeling approach implemented to generate the outer surface of the fuselage primitive is rather simple and aims at the generation of one, continuous aerodynamic surface extending from nose to tail. The procedure consists of two main steps:

- Definition of a skeleton of support curves

- Interpolation of a B-spline surface on top of this skeleton.

The first step is fundamental to the quality and accuracy of the overall fuselage design. In the current implementation, MMG requires the user to provide an input file which contains the planar points (at least 20) defining each circumferential curve and their location with respect to the global coordinate system (see Figure C.27). This method has the inconvenience that a lot of circumferential curves need to be provided by the user to properly model areas with large curvature gradient, such as the cockpit area. Nevertheless, this method has worked effectively for diverse fuselage shapes. The fuselage surface can be locally adjusted by modifying the points defining the support curves. Examples of different fuselage shapes generated in MMG using this parameterization is shown in Figure C.28.

C
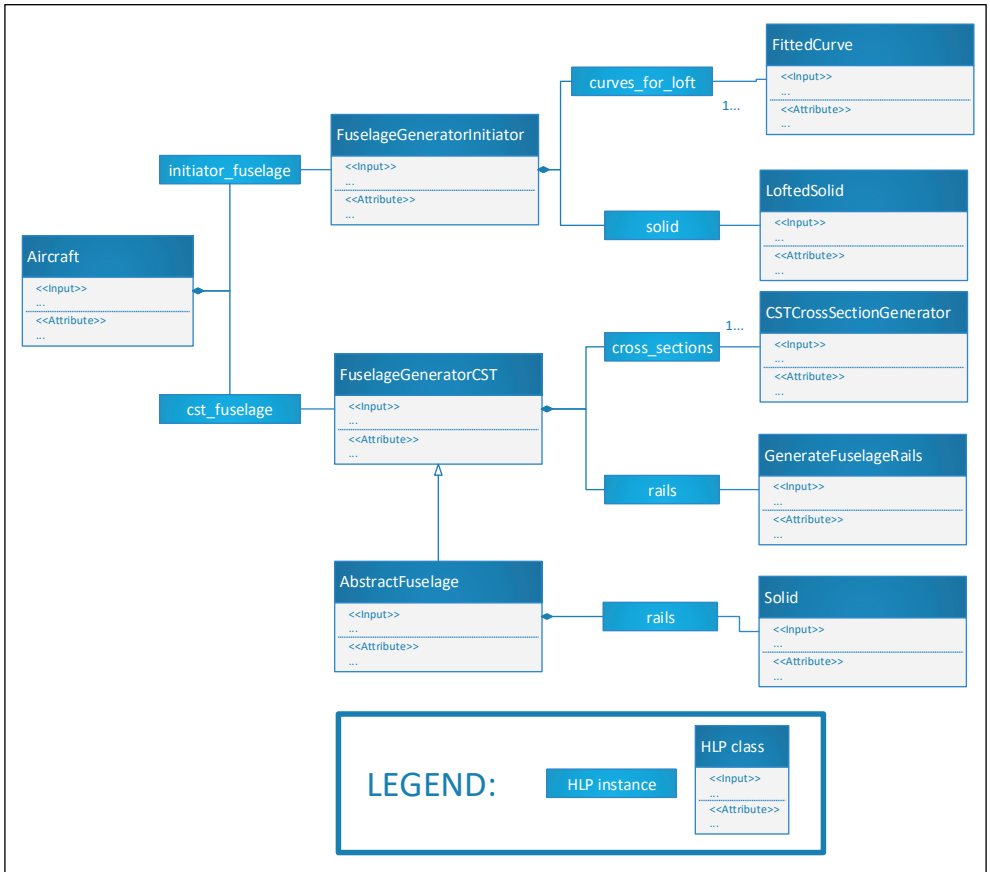
Figure C.26: UML class diagram of the fuselage HLP
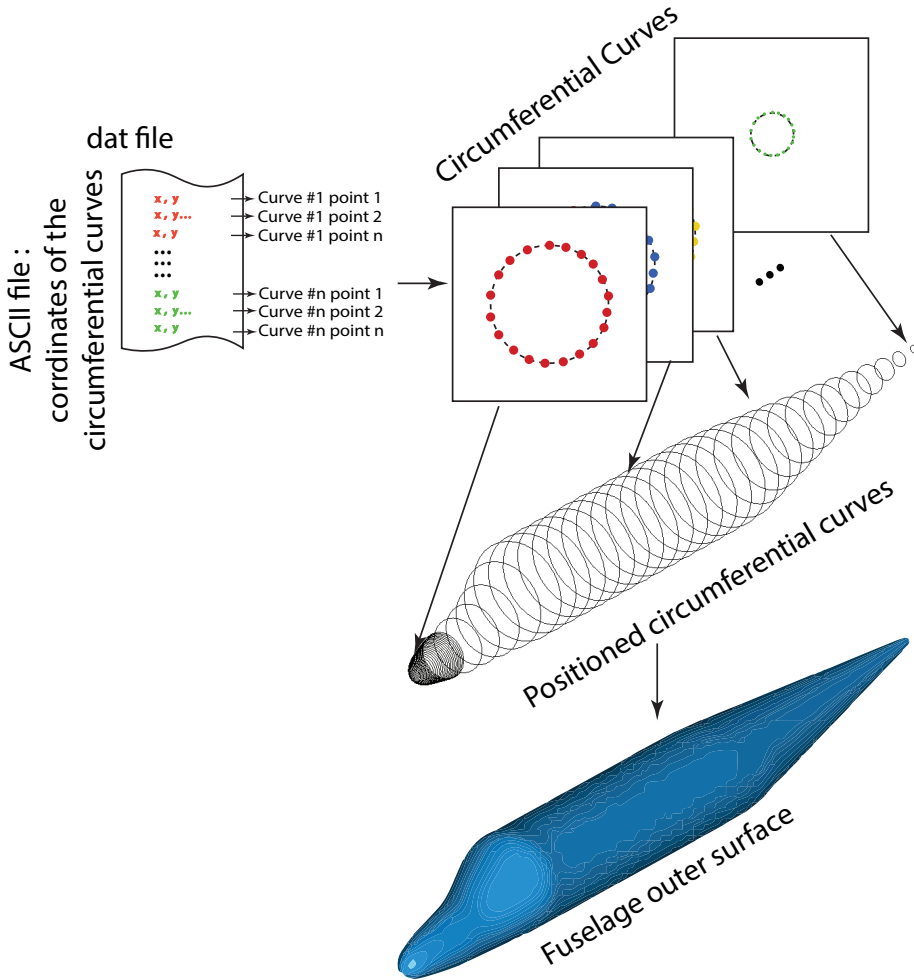
Figure C.27: Process showing the generation of Fuselage outer mold line from the data provided in the input file

C
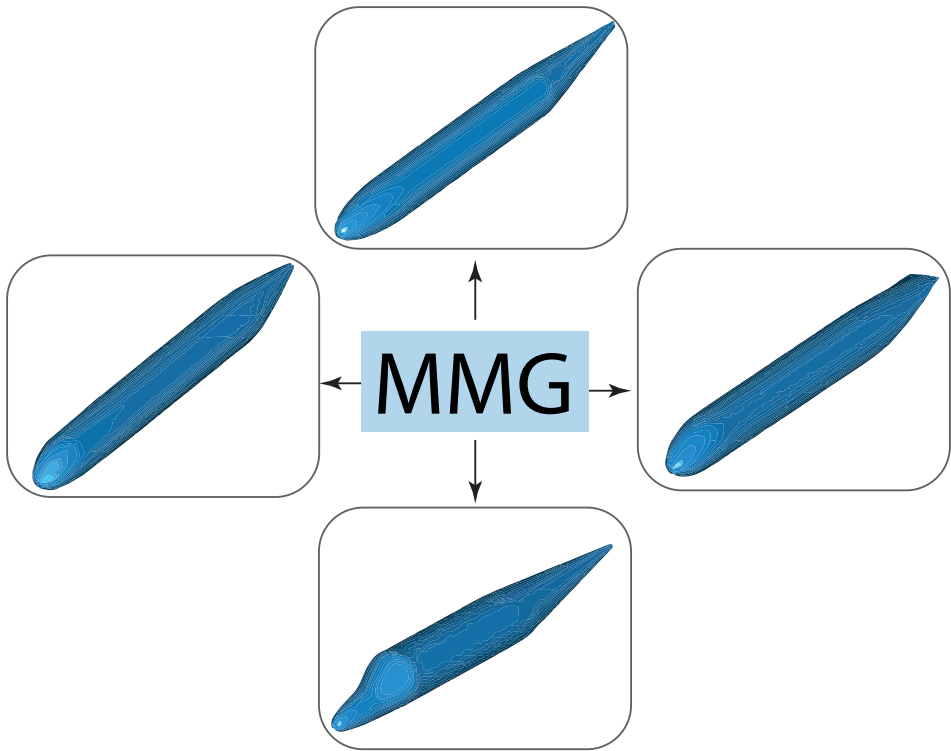
Figure C.28: Different fuselage shapes generated using the Fuselage HLP in MMG

D

VSAERO ANALYSIS FOR SFT MODEL DESIGN

VSAERO is commercial 3D panel code for calculating the subsonic aircraft characteristics of arbitrary configurations having vortex separation and strong vortex-surface interaction. This is achieved by using iterative execution of potential flow panel method coupled with integral boundary layer method and wake-shape iteration calculation [196].

VSAERO is a 3DPM code developed in the 1980s followed by a number of revisions and updates [194]. In this chapter, we compare the accuracy of the static-aerodynamic results generated by VSAERO with a wind-tunnel test performed at Delft University of Technology. Furthermore, we perform some Design of Experiments to verify whether the data generated by VSAERO is suitable for MDAO analysis (i.e., the data is not too noisy and the results are not discontinuous in the design space).

VSAERO analysis for validation: The dimensions of Variable Geometry Model (VGM) are fed into the MMG to generate the structured mesh (Figure 9.1). This mesh is used in VSAERO to simulate the angle of attack sweep from $-5°$ to $14°$ at Reynolds number of 500000. VSAERO was set to use potential flow solver with integral boundary layer equations and Prandtl-Glauert correction. The visualization of wake shape and pressure distribution for steady flight and pitch-up manoeuvre is shown in Figure D.1.

Comparison VSAERO & Wind-tunnel test results: Figure D.2 (a) shows the lift polar gathered from the wind tunnel test and the 3D panel code (VSAERO). This graph shows that VSAERO analysis and the wind-tunnel results have a good match up to $7°$ angle of attack (within 12% of one another). Beyond $7°$, VSAERO follows a linear slope (because of its inability to predict flow separation) whereas the wind-tunnel results indicate separation. The trends of the elevator deflection are correctly represented in the Figure D.2 (a), where, upward elevator deflection results in lower lift for a given angle of attack. Nevertheless, VSAERO demonstrates larger elevator effectiveness as compared to wind-tunnel
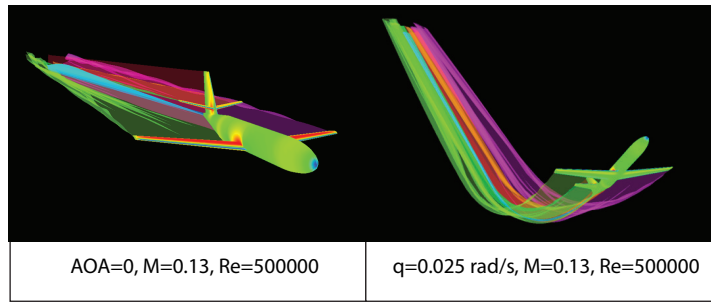
Figure D.1: Visualization of C_p distribution and wake deformation for VGM in steady flight and pitch-up rotation simulated using VSAERO

because VSAERO cannot model separation accurately that often occurs with upward deflection of elevators.

The drag polar is plotted in Figure D.2 (b). The drag obtained from VSAERO analysis is significantly lower (approximately 50% lower) than the wind-tunnel test. This is because VSAERO does not account for interference drag and only implements an approximate model to estimate boundary layer thickness. Thus, the predicted viscous drag is inaccurate. In addition, the separation is not included in the VSAERO model which further (negatively) influences the drag prediction at higher angles of attack. The lower drag has a significant effect on the phugoid motion.

It is important to note that the drag estimated by WT could be higher than drag that will be experienced by the model in SFT because the interference drag due to the presence of support stings has not be corrected in wind-tunnel results shown in Figure D.2 (b). Additionally, corrections have been made for blockage effects (i.e. wake blockage and solid blockage) and streamline curvature but these corrections are based on statistical methods and are not always accurate.

Thus, the actual drag difference between VSAERO analysis and the actual wind-tunnel test might be lower than that indicated in Figure D.2 (b). Nonetheless, even with the best correction to the wind-tunnel results, 50% difference between wind-tunnel and VSAERO results cannot be completely accounted (i.e., the drag modelling in VSAERO significantly under-predicts the interference and viscous drag). The severe drag under-prediction brings to question the accuracy of implementation of drag estimation method in VSAERO.

Figure D.2 (c) shows the moment polars. The moment estimated by VSAERO is lower than WT at low angles of attack and high elevator deflection angles due to the lower effectiveness of the elevator predicted by VSAERO as compared to WT. At high angles of attack, the difference in the moments between wind-tunnel and VSAERO is due to the discrepancies in lift due to the separation at the wing (not modelled in VSAERO), which increases the tail effectiveness thereby increasing pitch-down tendency.

Noise from the solver: For any optimizer to effectively function, the magnitude of numerical noise from a computational tool should be much smaller than the magnitude of the quantity of interest. Furthermore, the computational tool must be able to clearly
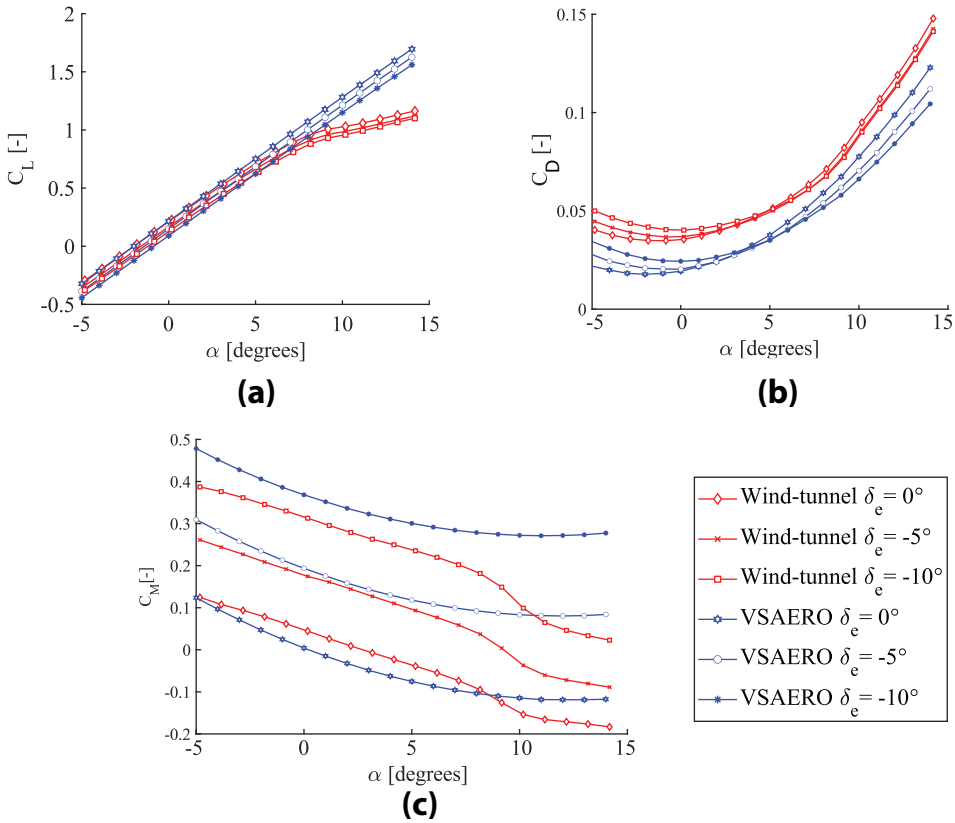
Figure D.2: Variation of static (longitudinal) aerodynamic coefficients ((a) lift coefficient, (b) drag-coefficient and (c) moment coefficient) with angle of attack

demonstrate the impact of varying the inputs on the quantity of interest.

To this end, we performed a design of experiment to determine the longitudinal stability derivatives on a number of geometrically scaled models of (an approximate) Cessna Citation II 550 (see dimensions used in Figure 9.5) at different test velocities. The results of the design of experiment are plotted in Figure D.3.

Figure D.3 shows that the results from VSAERO are noisy and no clear (continuous) trends can be seen. In order to ascertain that the noise is indeed from the solver and not due to the meshing or the setup of the problem, the design of experiment was performed by varying the mesh density, changing the convergence criteria, different compressibility conditions and by disabling integral boundary layer calculations. Irrespective of the problem set and/or mesh definition, random noise was seen in the results obtained from VSAERO[1]. The noise might be due to two main reasons:

---

[1] not all studies are reported here as one example provided in Figure D.3 demonstrates the noise and discontinuity in the results
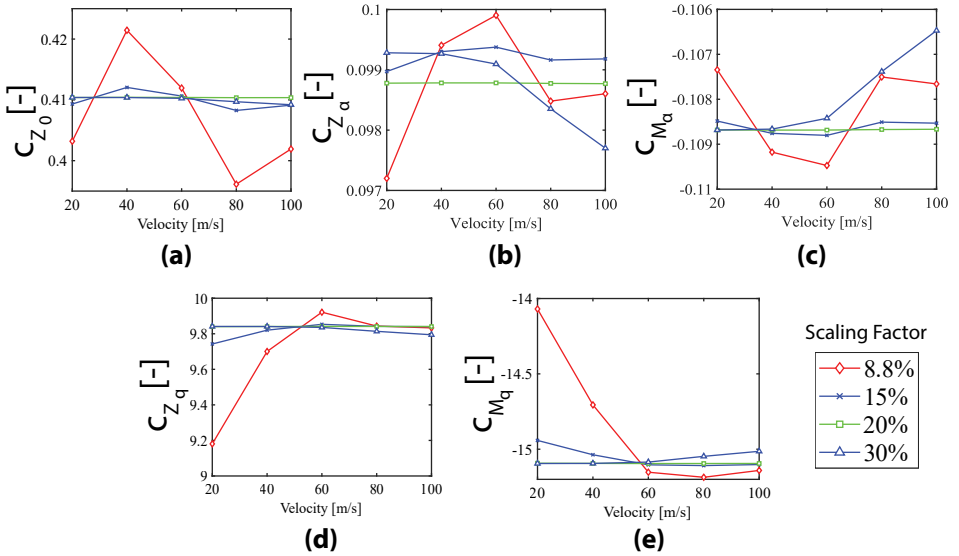
Figure D.3: Variation of different longitudinal stability derivatives (a) C_{Z_0}, (b) C_{Z_α}, (c) C_{M_α}, (d) C_{Z_q} and(e) C_{m_q} at different test velocities and geometric scaling factors evaluated using VSAERO

1. **Truncation error [194]:** due to the difference between the true (analytical) derivative of a function and its derivative obtained by numerical approximation. VSAERO assumes that the contribution from the linear and higher-order terms of both the potential and normal velocity can be neglected compared with the constant term to minimize the total number of unknowns. This leaves only one unknown, to be found for each panel. Higher-order codes, e.g., PAN-AIR, include one or more of the linear and quadratic terms in the potential, thereby having more than one unknown per panel requiring the evaluation of all the related influence coefficient (i.e., requiring longer solver time).

2. **Mean plane approximation [194]:** In order to generate the aerodynamic loads, panel method integrates the pressure/vorticity around the body. However, calculation of these integrals is challenging for a surface with arbitrary curvature. However, for flat panels the calculation is much simpler. VSAERO uses approximate flat panels instead of warped panels (see Figure D.4) and the difference in the influence coefficients between the flat and curved cases is ignored for body surface panels.

Analyzing the source code of a commercial software to identify cause of this behaviour is beyond the scope of this work. Nevertheless, for the purposes of this dissertation, it is important to note that the noisy nature of results is a key barrier in the use of VSAERO for MDAO based similarity maximization.
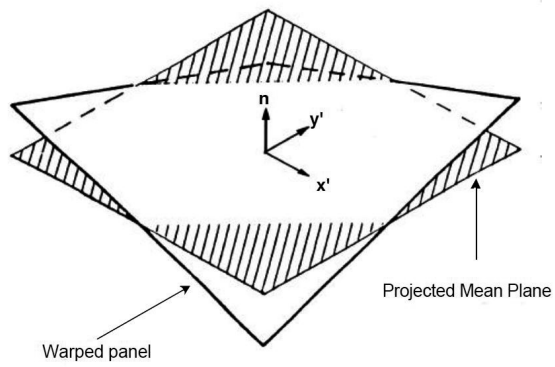
Figure D.4: Mean plane approximation used in VSAERO to overcome the complexities of warped panels
panels
Source: Nathman[194]

E

DESIGN VARIABLES USED IN CASE-STUDIES (INITIAL VALUES)

Table E.1: Design variables used for aerodynamic scaling of SFT model (applicable to case study 1, 4, 5 and 6)

Serial Number	Design Variable	Symbol	Initial values	Lower Bounds	Upper Bounds
1	Velocity [m/s]	v	45	20	80
2	Altitude [m]	h	1000	100	5000
3	Scaling Factor [-]	λ	0.2	0.05	0.3
4	Wing X - location [m]	x_{wing}	5265 * λ	3000 * λ	6700 * λ
5-10	CST root upper [-]	r_{upper}	[0.2064, 0.0775, 0.2387, 0.1592, 0.00147, 0.3012]	0.6*r_{upper}	1.4*r_{upper}
11-16	CST Root Lower [-]	r_{lower}	[-0.2011, -0.3124, -0.0687, -0.1762, -0.00147, 0.3726]	0.6*r_{lower}	1.4*r_{lower}
17-22	CST tip upper [-]	t_{upper}	[0.1780, 0.05208, 0.2156, 0.1358, 0.00126, 0.3017]	0.6*t_{upper}	1.4*t_{upper}
23-28	CST tip Lower [-]	t_{lower}	[-0.1712, -0.2810, -0.04858, -0.1513, -0.00126, 0.3608]	0.6*t_{lower}	1.4*t_{lower}

Table E.2: Design variables used to optimize CG of SFT model to maximize DoS (applicable to case study 2-6)

Serial Number	Design Variable	Symbol	Initial values	Lower Bounds	Upper Bounds
1	Floor #1 Start [% Fuselage length]	F_{1s}	0.1	0.05	0.2
2	Floor #2 Start [% Fuselage length]	F_{2s}	0.3	0.15	0.5
3	Floor #3 Start [% Fuselage length]	F_{3s}	0.6	0.45	0.8
4	Floor #1 End [% Fuselage length]	F_{1e}	0.35	0.27	0.5
5	Floor #2 End [% Fuselage length]	F_{2e}	0.65	0.5	0.85
6	Floor #3 End [% Fuselage length]	F_{3e}	0.8	0.79	0.9
7	Floor #1 Height [% Fuselage Diameter]	F_{1h}	0.2	0.1	0.4
8	Floor #2 Height [% Fuselage Diameter]	F_{2h}	0.5	0.4	0.75
9	Floor #3 Height [% Fuselage Diameter]	F_{3h}	0.2	0.1	0.4
10	Nose Landing Gear [% Fuselage length]	L_1	0.1	0.05	0.3
11	Main Landing Gear [% Fuselage length]	L_2	0.7	0.65	0.85

Table E.3: Additional design variables to case-study 2 (applicable to case study 3-6) variables used for the weight and balance scaling (see Table E.2 for first 11 design variables)

Serial Number	Variable name	Symbol	Initial values	Lower Bounds	Upper Bounds
12	Mass #1 [kg]	m_1	2.5	0	3
13	Mass #2 [kg]	m_2	2.5	0	3
14	Mass #3 [kg]	m_3	2.5	0	3
15	Mass #1 x location [% floor length]	x_{m1}	0.5	0	1
16	Mass #2 x location [% floor length]	x_{m2}	0.5	0	1
17	Mass #3 x location [% floor length]	x_{m3}	0.5	0	1
18	Mass #1 y location [% floor width]]	y_{m1}	0.5	0	1
19	Mass #2 y location [% floor width]]	y_{m2}	0.5	0	1
20	Mass #3 y location [% floor width]]	y_{m3}	0.5	0	1

E

Table E.4: Additional aerodynamic design variables used in Case-study 6

Serial Number	Variable name	Symbol	Initial values	Lower Bounds	Upper Bounds
29	Wing Scaling Factor [-]	λ_{wing}	0.2	0.04	0.4

Table E.5: Aerodynamic design variables (applicable to case study 7) used in the design of box-wing aircraft SFT model (see Figure 10.38)

Serial Number	Variable name	Symbol	Initial values	Lower Bounds	Upper Bounds
1	Velocity [m/s]	v	45	20	80
2	Altitude [m]	h	1000	100	5000
3	Scaling Factor [-]	λ	0.056	0.04	0.3
4	Front-wing root airfoil thickness [%]	$t_{f_{root}}$	100	60	140
5	Front-wing tip airfoil thickness [%]	$t_{f_{tip}}$	100	60	140
6	Rear-wing root airfoil thickness [%]	$t_{r_{root}}$	100	60	140
7	Rear-wing tip airfoil thickness [%]	$t_{r_{tip}}$	100	60	140

E

Table E.6: Weight & Balance Design variables used in case-study 7

Serial Number	Variable name	Symbol	Initial values	Lower Bounds	Upper Bounds
1	Floor #1 Start [% Fuselage length]	F_{1s}	0.05	0.03	0.25
2	Floor #2 Start [% Fuselage length]	F_{2s}	0.35	0.25	0.55
3	Floor #3 Start [% Fuselage length]	F_{3s}	0.7	0.65	0.9
4	Floor #1 End [% Fuselage length]	F_{1e}	0.2	0.15	0.5
5	Floor #2 End [% Fuselage length]	F_{2e}	0.55	0.4	0.85
6	Floor #3 End [% Fuselage length]	F_{3e}	0.81	0.7	0.98
7	Floor #1 Height [% Fuselage Diameter]	F_{1h}	0.4	0.1	0.4
8	Floor #2 Height [% Fuselage Diameter]	F_{2h}	0.6	0.4	0.9
9	Floor #3 Height [% Fuselage Diameter]	F_{3h}	0.4	0.1	0.7
10	Mass #1 [kg]	m_1	3	0	5
11	Mass #2 [kg]	m_2	0.01	0	3
12	Mass #3 [kg]	m_3	0.01	0	3
13	Mass #1 x location [% floor length]	x_{m1}	0.1	0	1
14	Mass #2 x location [% floor length]	x_{m2}	0.1	0	1
15	Mass #3 x location [% floor length]	x_{m3}	0.1	0	1
16	Mass #1 y location [% floor width]]	y_{m1}	0.5	0	1
17	Mass #2 y location [% floor width]]	y_{m2}	0.5	0	1
18	Mass #3 y location [% floor width]]	y_{m3}	0.5	0	1

E

F

DESIGN VARIABLES USED IN CASE-STUDIES (OPTIMIZED VALUES)

Table F.1: The values of design variables before and after optimization for Case-Study 1 (see initial values and bounds in Table E.1)

	Full-scale Aircraft	Geometrically Scaled Model	Aerodynamically Scaled Model
V [m/s]	200	50	31
h [m]	10000	1000	576
λ [-]	1.000	0.200	0.125
x_{wing} [m]	5.265*λ	5.265*λ	6.531*λ
r_{upper} [-]	[0.2064, 0.07759, 0.2387, 0.1592, 0.0014, 0.3012]	[0.2064, 0.07759, 0.2387, 0.1592, 0.0014, 0.3012]	[0.2475, 0.0621, 0.1912, 0.1275, 0.0012, 0.3592]
r_{lower} [$-$]	[-0.2011, -0.3124, -0.0687, -0.1762, -0.0014, 0.3726]	[-0.2011, -0.3124, -0.0687, -0.1762, -0.0014, 0.3726]	[-0.2392, -0.2503, -0.0825, -0.2112 -0.0017 0.4467]
t_{upper} [-]	[0.1780, 0.0520, 0.2156, 0.1358, 0.0012, 0.3017]	[0.1780, 0.0520, 0.2156, 0.1358, 0.0012, 0.3017]	[0.1415, 0.0624, 0.1727, 0.1079, 0.0014, 0.2398]
t_{lower} [-]	[-0.1712, -0.2810, -0.0485, -0.15135, -0.0012, 0.3608]	[-0.1712, -0.2810, -0.0485, -0.15135, -0.0012, 0.3608]	[-0.2042, -0.2234, -0.0389, -0.1202, -0.0010, 0.2891]

Table F.2: The final values of design variables obtained for the two CG optimization studies (Case-Study 2) performed using geometrically-scaled model and aerodynamically-scaled model obtained in Case-Study 1 (see initial values and bounds in Table E.2)

Serial Number	Variable name	Symbol	Geometric (Optimized COTS position)	Aerodynamic (Optimized COTS position)
1	Floor #1 Start [% Fuselage length]	F_{1s}	0.1	0.1
2	Floor #2 Start [% Fuselage length]	F_{2s}	0.15	0.26
3	Floor #3 Start [% Fuselage length]	F_{3s}	0.45	0.5625
4	Floor #1 End [% Fuselage length]	F_{1e}	0.35	0.35
5	Floor #2 End [% Fuselage length]	F_{2e}	0.65	0.65
6	Floor #3 End [% Fuselage length]	F_{3e}	0.9	0.9
7	Floor #1 Height [% Fuselage Diameter]	F_{1h}	0.21	0.11
8	Floor #2 Height [% Fuselage Diameter]	F_{2h}	0.48	0.49
9	Floor #3 Height [% Fuselage Diameter]	F_{3h}	0.26	0.19
10	Nose Landing Gear [% Fuselage length]	L_1	0.106	0.13
11	Main Landing Gear [% Fuselage length]	L_2	0.7	0.7

F

Table F.3: The final values of design variables obtained after weight and balance scaling optimization - Case-Study 3 (see initial values and bounds in Table E.2)

Serial Number	Design Variable	Symbol	Optimized values
1	Floor #1 Start [% Fuselage length]	F_{1s}	0.16
2	Floor #2 Start [% Fuselage length]	F_{2s}	0.15
3	Floor #3 Start [% Fuselage length]	F_{3s}	0.45
4	Floor #1 End [% Fuselage length]	F_{1e}	0.46
5	Floor #2 End [% Fuselage length]	F_{2e}	0.65
6	Floor #3 End [% Fuselage length]	F_{3e}	0.90
7	Floor #1 Height [% Fuselage length]	F_{1h}	0.19
8	Floor #2 Height [% Fuselage length]	F_{2h}	0.47
9	Floor #3 Height [% Fuselage length]	F_{3h}	0.20
10	Nose Landing Gear [% Fuselage length]	L_1	0.12
11	Main Landing Gear [% Fuselage length]	L_2	0.70
12	Mass #1 [kg]	m_1	1.29
13	Mass #2 [kg]	m_2	2.27
14	Mass #3 [kg]	m_3	3.01
15	Mass #1 x location [% Floor length]	x_{m1}	0.62
16	Mass #2 x location [% Floor length]	x_{m2}	0.62
17	Mass #3 x location [% Floor length]	x_{m3}	0.33
18	Mass #1 y location [% Floor length]	y_{m1}	0.50
19	Mass #2 y location [% Floor length]	y_{m2}	0.50
20	Mass #3 y location [% Floor length]	y_{m3}	0.50

F

Table F.4: The final values of aerodynamic design variables obtained after aerodynamic - W&B scaling optimization - Case-Study 4 (see initial values and bounds in Table E.1)

Sl. No.	Variables	Full-scale Aircraft	Optimized Design
1	V [m/s]	200	50.2
2	h [m]	10000	1017
3	λ [-]	1	0.158
4	x_{wing} [m]	5265*λ	6375*λ
5-10	r_{upper} [-]	[0.2064, 0.0775, 0.2387, 0.1592, 0.00147, 0.3012]	[0.2059, 0.0763, 0.2348, 0.1546, 0.0015,0.2875]
11-16	r_{lower} [-]	[-0.2011, -0.3124, -0.0687, -0.1762, -0.00147, 0.3726]	[-0.1942, -0.3134, -0.0647, -0.1720, -0.0014, 0.3642]
17-22	t_{upper} [-]	[0.1780, 0.05208,0.2156, 0.1358,0.00126, 0.3017]	[0.1760, 0.0526, 0.2101, 0.1322, 0.0012, 0.2831]
23-28	t_{lower} [-]	[-0.1712, -0.2810, -0.04858, -0.1513, -0.00126, 0.3608]	[-0.1651, -0.2639, -0.0505, -0.1468, -0.0012, 0.3446]

F

Table F.5: The final values of W&B design variables obtained after aerodynamic - W&B scaling optimization - Case-Study 4 (see initial values and bounds in Table E.2 and E.3)

Serial Number	Variable name	Symbol	Optimized values
1	Floor #1 Start [% Fuselage length]	F_{1s}	0.107
2	Floor #2 Start [% Fuselage length]	F_{2s}	0.32
3	Floor #3 Start [% Fuselage length]	F_{3s}	0.56
4	Floor #1 End [% Fuselage length]	F_{1e}	0.37
5	Floor #2 End [% Fuselage length]	F_{2e}	0.65
6	Floor #3 End [% Fuselage length]	F_{3e}	0.9
7	Floor #1 Height [% Fuselage length]	F_{1h}	0.19
8	Floor #2 Height [% Fuselage length]	F_{2h}	0.5
9	Floor #3 Height [% Fuselage length]	F_{3h}	0.19
10	Nose Landing Gear [% Fuselage length]	L_1	0.11
11	Main Landing Gear [% Fuselage length]	L_2	0.7
12	Mass #1 [kg]	m_1	2.63
13	Mass #2 [kg]	m_2	2.49
14	Mass #3 [kg]	m_3	2.25
15	Mass #1 x location [% Floor length]	x_{m1}	0.46
16	Mass #2 x location [% Floor length]	x_{m2}	0.45
17	Mass #3 x location [% Floor length]	x_{m3}	0.46
18	Mass #1 y location [% Floor length]	y_{m1}	0.5
19	Mass #2 y location [% Floor length]	y_{m2}	0.5
20	Mass #3 y location [% Floor length]	y_{m3}	0.5

F

Table F.6: The final values of aerodynamic design variables obtained after aerodynamic - W&B scaling optimization with flight mechanics constraints - Case-Study 5 (see initial values and bounds in Table E.1)

Sl. No.	Variables	Full-scale Aircraft	Optimized Design
1	V [m/s]	200	50.2
2	h [m]	10000	1006
3	λ [-]	1	0.1735
4	x_{wing} [m]	5265*λ	5953.3*λ
5-10	r_{upper} [-]	[0.2064, 0.0775, 0.2387, 0.1592, 0.00147, 0.3012]	[0.2068, 0.0720, 0.2392, 0.1598, 0.00147, 0.3015]
11-16	r_{lower} [-]	[-0.2011, -0.3124, -0.0687, -0.1762, -0.00147, 0.3726]	[-0.1869, -0.3154, -0.0685, -0.1773, -0.00147, 0.3739]
17-22	t_{upper} [-]	[0.1780, 0.05208, 0.2156, 0.1358, 0.00126, 0.3017]	[0.1796, 0.05179, 0.2135, 0.1349, 0.0012, 0.3025]
23-28	t_{lower} [-]	[-0.1712, -0.2810, -0.04858, -0.1513, -0.00126, 0.3608]	[-0.1705, -0.2796, -0.0488, -0.1523, -0.00127, 0.3604]

F

Table F.7: The final values of W&B design variables obtained after aerodynamic - W&B scaling optimization with flight mechanics constraints - Case-Study 5 (see initial values and bounds in Table E.2 and E.3)

Serial Number	Variable name	Symbol	Optimized values
1	Floor #1 Start [% Fuselage length]	F_{1s}	0.10
2	Floor #2 Start [% Fuselage length]	F_{2s}	0.27
3	Floor #3 Start [% Fuselage length]	F_{3s}	0.57
4	Floor #1 End [% Fuselage length]	F_{1e}	0.275
5	Floor #2 End [% Fuselage length]	F_{2e}	0.49
6	Floor #3 End [% Fuselage length]	F_{3e}	0.74
7	Floor #1 Height [% Fuselage length]	F_{1h}	0.20
8	Floor #2 Height [% Fuselage length]	F_{2h}	0.50
9	Floor #3 Height [% Fuselage length]	F_{3h}	0.19
10	Mass #1 [kg]	m_1	2.06
11	Mass #2 [kg]	m_2	2.52
12	Mass #3 [kg]	m_3	2.48
13	Mass #1 x location [% Floor length]	x_{m1}	0.09
14	Mass #2 x location [% Floor length]	x_{m2}	0.08
15	Mass #3 x location [% Floor length]	x_{m3}	0.10
16	Mass #1 y location [% Floor length]	y_{m1}	0.50
17	Mass #2 y location [% Floor length]	y_{m2}	0.50
18	Mass #3 y location [% Floor length]	y_{m3}	0.50

F

Table F.8: The final values of aerodynamic design variables obtained after aerodynamic - W&B scaling optimization with flight mechanics constraints - Case-Study 6 (see initial values and bounds in Table E.1 and E.4)

Sl. No.	Variables	Full-scale Aircraft	Optimized Design
1	V [m/s]	200	50.93
2	h [m]	10000	1040
3	λ [-]	1	0.165
4	x_{wing} [m]	5265*λ	6330*λ
5-10	r_{upper} [-]	[0.2064, 0.0775, 0.2387, 0.1592, 0.00147, 0.3012]	[0.2137, 0.0665, 0.2389, 0.1449, 0.0015, 0.2847]
11-16	r_{lower} [-]	[-0.2011, -0.3124, -0.0687, -0.1762, -0.00147, 0.3726]	[-0.1676, -0.3203, -0.0714, -0.17876, -0.00145, 0.3441]
17-22	t_{upper} [-]	[0.1780, 0.05208,0.2156, 0.1358,0.00126, 0.3017]	[0.15688, 0.0534, 0.2228, 0.1251, 0.00125, 0.2866]
23-28	t_{lower} [-]	[-0.1712, -0.2810, -0.04858, -0.1513, -0.00126, 0.3608]	[-0.17006, -0.2591, -0.0456, -0.1398, -0.0013, 0.3597]
29	λ_{wing} [-]	1	0.162

Table F.9: The final values of W&B design variables for short-period motion and roll-damping similarity - Case-Study 6 (see initial values and bounds in Table E.2 and E.3)

Serial Number	Variable name	Symbol	Optimized values
1	Floor #1 Start [% Fuselage] length]	F_{1s}	0.10
2	Floor #2 Start [% Fuselage] length]	F_{2s}	0.22
3	Floor #3 Start [% Fuselage] length]	F_{3s}	0.55
4	Floor #1 End [% Fuselage] length]	F_{1e}	0.28
5	Floor #2 End [% Fuselage] length]	F_{2e}	0.46
6	Floor #3 End [% Fuselage] length]	F_{3e}	0.74
7	Floor #1 Height [% Fuselage] length]	F_{1h}	0.20
8	Floor #2 Height [% Fuselage] length]	F_{2h}	0.50
9	Floor #3 Height [% Fuselage] length]	F_{3h}	0.19
10	Mass #1 [kg]	m_1	2.13
11	Mass #2 [kg]	m_2	2.65
12	Mass #3 [kg]	m_3	2.51
13	Mass #1 x location [% Floor length]	x_{m1}	0.10
14	Mass #2 x location [% Floor length]	x_{m2}	0.007
15	Mass #3 x location [% Floor length]	x_{m3}	0.10
16	Mass #1 y location [% Floor length]	y_{m1}	0.50
17	Mass #2 y location [% Floor length]	y_{m2}	0.50
18	Mass #3 y location [% Floor length]	y_{m3}	0.50

F

Table F.10: The final values of aerodynamic design variables obtained after aerodynamic - W&B scaling optimization with flight mechanics constraints for unconventional design - Case-Study 7 (see initial values and bounds in Table E.5)

Sl. No.	Variables	Full-scale Aircraft	Optimized Design
1	v [m/s]	200	42
2	h [m]	10000	323
3	λ [-]	1	0.04
4	$t_{f_{root}}$ [-]	100	129
5	$t_{f_{tip}}$ [-]	100	95
6	$t_{r_{root}}$ [-]	100	100
7	$t_{r_{tip}}$ [-]	100	91

F

Table F.11: The final values of W&B design variables for short-period motion of unconventional aircraft - Case-Study 7 (see initial values and bounds in Table E.6)

Serial Number	Variable name	Symbol	Optimized values
1	Floor #1 Start [% Fuselage length]	F_{1s}	0.05
2	Floor #2 Start [% Fuselage length]	F_{2s}	0.38
3	Floor #3 Start [% Fuselage length]	F_{3s}	0.65
4	Floor #1 End [% Fuselage length]	F_{1e}	0.32
5	Floor #2 End [% Fuselage length]	F_{2e}	0.52
6	Floor #3 End [% Fuselage length]	F_{3e}	0.76
7	Floor #1 Height [% Fuselage length]	F_{1h}	0.34
8	Floor #2 Height [% Fuselage length]	F_{2h}	0.40
9	Floor #3 Height [% Fuselage length]	F_{3h}	0.20
10	Mass #1 [kg]	m_1	2.29
11	Mass #2 [kg]	m_2	0
12	Mass #3 [kg]	m_3	0
13	Mass #1 x location [% Floor length]	x_{m1}	0.13
14	Mass #2 x location [% Floor length]	x_{m2}	0.06
15	Mass #3 x location [% Floor length]	x_{m3}	0.07
16	Mass #1 y location [% Floor length]	y_{m1}	0.50
17	Mass #2 y location [% Floor length]	y_{m2}	0.50
18	Mass #3 y location [% Floor length]	y_{m3}	0.50

F

G

xDSM USED IN CASE-STUDIES

Figure G.1: xDSM of the optimization problem solved in Case-Study 1

Figure G.2: xDSM of the optimization problem solved in Case-Study 2 and 3. Note, the design variables x_i, y_i and m_i are only applicable to case-study 3.
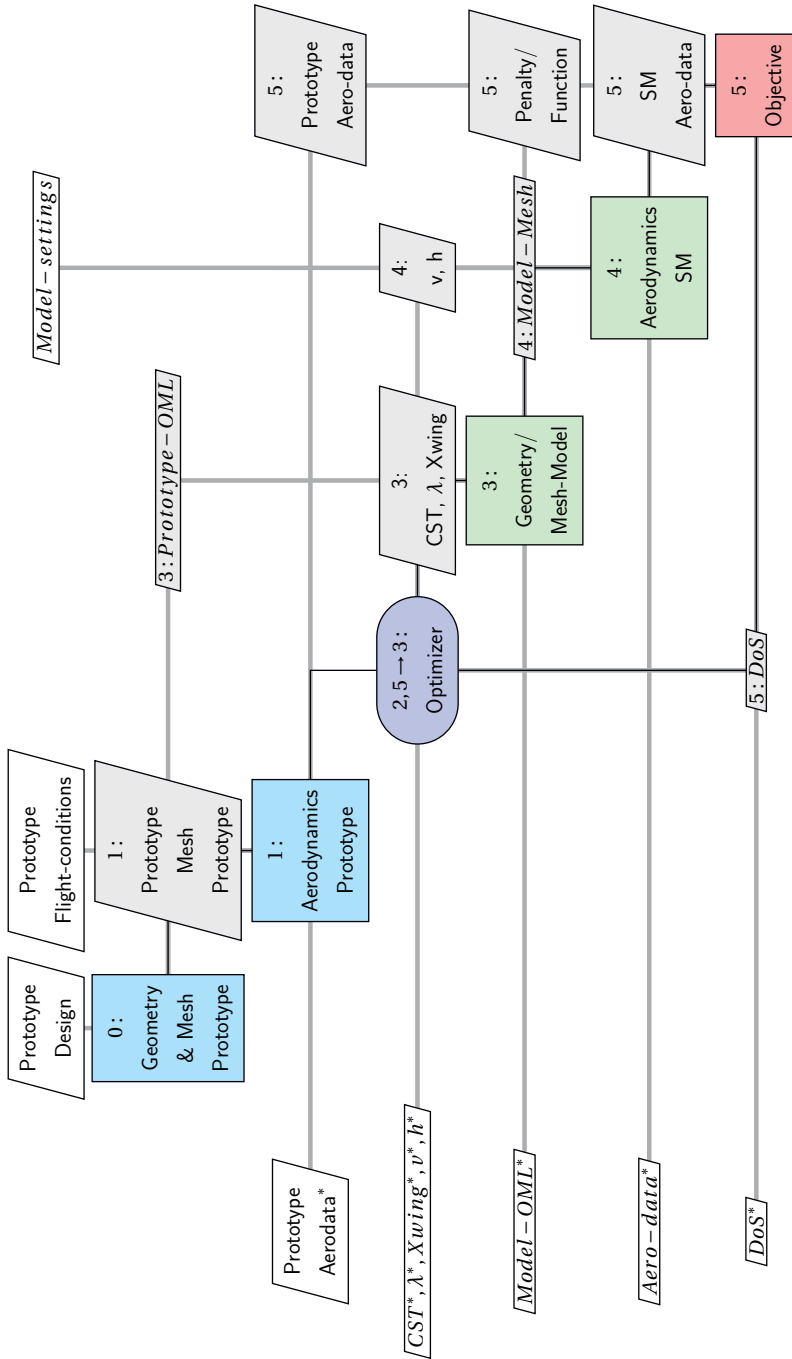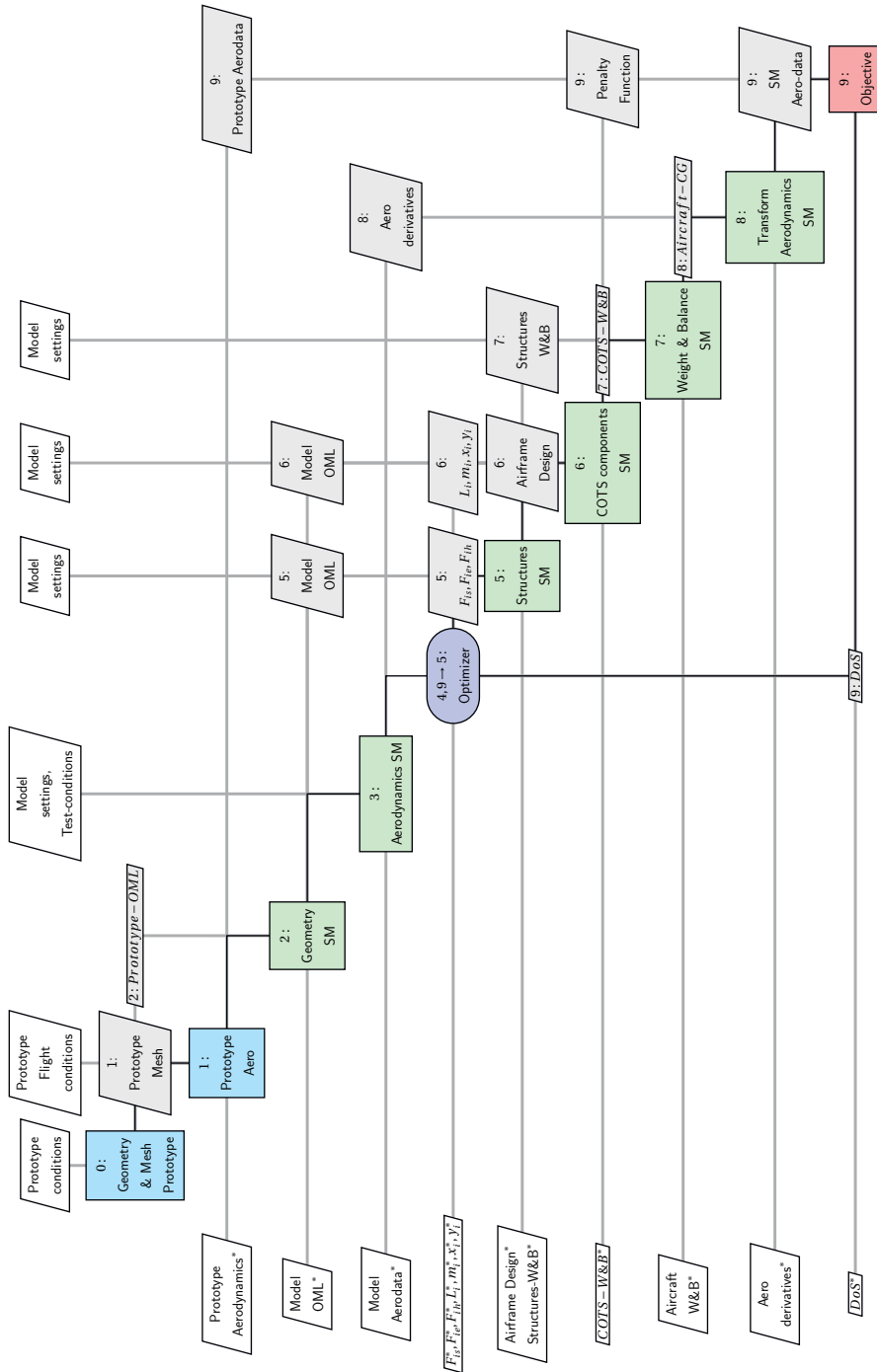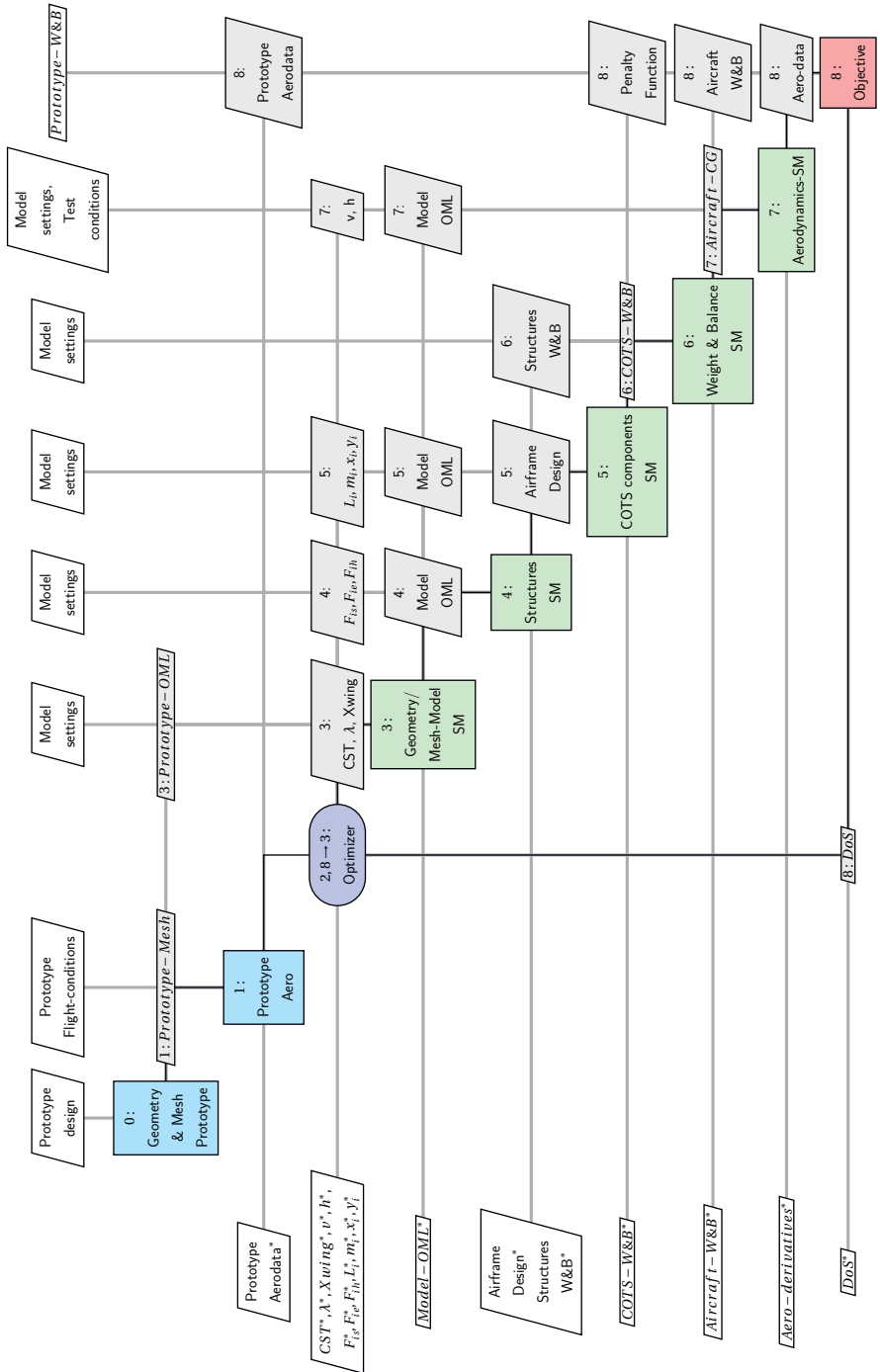
Figure G.3: xDSM of the optimization problem solved in Case-Study 4
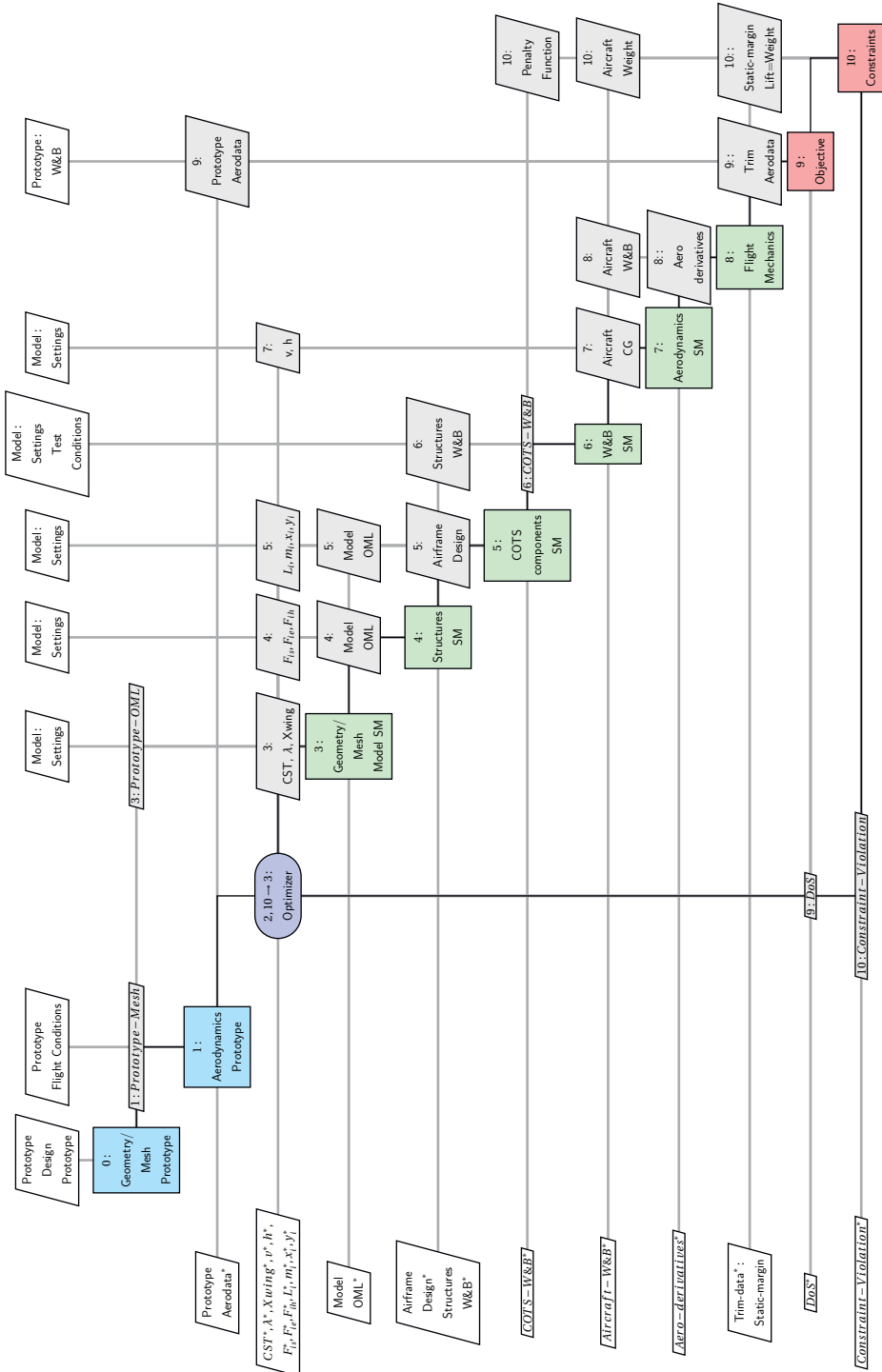
Figure G.4: xDSM of the optimization problem solved in Case-Study 5-7. Note, for case-study 7, instead of CST coefficients, airfoil thicknesses are used.

BIBLIOGRAPHY

[1]   *Facts & figures*. URL: https://www.atag.org/facts-figures.html (visited on 12/01/2020).

[2]   *The World of Air Transport in 2018*. URL: https://www.icao.int/annual-report-2018/Pages/the-world-of-air-transport-in-2018.aspx (visited on 12/01/2020).

[3]   *Air transport, passengers carried | Data*. URL: https://data.worldbank.org/indicator/IS.AIR.PSGR?end=2018&start=2000 (visited on 12/01/2020).

[4]   *Waypoint 2050*. URL: https://aviationbenefits.org/environmental-efficiency/climate-action/waypoint-2050/ (visited on 05/12/2021).

[5]   IATA. *IATA - Environmental Policy*. URL: http://www.iata.org/policy/environment/Pages/default.aspx (visited on 09/28/2017).

[6]   IATA. *IATA - Environment*. URL: http://www.iata.org/whatwedo/environment/Pages/index.aspx (visited on 09/28/2017).

[7]   IATA. *IATA - Aircraft Noise*. URL: http://www.iata.org/policy/environment/pages/aircraft-noise.aspx (visited on 09/28/2017).

[8]   IATA. *2036 Forecast Reveals Air Passengers Will Nearly Double to 7.8 Billion*. English. URL: https://www.iata.org/pressroom/pr/pages/2017-10-24-01.aspx (visited on 11/23/2018).

[9]   *Safety Reports*. URL: https://www.icao.int/safety/pages/safety-report.aspx (visited on 05/12/2021).

[10]   David S. Lee et al. "The contribution of global aviation to anthropogenic climate forcing for 2000 to 2018". In: *Atmospheric Environment* 244 (2021), p. 117834.

[11]   *Environmental noise in Europe — 2020 — European Environment Agency*. URL: https://www.eea.europa.eu/publications/environmental-noise-in-europe (visited on 12/03/2020).

[12]   The Technology Sub-Group of Air Travel – Greener by Design. *Air Travel – Greener by Design Mitigating the environmental impact of aviation: Opportunities and priorities | The Aeronautical Journal | Cambridge Core*. URL: https://www.cambridge.org/core/journals/aeronautical-journal/article/abs/air-travel-greener-by-design-mitigating-the-environmental-impact-of-aviation-opportunities-and-priorities/E4A2B1A182F2BEC94EFDAEBE9B05B417 (visited on 05/11/2021).

[13]   *Latest publications*. URL: https://www.atag.org/our-publications/latest-publications.html (visited on 12/01/2020).

[14]   *Aircraft Noise Exposure in the U.S.* Airlines For America. URL: https://www.airlines.org/dataset/u-s-airlines-tremendous-noise-record/ (visited on 12/05/2020).

[15]   European Aviation Safety Agency. and EAA. *European aviation environmental: report 2019*. LU: Publications Office, 2019. URL: https://data.europa.eu/doi/10.2822/309946 (visited on 12/05/2020).

[16]   Egbert Torenbeek. *Advanced aircraft design: conceptual design, analysis and optimization of subsonic civil airplanes*. John Wiley & Sons, 2013.

[17]   Egbert Torenbeek. *Synthesis of subsonic airplane design: an introduction to the preliminary design of subsonic general aviation and transport aircraft, with emphasis on layout, aerodynamic design, propulsion and performance*. Springer Science & Business Media, 2013.

[18]   Daniel Raymer. *Aircraft design: a conceptual approach*. American Institute of Aeronautics and Astronautics, Inc., 2012.

[19]   Aldo Frediani. "The prandtl wing". In: *von Karman Institute for Fluid Dynamics: VKI Lecture Series: Innovative Configurations and Advanced Concepts for Future Civil Transport Aircraft. Rhode St-Genèse: Von Kármán Institute for Fluid Dynamics* (2005).

[20]   R. Vos and M. F. M. Hoogreef. "System-level assessment of tail-mounted propellers for regional aircraft". en. In: *Proceedings of the 31st Congress of the International Council of the Aeronautical Sciences* (2018). URL: https://repository.tudelft.nl/islandora/object/uuid%3Aa1674c88-2df1-4365-8c3a-efde47de7f8c (visited on 04/15/2020).

[21]   H. Kok, Mark Voskuijl, and Michel van Tooren. "Distributed propulsion featuring boundary layer ingestion engines for the blended wing body subsonic transport". In: *51st AIAA/ASME/ASCE/AHS/ASC Structures, Structural Dynamics, and Materials Conference 18th AIAA/ASME/AHS Adaptive Structures Conference 12th*. 2010, p. 3064.

[22]   Benjamin J. Brelje and Joaquim R. R. A. Martins. "Electric, hybrid, and turboelectric fixed-wing aircraft: A review of concepts, models, and design approaches". en. In: *Progress in Aerospace Sciences* 104 (Jan. 2019), pp. 1–19. ISSN: 0376-0421. DOI: 10.1016/j.paerosci.2018.06.004. URL: http://www.sciencedirect.com/science/article/pii/S0376042118300356 (visited on 03/06/2020).

[23]   Joseph R. Chambers and Robert M. Hall. "Historical Review of Uncommanded Lateral-Directional Motions at Transonic Conditions". en. In: *Journal of Aircraft* 41.3 (May 2004), pp. 436–447. ISSN: 0021-8669, 1533-3868. DOI: 10.2514/1.4470. URL: https://arc.aiaa.org/doi/10.2514/1.4470 (visited on 12/17/2019).

[24]   Robert Hall et al. "Computational Methods for Stability and Control (COMSAC): The Time Has Come". en. In: *AIAA Atmospheric Flight Mechanics Conference and Exhibit*. San Francisco, California: American Institute of Aeronautics and Astronautics, Aug. 2005. ISBN: 978-1-62410-055-0. DOI: 10.2514/6.2005-6121. URL: http://arc.aiaa.org/doi/10.2514/6.2005-6121 (visited on 12/17/2019).

[25]   Glenn Murphy. *Similitude in engineering*. Ronald Press Co., 1950.

[26]   Wenbin Wei and Mark Hansen. "Cost Economics of Aircraft Size". In: *Journal of Transport Economics and Policy* 37.2 (2003), pp. 279–296. ISSN: 0022-5258. URL: `https://www.jstor.org/stable/20053934` (visited on 09/08/2020).

[27]   David Starkie and Simon Ellis. "The production economics of a very large civil aircraft". en. In: *Journal of Air Transport Management* 2.1 (Mar. 1995), pp. 11–16. ISSN: 09696997. DOI: `10.1016/0969-6997(95)00020-C`. URL: `https://linkinghub.elsevier.com/retrieve/pii/096969979500020C` (visited on 09/08/2020).

[28]   Dominique Paul Bergmann et al. "Innovative Scaled Test Platform e-Genius-Mod — Scaling Methods and Systems Design". In: *Aerospace* 6.2 (2019), p. 20.

[29]   Daniel Kuehme et al. "Flight Test Evaluation and System Identification of the Area-I Prototype-Technology-Evaluation Research Aircraft (PTERA)". In: *AIAA Flight Testing Conference*. 2014, p. 2577.

[30]   Christopher Jouannet et al. "Design of a very light jet and a dynamically scaled demonstrator". In: *46th AIAA Aerospace Sciences Meeting and Exhibit*. 2008, pp. 7–10.

[31]   TJD Models. *TJD Models Radio Control Trainer Planes*. URL: `https://www.tjdmodels.com/electric-aircraft-trainer-c-12_29_76.html` (visited on 11/19/2020).

[32]   Alexander Kurte. *HST® Impeller mit vollintegrierten Motoren*. de-de. URL: `https://schuebeler-jets.de/de/?Itemid=%7B107%7D` (visited on 11/19/2020).

[33]   Model Aircraft Company. *Micro turbines for remote controlled model jets - Model Aircraft Company*. URL: `http://modelaircraftcompany.com/newshop/en/18-micro-jet-turbines` (visited on 11/19/2020).

[34]   Jetcat. *Products - JetCat*. URL: `https://www.jetcat.de/en/products/` (visited on 10/09/2020).

[35]   A. Raju Kulkarni et al. "Sub-scale flight test model design: Developments, challenges and opportunities". In: *Progress in Aerospace Sciences* 130 (2022), p. 100798.

[36]   Joaquim R. R. A. Martins. "Perspectives on aerodynamic design optimization". In: *AIAA Scitech 2020 Forum*. American Institute of Aeronautics and Astronautics. DOI: `10.2514/6.2020-0043`. URL: `https://arc.aiaa.org/doi/abs/10.2514/6.2020-0043` (visited on 09/28/2020).

[37]   Yitong Fan and Weipeng Li. "Review of Far-Field Drag Decomposition Methods for Aircraft Design". In: *Journal of Aircraft* 56.1 (2019), pp. 11–21. DOI: `10.2514/1.C034781`. URL: `https://doi.org/10.2514/1.C034781` (visited on 09/28/2020).

[38]   Antonio Viviani et al. "CFD design capabilities for next generation high-speed aircraft". In: *Acta Astronautica* (2020).

[39]   Douglas Greenwell. "A review of unsteady aerodynamic modelling for flight dynamics of manoeuvrable aircraft". In: *AIAA Atmospheric Flight Mechanics Conference and Exhibit*. 2004, p. 5276.

[40]   Mehdi Ghoreyshi et al. "Framework for establishing limits of tabular aerodynamic
       models for flight dynamics analysis". In: *Journal of Aircraft* 48.1 (2011), pp. 42–55.

[41]   Joseph Chambers. *Modeling Flight NASA Latest Version: The role of dynamically
       scale Free Flight Models in support of NASA aerospace programs.* Vol. 3. Joseph
       Chambers, 2015. (Visited on 10/02/2017).

[42]   Chester H. Wolowicz, J. S. Brown Jr, and William P. Gilbert. "Similitude require-
       ments and scaling relationships as applied to model testing". In: (1979).

[43]   J. P. Fielding and Howard Smith. "FLAVIIR an innovative university/industry re-
       search program for collaborative research and demonstration of UAV technolo-
       gies". In: *Proceedings of the 25th International Congress of the Aeronautical Sci-
       ences, ICAS.* 2006.

[44]   Ali Yarf-Abbasi and J. P. Fielding. "Design integration of the eclipse and demon
       demonstrator UAVs". In: *Proceedings of the Seventh AIAA Aviation Technology,
       Integration and Operations Conference (ATIO), Belfast, UK.* 2007, pp. 18–20.

[45]   Or D. Dantsker and Renato Mancuso. "Flight Data Acquisition Platform Devel-
       opment, Integration, and Operation on Small- to Medium-Sized Unmanned Air-
       craft". In: *AIAA Scitech 2019 Forum.* AIAA SciTech Forum. American Institute of
       Aeronautics and Astronautics, Jan. 2019. DOI: 10.2514/6.2019-1262. URL:
       https://arc.aiaa.org/doi/10.2514/6.2019-1262 (visited on 03/20/2020).

[46]   Or D. Dantsker et al. "High-Frequency Sensor Data Acquisition System (SDAC)
       for Flight Control and Aerodynamic Data Collection". In: *32nd AIAA Applied Aero-
       dynamics Conference.* 2014, p. 2565.

[47]   Alejandro Sobron, David Lundström, and Petter Krus. "A Review of Current Re-
       search in Subscale Flight Testing and Analysis of Its Main Practical Challenges".
       In: *Aerospace* 8.3 (2021), p. 74.

[48]   Andreas Bergmann, Andreas Huebner, and Thomas Loeser. "Experimental and
       numerical research on the aerodynamics of unsteady moving aircraft". en. In:
       Progress in Aerospace Sciences 44.2 (Feb. 2008), pp. 121–137. ISSN: 0376-0421. DOI:
       10.1016/j.paerosci.2007.10.006. URL: http://www.sciencedirect.
       com/science/article/pii/S0376042107000838 (visited on 10/07/2020).

[49]   Dan D. Vicroy, Thomas D. Loeser, and Andreas Schütte. "Static and Forced-Oscillation
       Tests of a Generic Unmanned Combat Air Vehicle". en. In: *Journal of Aircraft*
       49.6 (Nov. 2012), pp. 1558–1583. ISSN: 0021-8669, 1533-3868. DOI: 10.2514/1.
       C031501. URL: https://arc.aiaa.org/doi/10.2514/1.C031501 (visited on
       10/14/2020).

[50]   Alessandro Casaburo et al. "A Review of Similitude Methods for Structural En-
       gineering". en. In: *Applied Mechanics Reviews* 71.3 (May 2019), p. 030802. ISSN:
       0003-6900, 2379-0407. DOI: 10.1115/1.4043787.

[51]   JAXA. *Aeroengine test facilities | Test facilities | Aeronautical Technology Directorate.*
       URL: https://www.aero.jaxa.jp/eng/facilities/aeroengine/ (visited
       on 05/31/2021).

[52] J. Schijve. "Fatigue of aircraft materials and structures". In: *International Journal of Fatigue* 16.1 (1994), pp. 21–32.

[53] DNW. *DNW Wind-tunnels*. URL: `https://www.dnw.aero//` (visited on 05/31/2021).

[54] Wolf R. Krüger et al. "Design and wind tunnel test of an actively controlled flexible wing". In: *Proc. International Forum on Aeroelasticity and Strucutural Dynamics 2019*. International Forum on Aeroelasticity and Structural Dynamics. Savannah, GA (USA), June 2019. URL: `https://elib.dlr.de/127970/` (visited on 05/31/2021).

[55] Milos Novak and Alan G. Davenport. "Aeroelastic Instability of Prisms in Turbulent Flow". In: *Journal of the Engineering Mechanics Division, 96(1), 17-39.* 96.1 (Feb. 1, 1970), pp. 17–39. DOI: 10.1061/JMCEA3.0001210. URL: `https://ascelibrary.org/doi/abs/10.1061/JMCEA3.0001210` (visited on 05/31/2021).

[56] T. Sinnige. "Aerodynamic and Aeroacoustic Interaction Effects for Tip-Mounted Propellers: An Experimental Study". PhD Thesis. Delft University of Technology, 2018.

[57] Melissa B. Rivers and Ashley Dittberner. "Experimental Investigations of the NASA Common Research Model". In: *Journal of Aircraft* 51.4 (2014), pp. 1183–1193. DOI: 10.2514/1.C032626. URL: `https://doi.org/10.2514/1.C032626` (visited on 05/31/2021).

[58] Dan Vicroy, Thomas Loeser, and Andreas Schuette. "SACCON Dynamic Wind Tunnel Tests at DNW-NWB and 14´x22´ NASA LaRC". en. In: *28th AIAA Applied Aerodynamics Conference*. Chicago, Illinois: American Institute of Aeronautics and Astronautics, June 2010. ISBN: 978-1-62410-141-0. DOI: 10.2514/6.2010-4394. URL: `http://arc.aiaa.org/doi/10.2514/6.2010-4394` (visited on 10/07/2020).

[59] Aurelia Cartieri. "Experimental investigations on the Common Research Model at ONERA-S2MA". In: *AIAA Scitech 2020 Forum*. 0 vols. AIAA SciTech Forum. American Institute of Aeronautics and Astronautics, Jan. 5, 2020. DOI: 10.2514/6.2020-0779. URL: `https://arc.aiaa.org/doi/10.2514/6.2020-0779` (visited on 05/31/2021).

[60] S. Gholizadeh. "A review of non-destructive testing methods of composite materials". In: *Procedia Structural Integrity* 1 (2016), pp. 50–57.

[61] Michael Chun-Yung Niu and Mike Niu. *Airframe Structural Design: Practical Design Information and Data on Aircraft Structures*. 2nd edition. Hong Kong: Adaso/Adastra Engineering Center, Oct. 31, 2011. ISBN: 978-962-7128-09-0.

[62] Thomas Henry Gordon Megson. *Aircraft structures for engineering students*. Butterworth-Heinemann, 2016.

[63] Safran. *A specific range of test equipment*. Safran Aero Boosters. Feb. 2, 2015. URL: `https://www.safran-aero-boosters.com/test-facilities/specific-range-test-equipment` (visited on 05/31/2021).

[64] T. C. A. Stokkermans. "Aerodynamics of Propellers in Interaction Dominated Flow-fields: An Application to Novel Aerospace Vehicles". In: (2020). DOI: 10.4233/uuid:46178824-bb80-4247-83f1-dc8a9ca7d8e3. (Visited on 05/31/2021).

[65] L. L. M. Veldhuis. "Propeller Wing Aerodynamic Interference". In: (2005). URL: https://repository.tudelft.nl/islandora/object/uuid%3A8ffbde9c-b483-40de-90e0-97095202fbe3 (visited on 06/01/2021).

[66] Yuan-cheng Fung. *An introduction to the theory of aeroelasticity*. Wiley, 1955.

[67] A. R. Collar. "The first fifty years of aeroelasticity". In: *Aerospace (Royal Aeronautical Society Journal)* 5.2 (1978), pp. 12–20.

[68] Christoph Mertens et al. "Determination of Collar's Triangle of Forces on a Flexible Wing based on Particle Tracking Velocimetry Measurements". In: *AIAA Scitech 2021 Forum*. 0 vols. AIAA SciTech Forum. American Institute of Aeronautics and Astronautics, Jan. 4, 2021. DOI: 10.2514/6.2021-0221. URL: https://arc.aiaa.org/doi/10.2514/6.2021-0221 (visited on 06/01/2021).

[69] Marvin E. Goldstein. "Aeroacoustics". In: *New York : McGraw-Hill International Book Co.* (1976).

[70] JE Ffowcs Williams. "Aeroacoustics". In: *Annual Review of Fluid Mechanics* 9.1 (1977), pp. 447–468.

[71] Christopher KW Tam. "Computational aeroacoustics: An overview of computational challenges and applications". In: *International Journal of Computational Fluid Dynamics* 18.6 (2004), pp. 547–567.

[72] Bruce Owens, David Cox, and Eugene Morelli. "Development of a Low-Cost Sub-Scale Aircraft for Flight Research: The FASER Project". en. In: *25th AIAA Aerodynamic Measurement Technology and Ground Testing Conference*. San Francisco, California: American Institute of Aeronautics and Astronautics, June 2006. ISBN: 978-1-62410-029-1. DOI: 10.2514/6.2006-3306. URL: http://arc.aiaa.org/doi/10.2514/6.2006-3306 (visited on 12/06/2019).

[73] Bruce Owens et al. "Overview of Dynamic Test Techniques for Flight Dynamics Research at NASA LaRC". en. In: *25th AIAA Aerodynamic Measurement Technology and Ground Testing Conference*. San Francisco, California: American Institute of Aeronautics and Astronautics, June 2006. ISBN: 978-1-62410-029-1. DOI: 10.2514/6.2006-3146. URL: http://arc.aiaa.org/doi/10.2514/6.2006-3146 (visited on 11/13/2019).

[74] D Vicroy. "X-48B Blended Wing Body Ground to Flight Correlation Update". In: *AIAA Aero Sciences Meeting January 4-7, 2011* (2011), p. 30.

[75] Anshal I. Neihouse, Walter J. Klinar, and Stanley H. Scher. *Status of spin research for recent airplane designs*. Vol. 57. National Aeronautics and Space Administration, 1960.

[76] James S. Bowman Jr. "Free-spinning-tunnel Investigation of Gyroscopic Effects of Jet-engine Rotating Parts (or of Rotating Propellers) - NACA Technical Note". In: (1955).

[77] James S. Browman Jr and Frederick M. Healy. "Free-Spinning-Tunnel Investigation of a 1/25-Scale Model of the Chance Vought F8U-1P Airplane - NACA Technical Note". In: (1959).

[78] Andrei Dorobantu et al. "System identification for small, low-cost, fixed-wing unmanned aircraft". In: *Journal of Aircraft* 50.4 (2013), pp. 1117–1130.

[79] Aaron T. Perry, Timothy Bretl, and Phillip J. Ansell. "System Identification and Dynamics Modeling of a Distributed Electric Propulsion Aircraft". In: *AIAA Aviation 2019 Forum*. 2019, p. 3086.

[80] David Fratello et al. "Use of the updated NASA Langley radio-controlled drop-model technique for high-alpha studies of the X-29A configuration". In: *14th Atmospheric Flight Mechanics Conference*. 1987, p. 2559.

[81] Mark Croom et al. "Research on the F/A-18E/F using a 22 percent-dynamically-scaled drop model". In: *Atmospheric Flight Mechanics Conference*. 2000, p. 3913.

[82] Euclid C. Holleman. *Summary of flight tests to determine the spin and controllability characteristics of a remotely piloted, large-scale (3/8) fighter airplane model*. National Aeronautics and Space Administration, 1976.

[83] EU. *Commission Implementing Regulation (EU) 2019/947 of 24 May 2019 on the rules and procedures for the operation of unmanned aircraft (Text with EEA relevance.)* June 11, 2019. URL: http://data.europa.eu/eli/reg_impl/2019/947/oj/eng (visited on 06/14/2021).

[84] The Netherlands Government. *Rules for flying drones*. business.gov.nl. URL: https://business.gov.nl/regulation/drones/ (visited on 06/14/2021).

[85] Wilfred E. Baker, Peter S. Westine, and Franklin T. Dodge. *Similarity methods in engineering dynamics: theory and practice of scale modeling*. Spartan Books;[distributed by] Hayden Book Co., 1973.

[86] Henry Louis Langhaar. *Dimensional analysis and theory of models*. Vol. 2. Wiley New York, 1951.

[87] Jeffrey P. Slotnick. "Integrated CFD validation experiments for prediction of turbulent separated flows for subsonic transport aircraft". In: *NATO Science and Technology Organization, Meeting Proceedings RDP, STO-MP-AVT-307*. 2019.

[88] Steven H. Goldthorpe et al. "X-48b blended wing body flight test performance of maximum sideslip and high to post stall angle-of-attack command tracking". In: *AIAA Guidance, Navigation, and Control Conference*. 2010, pp. 1–17.

[89] Thomas L. Jordan et al. "AirSTAR: A UAV platform for flight dynamics and control system testing". In: *25th AIAA Aerodynamic Measurement Technology and Ground Testing Conference*. 2006, pp. 2006–3307.

[90] Dong-Youn Kwak et al. "Flight test measurements of surface pressure on unmanned scaled supersonic experimental airplane". In: *AIAA paper* 3483 (2006), p. 2006.

[91] Edward M. Kraft. "The Air Force Digital Thread/Digital Twin - Life Cycle Integration and Use of Computational and Experimental Knowledge". In: *54th AIAA Aerospace Sciences Meeting*. 0 vols. AIAA SciTech Forum. American Institute of Aeronautics and Astronautics, Jan. 2, 2016. URL: http://arc.aiaa.org/doi/10.2514/6.2016-0897 (visited on 06/04/2021).

[92] James Hileman et al. "Airframe design for" silent aircraft"". In: *45th AIAA Aerospace Sciences Meeting and Exhibit*. 2007, p. 453.

[93] Kevin R. Moore and Andrew Ning. "Distributed electric propulsion effects on existing aircraft through multidisciplinary optimization". In: *2018 AIAA/ASCE/AHS/ASC Structures, Structural Dynamics, and Materials Conference*. 2018, p. 1652.

[94] Veer N. Vatsa et al. "CFD and Experimental Data Comparisons for Conventional and AFC-Enabled CRM High-Lift Configurations". In: *AIAA AVIATION 2020 FORUM*. 2020, p. 2939.

[95] Edward N. Tinoco. "An Evaluation and Recommendations for Further CFD Research Based on the NASA Common Research Model (CRM) Analysis from the AIAA Drag Prediction Workshop (DPW) Series". In: (2019).

[96] Alejandro Sobron. "On Subscale Flight Testing: Applications in Aircraft Conceptual Design". PhD Thesis. Linköping University Electronic Press, 2018.

[97] N. Matheny and G. Panageas. "HiMAT aerodynamic design and flight test experience". en. In: *1st Flight Test Conference*. Las Vegas,NV,U.S.A.: American Institute of Aeronautics and Astronautics, Nov. 1981. DOI: 10.2514/6.1981-2433. URL: http://arc.aiaa.org/doi/10.2514/6.1981-2433 (visited on 02/05/2020).

[98] J. L. Layton Lockenour. "RPRV research focus on HiMAT". In: *Astronautics and Aeronautics* (Apr. 1976). URL: https://ntrs.nasa.gov/search.jsp?R=19760042755 (visited on 02/05/2020).

[99] Dwain A. Deets. *HiMAT flight program: Test results and program assessment overview*. Vol. 86725. National Aeronautics, Space Administration, Scientific, and Technical Report, 1986.

[100] K. L. Petersen. "Flight control systems development of highly maneuverable aircraft technology /HiMAT/ vehicle". In: Aug. 20-22, 1979, Aug. 1979. URL: https://ntrs.nasa.gov/search.jsp?R=19790063865 (visited on 10/11/2017).

[101] Uichung Cho, Kristin L Wood, and H Crawford. "Novel Empirical Similarity Method for the reliable product test with rapid prototypes". en. In: *International Design Engineering Technical Conferences and Computers and Information in Engineering Conference (Vol. 80326, p. V002T02A029), American Society of Mechanical Engineers* (1998), p. 14.

[102] Raymond N. Chuk and Vincent J. Thomson. "A comparison of rapid prototyping techniques used for wind tunnel model fabrication". In: *Rapid Prototyping Journal* 4.4 (Jan. 1998), pp. 185–196. ISSN: 1355-2546. DOI: 10.1108/13552549810239030. URL: https://doi.org/10.1108/13552549810239030 (visited on 11/16/2020).

[103] Mark French. "An application of structural optimization in wind tunnel model design". en. In: *31st Structures, Structural Dynamics and Materials Conference*. Long Beach,CA,U.S.A.: American Institute of Aeronautics and Astronautics, Apr. 1990. DOI: 10.2514/6.1990-956. URL: http://arc.aiaa.org/doi/10.2514/6.1990-956 (visited on 01/29/2020).

[104] Thomas Duda and L. Venkat Raghavan. "3D Metal Printing Technology". en. In: *IFAC-PapersOnLine*. 17th IFAC Conference on International Stability, Technology and Culture TECIS 2016 49.29 (Jan. 2016), pp. 103–110. ISSN: 2405-8963. DOI: 10.1016/j.ifacol.2016.11.111. URL: http://www.sciencedirect.com/science/article/pii/S2405896316325496 (visited on 11/16/2020).

[105] Philip John. "The flapless air vehicle integrated industrial research (FLAVIIR) programme in aeronautical engineering". In: *Proceedings of the Institution of Mechanical Engineers, Part G: Journal of Aerospace Engineering* 224.4 (2010), pp. 355–363.

[106] Ray Kurzweil. *The Singularity Is Near: When Humans Transcend Biology*. en. Google-Books-ID: 9FtnppNpsT4C. Penguin, Sept. 2005. ISBN: 978-1-101-21888-4.

[107] Cardwave. *SD Cards: A trip down memory lane |Cardwave*. Apr. 5, 2019. URL: https://www.cardwave.com/knowledge-hub/sd-cards-a-trip-down-memory-lane/ (visited on 06/09/2021).

[108] KOOFR. *History and evolution of memory cards*. Koofr blog. URL: https://koofr.eu/blog/posts/history-and-evolution-of-memory-cards (visited on 06/09/2021).

[109] Roberto A. Bunge et al. "In-Flight Measurement of Wing Surface Pressures on a Small-Scale UAV During Stall/Spin Maneuvers". In: *AIAA Flight Testing Conference*. AIAA Flight Testing Conference. Washington, D.C.: American Institute of Aeronautics and Astronautics, June 13, 2016. ISBN: 978-1-62410-431-2. DOI: 10.2514/6.2016-3652. URL: https://arc.aiaa.org/doi/10.2514/6.2016-3652 (visited on 06/08/2021).

[110] Lorenz Meier et al. "Pixhawk: A system for autonomous flight using onboard computer vision". In: *2011 IEEE International Conference on Robotics and Automation*. IEEE, 2011, pp. 2992–2997.

[111] *Urban Air Mobility |Airbus*. 2021. URL: https://www.airbus.com/en/innovation/zero-emission/urban-air-mobility (visited on 12/16/2021).

[112] *Advancing Aerial Mobility: A National Blueprint | The National Academies Press*. 2021. URL: https://www.nap.edu/download/25646 (visited on 12/16/2021).

[113] TU Delft. *DUUC aircraft with the innovative 'Propulsive Empennage' concept*. URL: https://www.youtube.com/watch?v=VDbJBkcQBPI (visited on 04/16/2020).

[114] Kevin Hameeteman. "Unconventional Propulsive Empennage - Future or Fiction?: Stability and control analysis and the effect of scaling of the DUUC". en. In: (2017). URL: https://repository.tudelft.nl/islandora/object/uuid%3A8a0d0131-6961-4a19-baa5-32fac80d6b5c (visited on 04/15/2020).

[115]   Laurence A. Walker. *Flight Testing the X-36: The Test Pilots Perspective*. Tech. rep. Oct. 1997. URL: https://ntrs.nasa.gov/search.jsp?R=19970031950 (visited on 02/05/2020).

[116]   Michael A. Dornheim. "Mcdonnell douglas rolls out X-36". In: *AW & ST* 25 (1996), pp. 20–22.

[117]   Philip Woods. "FLAVIIR–An Integrated Programme of Research for UAVs". In: *Proc. of the 3rd AIAA Flow Control Conference, San Francisco*. 2008, pp. 5–7. URL: https://arc.aiaa.org/doi/pdfplus/10.2514/6.2006-3504 (visited on 10/02/2017).

[118]   A. Yarf-Abbasi et al. "Design and development of the eclipse and demon demonstrator UAVs". In: *Proceedings of the 26th Congress of International Council of Aeronautical Sciences (ICAS 2008), Canada*. 2008.

[119]   Christopher Jouannet et al. "Design and Flight Testing of an ECO-Sport Aircraft". en. In: *48th AIAA Aerospace Sciences Meeting Including the New Horizons Forum and Aerospace Exposition*. Orlando, Florida: American Institute of Aeronautics and Astronautics, Jan. 2010. ISBN: 978-1-60086-959-4. DOI: 10.2514/6.2010-1206. URL: http://arc.aiaa.org/doi/10.2514/6.2010-1206 (visited on 02/05/2020).

[120]   William J. McSwain Fredericks. *Greased Lightning (GL-10) Flight Testing Campaign*. Tech. rep. July 2017. URL: https://ntrs.nasa.gov/search.jsp?R=20170007194 (visited on 02/06/2020).

[121]   P. Schmollgruber et al. "An innovative evaluation platform for new aircraft concepts". en. In: *The Aeronautical Journal* 114.1157 (July 2010), pp. 451–456. ISSN: 0001-9240, 2059-6464. DOI: 10.1017/S0001924000003936. URL: https://www.cambridge.org/core/journals/aeronautical-journal/article/an-innovative-evaluation-platform-for-new-aircraft-concepts/F202F2A88561E91FFD66AE15685B64C7 (visited on 02/12/2020).

[122]   Zdobyslaw Goraj et al. "Design and Integration of Flexi-Bird-a Low Cost Sub-Scale Research Aircraft for Safety and Environmental Issues". In: *27th International Congress of the Aeronautical Sciences, Nice,[September 2010]*. 2010.

[123]   Or D. Dantsker et al. "Flight & Ground Testing Data Set for an Unmanned Aircraft: Great Planes Avistar Elite". In: *AIAA Scitech 2020 Forum*. American Institute of Aeronautics and Astronautics. DOI: 10.2514/6.2020-0780. URL: https://arc.aiaa.org/doi/abs/10.2514/6.2020-0780 (visited on 04/15/2020).

[124]   Airbus. *The albatross is inspiring tomorrow's aircraft wings*. en. URL: https://www.airbus.com/newsroom/stories/the-albatross-is-inspiring-tomorrows-next-generation-of-aircraft-wings.html (visited on 02/06/2020).

[125]   Airbus. *Airbus Unveils 'Maverick', Its Blended Wing Aircraft Demonstrator*. en. URL: https://www.gonewsindia.com/latest-news/technology/airbus-unveils-maverick-a-blended-wing-aircraft-demonstrator-8832 (visited on 02/12/2020).

[126] Yiyuan Ma et al. "Sizing Method and Sensitivity Analysis for Distributed Electric Propulsion Aircraft". In: *Journal of Aircraft* (Mar. 2020), pp. 1–12. DOI: 10.2514/1.C035581. URL: https://arc.aiaa.org/doi/10.2514/1.C035581 (visited on 04/15/2020).

[127] TU Delft. *Flying-V*. TU Delft. en. URL: https://www.tudelft.nl/en/ae/flying-v/ (visited on 10/30/2020).

[128] Marco Palermo and Roelof Vos. "Experimental aerodynamic analysis of a 4.6%-scale flying-v subsonic transport". In: *AIAA Scitech 2020 Forum*. 2020, p. 2228.

[129] Christopher Courtin, R. John Hansman, and Mark Drela. "Flight Test Results of a Subscale Super-STOL Aircraft". In: *AIAA Scitech 2020 Forum*. 2020, p. 0977.

[130] Andreas Gross et al. "1/5 Scale Model of Aeromot 200S SuperXimango for Scaled Flight Research". en. In: *26th AIAA Applied Aerodynamics Conference*. Honolulu, Hawaii: American Institute of Aeronautics and Astronautics, Aug. 2008. ISBN: 978-1-60086-987-7. DOI: 10.2514/6.2008-6416. URL: http://arc.aiaa.org/doi/10.2514/6.2008-6416 (visited on 12/10/2019).

[131] Or D. Dantsker, Gavin K. Ananda, and Michael S. Selig. "GA-USTAR Phase 1: Development and Flight Testing of the Baseline Upset and Stall Research Aircraft". en. In: *35th AIAA Applied Aerodynamics Conference*. Denver, Colorado: American Institute of Aeronautics and Astronautics, June 2017. ISBN: 978-1-62410-501-2. DOI: 10.2514/6.2017-4078. URL: https://arc.aiaa.org/doi/10.2514/6.2017-4078 (visited on 04/21/2020).

[132] Thomas Jordan et al. "Development of a dynamically scaled generic transport model testbed for flight research experiments". In: *NASA Technical Report* (2004).

[133] Christopher Regan. "In-flight stability analysis of the X-48B aircraft". In: *AIAA atmospheric flight mechanics conference and exhibit* (2008), p. 6571.

[134] Tim Risch et al. "X-48B flight-test progress overview". In: *47th AIAA aerospace sciences meeting including the new horizons forum and aerospace exposition*. 2009.

[135] Kristian Amadori, Christopher Jouannet, and Patrick Berry. "Development of a subscale flight testing platform for a generic future fighter". In: *27TH International Congress of the Aeronautical Sciences-ICAS 2010*. 2010.

[136] Alejandro Sobron. *On Subscale Flight Testing: Applications in Aircraft Conceptual Design*. Vol. 1819. Linköping University Electronic Press, 2018.

[137] Kyle Pieper et al. "Design and Development of a Dynamically, Scaled Distributed Electric Propulsion Aircraft Testbed". In: *2018 AIAA/IEEE Electric Aircraft Technologies Symposium (EATS)*. ISSN: null. July 2018, pp. 1–2.

[138] Daniel P. Raymer. *Dan Raymer's simplified aircraft design for homebuilders*. 1st ed. Los Angeles, CA: Design Dimension Press, 2003. 143 pp. ISBN: 978-0-9722397-0-7.

[139] Richard M. Hueschen. *Development of the Transport Class Model (TCM) Aircraft Simulation From a Sub-Scale Generic Transport Model (GTM) Simulation*. Tech. rep. Aug. 2011. URL: https://ntrs.nasa.gov/search.jsp?R=20110014509 (visited on 12/17/2019).

[140] Gina Hagler. "William Froude". en. In: *Modeling Ships and Space Craft*. New York, NY: Springer New York, 2013, pp. 109–134. ISBN: 978-1-4614-4595-1 978-1-4614-4596-8. DOI: 10.1007/978-1-4614-4596-8_6. URL: http://link.springer.com/10.1007/978-1-4614-4596-8_6 (visited on 01/07/2020).

[141] Derek Jackson and Brian Launder. "Osborne Reynolds and the Publication of His Papers on Turbulent Flow". In: *Annual Review of Fluid Mechanics* 39.1 (2007), pp. 19–35. DOI: 10.1146/annurev.fluid.39.050905.110241. URL: https://doi.org/10.1146/annurev.fluid.39.050905.110241 (visited on 01/07/2020).

[142] Osborne Reynolds. "IV. On the dynamical theory of incompressible viscous fluids and the determination of the criterion". In: *Philosophical Transactions of the Royal Society of London. (A.)* 186 (Jan. 1895), pp. 123–164. DOI: 10.1098/rsta.1895.0004. URL: https://royalsocietypublishing.org/doi/abs/10.1098/rsta.1895.0004 (visited on 01/07/2020).

[143] E. Buckingham. "On Physically Similar Systems; Illustrations of the Use of Dimensional Equations". en. In: *Physical Review* 4.4 (Oct. 1914), pp. 345–376. ISSN: 0031-899X. DOI: 10.1103/PhysRev.4.345. URL: https://link.aps.org/doi/10.1103/PhysRev.4.345 (visited on 01/07/2020).

[144] Lord Rayleigh. "The principle of similitude". In: *Nature* 95 (1915), p. 66.

[145] Stephen J. Kline. *Similitude and approximation theory*. Springer Science & Business Media, 2012.

[146] Enzo O. Macagno. "Historico-critical review of dimensional analysis". en. In: *Journal of the Franklin Institute* 292.6 (Dec. 1971), pp. 391–402. ISSN: 0016-0032. DOI: 10.1016/0016-0032(71)90160-8. URL: http://www.sciencedirect.com/science/article/pii/0016003271901608 (visited on 11/05/2020).

[147] E. Szücs. *Similitude and Modelling*. en. Google-Books-ID: ORQ7AAAAQBAJ. Elsevier, Dec. 2012. ISBN: 978-0-08-098378-3.

[148] Max Scherberg and R. V. Rhode. "Mass distribution and performance of free flight models". en. In: (Oct. 1927). URL: http://ntrs.nasa.gov/search.jsp?R=19930081026 (visited on 12/16/2019).

[149] Anshal I. Neihouse and Philip W. Pepoon. "Dynamic similitude between a model and a full-scale body for model investigation at full-scale Mach number". In: (1950).

[150] Leonid Ivanovich Sedov. *Similarity and dimensional methods in mechanics*. CRC press, 2018.

[151] James Norman Goodier and W. T. Thomson. *Applicability of similarity principles to structural models*. 933. National Advisory Committee for Aeronautics, 1944.

[152] Percy Williams Bridgman. *Dimensional analysis*. Yale university press, 1922.

[153] Joan Mas Colomer et al. "Similarity Maximization of a Scaled Aeroelastic Flight Demonstrator via Multidisciplinary Optimization". In: *58th AIAA/ASCE/AHS/ASC Structures, Structural Dynamics, and Materials Conference*. 2017, p. 0573. URL: `http://arc.aiaa.org/doi/pdf/10.2514/6.2017-0573` (visited on 02/14/2017).

[154] Christian Adams, Joachim Bs, and Tobias Melz. "An experimental investigation of vibrating plates in similitude and the possibility to replicate the responses using sensitivity-based scaling laws". In: *INTER-NOISE and NOISE-CON congress and conference proceedings*. Vol. 257. Institute of Noise Control Engineering, 2018, pp. 799–810.

[155] Pedro Pereira et al. "Aeroelastic scaling and optimization of a joined-wing aircraft concept". In: *48th AIAA/ASME/ASCE/AHS/ASC Structures, Structural Dynamics, and Materials Conference*. 2007, p. 1889.

[156] Mark French. "An application of structural optimization in wind tunnel model design". In: *31st Structures, Structural Dynamics and Materials Conference*. 1990, p. 956.

[157] Anthony Ricciardi et al. "Nonlinear aeroelastic scaling of a joined wing aircraft". In: *53rd AIAA/ASME/ASCE/AHS/ASC Structures, Structural Dynamics and Materials Conference 20th AIAA/ASME/AHS Adaptive Structures Conference 14th AIAA*. 2012, p. 1454.

[158] JW Wissmann. "Dynamic stability of space vehicles. Structural dynamics model testing(Dimensional analysis, and similitude and scaling laws for structural dynamics model testing of spacecraft dynamic stability)". In: (1968).

[159] Joan Mas-Colomer. "Aeroelastic Similarity of a Flight Demonstrator via Multidisciplinary Optimization". en. PhD thesis. DOCTORAT DE L'UNIVERSITÉ DE TOULOUSE Délivré par : l'Institut Supérieur de l'Aéronautique et de l'Espace (ISAE), Dec. 2018. URL: `https://hal.archives-ouvertes.fr/tel-02023612` (visited on 11/09/2020).

[160] Qingqing Ye et al. "Effect of Surface Roughness Geometry on Boundary-Layer Transition and Far-Field Noise". In: *AIAA Journal* (2021), pp. 1–13.

[161] P. S. Klebanoff and K. D. Tidstrom. "Mechanism by Which a Two-Dimensional Roughness Element Induces Boundary-Layer Transition". In: *The Physics of Fluids* 15.7 (1972), pp. 1173–1188.

[162] William Saric, Edward White, and Helen Reed. "Boundary-layer receptivity to freestream disturbances and its role in transition". In: *30th fluid dynamics conference*. 1999, p. 3788.

[163] Arthur G. Hansen. "Similarity analyses of boundary value problems in engineering(Text on similarity solutions of partial differential equations for boundary value problems in engineering)". In: *ENGLEWOOD CLIFFS, N. J., PRENTICE-HALL, INC., 1964. 114 P* (1964).

[164] Dennis M. Bushnell. "Scaling: Wind tunnel to flight". In: *Annual Review of Fluid Mechanics* 38 (2006), pp. 111–128.

[165]   Karl Pettersson and Arthur Rizzi. "Aerodynamic scaling to free flight conditions: Past and present". In: *Progress in Aerospace Sciences* 44.4 (May 2008), pp. 295–313. ISSN: 0376-0421. DOI: 10.1016/j.paerosci.2008.03.002. URL: http://www.sciencedirect.com/science/article/pii/S0376042108000262 (visited on 06/06/2018).

[166]   Johnhenri R. Richardson et al. "Scaling of Airplane Dynamic Response to Stochastic Gusts". en. In: *Journal of Aircraft* 51.5 (Sept. 2014), pp. 1554–1566. ISSN: 0021-8669, 1533-3868. DOI: 10.2514/1.C032410. URL: http://arc.aiaa.org/doi/10.2514/1.C032410 (visited on 10/17/2019).

[167]   Anthony P. Ricciardi et al. "Nonlinear Aeroelastic Scaled-Model Design". en. In: *Journal of Aircraft* 53.1 (Jan. 2016), pp. 20–32. ISSN: 0021-8669, 1533-3868. DOI: 10.2514/1.C033171. URL: http://arc.aiaa.org/doi/10.2514/1.C033171 (visited on 11/09/2020).

[168]   Cristiano P. Coutinho, António J. Baptista, and José Dias Rodrigues. "Reduced scale models based on similitude theory: A review up to 2015". en. In: *Engineering Structures* 119 (July 2016), pp. 81–94. ISSN: 0141-0296. DOI: 10.1016/j.engstruct.2016.04.016. URL: http://www.sciencedirect.com/science/article/pii/S0141029616301274 (visited on 03/30/2020).

[169]   Robert C. Nelson. *Flight stability and automatic control.* Vol. 2. WCB/McGraw Hill New York, 1998. (Visited on 10/02/2017).

[170]   W. H. J. J. Van Staveren. "Analyses of Aircraft Responses to Atmospheric Turbulence". en. In: (2003). URL: https://repository.tudelft.nl/islandora/object/uuid%3Ac639ce70-4ea9-4c9b-8594-bb4b51e42c73 (visited on 04/21/2020).

[171]   Warren Williams. "UAV handling qualities... you must be joking". In: *Aerospace Sciences Corporation Pty. Ltd* (2003).

[172]   Or D. Dantsker et al. "Flight Testing Automation to Parameterize Unmanned Aircraft Dynamics". In: *AIAA Aviation 2019 Forum.* 2019, p. 3230.

[173]   Robert Shishko and Robert Aster. "NASA Special Publication". In: 6105 (1995).

[174]   D. M. Hamby. "A review of techniques for parameter sensitivity analysis of environmental models". en. In: *Environmental Monitoring and Assessment* 32.2 (Sept. 1994), pp. 135–154. ISSN: 1573-2959. DOI: 10.1007/BF00547132. URL: https://doi.org/10.1007/BF00547132 (visited on 02/02/2022).

[175]   F.O. Hoffman and C.W. Miller. *Uncertainties in environmental radiological assessment models and their implications.* Tech. rep. United States, 1983, p. 57.

[176]   Joaquim RRA Martins and Andrew B. Lambe. "Multidisciplinary design optimization: a survey of architectures". In: *AIAA journal* 51.9 (2013), pp. 2049–2075. URL: http://arc.aiaa.org/doi/abs/10.2514/1.J051895 (visited on 02/14/2017).

[177]   Akshay Raju Kulkarni et al. "Assessment of Sub-scale Designs for Scaled Flight Testing". In: *AIAA Aviation 2019 Forum.* 2019, p. 3089.

[178] Akshay Raju Kulkarni, Gianfranco La Rocca, and Leo Veldhuis. "Knowledge Based Engineering tool to estimate the degree of similitude for scaled models". In: San Diego, USA: AIAA, Jan. 2019.

[179] Jan Vandenbrande, Thomas Grandine, and Thomas Hogan. "The search for the perfect body: Shape control for multidisciplinary design optimization". In: *44th AIAA Aerospace Sciences Meeting and Exhibit*. 2006, p. 928.

[180] T. Van den Berg. "Harnessing the potential of Knowledge Based Engineering in manufacturing design". en. In: (2013). (Visited on 07/13/2022).

[181] Z. Zhu. "Automatic 3D Routing for the Physical Design of Electrical Wiring Interconnection Systems for Aircraft". en. In: (2016). DOI: 10.4233/uuid:2ca107b4-202d-4638-a044-d45649b89275. (Visited on 07/13/2022).

[182] H. Wang. "Global-local Knowledge Coupling Approach to Support Airframe Structural Design". en. In: (2014). (Visited on 07/13/2022).

[183] Jaroslaw Sobieszczanski-Sobieski, Alan Morris, and Michel Van Tooren. *Multidisciplinary design optimization supported by knowledge based engineering*. John Wiley & Sons, 2015.

[184] G. La Rocca. "Knowledge based engineering techniques to support aircraft design and optimization". en. PhD thesis. Apr. 2011. URL: http://resolver.tudelft.nl/uuid:45ed17b3-4743-4adc-bd65-65dd203e4a09 (visited on 02/28/2022).

[185] G. La Rocca. "Knowledge based engineering techniques to support aircraft design and optimization". en. In: (2011). URL: https://repository.tudelft.nl/islandora/object/uuid%3A45ed17b3-4743-4adc-bd65-65dd203e4a09 (visited on 04/17/2020).

[186] R. J. M. Elmendorp, Roelof Vos, and Gianfranco La Rocca. "A conceptual design and analysis method for conventional and unconventional airplanes". In: *ICAS 2014: Proceedings of the 29th Congress of the International Council of the Aeronautical Sciences, St. Petersburg, Russia, 7-12 September 2014*. International Council of Aeronautical Sciences, 2014.

[187] JPTJ Berends and M. J. L. Van Tooren. "Design of a Multi Agent Task Environment Framework to Support Multidisciplinary Design and Optimisation". In: *45th AIAA Aerospace Sciences Meeting and Exhibit*. 2007, p. 969.

[188] Nicholas Ross Milton. *Knowledge acquisition in practice: a step-by-step guide*. Springer Science & Business Media, 2007.

[189] Anthony J. Rhem. *Knowledge management in practice*. Auerbach Publications, 2016.

[190] Daniel P. Raymer. *Simplified Aircraft Design for Homebuilders*. English. Los Angeles, CA: Design Dimension Press, Oct. 2002. ISBN: 978-0-9722397-0-7.

[191] Berta Rubio Pascual. "Engine-Airframe Integration for the Flying-V". en. In: (2018). URL: https://repository.tudelft.nl/islandora/object/uuid%5C%3A75be27a7-6fd4-4112-a600-45df2999758f (visited on 02/28/2022).

[192]   F. Faggiano. "Aerodynamic Design Optimization of a Flying V Aircraft". en. In: (2016). URL: https://repository.tudelft.nl/islandora/object/uuid%5C%3A0b1472a5-3aad-433c-9a64-242c84b114fd (visited on 02/28/2022).

[193]   *All there is to know about different mesh types in CFD!* en. June 2016. URL: https://www.manchestercfd.co.uk/post/all-there-is-to-know-about-different-mesh-types-in-cfd (visited on 02/15/2022).

[194]   James K. Nathman. *VSAERO User's manual*. 1999th ed. Vol. 6.1. Remond Washington.

[195]   Larry L. Erickson. *Panel methods: An introduction*. Tech. rep. 1990.

[196]   B. Maskew. "Calculation of Flow Characteristics for General Configurations Using Panel Methods". en. In: *Panel Methods in Fluid Mechanics with Emphasis on Aerodynamics: Proceedings of the Third GAMM-Seminar Kiel, January 16 to 18, 1987*. Ed. by Josel Ballmann, Richard Eppler, and Wolfgang Hackbusch. Notes on Numerical Fluid Mechanics. Vieweg Teubner Verlag, 1988, pp. 156–165. ISBN: 978-3-663-13997-3. DOI: 10.1007/978-3-663-13997-3_13. URL: https://doi.org/10.1007/978-3-663-13997-3_13 (visited on 04/28/2022).

[197]   Vivek Ahuja and R. J. Hartfield. "Aerodynamic Loads over Arbitrary Bodies by Method of Integrated Circulation". en. In: *Journal of Aircraft* 53.6 (Nov. 2016), pp. 1719–1730. ISSN: 0021-8669, 1533-3868. DOI: 10.2514/1.C033619. URL: https://arc.aiaa.org/doi/10.2514/1.C033619 (visited on 04/29/2022).

[198]   T. W. Swafford. "Analytical approximation of two-dimensional separated turbulent boundary-layer velocity profiles". In: *AIAA journal* 21.6 (1983), pp. 923–926.

[199]   Ali Elham and Michel JL van Tooren. "Tool for preliminary structural sizing, weight estimation, and aeroelastic optimization of lifting surfaces". In: *Proceedings of the Institution of Mechanical Engineers, Part G: Journal of Aerospace Engineering* 230.2 (2016), pp. 280–295.

[200]   C Varriale et al. "A Thrust-Elevator Interaction Criterion for Aircraft Optimal Longitudinal Control". In: Dallas: AIAA, June 2019.

[201]   Till Pfeiffer et al. "Implementation of a heterogeneous, variable-fidelity framework for flight mechanics analysis in preliminary aircraft design". In: *60th German Aerospace Congress (DLRK)*. 2011.

[202]   Fengnian Tian and Mark Voskuijl. "Automated generation of multiphysics simulation models to support multidisciplinary design optimization". In: *Advanced Engineering Informatics* 29.4 (2015), pp. 1110–1125.

[203]   C. Varriale. *Flight Mechanics and Performance of Direct Lift Control: Applying Control Allocation Methods to a Staggered Box-Wing Aircraft Configuration*. en. 2022. DOI: 10.4233/uuid:8b868c52-f34f-4307-8fc0-b1176eaf9d04. URL: https://repository.tudelft.nl/islandora/object/uuid%3A8b868c52-f34f-4307-8fc0-b1176eaf9d04 (visited on 04/19/2022).

[204]   G E Cooper and R P Harper Jr. *The Use of Pilot Rating in the Evaluation of Aircraft Handling Qualities*. Tech. rep. NASA TN D-5153. Washington D. C.: NASA, 1969.

[205] John P. Campbell and Marion O. McKinney. *Summary of Methods for Calculating Dynamic Lateral Stability and Response and for Estimating Lateral Stability Derivatives*. en. Tech. rep. NASA, July 1951. URL: https://apps.dtic.mil/sti/citations/ADA382075 (visited on 06/27/2022).

[206] Slawomir Koziel and Leifur Leifsson. *Surrogate-based modeling and optimization*. Springer, 2013.

[207] ICAO. *Manual on Remotely Piloted Aircraft Systems (RPAS), 1st ed.; International Civil Aviation Organization: Montreal, QC, Canada, 2015. - Google Search*. URL: https://skybrary.aero/sites/default/files/bookshelf/4053.pdf (visited on 06/12/2021).

[208] Pieter-Jan Proesmans. "Preliminary Propulsion System Design and Integration for a Box-Wing Aircraft Configuration: A Knowledge Based Engineering Approach". en. In: (2019). URL: https://repository.tudelft.nl/islandora/object/uuid%3A0d2ebc46-09ee-493f-bb4c-c871133bff6f (visited on 07/29/2022).

[209] Roy Groot. "Stability &amp; control derivatives prediction for box wing aircraft configurations". en. In: (2019). URL: https://repository.tudelft.nl/islandora/object/uuid%5C%3A150c648c-0ba4-466f-bc6d-837df3e0d053 (visited on 07/27/2022).

[210] Luc de Ruiter. "Weight &amp; Balance Estimation with Automated Structural Analysis for Subscale Flight Models: A Knowledge Based Engineering Approach". en. In: (2020). URL: https://repository.tudelft.nl/islandora/object/uuid%3A57064c65-03d1-4c42-953d-a6d59f2a34c6 (visited on 07/29/2022).

[211] András Sóbester and Alexander IJ Forrester. *Aircraft aerodynamic design: geometry and optimization*. John Wiley & Sons, 2014.

[212] G. La Rocca and M.J.L. Van Tooren. "Knowledge-based engineering to support aircraft multidisciplinary design and optimization". In: *Proceedings of the Institution of Mechanical Engineers, Part G: Journal of Aerospace Engineering* 224.9 (2010), pp. 1041–1055. DOI: 10.1243/09544100JAERO592.

[213] Brenda M. Kulfan. "Universal parametric geometry representation method". In: *Journal of aircraft* 45.1 (2008), pp. 142–158.

[214] Colin Heimans. "Aerodynamic Analysis of Engine Integration during the Preliminary Design Phase". en. In: (2021). URL: https://repository.tudelft.nl/islandora/object/uuid%5C%3Aa3e588a9-9d21-4170-a973-c53eb3b45afc (visited on 07/27/2022).

[215] J. H. Wei. "Parametric modelling for determining aircraft stability & control derivatives". en. In: (2016). URL: https://repository.tudelft.nl/islandora/object/uuid%5C%3Acd095318-3272-400a-822d-e7990480a904 (visited on 07/28/2022).

LIST OF PUBLICATIONS

7. **Raju Kulkarni, A., La Rocca, G., Veldhuis, L.L.M. and Eitelberg, G.**, *Sub-scale flight test model design: Developments, challenges and opportunities,* Progress in Aerospace Sciences 130 (2022): 100798.

6. **Raju Kulkarni, A., Varriale, C., Voskuijl, M., La Rocca, G. and Veldhuis, L.L.M.**, *Assessment of Sub-scale Designs for Scaled Flight Testing,* AIAA Aviation 2019 Forum.

5. **Varriale, C., Raju Kulkarni, A., Voskuijl, M. and La Rocca, G.**, *A hybrid, Configuration-Agnostic approach to aircraft control surface sizing,* Proceedings of the 25th International Congress of the Italian Association of Aeronautics and Astronautics (2019).

4. **Raju Kulkarni, A., La Rocca, G. and Veldhuis, L.L.M.**, *Degree of similitude estimation for sub-scale flight testing,* AIAA Scitech 2019 Forum.

3. **Marcus, E.A., de Vries, R. and Raju Kulkarni, A. and Veldhuis, L.L.M.**, *Aerodynamic investigation of an over-the-wing propeller for distributed propulsion,* 2018 AIAA Aerospace Sciences Meeting.

2. **Raju Kulkarni, A., Hoogreef, M. and La Rocca, G.**, *Combining semantic web technologies and KBE to solve industrial MDO problems,* 18th AIAA/ISSMO Multidisciplinary Analysis and Optimization Conference (2017).

1. **Raju Kulkarni, A., La Rocca, G., van den Berg, T. and van Dijk, R.**, *A knowledge based engineering tool to support front-loading and multi-disciplinary design optimization of the fin-rudder interface,* Aerospace Europe 6th CEAS Conference (2017).

ACKNOWLEDGEMENTS

Anyone who has undertaken PhD can vouch that the process is laborious, time consuming and solitary with myriad dead-ends. However, the people we meet along our PhD journey makes it pleasurable, fruitful and most importantly enlightening. Indeed, I have been blessed with the support of my friends, family and mentors. First, I would like to thank my supervisors Gianfranco and Leo for their calm, mature and ceaseless support. My respect and value for their support only grows as I enter the last phase of my PhD.

In the last eight years that I have known Gianfranco, I have gained a lot from his experience, knowledge of advanced design methods and his vast network of experts in aerospace community. In addition to supporting my research and assisting me in critically assessing my work, Gianfranco has been tirelessly helping me improve my writing skills. The review provided by Gianfranco on my writing has greatly helped in improving the quality of all our publications and this dissertation. I would like to thank Gianfranco for all his support, without which this thesis would not have been possible.

Leo gave me an opportunity to work as a researcher in the NOVAIR project. I have learnt a great deal from his management and mentoring. In particular, I have experienced his ability to get work done using gentle words without pressurizing people and I hope to emulate him in my future endeavours. My sincere thanks to Leo for all the support and care he has shown to me in the completion of this dissertation.

As a researcher in a European project, a significant amount of time and energy is invested in collaborating with other companies and research institutes. I have been lucky to have been involved in IDealiSM, AGILE, Parsifal, NOVAIR and DEFAINE projects in my time as a PhD candidate. These projects have provided me with insights on the needs of the aerospace community and helped me build relationships that will last well beyond my PhD days. My special thanks to Tobie, Erwin, Prajwal, Francesco, Pier, Natalie, Bjorn, Henk, Ton, Bastian, Stefan, Max, Reinier, Noel, Robin, Roberto and Marco for all the collaborations.

At the end of the first half of my PhD, I experienced dead-ends with my work as the tools and methods I was using were not robust enough to support my technical progress. I would like to thank Vivek Ahuja for stepping in at such a critical stage and supporting my research work by providing his commercial software Flightstream and offering software support and technical help to me and my students. In addition, I owe my gratitude to my colleagues at TU Delft who have consistently collaborated with me and helped me with my PhD. I thank Carmine, Maurice, Anne-Liza, Reno and Pieter-Jan for supporting my work and providing technical inputs. I would also like to thank Nando for giving me valuable time from his wind-tunnel slot and helping me acquire validation data which has helped me answer a lot of questions about my work.

Special thanks to my master students Julia, Roy, Marco (Palermo and Mangano), Rob, Adithya, San, Fabio and Luc for all your contributions. This thesis relies on the results

of your work and would not have been possible without your contributions. I hope that you all have learnt as much as I have.

I also appreciate the contributions of my office mates in Room 7.15 over the years, Tomas, Maurice, Imco, Tom, Carmine, Anne-Liza, Sarah, Pieter-Jan and Jente who have made my PhD fun and enjoyable. You make me look forward to going to work everyday. Thanks for being so sensitive towards each other. The smallest sign of worry is immediately identified by the office mates and their best means are employed to allay any discomfort. A special mention to all other FPP colleagues Adam, Fabrizio, Sonia, Sumit, Nitish, Nando, Lucia, Biagio, Reynard, Sebastian, Antonio, Salvo, Joris, Andre, Roelof and Martijn for all the interesting discussions and excellent travel adventures. PhD wouldn't have been the same joy without you all.

My parents who have been so involved with my progress and interests need a special mention. I would never have been able to dream big if they did not give me the wings to fly. My words of gratitude pales in comparison to their efforts, sacrifices and involvement. Nevertheless, thanks a lot for being my invisible shoulders and supporting my ventures wholeheartedly.

Last but definitely not the least, my dear wife Spoorti. She has been a partner of mine in this PhD journey. She has been my punching bag in stress and championing me since I started my PhD. She was also the very first person to say I would go on to do a PhD (on the day I got an MSc). I hope my efforts to make your words come true are worth it. In any case, thanks a lot for all your sacrifices, support and for the beautiful bundle of joy, Anika.

Curriculum Vitæ

Akshay Raju Kulkarni

01-04-1991   Born in Bharuch, India.

Research and Engineering

2021–2022   **Researcher - DEFAINE project**
Delft University of Technology, Delft, The Netherlands

2017–2022   **Researcher - NOVAIR project**
Delft University of Technology, Delft, The Netherlands

2016–2018   **Researcher - IDEALISM project**
Delft University of Technology, Delft, The Netherlands

Education

2017–2022   **Doctor of Philosophy (PhD) in Sub-Scale Flight Testing**
Delft University of Technology, Delft, The Netherlands
Thesis: Similitude Augmentation in Sub-scale Flight Test Model Design
Promotors: dr.ir. G. La Rocca & prof.dr.ir. L.L.M. Veldhuis

2013–2015   **Master of Science (MSc) in Aerospace Engineering**
Delft University of Technology, Delft, The Netherlands
Thesis: Development of KBE tool to support Fin-Rudder Interface Design and Optimization
Supervisors: dr.ir. G. La Rocca & dr.ir.T. van den Burg

2009–2013   **Bachelor of Engineering (B.E.) in Mechanical Engineering**
University Visvesvaraya College of Engineering,
Bangalore University, Bangalore, India

2007–2009   **All India Senior School Certificate Examination**,
Kendriya Vidyalaya Malleswaram, Bangalore, India